(1)

ADIABATIC SHEAR BANDS IN SIMPLE AND DIPOLAR VISCOPLASTIC MATERIALS

FINAL REPORT

ROMESH C. BATRA

U. S. ARMY RESEARCH OFFICE

CONTRACT NO. DAAL03-88-K-0184

UNIVERSITY OF MISSOURI - ROLLA
ROLLA, MO 65401

APPROVED FOR PUBLIC RELEASE
DISTRIBUTION UNLIMITED

CONTENTS

1. STATEMENT OF THE PROBLEM STUDIED

Adiabatic shear is the name given to a localization phenomenon that occurs during high-rate plastic deformation such as machining, explosive forming, shock impact loading, ballistic penetration, fragmentation, ore crushing, impact tooling failure, and metal shaping and forming processes. The localization of shear strain has been observe in steels, nonferrous metals, and polymers. Practical interest in the phenomenon derives from the fact that progressive shearing on an intense shear band provides an undesirable mode of material resistance to imposed deformation, and the bands are often precursors of shear fractures.

The localization of deformation is exemplified by the deformed shear band in the aluminum alloy 2014-T6, shown in Figure 1, which is taken from Rogers' review article [1].

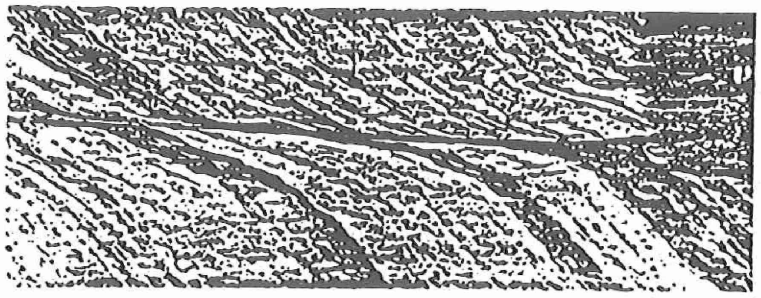

Figure 1. Deformed shear band produced below a flat-ended projectile in aluminum alloy 2014-T6, showing the high degree of shear in the band.[1]

Precipitate particles and grain boundaries provide the markers for shear strain delineation, which is obviously very high in an extremely thin zone of deformation. There is no evidence from the microstructure that this was an adiabatic shear band; only the knowledge that the deformation was caused by projectile impact would necessitate considering deformation heating as a contributing factor in strain localization. Moss [2] used an explosively driven punch to shear plugs from Ni-Cr steel plates, and thereby observe strain and strain rates in the resulting shear bands. His findings, illustrated in Figures 2 and 3, clearly indicate that a maximum shear strain rate as large as 9.4×10^7 sec^{-1} occurred.

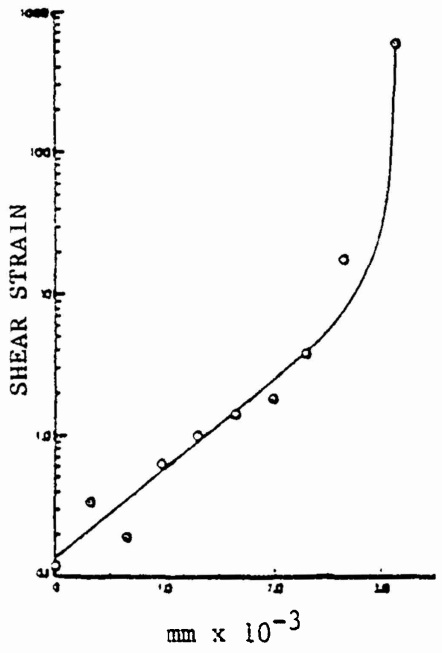

Figure 2. Shear strain versus distance through an adiabatic shear band.[2]

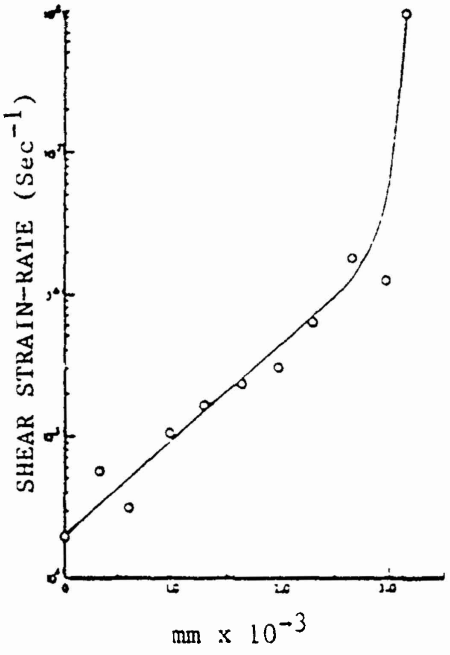

Figure 3. Shear strain rate versus distance through an adiabatic shear band.[2]

Zener and Hollomon [3] observed 32 μm wide shear bands in a steel plate punched by a standard die, and estimated the maximum strain in the band to be 100. They recognized the destabilizing effect of thermal softening in reducing the slope of the stress-strain curve in nearly adiabatic deformations, and postulated that a negative slope of the stress-strain curve implies an intrinsic instability of the material.

According to Johnson [4], adiabatic shear bands had been observed by Tresca [5] in 1878 and Massey[6] in 1921 during the hot forging of platinum. They called them hot lines.

Recent experimental [7-9] investigations have established that the localization of the deformation initiates in earnest at a value of the average strain much greater than the value at which the shear stress or the effective stress attains its peak value. Experimental findings of Marchand and Duffy [7] on HY-100 steel, and of Marchand, Cho, and Duffy [9] on AISI 1018 cold-rolled steel indicate that the shear strain localization phenomenon consists of three stages. In the first stage, the deformation stays homogeneous. Stage two, stipulated to initiate when the shear stress attains its peak value, involves non-homogeneous deformations of the block. In stage three, the shear stress drops precipitously and the severely

deforming region narrows down considerably. Thus, the stability criterion [10] based on the stress attaining a maximum value will predict the initiation of stage two rather than the beginning of the intense localization of the deformation.

We have developed a robust computer code to integrate field equations governing the thermomechanical deformations of a viscoplastic body deformed in either simple shear or plane strain compression. The code has been used to study the initiation and growth of shear bands with the following objectives:

(a) identifying the most appropriate constitutive model for the study of shear bands,

(b) assessing the effect of different ways of modeling a material inhomogeneity,

(c) identifying material parameters that affect significantly the initiation and subsequent development of shear bands,

(d) investigating the interaction among two or more bands, and

(e) finding the effect of the deformation mode (i.e., simple shear or plane strain compression) on the initiation and growth of adiabatic shear bands.

2. SUMMARY OF IMPORTANT RESULTS

From the research completed under this contract, the following salient conclusions can be drawn.

1. Of the five constitutive relations, namely, the Bodner-Partom law, the Litonski law, the Power law, the Johnson-Cook law, and the Wright-Batra law for dipolar materials, used to model the thermoviscoplastic response of materials in simple shear, the Bodner-Partom law and the Wright-Batra dipolar theory predict results which are in better agreement with the experimental observations of Marchand and Duffy on HY-100 steel than are the predictions from the other three constitutive relations.

2. The plots of the band width w computed when the ratio of the average shear stress in the specimen to the maximum shear stress equalled 0.95, 0.90, 0.85, 0.80, 0.75, and 0.70 versus the square root of the thermal conductivity k revealed that w decreases with a decrease in k for each of the three constitutive relations, viz, the Litonski law, the Bodner-Partom law, and the Johnson-Cook law, and that the relationship between w and $(k)^{1/2}$ is not linear.

3. The consideration of inertia forces delays the initiation of shear bands. For materials exhibiting large thermal softening effect in the Litonski law, the stress drop within the band is rapid enough to cause an elastic unloading wave to emanate outward from the shear band.

4. When the dependence of material properties upon the temperature is accounted for, and the Bodner-Partom law is used to model the viscoplastic response of the material, it was found that an increase in the initial temperature delayed the initiation of shear bands and resulted in wider bands.

5. When the initiation and development of shear bands in six ductile and six less ductile materials was studied by using the Johnson-Cook law, the homologous temperature of a material point at the band center when the shear stress had dropped to 85% of its maximum value was found to be independent of the defect size.

6. For dipolar materials, the initiation of the localization process was delayed, the shear stress dropped less rapidly, and bands were wider as compared to that for the nonpolar case.

7. For a hollow viscoplastic cylinder containing two ellipsoidal voids symmetrically located on a radial line with their centers at the midpoints of the cylinder thickness, the shear bands initiate at void tips near the inner surface of the cylinder and propagate toward this surface. Even though the strain near the other void tips is high, no bands were found to diffuse out from them.

8. The modelling of a material defect by either (i) introducing a temperature perturbation, (ii) assuming that the material at the site of the defect is weaker than the rest of the material, (iii) there is a non-heat-conducting rigid ellipsoidal inclusion, or (iv) there is an ellipsoidal void at the defect site, give similar qualitative results.

9. For a bimetallic body containing a thin layer of a weak material, and also an ellipsoidal void and deformed in plane strain compression, shear bands also originate from points where the thin layer meets the free boundaries and propagate into the weaker layer material. These bands propagate along the thin layer first and then bifurcate into two bands that propagate into the matrix material in the direction of the maximum shear stress.

10. The rate of evolution of the stress, strain, and temperature at the band center in a viscoplastic body undergoing plane strain deformations is different from that in the same body deformed in simple shear. For example, the temperature rises extremely sharply in the latter case, but rather gradually in the former.

3. BRIEF REVIEW OF THE COMPLETED WORK

The thrust of the research has been to increase our understanding of the physics of adiabatic shear banding, delineate the post-localization response of the material, find the structure within the band, and assess the effect of various material and geometric parameters on the initiation and development of the shear band. For this purpose, a robust computer code that gives stable and reliable results, even after the localization has set in and the band has formed, has been developed. We first outline briefly results for the simple shearing problem, and then for the two-dimensional problems involving plane strain deformations of a thermally softening viscoplastic body. Throughout our work, we have assumed that softening is caused by the heating of the body due to plastic working, and the material can undergo unlimited plastic deformation.

a. Results for the Simple Shearing Problem.

When studying the initiation and growth of shear bands in a body undergoing overall simple shearing deformations, we have modeled its material as elastic-viscoplastic that exhibits strain-hardening, strain-rate hardening, and thermal softening. A material inhomogeneity or defect has been modeled by either introducing a temperature perturbation or by assuming that the block has a non-uniform thickness. We found values of the material parameters in the Bodner-Partom [11] constitutive relation, Litonski law [12], Johnson-Cook law [13], Power law [14], and the Wright-Batra [15] dipolar theory by ensuring that the computed shear stress-shear strain curve for a block without any defect matched well with that reported by Marchand and Duffy [7] for a HY-100 steel specimen subjected to torsional loading at room temperature and deformed at a nominal strain-rate of 3300 sec^{-1}. The size of the defect was determined by numerical experiments, so that the sharp drop in stress occurred at about the experimental value of the nominal strain. Subsequently, computed band-width, temperature rise, evolution of the strain within the band, and the rate of stress drop for tests done at nominal strain rates of 1600 sec^{-1} and 1400 sec^{-1} were compared with the experimental findings. This comparison [16] revealed that the predictions from the Bodner-Partom law and the Wright-Batra dipolar theory are in better agreement with experimental observations than those from the other three flow rules. Each one of the five constitutive relations predicted the three stages of the localization phenomenon reported by Marchand and Duffy. However, the rate of evolution of the temperature within the band and/or the rate of drop of the shear stress within the band depended upon the constitutive relation used.

We [17] have used the Litonski law, the Bodner-Partom law and the Johnson-Cook law to model the viscoplastic response of the material and computed results for five different values, i.e., 0, 5, 50, 500, and 5000 W/m ° C, of the thermal conductivity k. The thickness of the block was assumed to vary smoothly, with the thickness at the specimen center being 5% smaller than that at the outer edges. For each of these three constitutive

relations, the rates of evolution of the temperature and the shear strain at the specimen center were steepest for k = 0, and decreased with an increase in the value of k. Marchand and Duffy [7] defined the band-width as the width of the region over which the shear strain equalled its peak value. For most of our computations, this definition will give the band-width to be zero. Therefore, we defined the band-width as the width of the region over which the shear strain exceeds 95% of its value at the center. The band-width depends upon how far the localization of the deformation has progressed, or how much the shear stress at the specimen center has dropped. The plots of the band-width w computed when the ratio of the average stress in the specimen to the maximum shear stress equalled 0.95, 0.90, 0.85, 0.80, 0.75, and 0.70 versus $(k)^{1/2}$ revealed that w decreased with a decrease in the value of k, irrespective of the constitutive relation employed, and that the relationship between w and $(k)^{1/2}$ was not linear as asserted by Dodd and Bai [18]. The Litonski law and Johnson-Cook law gave zero band width for k = 0, but the Bodner-Partom law gave a finite value of the band-width for k = 0.

We [19] examined the effect of inertia forces on the initiation of shear bands with each one of the aforestated five constitutive relations. It was found that the consideration of inertia forces delayed the initiation of shear bands. With the Litonski law and when inertia forces were considered, the stress drop within the band was rapid enough to cause an elastic unloading wave to emanate outward from the shear band. The difference between the computed speed of this elastic unloading wave and $(\mu/\rho)^{1/2}$ was less than 1%. Here μ and ρ equal, respectively, the shear modulus and the mass density of the material of the body. No such wave effect was observed with the other constitutive relations.

When studying the effect of the initial temperature of the specimen upon the initiation and development of shear bands, we [20] modeled the viscoplastic response of the material by the Bodner-Partom law and accounted for the dependence of the specific heat, thermal conductivity, and shear modulus upon the temperature. It was found that an increase in the initial temperature delayed the initiation of shear bands and resulted in

wider bands. This suggests that at higher initial temperatures of the specimen, larger changes of shape can be accommodated without damaging the workpiece due to the occurrence of shear bands.

In an attempt to correlate the information regarding the initiation and development of shear bands in different materials, we [21] have investigated the overall simple shearing deformations of an elastic-viscoplastic block deformed at a nominal strain-rate of 1500 sec^{-1}, and made of 12 different materials, namely, OFHC copper, Cartridge brass, Nickel 200, Armco IF (interstitial free) iron, Carpenter electric iron, 1006 steel, 2024-T351 aluminum, 7039 aluminum, low alloy steel, S-7 tool steel, Tungsten alloy, and Depleted Uranium (DU-0.75 Ti). The thermomechanical response of these materials is represented by the Johnson-Cook law, the material parameters are assigned values given by Johnson et al. [22], and the thickness of the block is least at its center, and its ends are kept at a constant temperature. It is found that the localization of the deformation begins earnestly when the shear stress at the weakest point has dropped to somewhere between 90 and 95% of its maximum value. The ratio of the maximum shear strain within the band to the nominal strain is found to depend strongly upon $\log \delta$, where δ is the percentage decrease in the specimen thickness at the center as compared to that at its edges. Larger defects result in more severe localization of the deformation for the same value of the ratio of the shear stress within the band to the maximum shear stress. The defect size has very little effect on the value of the homologous temperature, defined as the ratio of the absolute temperature of a material point to its melting temperature, when the shear stress at the specimen center attained its peak value, and when it had dropped to 85% of its maximum value. The band-width, defined above, computed when the shear stress at the specimen center has dropped to 85% of its maximum value, was found to be much longer for copper than for any of the other eleven materials studied. The computed band-width was different for the Armco IF iron, 1006 steel, and S-7 tool steel, even though each was assigned the same value of the thermal conductivity. No simple correlation was found between the

band-width and the thermal conductivity for these twelve materials.

When dipolar effects, i.e., the strain gradient considered as an independent kinematic variable and the corresponding higher order stress included in the balance of linear momentum and the balance of energy, were considered, initiation of the localization process was delayed, the shear stress dropped less rapidly, and the computed band-width was more as compared to the corresponding results for the nonpolar case [23]. The band-width and the value of the strain when the shear band initiated decreased monotonically and nonlinearly with a decrease in the value of the material characteristic length. Also, no unloading wave emanated outward from the severely deforming region in the problem wherein such a wave was computed in the absence of dipolar effects.

b. Results for the Plane-Strain Problems.

We [24-26] have analyzed the phenomenon of shear banding in a viscoplastic prismatic body of square cross-section undergoing overall adiabatic plane strain thermomechanical deformations. Two different loadings, namely, simple shearing and simple compression, at a nominal strain-rate of 5000 sec^{-1} are considered. A material defect is modeled by either (i) introducing a temperature perturbation at the specimen center, (ii) assuming that the material in a narrow region around the center of the specimen is weaker than the rest of the material, (iii) there is a rigid non-heat-conducting ellipsoidal inclusion (the inclusion simulates an impurity or a second phase particle such as carbide or manganese sulfide in a steel) at the center, or (iv) there is an ellipsoidal void at the center and also a narrow horizontal layer of a different material whose yield stress in simple compression equals either one-fifth or five times that of the surrounding matrix material. The thermo-viscoplastic response of the material was represented by a constitutive relation obtained by generalizing Litonski's law. In each case, bands of intense shear diffuse out from the point abutting the defect and propagate in the direction of maximum shearing. The velocity field suffers a sharp jump across the shear band, as asserted by Tresca [5] and Massey [6] in 1878 and 1921, respectively. As the temperature within the band increases, the effective stress in

it drops and the strain-rate rises. At a point near the inclusion tip or the void tip, the effective stress drops first. This is followed, much later, by a sharp increase in the maximum principal logarithmic strain ϵ at the same point. The rate of drop of the effective stress and the rate of growth of ϵ are much lower than those found in the one-dimensional simple shearing problem (e.g., see the Fig.). These differences are possibly due to the constraining effects of the relatively strong material surrounding the weakened material within the shear band. A similar phenomenon was observed in the study of shear bands originating from void tips in a long hollow cylinder whose inner surface is subjected to a prescribed radial velocity [27]. Note that the deformations of the cylinder are non-homogeneous, even when there are no voids. The shear bands were found to initiate first at void tips closer to the center of the cylinder, and propagate toward the inner surface. The shear bands originating from the other void tips propagated toward the outer surface of the cylinder.

For the bimetallic body containing a thin layer of a different material and also an ellipsoidal void [26], the shear bands initiating from the tips of the void on the major axes propagate in the direction of the maximum shear stress. These bands are arrested by the strong virtually rigid material of the thin layer, but pass through the weaker thin layer rather easily. Other shear bands originate from points at which the thin layers meet the free boundaries and propagate into the weaker material. The band in the weaker thin layer propagates horizontally first, and then bifurcates into two bands that propagate into the matrix material in the direction of maximum shear stress. Within the band near the void tips, the effective stress drops quite rapidly and the temperature there rises sharply at about the same time. However, the sharp rise in the maximum principal logarithmic strain there occurs much later because parts of the void near the tips had coalesced.

Thus, histories of the evolution of the temperature, effective stress, and effective strain at a point within a shear band for the two-dimensional problems are strikingly different from those for the one-dimensional simple shearing problem.

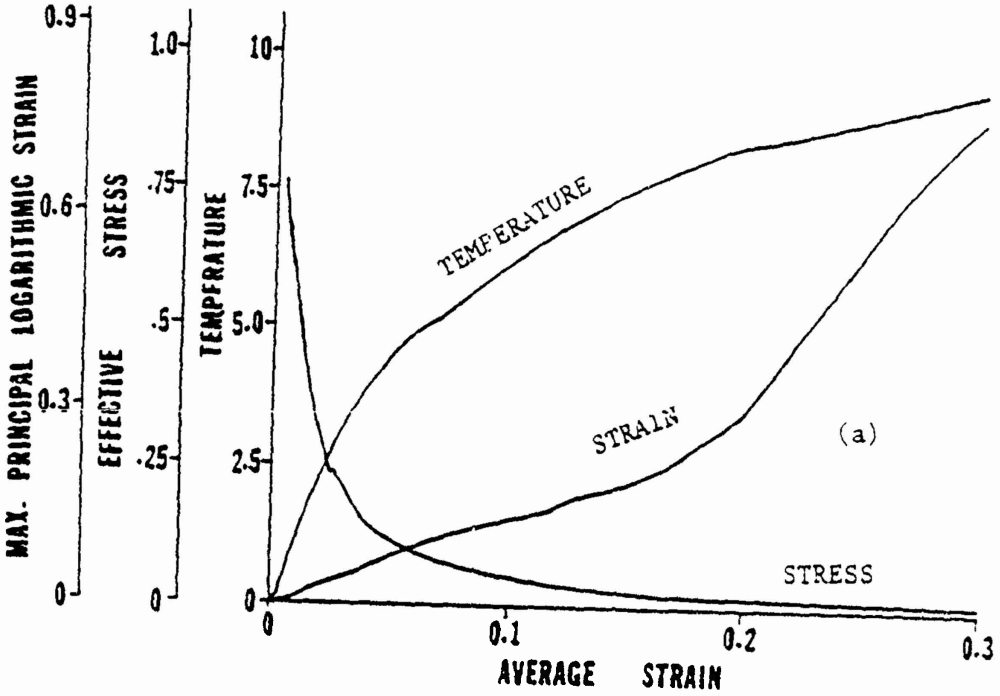

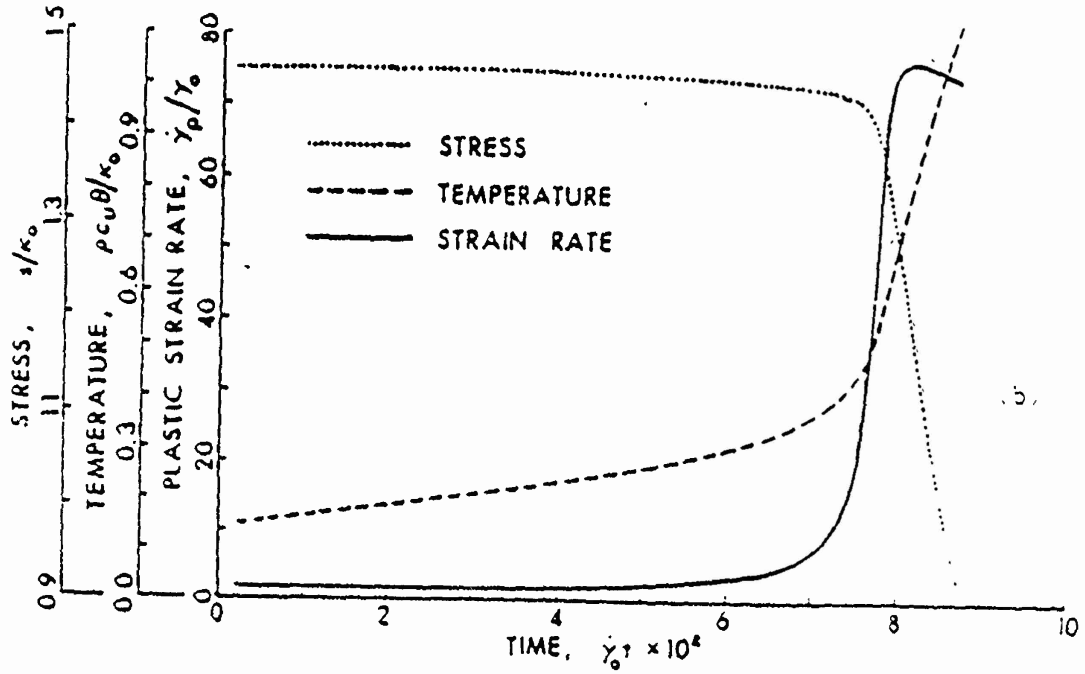

Figure a. Evolution of the Effective Stress, Temperature and the Maximum Principal Logarithmic Strain at a Point Near the Rigid Non-Heat-Conducting Ellipsoidal Tip during Plane Strain Compression of a Rectangular Viscoplastic Block Containing the Inclusion at Its Center.

Figure b. Evolution of the Shear Stress, Temperature and Strain-Rate at the Band Center in a Viscoplastic Block Undergoing Overall Simple Shearing Deformations.

4. PUBLICATIONS

a) ARTICLES IN REFEREED JOURNALS

1. R. C. Batra and Y. W. Kwon, Adiabatic Shear Banding in a Bimetallic Body, Acta Mechanica, 77, 281-297, 1989.

2. R. C. Batra and D-Shin Liu, Adiabatic Shear Banding in Dynamic Plane Strain Problems, J. Appl. Mechs., 56, 527-534, 1989.

3. R. C. Batra and De-Shin Liu, Adiabatic Shear Banding in Dynamic Plane Strain Compression of a Viscoplastic Material, Int. J. Plasticity 6, 231-246, 1990.

4. R. C. Batra and C. H. Kim, Adiabatic Shear Banding in Elastic-Viscoplastic Nonpolar and Dipolar Materials, Int. J. Plasticity, 6, 127-141, 1990.

5. R. C. Batra and C. H. Kim, An Adaptive Mesh Refinement Technique for the Analysis of Adiabatic Shear Banding, Mechs. Research Communications, 17, 81-91, 1990.

6. R. C. Batra and C. H. Kim, Effect of Integration Methods on the Solution of an Adiabatic Shear Banding Problem, Int. J. Numerical Methods Engineering, 29, 1639-1652, 1990.

7. R. C. Batra and C. H. Kim, Effect of Viscoplastic Flow Rules on the Initiation and Growth of Shear Bands at High Strain Rates, J. Mechs. Phys. Solids, 38, 859-874, 1990.

8. Z. G. Zhu and R. C. Batra, "Dynamic Shear Band Development in Plane Strain Compression of a Viscoplastic Body Containing a Rigid Inclusion", Acta Mechanica, 84, 89-107, 1990.

9. R. C. Batra and C. H. Kim, "The Interaction Among Adiabatic Shear Bands in Simple and Dipolar Materials", Int. J. Engr. Science, 28, 927-942, 1990.

10. R. C. Batra and Xiang-Tong Zhang, "Shear Band Development in Dynamic Loading of a Viscoplastic Cylinder Containing Two Voids", Acta Mechanica, 85, 221-234, 1990.

11. R. C. Batra and C. H. Kim, Effect of Thermal Conductivity on the Initiation, Growth, and Band Width of Adiabatic Shear Bands, Int. J. Engng. Sci., 29, 949-960, 1991.

12. R. C. Batra and Z. G. Zhu, Dynamic Adiabatic Shear Band Development in a Bimetallic Body Containing a Void, Int. J. Solids Structures, 27, 1829-1854, 1991.

13. R. C. Batra and Z. G. Zhu, Dynamic Band Development in a Thermally Softening Bimetallic Body Containing Two Voids, Acta Mechanica, 86, 31-52, 1991.

14. Z. G. Zhu and R. C. Batra, Shear Band Development in a Thermally Softening Viscoplastic Body, Computers and Structures, 39, 459-472, 1991.

15. R. C. Batra and C. H. Kim, Analysis of Shear Banding in Twelve Materials, Int. J. Plasticity, (in press).

16. Z. G. Zhu and R. C. Batra, Analysis of Shear Banding in Plane Strain Compression of a Bimetallic Thermally Softening Viscoplastic Body Containing an Elliptical Void, J. Engr. Mat. and Tech., (in press).

17. C. H. Kim and R. C. Batra, Effect of Initial Temperature on the Initiation and Growth of Shear Bands in a Plain Carbon Steel, Int. J. Nonlinear Mechs., (in press).

18. Xiang-Tong Zhang and R. C. Batra, An Approximate Linear Stability Analysis of Simple Shearing Deformations of a Dipolar Viscoplastic Material, J. Math. Physical Sciences (in press).

b) ARTICLES IN CONFERENCE PROCEEDINGS

19. R. C. Batra, A Mathematical Model of Adiabatic Shear Banding, in Mathematical Modelling in Science and Technology, (N. V. C. Swamy, P. Achuthan and S. N. Majhi eds.) Tata McGraw Hill, pp. 302-312, 1988.

20. R. C. Batra and De-Shin Liu, Shear Band Development in Dynamic Plane Strain Compression of a Viscoplastic Material, Proc. Army Symp. Solid Mechs.: Mechanics of Engineered Materials and Applications, Newport, May 16-18, 1989, pp. 118-122.

21. R. C. Batra, Effect of Nominal Strain Rates on Adiabatic Shear Banding in Dipolar Materials, Pan American Congress of Applied Mechs., Rio de Janeiro, Brazil, Jan. 1989, pp. 79-82.

22. R. C. Batra and C. H. Kim, Effect of Constitutive Modelling on Dynamic Development of Shear Bands in Viscoplastic Materials, Proc. 7th U. S. Army Conf. Appl. Math. and Computing, (F. Dressel, ed.), pp 182-192, 1990.

23. Z. G. Zhu and R. C. Batra, Analysis of Shear Banding in Plane Strain Compression of a Bimetallic Thermally Softening Viscoplastic Body Containing an Elliptical Void, Thermal Effects on Structures and Materials (V. Birman and D. Hui, eds.) ASME Press, AMD-Vol. 110, pp. 77-92, 1990.

24. R. C. Batra and C. H. Kim, Modelling of Shear Bands in a HY-100 Structural Steel, Computational Mechanics 91 (S. N. Atluri, D. E. Beskos, and G. Yagawa, eds.), Springer-Verlag (in press).

25. R. C. Batra and Z. G. Zhu, Dynamic Shear Band Development in Plane Strain Compression of a Bimetallic Body, Trans. 8th Army Conf. Applied Math & Computing, (F. Dressel, ed.), pp. 127-136, 1991.

5. PRESENTATIONS

1. R. C. Batra and C. H. Kim, Adiabatic Shear Banding in Elastic Viscoplastic Materials, 17th Int. Cong. of Theoretical and Appl. Mechs., Grenoble, France, August 1988.

2. R. C. Batra, A Mathematical Model of Adiabatic Shear Banding, Int. Conf. on Math. Modelling in Science and Technology, Madras, India, August 1988.

3. R. C. Batra and C. H. Kim, Effect of Material Characteristic Length on the Initiation, Growth, and Band Width of Adiabatic Shear Bands in Dipolar Materials, 2nd Int. Conf. on Mechanical and Physical Behavior of Materials Under Dynamic Loading, Ajaccio, France, September 1988.

4. Adiabatic Shear Banding in Viscoplastic Materials, Seminar, University of Missouri-Rolla, October 1988.

5. R. C. Batra, Dynamic Adiabatic Shear Band Development in Viscoplastic Materials, Federal University of Rio de Janeiro, Instituto de Matematica, Seminar, Rio de Janeiro, Brazil, Jan. 1989.

6. R. C. Batra, Effect of Nominal Strain Rates on Adiabatic Shear Banding in Dipolar Materials, Pan American Congress of Applied Mechanics, Rio de Janeiro, Brazil, Jan. 1989.

7. R. C. Batra, Adiabatic Shear Banding in Viscoplastic Materials, Plasticity Minisymposium, Institute of Mathematics and Its Applications, Univ. of Minnesota, Feb. 1989.

8. R. C. Batra and De-Shin Liu, Shear Band Development in Dynamic Plane Strain Compression of a Viscoplastic Material, U. S. Army Symposium on Solid Mechanics, Newport, RI, May 16-18, 1989.

9. R. C. Batra and Chang-Ho Kim, Effect of Constitutive Modelling on the Dynamic Development of Shear Bands in Viscoplastic Materials, 7th U. S. Army Conference on Applied Mathematics and Computing, West Point, NY, June 6-9, 1989.

10. R. C. Batra, Shear Band Development in Viscoplastic Materials, Seminar, National Chung-Hsing University, Taichung, Taiwan, July, 1989.

11. R. C. Batra and De-Shin Liu, Dynamic Shear Band Development in Thermally Softening Viscoplastic Materials, 2nd International Symposium on Plasticity, Mie University, Tsu, Japan, July 31 - Aug. 4, 1989.

12. R. C. Batra and De-Shin Liu, Adiabatic Shear Band Development in Simple Shearing Deformations of a Viscoplastic Material, 21st Midwestern Mechanics Conference, Michigan Technological Univ., Houghton, Aug. 13-16, 1989.

13. R. C. Batra, Effect of Inertia Forces on the Initiation and Growth of Shear Bands in Viscoplastic Materials, 26th Annual Technical Meeting of the Society of Engr. Science, University of Michigan, Ann Arbor, Sept. 18-20, 1989.

14. R. C. Batra and De-Shin Liu, Adiabatic Shear Banding in Plane Strain Problems, ASME 1989 Winter Annual Meeting, San Francisco, Dec. 10-15, 1989.

15. R. C. Batra, Effect of Viscoplastic Flow Rules on the Initiation and Growth of Shear Bands at High Strain Rates, ASME 1989 Winter Annual Meeting, San Francisco, Dec. 10-15, 1989.

16. R. C. Batra, Adiabatic Shear Banding in Simple and Dipolar Viscoplastic Materials, Seminar, University of Pittsburgh, March 1990.

17. R. C. Batra, Adiabatic Shear Banding in Simple and Dipolar Viscoplastic Materials, Seminar, Dublin College, Ireland, May 1990.

18. Z. G. Zhu and R. C. Batra, Dynamic Shear Band Development in Plane Strain Compression of a Viscoplastic Body Containing a Rigid Inclusion, XI U. S. Nat'l Cong. Appl. Mechs., The Univ. of Arizona, Tucson, May 1990.

19. R. C. Batra, Z. G. Zhu and Xiang-Tong Zhang, Shear Band Development in Dynamic Plane Strain Problems, 8th Army Conference on Appl. Math. and Computing, Cornell Univ., Ithaca, June 1990.

20. R. C. Batra and C. H. Kim, Analysis of Adiabatic Shear Bands in Twelve Metals, 27th Annual Meeting of the Society of Engineering Science, Santa Fe, NM, October 21-24, 1990.

21. Z. G. Zhu and R. C. Batra, Analysis of Shear Banding in Plane Strain Compression of a Bimetallic Thermally Softening Viscoplastic Body Containing an Elliptical Void, ASME Winter Annual Meeting, November 1990.

22. R. C. Batra and C. H. Kim, Analysis of Shear Banding in Twelve Materials, 9th Army Conference on Applied Math. and Computing, Minneapolis, June 1991.

6. DISSERTATIONS COMPLETED

Ph.D., 1989, De-Shin Liu

Dynamic Adiabatic Shear Band Development in Plane Strain Deformations of a Viscoplastic Material

Ph.D., 1989, Chang-Ho Kim
Shear Strain Localization in Elastic-Viscoplastic Materials

7. PARTICIPATING SCIENTIFIC PERSONNEL

Romesh C. Batra
Zhen-Guo Zhu
Chang-Ho Kim
De-Shin Liu
Yinhe Cao
Kwang-Il Ko
Jungsun Hwang

8. BIBLIOGRAPHY

1. H. C. Rogers, Ann. Rev. Mat. Sci., 9, 283 (1979).

2. G. L. Moss in Shock Waves and High Strain-Rate Phenomena in Metals, M. A. Meyers and L. E. Murr, eds., Plenum Press, New York, pp. 299-312 (1981).

3. C. Zener and J. H. Hollomon, J. Appl. Phys. 15, 22 (1944).

4. W. Johnson, Int. J. Mech. Sci., 29, 301 (1987).

5. H. Tresca, Proc. Inst. Mech. Engr., 30, 301-330 (1878).

6. H. F. Massey, Proc. Manchester Assoc. Engrs., 21-26 (1921).

7. A. Marchand and J. Duffy, J. Mechs. Phys. Solids, 36, 251 (1988).

8. J. H. Giovanola, Mechs. Materials, 7, 59 (1988).

9. A. Marchand, K. Cho, and J. Duffy, The Formations of Adiabatic Shear Bands in an AISI 1018 CRS, Brown Univ. Report (1988).

10. R. F. Recht, J. Appl. Mech. 31, 189 (1964).

11. S. R. Bodner and Y. Partom, J. Appl. Mech., 42, 385 (1975).

12. J. Litonski, Bulletin de l'Acadé mie Pololnaise des Sciences, 25, 7 (1977).

13. G. R. Johnson and W. H. Cook, Proc. 7th Int. Symp. Ballistics, The Hague, The Netherlands, p.1.

14. T. G. Shawki and R. J. Clifton, Mechs. Materials, 8, 13 (1989).

15. T. W. Wright and R. C. Batra, Proc. IUTAM Symp. on Macro- and Micro-Mechanics of High Velocity Deformation and Fracture, K. Kawata and J. Shioiri, eds., Springer-Verlag, New York, 1987, pp. 189-201.

16. R. C. Batra and C. H. Kim, J. Mechs. Phys. Solids, 38, 859 (1990).

17. R. C. Batra and C. H. Kim, Int. J. Engng. Sci., 29, 949 (1991).

18. B. Dodd and Y. Bai, Mat. Sci. Tech. 1, 38 (1985).

19. R. C. Batra, Unpublished work. (For wave speeds, see R. C. Batra and C. H. Kim, Int. J. Plasticity, 6, 127 (1990)).

20. C. H. Kim and R. C. Batra, Effect of Initial Temperature on the Initiation and Growth of Shear Bands in a Plain Carbon Steel, Int. J. Nonlinear Mechs. (in press).

21. R. C. Batra and C. H. Kim, Analysis of Shear Banding in Twelve Materials, Int. J. Plasticity (in press).

22. G. R. Johnson, J. M. Hoegfeldt, U. S. Lindholm, and A. Nagy, J. Engr. Mat. Tech., 105, 42 (1983).

23. R. C. Batra and C. H. Kim, J. Physique, 49 (C3), 41 (1988).

24. R. C. Batra and De-Shin Liu, J. Appl. Mechs., 56, 527 (1989); Int. J. Plasticity, 6, 231 (1990).

25. Z. G. Zhu and R. C. Batra, Acta Mechanica, 84, 89 (1990).

26. R. C. Batra and Z. G. Zhu, Int. J. Solids Structures, 27, 1829 (1991).

27. R. C. Batra and X.-T. Zhang, Acta Mechanica, 85, 221 (1990).

9. APPENDIX

A Copy of each of the following ten papers is included.

1. R. C. Batra and De-Shin Liu, "Adiabatic Shear Banding in Plane Strain Problems", ASME J. Appl. Mechs., 56, 527-534, 1989.

2. R. C. Batra and C. H. Kim, "Adiabatic Shear Banding in Elastic-Viscoplastic Nonpolar and Dipolar Materials", Int. J. Plasticity, 6, 127-141, 1990.

3. R. C. Batra and De-Shin Liu, "Adiabatic Shear Banding in Dynamic Plane Strain Compression of a Viscoplastic Material", Int. J. Plasticity, 6, 231-246, 1990.

4. Z. G. Zhu and R. C. Batra, Shear Band Development in a Thermally Softening Viscoplastic Body, Computers & Structures, 39, 459-472, 1991.

5. R. C. Batra and C. H. Kim, "An Adaptive Mesh Refinement Technique for the Analysis of Adiabatic Shear Banding", Mechs. Research Communications, 17, 81-91, 1990.

6. R. C. Batra and C. H. Kim, "Effect of Viscoplastic Flow Rules on the Initiation and Growth of Shear Bands at High Strain Rates", J. Mechs. Phys. Solids, 38, 859-874, 1990.

7. Z. G. Zhu and R. C. Batra, "Dynamic Shear Band Development in Plane Strain Compression of a Viscoplastic Body Containing a Rigid Inclusion", Acta Mechanica, 84, 89-107, 1990.

8. R. C. Batra and X.-T. Zhang, "Shear Band Development in Dynamic Loading of a Viscoplastic Cylinder Containing Two Voids", Acta Mechanica, 85, 221-234, 1990.

9. R. C. Batra and Z. G. Zhu, "Dynamic Shear Band Development in a Thermally Softening Bimetallic Body Containing Two Voids", Acta Mechanica, 86, 31-52, 1991.

10. R. C. Batra and C. H. Kim, "Effect of Thermal Conductivity on the Initiation, Growth, and Band Width of Adiabatic Shear Bands", Int. J. Engng. Sci., 29, 949-960, 1991.

THE AMERICAN SOCIETY OF MECHANICAL ENGINEERS
345 E. 47 St., New York, N.Y. 10017

89-WA/APM-16

Adiabatic Shear Banding in Plane Strain Problems

R. C. Batra
Mem. ASME

De-Shin Liu

Department of Mechanical and Aerospace Engineering and Engineering Mechanics, University of Missouri-Rolla, Rolla, Mo. 65401-0249

Plane strain thermomechanical deformations of a viscoplastic body are studied with the objective of analyzing the localization of deformation into narrow bands of intense straining. Two different loadings, namely, the top and bottom surfaces subjected to a prescribed tangential velocity, and these two surfaces subjected to a preassigned normal velocity, are considered. In each case a material defect, flaw, or inhomogeneity is modeled by introducing a temperature bump at the center of the specimen. The solution of the initial boundary value problem by the Galerkin-Adams method reveals that the deformation eventually localizes into a narrow band aligned along the direction of the maximum shearing strain. For both problems, bands of intense shearing appear to diffuse out from the center of the specimen.

1 Introduction

Adiabatic shear banding is the name given to a localization phenomenon that occurs during high-rate plastic deformation such as machining, explosive forming, shock-impact loading, ballistic penetration, fragmentation, ore crushing, impact tooling failure, and metal shaping and forming processes. The localization of the deformation has been observed in steels, nonferrous metals, and polymers. Practical interest in the phenomenon derives from the fact that progressive shearing on an intense shear band provides an undesirable mode of material resistance to imposed deformations, and the bands are often precursors to shear fractures. Of the many processes just stated in which adiabatic shear bands have been found to occur, flat sheet rolling and certain forging operations can be modeled as plane strain operations.

Since the time Zener and Hollomon (1944) recognized the destabilizing effect of thermal softening in reducing the slope of the stress-strain curve in nearly adiabatic deformations, there have been numerous studies aimed at delineating material parameters that enhance or retard the initiation and growth of adiabatic shear bands. Most of the effort has been concentrated in analyzing the simple shearing problem. Clifton (1980) and Bai (1981) studied the growth of infinitesimal periodic perturbations superimposed on a body deformed by a finite amount in simple shear. Burns (1985) used a dual asymptotic expansion to account for the time dependence of the homogeneous solution in the analysis of the growth of superimposed periodic perturbations. Merzer (1982) used the constitutive relation proposed by Bodner and Partom (1975) to study the problem of twisting of a thin tubular specimen having a notch in its periphery. He concluded that the band width depends upon the thermal conductivity. Wu and Freund (1984) used a different material model and studied wave propagation in an infinite medium. They concluded that the thermal conductivity has essentially no effect on the width of a shear band. Other works analyzing the initiation and growth of adiabatic shear bands include those due to Clifton et al. (1984), Wright and Batra (1985), Wright and Walter (1987), Batra (1987), and Batra and Kim, (1989). Rogers (1979, 1983) and Timothy (1987) have reviewed various aspects of adiabatic shear banding, especially from a materials point of view.

Experimental studies dealing with adiabatic shear banding include those of Zener and Hollomon (1944), Moss (1981), Costin et al. (1979), Lindholm and Johnson (1983), and Marchand and Duffy (1988). Marchand and Duffy have given a detailed history of the temperature and strain fields within a band.

Needleman (1989) has recently studied the initiation and growth of shear bands in plane strain deformations of viscoplastic materials. He studied a purely mechanical problem and approximated the effect of thermal softening by assuming that the stress-strain curve has a peak in it. He modeled a material inhomogeneity by assuming that the flow stress for a small amount of material near the center of the block was less than that of the surrounding material. We study herein the thermomechanical plane strain deformations of a thermally softening viscoplastic solid and model the material inhomogeneity by introducing a temperature bump at the center of the block. The block boundaries are assumed to be perfectly insulated. Two different deformation states, namely, that of a simple shearing of the block, and the block deformed in simple compression are analyzed. In each case a shear band develops along the direction of maximum shearing strain. Whereas the deformation localizes at an average compressive strain of 0.059 when the block is deformed in compression, the average shear strain equals 0.227 when the block is deformed in simple shear.

Contributed by the Applied Mechanics Division of THE AMERICAN SOCIETY OF MECHANICAL ENGINEERS for presentation at the Winter Annual Meeting, San Francisco, Calif., December 10–15, 1989.

Discussion on this paper should be addressed to the Editorial Department, ASME, United Engineering Center, 345 East 47th Street, New York, N.Y. 10017, and will be accepted until two months after final publication of the paper itself in the JOURNAL OF APPLIED MECHANICS. Manuscript received by the ASME Applied Mechanics Division, July 29, 1988; final revision, November 18, 1988. Paper No. 89-WA/APM-16.

2 Formulation of the Problem

We use a fixed set of rectangular Cartesian coordinate axes to describe the thermomechanical deformations of the body. In terms of the referential description the governing equations are

$$(\rho J)^{\cdot} = 0, \tag{1}$$

$$\rho_0 v_i = T_{i\alpha,\alpha}, \tag{2}$$

$$\rho_0 \dot{e} = -Q_{\alpha,\alpha} + T_{i\alpha} v_{i,\alpha}, \tag{3}$$

and a suitable set of initial and boundary conditions. Equation (1) expresses the balance of mass, (2) the balance of linear momentum, and (3) the balance of internal energy. In these equations, ρ is the current mass density, ρ_0 the mass density in the reference configuration, J is the determinant of the deformation gradient, v_i the velocity of a material particle in the x_i direction, Q_α the heat flux, e the specific internal energy, $T_{i\alpha}$ the first Piola-Kirchoff stress tensor, a superimposed dot stands for the material time derivative, and a comma followed by an index α (i) implies partial differentiation with respect to X_α (x_i). Also $\mathbf{x}$ denotes the present position of a material particle that occupied the place $\mathbf{X}$ in the reference configuration, and a repeated index implies summation over the range of the index. For plane strain deformations, $x_3 = X_3$ and the indices i and α take on values 1 and 2.

For the constitutive relations we take

$$\sigma = -p(\rho)\mathbf{1} + 2\mu\mathbf{D}, \quad T_{i\alpha} = \frac{\rho_0}{\rho} X_{\alpha,j}\sigma_{ij}, \tag{4}$$

$$2\mu = \frac{\sigma_0}{\sqrt{3I}}(1-\nu\theta)(1+bI)^m, \quad 2D_{ij} = v_{i,j} + v_{j,i}, \tag{5}$$

$$I = \frac{1}{2}\mathrm{tr}\tilde{\mathbf{D}}^2, \quad \tilde{\mathbf{D}} = \mathbf{D} - \frac{1}{3}(\mathrm{tr}\mathbf{D})\mathbf{1}, \tag{6}$$

$$p(\rho) = B\left(\frac{\rho}{\rho_0} - 1\right), \tag{7}$$

$$Q_\alpha = -k\theta_{,\alpha}, \tag{8}$$

$$e = c\theta + p\rho(\rho)/(\rho\rho_0). \tag{9}$$

Here, σ_0 is the yield stress in simple tension or compression, ν is the coefficient of thermal softening, parameters b and m represent the strain rate sensitivity of the material, B may be thought of as the bulk modulus, k is the thermal conductivity, and c the specific heat. Equation (7) is a part of the Tillotson (1962) equation wherein the dependence of the pressure upon the changes in temperature has not been considered, and equation (8) is the Fourier law of heat conduction.

Defining $\mathbf{s}$ as

$$\mathbf{s} = \sigma - \left(p - \frac{2\mu}{3}\mathrm{tr}\mathbf{D}\right)\mathbf{1}, \tag{10}$$

$$= 2\mu\tilde{\mathbf{D}}. \tag{11}$$

equations (4) and (5) give

$$\left(\frac{1}{2}\mathrm{tr}\mathbf{s}^2\right) = \frac{\sigma_0}{\sqrt{3}}(1-\nu\theta)(1+bI)^m, \tag{12}$$

which can be viewed as a generalized von Mises yield surface when the flow stress (given by the right-hand side of (12)) at a material particle depends upon its strain rate and temperature. The linear dependence of the flow stress upon the temperature change has been observed by Bell (1968), Lindholm and Jonnson (1983), and Lin and Wagoner (1986). A constitutive relation similar to equation (4) has been used by Zienkiewicz et al. (1981) in analyzing the extrusion problem, by Batra (1988) in studying the steady-state penetration of a viscoplastic target by a rigid cylindrical penetrator, and by Batra and Lin (1989) in studying the steady-state axisymmetric deformations of a cylindrical viscoplastic rod upset at the bottom of a hemispherical rigid cavity. Equation (4) may be interpreted as a constitutive relation for a non-Newtonian fluid whose viscosity μ depends upon the strain rate and temperature

We introduce nondimensional variables as follows:

$$\hat{\sigma} = \sigma/\sigma_0, \ \hat{p} = p/\sigma_0, \hat{\mathbf{s}} = \mathbf{s}/\sigma_0, \hat{\mathbf{v}} = \mathbf{v}/v_0, \ \hat{t} = tv_0/H, \ \hat{\mathbf{T}} = \mathbf{T}/\sigma_0,$$
$$\hat{\mathbf{x}} = \mathbf{x}/H, \ \hat{\theta} = \theta/\theta_0, \ \hat{b} = b\frac{v_0}{H}, \ \hat{\nu} = \nu\theta_0, \ \hat{\rho} = \rho/\rho_0, \ \hat{\mathbf{X}} = \mathbf{X}/H,$$
$$\hat{\delta} = \rho_0 v_0^2/\sigma_0, \ \beta = k/(\rho_0 c v_0 H), \ \theta_0 = \sigma_0/(\rho_0 c), \ \hat{B} = B/\sigma_0. \tag{13}$$

Here, $2H$ is the height of the block, v_0 is the imposed velocity on the top and bottom surfaces, and ρ_0 is the mass density in the unstressed reference configuration. Substituting from equations (4) through (9) into the balance laws (1) through (3), rewriting these in terms of nondimensional variables, denoting the partial differentiation with respect to $\hat{x}$ ($\hat{X}_\alpha$) by a comma followed by an index $i(\alpha)$, material differentiation with respect to $\hat{t}$ by a superimposed dot, and dropping the superimposed bars, we arrive at the following set of equations

$$\dot{\rho} + \rho v_{i,i} = 0 \tag{14}$$

$$\delta\dot{v}_i = T_{\alpha i,\alpha}, \tag{15}$$

$$\dot{\theta} = \beta\theta_{,\alpha\alpha} + [1/(\sqrt{3}I_D)](1-\nu\theta)(1+bI)^m D_{ij}D_{ij}, \tag{16}$$

$$\sigma = -B(\rho - 1)\mathbf{1} + \frac{1}{\sqrt{3I}}(1+bI)^m(1-\nu\theta)\mathbf{D}. \tag{17}$$

It is simpler to state boundary conditions for the specific problem studied. We analyze plane strain thermomechanical deformations of an initially-square block of dimension $2H \times 2H$. The $X_1 - X_2$ plane, with the origin of the coordinate system located at the center of the block, is taken as the plane of deformation. For the simple shearing problem the boundary conditions are taken to be

$$v_1 = \pm f(t), \ v_2 = 0, \ Q_\alpha N_\alpha = 0 \text{ at } X_2 = \pm H, \tag{18}$$

$$n_i T_{i\alpha} N_\alpha = 0, \ e_i T_{i\alpha} N_\alpha = h(t), \ Q_\alpha N_\alpha = 0 \text{ at } X_1 = \pm H, \tag{19}$$

where $\mathbf{n}$ is a unit outward normal and $\mathbf{e}$ is a unit vector tangent to the surface in the present configuration and $\mathbf{N}$ is a unit outward normal in the reference configuration. Equations (18) and (19) imply that the boundaries of the block are perfectly insulated, the top and bottom faces are placed in a hard loading device and are subjected to a known velocity field. On the other two faces of the block, zero normal tractions are assigned and the tangential tractions are such as to equilibrate the ones acting on the top and bottom faces. For a known function f, the values of h depend upon the constitutive relation for the material of the block, and hence, are not known *a priori*. As discussed in Section 3, we solve the resulting system of equations iteratively and find h as a part of the solution of the problem.

For the simple compression problem, we restrict ourselves to the deformations that remain symmetric about both $X_1 = 0$ and $X_2 = 0$. The boundary conditions for the quadrant analyzed numerically are

$$v_1 = 0, \ T_{21} = 0, \ Q_1(Ku)_1 = 0, \text{ at } x_1 = X_1 = 0, \tag{20}$$

$$v_2 = 0, \ T_{12} = 0, \ Q_2 = 0, \text{ at } x_2 = X_2 = 0, \tag{21}$$

$$T_{\alpha 1}N_\alpha = 0, \ Q_\alpha N_\alpha = 0, \text{ at } X_1 = H, \tag{22}$$

$$v_2 = U(t), \ e_i T_{i\alpha}N_\alpha = 0, \ Q_\alpha N_\alpha = 0, \text{ at } X_2 = H \tag{23}$$

That is boundary conditions resulting from the assumed symmetry of deformations are applied to the left and bottom faces, the right face of the block is taken to be traction free, and a prescribed normal velocity field and zero tangential tractions are applied on the top face. All four sides of the block are assumed to be perfectly insulated.

In each of the two problems, a material inhomogeneity or flaw is modeled by adding a temperature bump at the center of the block to the temperature field that corresponds to a homogeneous deformation of the block.

3 Finite Element Formulation of the Problem

In order to avoid having to deal with a severely distorted finite element mesh within the region of localization of the deformation, we employ an updated Lagrangian formulation. Thus to find the deformed shape of the body at time $t + \Delta t$, we take the configuration at time t as the reference configuration, and denote the region occupied by the body at time t by Ω. At subsequent times the current locations of the nodes are computed and Ω equals the union of the 9-noded quadrilateral elements obtained by joining these nodes. No attempt was made to ensure that when the deformation localizes, the element sides will be aligned along the direction of the maximum shearing strain (cf., Needleman, 1989). However, for the simple shearing problem, the element sides are so aligned at the initiation of the localization of the deformation.

We first rewrite equations (14)–(16) so that terms involving the partial derivative with respect to time t only are on the left-hand side and then use the Galerkin method and the lumped mass matrix (e.g., see Hughes (1987)) to derive the following semi-discrete formulation of the problem.

$$\mathbf{d} = \mathbf{F}(\mathbf{d}, \delta, \beta, b, m, \nu). \tag{24}$$

Here, $\mathbf{d}$ is the vector of nodal values of the mass density, two components of the velocity, and the temperature. Thus the total number of unknowns or the number of components of $\mathbf{d}$ equals four times the number of nodes. The vector-valued function $\mathbf{F}$ on the right-hand side of equation (24) is a nonlinear function of $\mathbf{d}$ and of the material parameters δ, β, b, m, and ν. For a given set of initial values of ρ, v and θ, one can deduce the initial conditions on $\mathbf{d}$. The nonlinear coupled set of ordinary differential equations (24) are solved by using the backward-difference Adams method included in the IMSL subroutine LSODE. During the solution of these equations, the tangential traction on the current position of the faces $X_1 = \pm H$ as determined from the immediately preceding solution, is applied. The subroutine LSODE has the option to use the modified Gear method appropriate for stiff equations. This could not be used because of the limited core storage available on the local FPS164 processor attached to IBM 4381 computer. For the Adams method, the subroutine LSODE adjusts the size of the time increment adaptively until it can compute a solution of the nonlinear equations (24) to the prescribed accuracy.

4 Computation and Discussion of Results

We took the following values of various material and geometric parameters to compute numerical results.

$$b = 10{,}000 \text{ sec}, \nu = 0.0222^\circ\text{C}^{-1}, \sigma_0 = 333\text{MPa}, m = 0.025,$$

$$k = 1.22 \text{ Wm}^{-1}{}^\circ\text{C}^{-1}, c = 473\text{Jkg}^{-1}{}^\circ\text{C}^{-1}, \rho_0 = 7{,}800 \text{ kgm}^{-3},$$

$$B = 128\text{GPa}, H = 5\text{mm}, v_0 = 25 \text{ msec}^{-1} \tag{25}$$

For these choices, $\theta_0 = 89.6^\circ\text{C}$, the nondimensional melting temperature equals 0.5027, and the overall applied strain rate is 5000 sec^{-1}. We assigned a rather large value to the thermal softening coefficient ν to reduce the CPU time required to solve the problem.

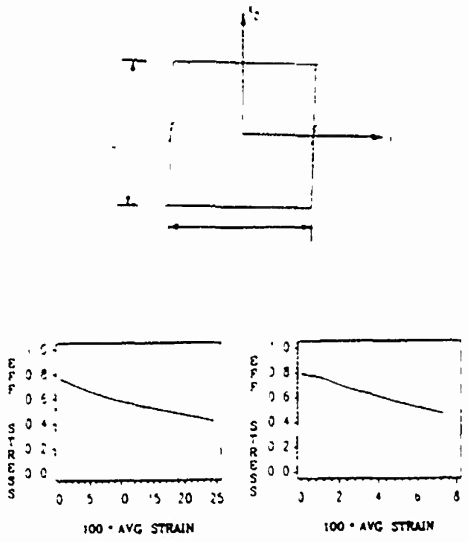

Fig. 1 (a) The shape of the block in the reference configuration and after it has been deformed uniformly in simple shear, (b) Stress-strain curve in simpler shear, and (c) Stress-strain curve in simple compression

Figure 1 depicts the block in the undeformed reference configuration and its shape after it has been deformed uniformly in simple shear. Also plotted are the stress strain curves for the material defined by parameters (25) when the block is deformed in simple shear and simple compression. It is obvious that the softening caused by the heating of the material exceeds the hardening due to strain rate effects right from the beginning. This is due to the rather high value of the thermal softening coefficient assumed for the material of the block. Once the deformation begins to localize, equations (24) become stiff and the maximum size of the time step one can use and still integrate these equations to the desired degree of accuracy becomes extremely small. Ideally, one should then use the Gear method. But, as stated previously, we could not do so because of the limited core storage available. The results presented and discussed next are up to the moment when the deformation has localized into a narrow band. Results computed earlier for the one-dimensional problem (Batra (1987), Batra and Kim (1989), and Wright and Walter (1987)) suggest that the presently computed results represent essentially all of the salient features of the localization of the deformation. We first discuss results for the simple shearing problem, and then the compression problem.

(a) Results for the Simple Shearing Problem. The square region in the configuration at time $t = 0$ is divided into 16×16 uniform 9-noded square elements. The velocity field

$$v_1 = x_2, v_2 = 0 \tag{26}$$

that corresponds to steady shearing of the block, and the temperature field

$$\theta = 0 \tag{27}$$

are taken as the initial conditions at time $t = 0$, and for the boundary conditions we take

$$f(t) = 1.0, t > 0.$$

Thus, the effect of initial transients is assumed to have died out. This reduces the computational effort required without altering noticeably the computed results. Subsequent calculations with zero-initial conditions for v_1, v_2, and θ have given essentially similar results.

At time $t = 0$, a temperature bump given by

$$\Delta\theta = 0.2(1 - r^2)^9 \exp(-5r^2),\ r^2 = X_1^2 + X_2^2 \qquad (28)$$

was introduced and the resulting initial boundary value problem solved. The temperature bump (28) simulates a material inhomogeneity or defect; the height of the bump represents, in some sense, the strength of the singularity. Without the temperature bump or some other mechanism to make the deformation nonhomogeneous, the block will undergo unlimited simple shearing deformations and no localization of the deformation will occur. We note that other ways to model an initial imperfection in the body include having a notch (Clifton et al., 1984) and a small region with a slightly lower value of the yield stress (Needleman, 1989). For strain hardening materials the introduction of a temperature bump, a notch or a softer region does not, in general, lead to the localization of the deformation. The average strain at which a shear band forms depends upon, among other factors, the amplitude and shape of the temperature bump.

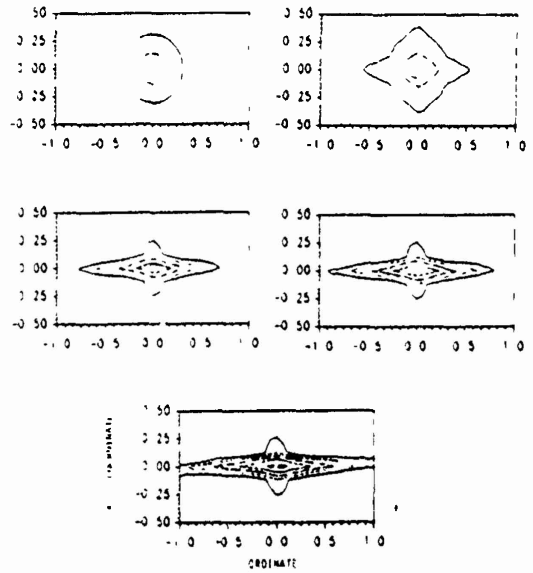

Fig. 2 Isotherms plotted in the reference configuration at different values of the average strain for simple shearing deformations of the block: (a) $\gamma_{avg} = 0$, $\theta_{max} = 0.2$, — 0.15, · · · · 0.10, —·—·—· 0.15, 0.05, (b) $\gamma_{avg} = 0.13$, $\theta_{max} = 0.344$, — 0.15, · · · · 0.20, —·—·—· 0.25, - - - - 0.30, (c) $\gamma_{avg} = 0.208$, $\theta_{max} = 0.441$, — 0.25, · · · · 0.30, —·—·—· 0.35, - - - - 0.40, — — — 0.45, (d) $\gamma_{avg} = 0.215$, $\theta_{max} = 0.449$ (see part (c) for values of θ corresponding to different curves), and (e) $\gamma_{avg} = 0.227$, $\theta_{max} = 0.463$ (see part (c) for values of θ corresponding to different curves)

Figure 2 shows isotherms in the reference configuration of the block at four different values of the average strain γ_{avg}. Initially, these isotherms look elliptical because of the different choice of scales along the horizontal and vertical axes. The temperature bump is symmetrical in x_1 and x_2. A reason for selecting different scales along the two axes is that the isotherms eventually flaten out and spread to the vertical boundaries of the block. Thus, larger scale is chosen along the vertical axis to decipher these isotherms. The initial temperature equals 0.20 only at the origin. At an average strain of 13 percent, the isotherms have changed shape; those for a lower temperature look like a rhombus and the ones for the higher temperature resemble closed polygons. Because of the plastic working and zero heat flux boundary conditions the temperature rises everywhere. The heat is continuously being conducted outwards from the central hotter region. Near the corners of the block deformation is nonhomogeneous (e.g., see Fig. 5) and the temperature rise there is more than that at other points except possibly near the center of the block. The nonhomogeneity of the deformation near the corners is a numerical artifact rather than due to the physics of the problem. The use of a very fine mesh should reduce the effect considerably, but a mesh finer than the one employed here could not be used because of the limited core storage available. Once the deformation begins to localize, the temperature rise within the band is significantly more than what it is elsewhere. The temperature contours at average strains of 20.8 percent, 21.5 percent, and 22.7 percent bear this out. At an average strain of 22.7 percent the maximum temperature at the center equals 92 percent of the presumed melting temperature of the material. The isotherms are quite narrow in the vertical direction and progressively become narrower as the deformation localizes.

Figure 3 depicts the v_1-velocity field in the reference configuration of the block at average strains of 0 percent, 18.5 percent, 20.8 percent, and 22.7 percent. Because of the initial temperature bump, the deformation becomes nonhomo-

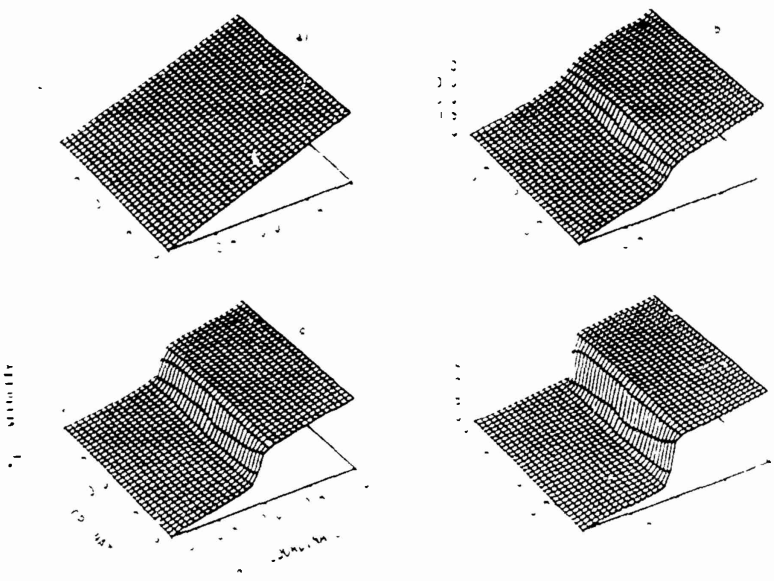

Fig. 3 Velocity field in the direction of shearing at several values of the average strain: (a) $\gamma_{avg} = 0$, (b) $\gamma_{avg} = 0.185$, (c) $\gamma_{avg} = 0.208$, and (d) $\gamma_{avg} = 0.227$

geneous. This nonuniformity becomes perceptible at an average strain of 18.5 percent and is quite noticeable when the average strain equals 20.8 percent and 22.7 percent. The nonhomogeneity in the deformation at the corners is not noticeable in these plots probably because of the scale chosen to plot the data. The v_1-velocity field appears to stay antisymmetric in x_2 even through the localization of the deformation. At an average strain of 20.8 percent the shearing strain rate at the center is noticeably higher than what it is within the region $|x_2| \geq 0.1$. During the ensuing deformations of the block, the region near the center undergoes intense straining and that outside of the domain $|x_2| \leq 0.1$ deforms at a strain rate much smaller than the imposed strain rate of 5000 sec^{-1}. With a finer mesh one could sharpen a bit more the boundaries of the two domains.

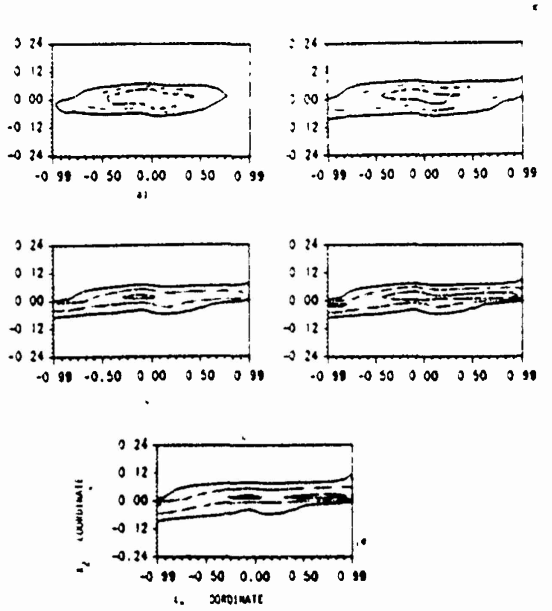

Fig. 4 Contours of the second invariant I of the deviatoric strain rate tensor at different values of the average strain; (a) $\gamma_{avg} = 0.185$, $I_{max} = 3.47$; — 1.5, · · · · · · 2.0, —·—·—· 3.5, (b) $\gamma_{avg} = 0.198$, $I_{max} = 4.45$; — 1.5, · · · · · · 2.5, —·—·—· 3.5, (c) $\gamma_{avg} = 0.208$, $I_{max} = 5.51$; — 2.5, · · · · · · 3.75, —·—·—· 5.0, (d) $\gamma_{avg} = 0.215$, $I_{max} = 6.23$; — 2.5, · · · · · · 3.75, —·—·—· 5.0, and (e) $\gamma_{avg} = 0.227$, $I_{max} = 8.45$; — 2.5, · · · · · · 5.0, —·—·—· 7.5

In Fig. 4 we have plotted the contours of the second invariant I of the deviatoric strain rate tensor $\bar{\mathbf{D}}$ at different stages of the localization process. At an average strain of 18.5 percent the peak value of I equals 3.47 and it equals 4.45 when the average strain is 19.8 percent. We note that these are plotted in the reference configuration. It is clear that during the deformation of the block from 18.5 percent average strain to 19.8 percent average strain, the contour of $I = 2.5$ has spread out horizontally and become narrower in the vertical direction. The various plots in Fig. 4 give the impression that there is a kind of source term for I at the center. Once the deformation has started to localize, contours of successively higher values of I seem to originate at the center and fan out. They spread out in the direction of shearing. As noted earlier, severe deformations of the block occur now in this narrow region.

Figure 5 depicts the distribution of the effective stress s_e, defined as being equal to the right-hand side of equation (12) within the block at average strains of 0 percent, 18.5 percent, 20.8 percent, and 22.7 percent. Initially it looks like an inverted hat because every material point is assumed to lie on its yield surface. We note that for the simple shearing problem being studied, σ_{12} is the only component of stress having significant values. Because of the higher temperature at points near the center, the flow stress there is reduced. As the body continues to be deformed, the stress distribution within the block, and especially in the region surrounding the center of the block, alters. The nonhomogeneity of the deformation near the corners is now evident. The temperature rise within the block reduces the flow stress needed to deform the material. Consequently, the value of s_e drops at all points. Even though the strain rate invariant I assumes very high values at points within the region of localization, the softening caused by the temperature rise exceeds the hardening due to strain rate effects and the stress drop in the severely deforming region is enormous. For very high rate of drop of s_e, an unloading elastic wave emanates outwards from the shear band (Batra and Kim, 1989). No such unloading wave was observed in this case. It could be due to the coarseness of the mesh, the integration scheme used, or the rate of the drop of s_e was not too high.

The deformed mesh at average strain of 22.7 percent is shown in Fig. 6. The relatively severe deformations within the region of localization, and nonuniformity of deformations near the corners, is evident.

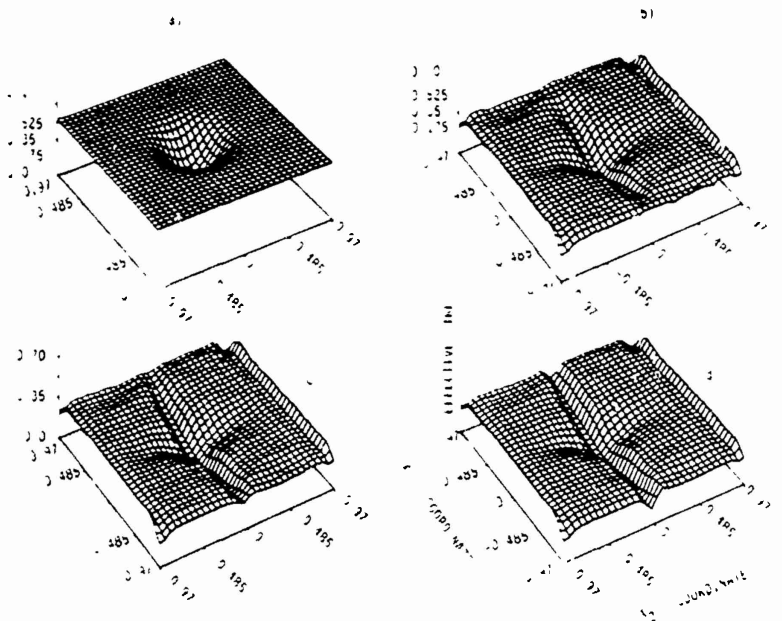

Fig. 5 Distribution of the effective stress within the block at different values of the average strain; (a) $\gamma_{avg} = 0$, (b) $\gamma_{avg} = 0.185$, (c) $\gamma_{avg} = 0.208$, and (d) $\gamma_{avg} = 0.227$

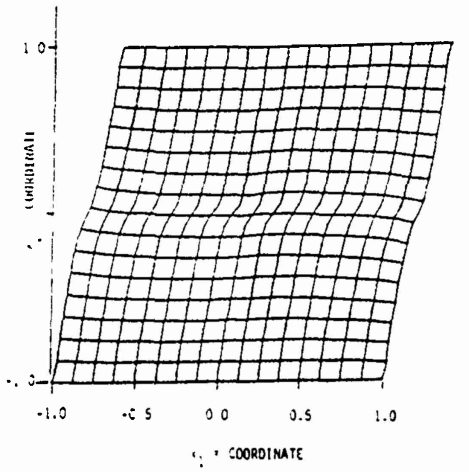

Fig. 6 Deformed mesh at an average strain of 0.227 (simple shearing deformations of the block)

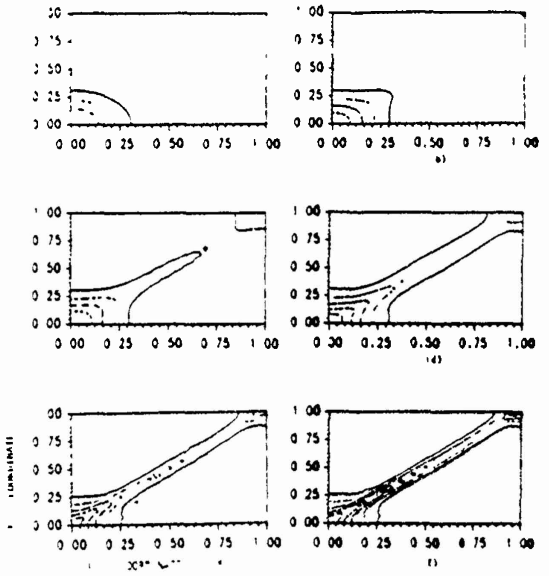

Fig. 7 Isotherms plotted in the reference configuration at different values of the average compressive strain; (a) $\gamma_{avg} = 0.0$, $\theta_{max} = 0.2$, — 0.05, · · · · 0.10, —·—·— 0.15, (b) $\gamma_{avg} = 0.035$, $\theta_{max} = 0.286$, — 0.10, · · · · 0.15, —·—·— 0.20, - - - - 0.25, (c) $\gamma_{avg} = 0.040$, $\theta_{max} = 0.313$, see part (b) for values of θ corresponding to different curves, (d) $\gamma_{avg} = 0.045$, $\theta_{max} = 0.353$, — 0.10, · · · · · 0.15, —·—·— 0.20, - - - - 0.25, — — — 0.30, (e) $\gamma_{avg} = 0.055$, $\theta_{max} = 0.426$, — 0.15, · · · · · 0.20, —·—·— 0.25, - - - - 0.30, — — — 0.35, and (f) $\gamma_{avg} = 0.059$, $\theta_{max} = 0.449$, (see part (e) for values of θ corresponding to different curves)

(b) Results for the Compression Problem. Because of the assumed symmetry of the deformation field, the deformations of the block within the first quadrant are analyzed. Several trial runs without introducing any temperature perturbation yielded the following values of the steady-state solution:

$$v_1 = 0.37x_1, \; v_2 = -x_2 \tag{29}$$

for an average applied strain rate of 5000 sec^{-1}. Subsequently this velocity field, and the temperature field given by equation (28), were taken as the initial conditions and the initial boundary value problem solved. A closer look at the results computed by Batra (1987a, 1987b) for the one-dimensional simple shearing problem reveals that the initial state where the perturbation is introduced has very little effect, if any, on the qualitative nature of the results. Figure 7 depicts the

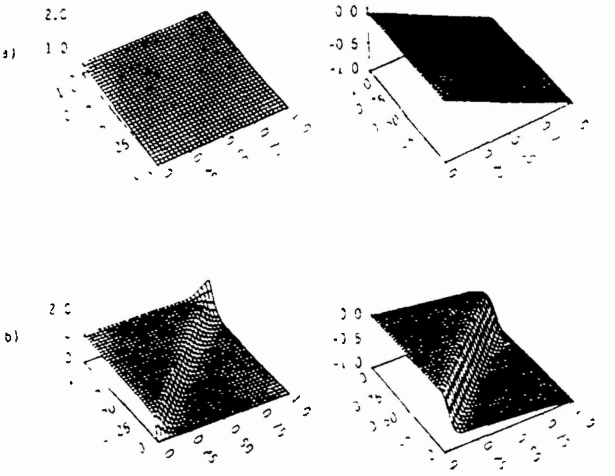

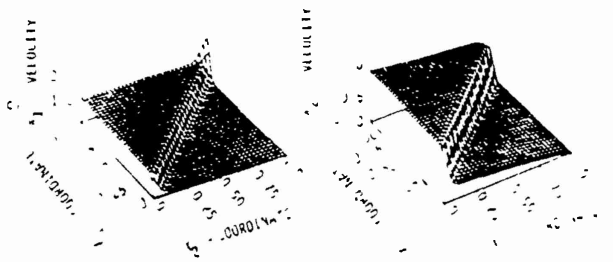

Fig. 8 Velocity field within the block at different values of the average compressive strain; (a) $\gamma_{avg} = 0$, (b) $\gamma_{avg} = 0.045$, (c) $\gamma_{avg} = 0.059$

temperature distribution at several values of the average compressive strain. At an average strain of 3.5 percent the isotherms have changed in shape from elliptic to rhombus and the peak temperature at the center has risen from 0.20 to 0.286. Because of the nonhomogeneous deformations near the top right corner, the temperature rise there is more than that at other points within the block except, of course, those near the center which are undergoing severe deformations. As the temperature plots at average compressive strains of 4 percent, 4.5 percent, 5.5 percent, and 5.9 percent show vividly, the isotherms spread out diagonally indicating that the material around the main diagonal is deforming severely. At these average strains the peak temperature occurs at the center and equals 0.313, 0.353, 0.426, and 0.449, respectively. Thus, the rate of temperature rise at the center is small initially, increases as the deformation begins to localize, and tapers off during the late stages of the localization. Even though heat is being conducted out of this central region the heat produced due to the plastic dissipation exceeds that lost due to conduction. Once the localization process is initiated, the heat generated due to plastic working becomes quite high and the rate of temperature rise within the central region picks up. However, the stress required to deform the material drops and thus reduces the energy dissipated due to plastic working. This and the heat conducted out of the central hotter region explains the slow rate of temperature rise during the late stages of the localization of the deformation.

In Fig. 8 we have plotted the v_1- and v_2-velocity fields at average strains of 0, 4.5 percent, and 5.9 percent. Except at points around the diagonal passing through the top right corner, both v_1 and v_2 vary slowly and nearly linearly, thereby implying that the material region within a narrow zone on both sides of the diagonal line is undergoing severe deformations. Figure 9 shows the contours of the second invariant I_2 of the deviatoric strain rate tensor at average compressive strains

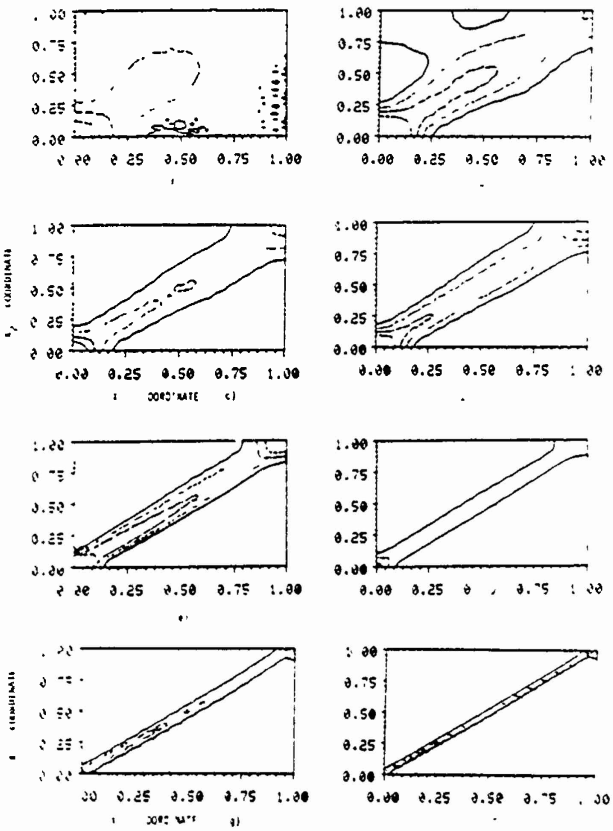

Fig. 9 Contours of the second invariant I of the deviatoric strain rate tensor at different values of the average compressive strain; (*a*) $\gamma_{avg} = 0.012$, $I_{max} = 2.0$. — 1.0, · · · · · · 1.25, —·—·—· 1.50, - - - - 1.75, (*b*) $\gamma_{avg} = 0.018$, $I_{max} = 2.53$, — 1.0, · · · · · · 1.25, —·—·—· 1.50, - - - - 1.75, (*c*) $\gamma_{avg} = 0.025$, $I_{max} = 2.95$. — 1.0, · · · · · · 1.5, —·—·—· 2.0, - - - - 2.5, (*d*) $\gamma_{avg} = 0.03$, $I_{max} = 3.70$, see part (*c*) for values of I corresponding to different curves, (*e*) $\gamma_{avg} = 0.035$, $I_{max} = 5.53$, — 1.5, · · · · · · 2.0, —·—·—· 2.5, - - - - 3.0, (*f*) $\gamma_{avg} = 0.040$, $I_{max} = 8.73$, — 2.5, · · · · · · 5.0, —·—·—· 7.5, (*g*) $\gamma_{avg} = 0.053$, $I_{max} = 16.92$, — 2.5, · · · · · · 7.5, —·—·—· 12.5, and (*h*) $\gamma_{avg} = 0.060$, $I_{max} = 20.7$, — 7.5, · · · · · · 12.5, —·—·—· 17.5

of 0.012, 0.018, 0.025, 0.03, 0.035, 0.04, 0.055, and 0.059. As for the simple shearing problem, the maximum value of I occurs at points near the center of the block and these contours seem to originate at the center and spread out along and perpendicular to the direction of maximum shearing strain; their speed probably depends upon the mesh size. Also, the width of the severely deforming region depends upon the mesh size, too.

Figure 10 depicts the distribution of the effective stress s_e at average strains of 0, 0.027, 0.045, and 0.059. Initially the stress is uniform everywhere except in a narrow region near the center where the flow stress has been reduced due to the higher value of the temperature at these points. The plot at $\gamma_{avg} = 0.027$ reveals that the flow stress has dropped everywhere due to the rise in the temperature of material particles. Still, the effective stress is uniformly distributed except at points near the center of the block. It seems that the localization of the deformation begins in earnest at $\gamma_{avg} = 0.045$. At $\gamma_{avg} = 0.059$ the material region around the main diagonal has severely deformed. The deformed mesh for $\gamma_{avg} = 0.059$ is shown in Fig. 11. That the band has formed is difficult to visualize from the deformed mesh shown. Also, the mesh is incapable of resolving sharp deformation gradients within the localized region.

5 Discussion and Conclusions

The 9-noded quadrilateral element used herein seems to have performed satisfactorily as far as the initiation and some growth of the adiabatic shear band is concerned. As for computations with one-dimensional problems (Batra, 1987a; Batra and Kim, 1989), it is probably due to the coarseness of the mesh that sharp gradients of the deformation within the region of localization could not be completely resolved. This is also supported by the recent work of Shuttle and Smith (1988) on the numerical simulation of shear band formation in soils. Both for plane strain, simple shearing deformations of the block and plane strain compression of the block, the shear band is formed along the direction of maximum shearing. For the compression problem the shear band formed at an average strain of 0.059, and for the simple shearing problem it formed when the average strain equaled 0.229. The results computed

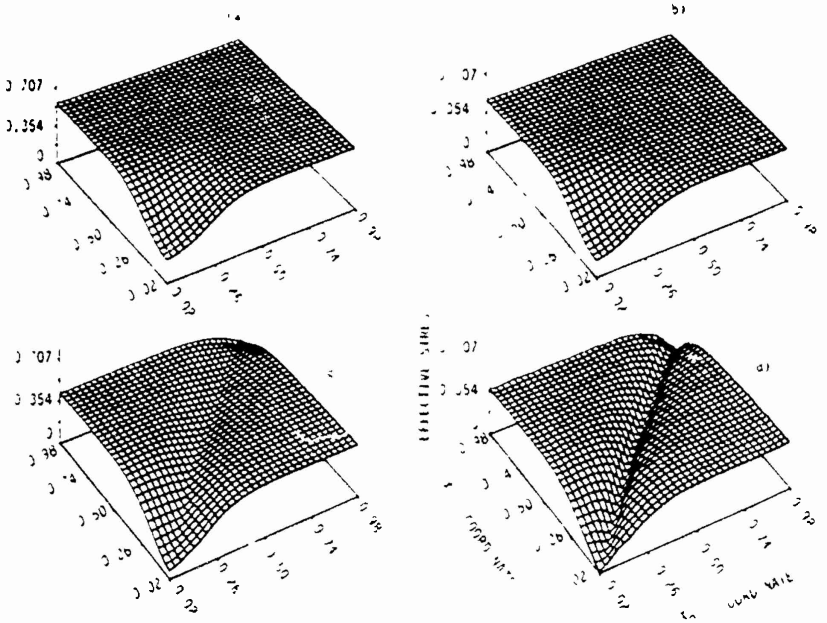

Fig. 10 Distribution of the effective stress within the block at different values of the average strain: (*a*) $\gamma_{avg} = 0$, (*b*) $\gamma_{avg} = 0.027$, (*c*) $\gamma_{avg} = 0.045$, and (*d*) $\gamma_{avg} = 0.059$

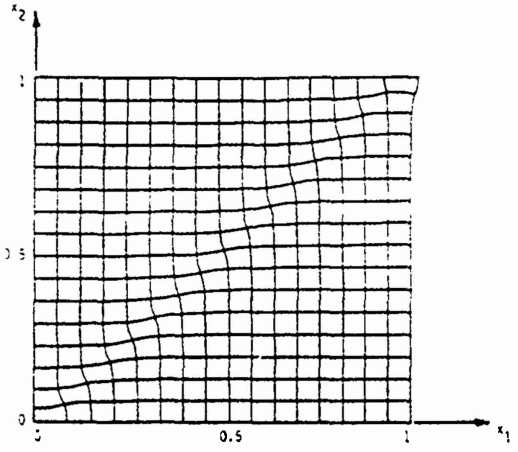

Fig. 11 Deformed mesh at an average compressive strain of 0.059

herein are in qualitative agreement with those of Needleman (1989). Because of the different constitutive assumptions made and the difference in modeling a material inhomogeneity, it is hard to make any quantitative comparisons.

Acknowledgments

This work was supported by the U.S. National Science Foundation grant MSM-8715952 and the U.S. Army Research Office Contract DAAL03-88K-0184 to the University of Missouri-Rolla.

References

Bai, Y. L., 1981, "A Criterion for Thermoplastic Shear Instability," *Shock Waves and High Strain-Rate Phenomena in Metals*, M. A. Myers, and L. E. Murr, eds., Plenum Press, New York, pp. 277–283.

Batra, R. C., 1987a, "The Initiation and Growth of, and the Interaction Among Adiabatic Shear Bands in Simple and Dipolar Materials," *Int. J. Plasticity*, Vol. 3, pp. 75–89.

Batra, R. C., 1988, "Steady State Penetration of Thermoviscoplastic Targets," *Comp. Mech.*, Vol. 3, pp. 1–12.

Batra, R. C., and Kim, C. H., 1989, "Adiabatic Shear Banding in Elastic-Viscoplastic Nonpolar and Dipolar Materials," *Int. J. Plasticity*, Vol. 5, to appear.

Batra, R. C., and Lin, Pei-Rong, 1989, "Steady State Axisymmetric Deformations of a Thermoviscoplastic Rod Striking a Hemispherical Rigid Cavity," *Int. J. Impact Engng.*, Vol. 8, to appear.

Bell, J. F., 1968, *Physics of Large Deformations of Crystalline Solids*, Springer-Verlag, New York.

Bodner, S. R., and Partom, Y., 1975, "Mechanical Properties at High Rate of Strain," *Inst. Phys. Conf.*, Ser. No. 21, pp. 102–110.

Burns, T. J., 1985, "Approximate Linear Stability Analysis of a Model of Adiabatic Shear Band Formation," *Q. Appl. Math.*, Vol. 43, pp. 65–84.

Clifton, R. J., 1980, "Adiabatic Shear in Material Response to Ultrahigh Loading Rates," U.S. NRC National Material Advisory Board Report NMAB-356, W. Herrman et al., eds.

Clifton, R. J., Duffy, J., Hartley, K. A., and Shawki, T. G., 1984, "On Critical Conditions for Shear Band Formation at High Strain Rates," *Scripta Metall.*, Vol. 18, pp. 443–448.

Costin, L. S., Crisman, E. E., Hawley, R. H., and Duffy, J., 1979, "On the Localization of Plastic Flow in Mild Steel Tubes Under Dynamic Torsion Loading," *Inst. Phys. Conf. Ser.*, Vol. 47, pp. 90–100.

Hughes, T. J. R., 1987, *The Finite Element Method Linear Static and Dynamic Finite Element Analysis*, Prentice-Hall, Englewood Cliffs, N.J.

Lin, M. R., and Wagoner, R. H., 1986, "Effect of Temperature, Strain and Strain-Rate on the Tensile Flow Stress of I. F. Steel and Stainless Steel Type 310," *Scripta Metall.*, Vol. 20, pp. 143–148.

Lindholm, U. S., and Johnson, G. R., 1983, "Strain-Rate Effects in Metals at Large Strain-Rates," *Material Behavior Under High Stresses and Ultrahigh Loading Rates*, J. Mescal, and V. Weiss, eds., pp. 61–79.

Marchand, A., and Duffy, J., 1988, "An Experimental Study of the Formation Process of Adiabatic Shear Bands in a Structural Steel," *J. Mech. Phys. Solids*, Vol. 36, pp. 251–283.

Merzer, A. M., 1983, "Modelling of Adiabatic Shear Band Development from Small Imperfections," *J. Mech. Phys. Sol.*, Vol. 30, pp. 323–338.

Moss, G. L., 1981, "Shear Strain, Strain Rates and Temperature Changes in Adiabatic Shear Bands," *Shock Waves and High Strain-Rate Phenomenon in Metals*, M. A. Meyers and L. E. Murr, eds., Plenum Press, New York, pp. 299–312.

Needleman, A., 1989, "Dynamic Shear Band Development in Plane Strain," ASME JOURNAL OF APPLIED MECHANICS, Vol. 56, pp. 1–9.

Rogers, H. C., 1979, "Adiabatic Plastic Deformation," *Ann. Rev. Mat. Sci.*, Vol. 9, pp. 283–311.

Rogers, H. C., 1983, "A Review of Adiabatic Shearing," *Material Behavior Under High Stress and Ultrahigh Loading Rates*, J. Mescall and V. Weiss, eds., Plenum Press, New York, pp. 101–118.

Shuttle, D. A., and Smith, I. M., 1988, "Numerical Simulation of Shear Band Formation in Soils," *Int. J. for Numerical and Analytical Methods in Geomechanics*, Vol. 12, pp. 611–626.

Tillotson, J. H., 1962, General Atomic Report GA-3216.

Timothy, S. P., 1987, "The Structure of Adiabatic Shear Bands in Metals. A Critical Review," *Acta Metall.*, Vol. 35, pp. 301–306.

Wright, T. W., and Batra, R. C., 1985, "The Initiation and Growth of Adiabatic Shear Bands," *Int. J. Plasticity*, Vol. 1, pp. 205–212.

Wright, T. W., and Walter, J., 1987, "On Stress Collapse in Adiabatic Shear Bands," *J. Mech. Phys. Solids*, Vol. 35, pp. 701–716.

Wu, F. H., and Freund, L. B., 1984, "Deformation Trapping Due to Thermoplastic Instability in One-Dimensional Wave Propagation," *J. Mech. Phys. Solids*, Vol. 32, pp. 119–132.

Zener, C., and Hollomon, J. H., 1944, "Effect of Strain-Rate on Plastic Flow of Steel," *J. Appl. Phys.*, Vol. 14, pp. 22–32.

Zienkiewicz, O. C., Onate, E., and Heinrich, J. C., 1981, "A General Formulation for Coupled Thermal Flow of Metals Using Finite Elements," *Int. J. Numer. Methods Eng.*, Vol. 17, pp. 1497–1514.

Printed in U.S.A.

International Journal of Plasticity, Vol 6 pp 127-141, 1990
Printed in the U S A

0749-6419/90 $3 00 + 00

ADIABATIC SHEAR BANDING IN ELASTIC-VISCOPLASTIC NONPOLAR AND DIPOLAR MATERIALS

R.C. BATRA and C.H. KIM

University of Missouri-Rolla

Abstract—Simple shearing deformations of a block made of an elastic-viscoplastic material are studied. The material of the block is presumed to exhibit strain hardening, strain-rate hardening and thermal softening. The effect of modeling the material of the block as a dipolar material in which the strain gradient is also taken as an independent variable has been investigated The uniform fields of temperature and shear stress in the block are perturbed by superimposing a temperature bump at the center of the block, and the resulting initial-boundary-value problem is solved by the Galerkin-Gear method. It is found that for simple materials as the shear stress within the region of localization begins to collapse, an unloading elastic shear wave emanates outwards from the edges of the shear band. For dipolar materials, the localization of the deformation is considerably delayed as compared to that for nonpolar materials, the shear stress does not collapse suddenly but decreases gradually, there is no unloading wave traveling outwards from the edges of the band, and the region of localized deformation is wider as compared to that for nonpolar materials.

1. INTRODUCTION

Since the time ZENER and HOLLOMON [1944] observed 32 μm wide shear bands in a steel plate punched by a standard die and estimated the maximum strain in the band to be 100, there has been a considerable amount of research done in understanding factors that influence the initiation and growth of adiabatic shear bands. ROGERS [1979,1983] has vividly summarized in his review articles the work done on adiabatic shear banding until 1982. References to some of the other experimental, analytical and numerical studies may be found in CLIFTON *et al.* [1984] and BATRA [1987].

Recently, MARCHAND and DUFFY [1988] have given a detailed history of the temperature and strain fields within a band. Their experimental observations confirm the earlier prediction by WRIGHT and WALTER [1987] that the shear stress within a band collapses as the deformation localizes. Wright and Walter gave details of the shear band morphology for a rigid viscoplastic material. Herein we also account for (i) the material elasticity, (ii) work hardening, and (iii) the consideration of strain gradient as an independent variable. For simple materials, it is found that as the deformation begins to localize the shear stress collapses and an unloading elastic shear wave travels outwards from the region of severe deformation. For dipolar materials the shear stress drops gradually and there is no unloading elastic wave observed. The region of sevère deformation is wider for dipolar materials as compared to that for nonpolar materials.

Whereas CLIFTON *et al.* [1984], WRIGHT and BATRA [1985], and BATRA [1987] accounted for the effect of material elasticity, their calculations were not carried far enough in time to see what effect, if any, the material elasticity has once a shear band has formed. Wright and Batra, and Batra used, respectively, the forward-difference method and the Crank-Nicolson method to integrate the ordinary differential equations obtained by applying the Galerkin approximation to the governing partial differential

equations. Both these methods became unstable once the deformation started to localize. The Gear method used by WRIGHT and WALTER [1987] and also employed here enables us to study the details of the deformation within the severely deformed region. The results presented here should help to better understand the mechanics of the shear band formation.

II. FORMULATION OF THE PROBLEM

Equations governing the thermomechanical deformations of a block of material undergoing simple shearing motion are:

$$\text{The balance of linear momentum, } \rho u = (s - \sigma_{,y})_{,y}, \tag{1}$$

$$\text{The balance of internal energy, } \rho e = -q_{,y} + sv_{,y} + \sigma v_{,yy}. \tag{2}$$

Here ρ is the mass density, u is the x-displacement and v the x-velocity of a material particle, s is the shear stress, σ is the dipolar stress associated with the kinematic variable $u_{,yy}$, q is the heat flux, e is the specific internal energy, a comma followed by y implies partial differentiation with respect to y, and a superimposed dot signifies material time differentiation. For the sake of completeness and brevity, we give only the equations which are absolutely necessary for our work. Detailed discussions of these equations and those given below may be found in GREEN, MCINNIS and NAGHDI [1968] and WRIGHT and BATRA [1987].

COLEMAN and HODGDON [1985] have developed a theory of shear banding in which the shear yield stress depends upon the accumulated shear strain $\bar{\gamma}$ and its second spatial gradient. For monotonic loading the accumulated shear strain equals the present value of the shear strain γ. Previous numerical (e.g., BATRA [1987]) and experimental work (MARCHAND & DUFFY [1988]) on the adiabatic shearing problem indicates that peak strain gradients are of the order of 10^7 per meter. It seems reasonable to assume that such a deforming region will experience a force which opposes these sharp gradients of γ. COLEMAN and HODGDON [1985] introduced such a force into the theory by adding, to the expression for the stress in the classical flow rule, a term linear in the second spatial derivative of γ. Here we account for this force by taking the first spatial derivative of γ as a kinematic variable and account for the effects of the associated dipolar stress σ on the deformations of the body.

We presume that the shear strain γ and the shear strain gradient d have additive decompositions into elastic (γ_e, d_e) and plastic (γ_p, d_p) parts. That is,

$$\gamma \equiv u_{,y} = \gamma_e + \gamma_p, \tag{3}$$

$$d \equiv u_{,yy} = d_e + d_p. \tag{4}$$

For the constitutive relations we take

$$q = -k\theta_{,y}, \tag{5}$$

$$s = \mu\gamma_e, \tag{6}$$

$$\sigma = \nu d_e, \tag{7}$$

$$e = c\theta + s\gamma_e + \sigma d_e, \tag{8}$$

$$\gamma_p = \Lambda s, \tag{9}$$

$$d_p = \frac{\Lambda}{\ell_1^2}\,\sigma, \tag{10}$$

where k is the thermal conductivity, c the specific heat, θ the change in the temperature of a material particle from its temperature in the reference configuration, μ is the shear modulus, ν is the modulus associated with the dipolar effects, ℓ_1 is a material characteristic length, and $\Lambda = \Lambda(s, \sigma, \gamma_p, d_p)$ is positive for plastic deformations and equals zero when the deformations are elastic. All of the material parameters μ, k, c and ν are assumed to be constants.

To decide whether the ensuing deformations are elastic or plastic, we presume that there exists a loading function

$$f(s, \sigma, \gamma_p, d_p, \theta) = \kappa(\gamma_p, d_p) \tag{11}$$

such that for all positive λ and real numbers a and b,

$$\frac{\partial f}{\partial \lambda}(s, \sigma, \lambda a, \lambda b, \theta) < 0. \tag{12}$$

The function κ on the right-hand side of eqn (11) describes the work hardening of the material. The condition (12) ensures that the equation

$$f\left(s, \sigma, \Lambda s, \frac{\Lambda}{\ell_1^2}\,\sigma, \theta\right) = \kappa(\gamma_p, d_p) \tag{13}$$

has a unique solution for Λ. We make the following choices for f and κ

$$f = \left(s^2 + \frac{\sigma^2}{\ell_1^2}\right)^{1/2} \frac{1}{(1 - a\theta)}\,(1 + b(\gamma_p^2 + \ell_1^2 d_p^2))^{m/2n}, \tag{14}$$

$$\kappa = \kappa_0\left(1 + \frac{\psi}{\psi_0}\right)^n, \tag{15}$$

$$\kappa\psi = s\gamma_p - \sigma d_p. \tag{16}$$

The parameter a describes the thermal softening of the material, b and m its strain-rate hardening, ψ_0 and n characterize its work hardening, and κ_0 is the yield stress in a quasi-static isothermal test. The parameter ψ introduced through eqns (15) and (16) may be thought of as an internal variable. It describes the effect of the history of the deformation on the current value of the yield stress in a quasi-static and isothermal test. It is referred to as the work hardening parameter below.

Substitution from (14), (15), (9) and (10) into (11) yields

$$\left(s^2+\frac{\sigma^2}{\ell_1^2}\right)^{1/2}=\kappa_0\left(1+\frac{\dot\psi}{\dot\psi_0}\right)^n(1-a\theta)\left(1+b\Lambda\left(s^2+\frac{\ell_2^2}{\ell_1^4}\sigma^2\right)^{1/2}\right)^m \tag{17}$$

which is to be solved for Λ when plastic deformation is occurring; otherwise Λ is zero. The constitutive eqn (17) is a simple variation of the "overstress" idea, due to MALVERN [1984], where the overstress in the present case is obtained through the use of a multiplicative factor rather than an additive one. When the dipolar effects are neglected and the material is presumed to be viscoplastic without any yield surface, then eqn (17) reduces to LITONSKI's [1977] constitutive relation.

Before discussing the initial and boundary conditions, we nondimensionalize the variables as follows:

$$\begin{gathered}
y=H\bar y,\quad u=H\bar u,\quad \ell_1=\bar\ell_1 H,\quad \ell_2=\bar\ell_2 H,\quad \gamma=\bar\gamma,\quad d=\bar d/H,\quad \psi=\bar\psi,\\
s=\kappa_0\bar s,\quad \sigma=\kappa_0\ell_2\bar\sigma,\quad \kappa=\kappa_0\bar\kappa,\quad \Lambda=\frac{\gamma_0}{\kappa_0}\bar\Lambda,\quad t=\frac{\bar t}{\gamma_0},\quad \theta=\theta_0\bar\theta,\\
\frac{\rho H^2\gamma_0^2}{\kappa_0}=\bar\rho,\quad \frac{k}{\rho c\gamma_0 H^2}=\bar k,\quad a\theta_0=\bar a,\quad b\gamma_0=\bar b,\quad \theta_0\equiv\frac{\kappa_0}{\rho c},\\
\bar\mu\kappa_0=\mu,\quad \bar\nu\kappa_0\ell_3^2=\nu,\quad \ell_3=\bar\ell_3 H.
\end{gathered} \tag{18}$$

Here 2H is the height of the block, γ_0 is the average strain-rate, ℓ_3 is a material characteristic length, and the overbar indicates the nondimensional quantity. Below we drop the overbars and give a summary of the equations in terms of nondimensional variables.

$$\rho v=(s-\ell\sigma_{,y})_{,y}, \tag{19}$$

$$\theta=k\theta_{,yy}+\Lambda(s^2+\sigma^2), \tag{20}$$

$$s=\mu(v_{,y}-\Lambda s), \tag{21}$$

$$\sigma=\mu\ell\left(v_{,yy}-\frac{\Lambda\sigma}{\ell}\right), \tag{22}$$

$$\Lambda=\frac{(s^2+\sigma^2)}{\left(1+\dfrac{\dot\psi}{\dot\psi_0}\right)^n}, \tag{23}$$

$$\Lambda=\max\left\{0,\left(\left(\frac{(s^2+\sigma^2)^{1/2}}{(1-a\theta)\left(1+\dfrac{\dot\psi}{\dot\psi_0}\right)^n}\right)^{1/m}-1\right)\Big/\,b(s^2+\sigma^2)^{1/2}\right\} \tag{24}$$

In writing these equations we have set $\ell=\ell_1=\ell_2=\ell_3=\ell$ since no information is currently available on their relative magnitudes. This was also done by WRIGHT and BATRA [1987] and by BATRA [1987]. Note that in the energy equation, all of the plastic working is taken to be converted into heat.

We presume that the specimen is placed in a hard insulated loading device so that the velocity is prescribed on its top and bottom surfaces. With the origin of the rectangular Cartesian system of axes located at the center of the specimen, we seek solutions of the governing equations which exhibit the following properties.

$$v(-y,t) = -v(y,t), \quad \theta(-y,t) = \theta(y,t), \quad \psi(-y,t) = \psi(y,t),$$
$$s(-y,t) = s(y,t), \quad \sigma(-y,t) = -\sigma(y,t). \tag{25}$$

Thus the problem for the upper half of the block will be solved under the following boundary conditions.

$$v(1,t) = 1, \quad \theta_{,y}(1,t) = 0, \quad \sigma(1,t) = 0,$$
$$v(0,t) = 0, \quad \theta_{,y}(0,t) = 0, \quad \sigma(0,t) = 0. \tag{26}$$

Figure 1 depicts a solution of eqns (19) through (24), (26), the initial conditions

$$v(y,0) = y, \quad \theta(y,0) = \sigma(y,0) = s(y,0) = \psi(y,0) = 0 \tag{27}$$

and

$$\rho = 3.928 \times 10^{-5}, \quad k = 3.978 \times 10^{-3}, \quad a = 0.4973, \quad \mu = 240.3,$$
$$n = 0.09, \ \psi_0 = 0.017, \ b = 5 \times 10^6, \ m = 0.025. \tag{28}$$

The aforementioned values of various parameters are for a typical steel, the average applied strain-rate of 500 $\sec^{-1}$, and H = 2580 μm. However, we have taken a rather large value of the thermal softening coefficient a to reduce the computational effort required to simulate the formation of a shear band. The chosen value of a gives the nondimen-

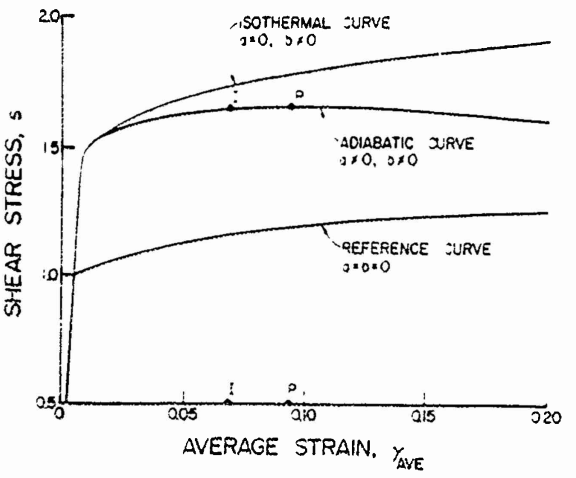

Fig. 1. Average shear stress–average shear strain curve for a typical steel at a nominal strain-rate of 500 sec

sional melting temperature to be 2.011. For homogeneous deformations of the block, $\sigma \equiv 0$, and the peak (marked as point P in Fig. 1) in the shear stress-shear strain curve occurs at a strain of 0.093. The uniform temperature $\theta_0 = 0.1003$ in the block when $\gamma = 0.0692$, corresponding to point I in Fig. 1 is perturbed by *adding* a smooth temperature bump

$$\bar{\theta}(y) = 0.1(1 - y^2)^9 e^{-5y^2},$$

and the initial-boundary-value problem described by equations (19)-(24), (26), and the initial conditions

$$\begin{aligned} &v(y,0) = y, \quad \sigma(y,0) = 0, \quad \psi(y,0) = 0.1, \\ &\theta(y,0) = 0.1003 + 0.1(1 - y^2)^9 e^{-5y^2}, \\ &s(y,0) = \left(1 + \frac{0.1}{\psi_0}\right)^n (1 - a\theta(y,0))(1 + b)^m \end{aligned} \tag{29}$$

is solved numerically by using the Galerkin-Gear method. The Galerkin method is used to reduce the partial differential equations to coupled nonlinear ordinary differential equations which are then integrated by using the Gear method for stiff differential equations (GEAR [1971]). We used the subroutine LSODE, taken from the package ODEPACK, developed by HINDMARSH [1983], and employed the option of using the full Jacobian matrix.

III. COMPUTATION AND DISCUSSION OF RESULTS

Guided by the work of WRIGHT and WALTER [1987] on rigid/visco-plastic materials, we selected a finite element mesh with coordinates of node points given by

$$y_n = \left(\frac{n-1}{160}\right)^p \qquad 1 \le n \le 161,$$

and computed results for $p = 3, 5, 7$ on the Floating Point System machine. We tested these meshes on the problem analyzed by Wright and Walter and obtained results virtually identical to their findings. This assured us of the accuracy of the code and the adequacy of the finite element meshes used. All three meshes gave results which were essentially indistinguishable from each other. We first present and discuss results for nonpolar ($\ell' = 0.0$) materials and then for dipolar materials with $\ell' = 0.01$.

III.1 *Nonpolar materials*

For homogeneous deformations of the block, the peak in the shear stress-shear strain curve occurs at an average strain of 0.093. The temperature perturbation (29) was introduced when the block had undergone deformations corresponding to point I in Fig. 1 and the resulting initial-boundary-value problem was solved. We recall that (BATRA

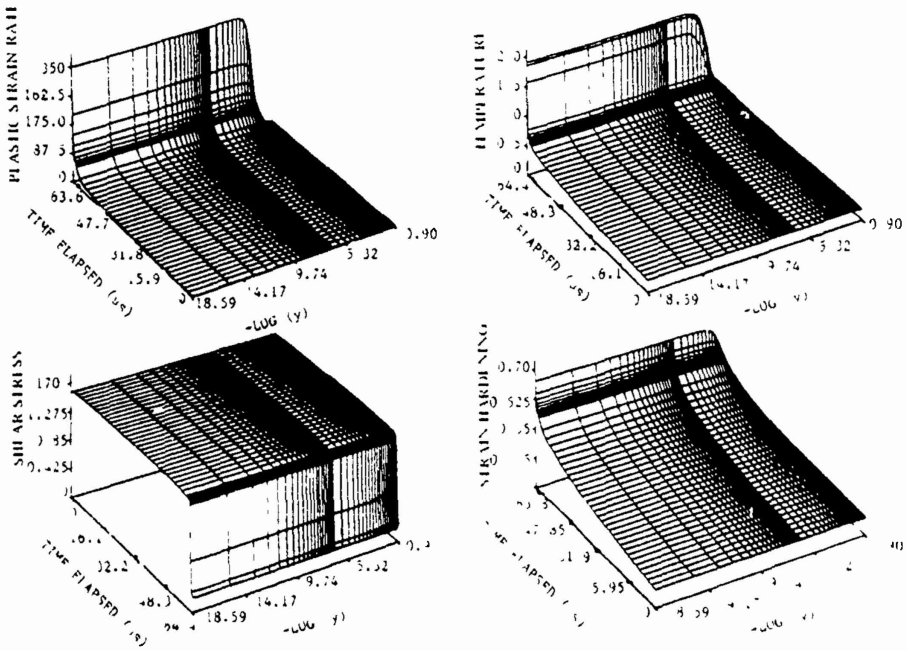

Fig. 2. Evolution of the shear stress, plastic strain-rate, temperature and work-hardening parameter at points near the center of the specimen for nonpolar materials.

[1987]) the average strain at which the deformation begins to localize depends upon, among other factors, the size and the shape of the temperature perturbation. Figure 2 shows the evolution of the shear stress, plastic strain-rate, the temperature and the work-hardening parameter ψ. Initially, the temperature, plastic strain-rate and the work hardening parameter ψ increase slowly, and the values of the temperature and ψ at a point differ approximately by the magnitude of the initial temperature bump. When the average strain in the block equals 0.1002 the rate of increase of the plastic strain rate at points near the center of the block rises sharply and shoots up at an average strain of 0.1011. Thus, for the present problem, the localization of the deformation begins in earnest at an average strain close to 0.1011.

Figure 3 shows the evolution of the plastic strain-rate and the shear stress during the time the severe localization of the deformation is occurring. It is clear from these plots that the shear stress drops to essentially zero in nearly one micro-second even when the strain-hardening effects are included. The shear stress stayed uniform throughout the specimen prior to the initiation of the localization, and during the initial stages of the sudden collapse. But it became nonuniform during the time the localization of the deformation was in progress. This prompted us to examine the field variables more closely.

Figure 4 depicts the distribution of the shear stress and the particle velocity within the specimen at intervals of one-tenth of a microsecond starting with the time when the deformation begins to localize. It is clear that an unloading elastic shear wave emanates outwards from the region of severe deformation. The emanation of the elastic unloading wave is probably associated with the sudden collapse of the shear stress within the band. The computed speed, 3178 m/sec, of the wave essentially equals $(\mu/\rho)^{1/2}$, since

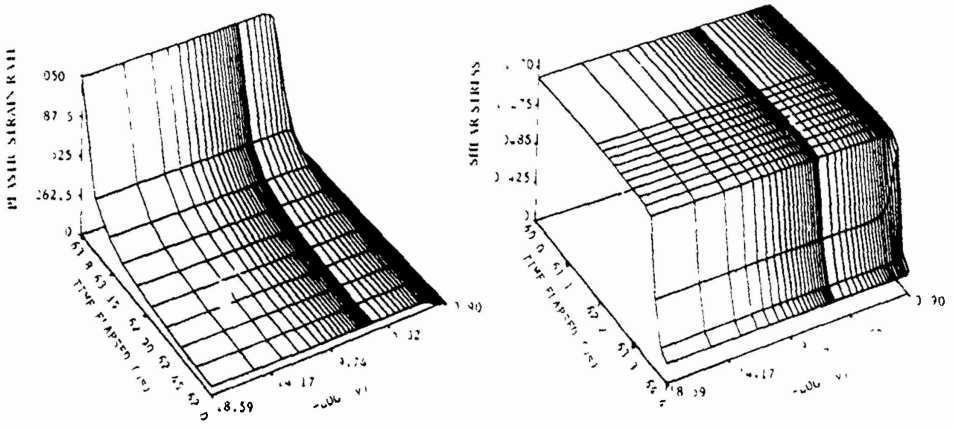

Fig. 3. Collapse of the shear stress and rise of the plastic strain-rate during the localization of the deformation for nonpolar materials

$$\sqrt{\frac{\mu}{\rho}} = \left(\frac{80 \times 10^9}{7860}\right)^{1/2} = 3{,}190 \text{ m/sec.}$$

It takes 0.807 μs for the shear wave to reach the outer boundary from which it is reflected back with a negative value of the shear stress. The numerical calculations were not pursued any further.

Figures 5 and 6 depict, at different times, the particle velocity, temperature, plastic strain-rate, work-hardening parameter ψ, and the shear stress within the region of localization. These results show that the calculations stay stable throughout the severe localization of the deformation. The plots of the plastic strain-rate and ψ vs. y at different times indicate that the region of severe deformation becomes smaller with time. Even though the values of ψ at points near the center of the specimen keep on increasing monotonically, those of γ_p begin to oscillate. A possible explanation for this is that

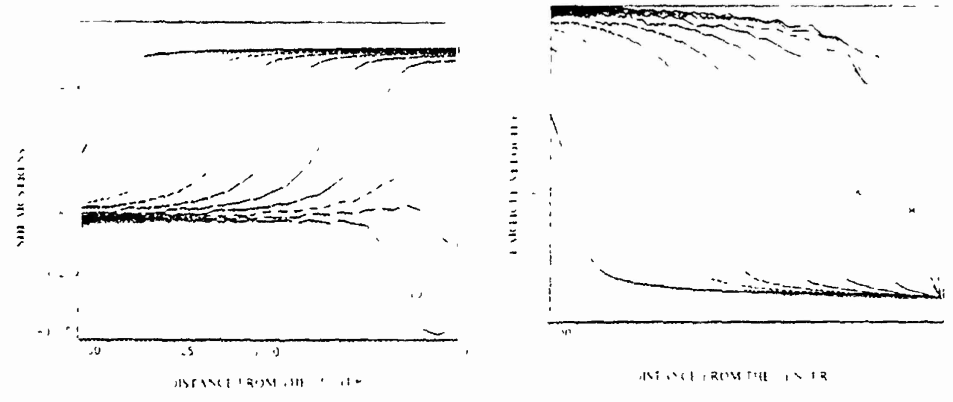

Fig. 4. Distribution of the shear stress and the particle velocity within the specimen at different times during the localization of the deformation for nonpolar materials. These curves are plotted at intervals of 0.1 μs with curve 1 at t = 64.0 μs, curve 2 at t = 64.1 μs, curve 3 at t = 64.2 μs, ... and curve 10 at t = 64.9 μs

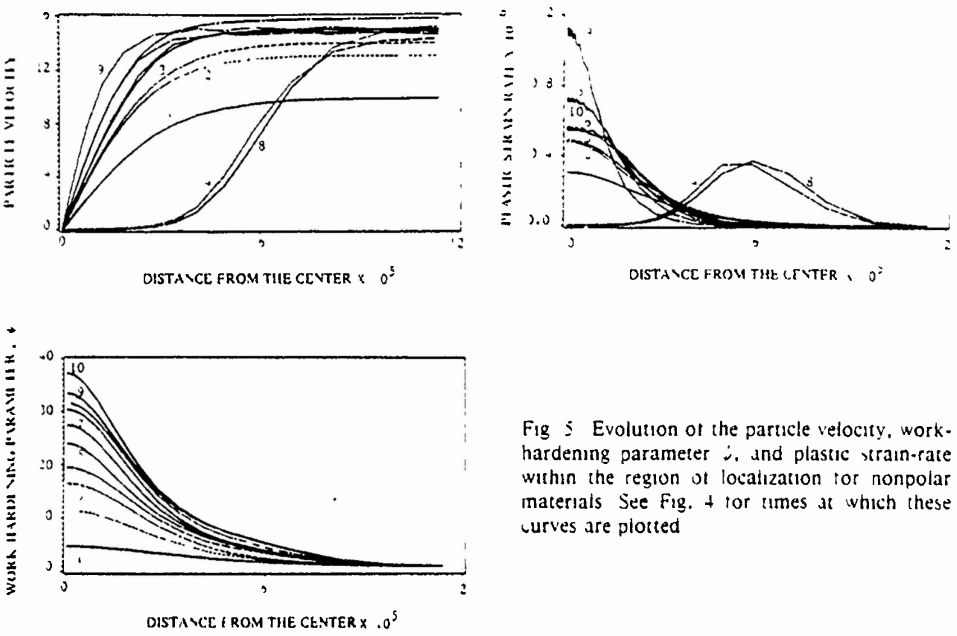

Fig 5 Evolution of the particle velocity, work-hardening parameter ψ, and plastic strain-rate within the region of localization for nonpolar materials See Fig. 4 for times at which these curves are plotted

there is a diffusive term present in the energy equation, but there is no such term in the equation representing the evolution of ψ with time. Because of the sharp temperature gradients at points near the center of the specimen, the rate of heat conducted out of the region of localization is high and at times balances the rate of heat generation due to plastic working. When this happens, the softening of the material caused by the rise in its temperature cannot overcome the hardening due to the increase in the value of ψ and the plastic strain at that material point drops significantly. This in turn reduces the shear stress required for the material to deform plastically because of the reduced hardening due to plastic strain-rate effects. Hence the plastic strain rate begins to increase again

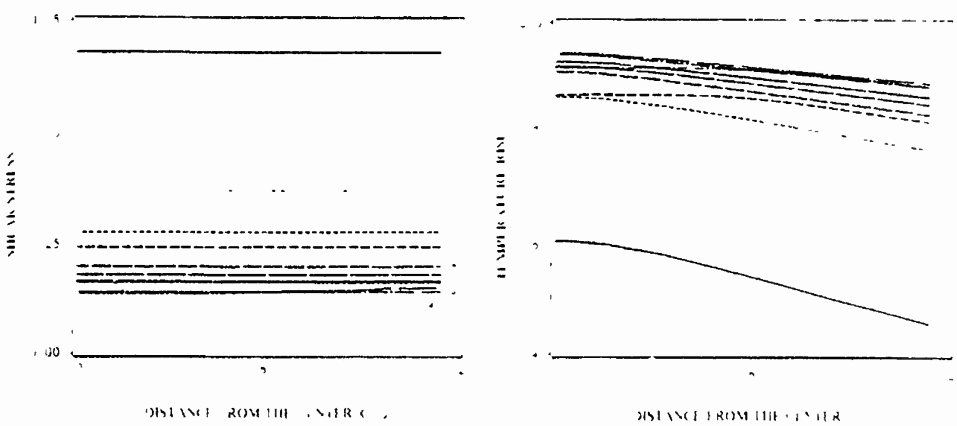

Fig 6 Evolution of the shear stress and temperature within the region of localization for nonpolar materials See Fig. 4 for times at which these curves are plotted

and the phenomenon is repeated though not with any periodicity. The nondimensional plastic strain-rate drops at the center by nearly four-tenth of a million during each one-tenth of a micro-second beginning at $t = 64.2\ \mu s$, $64.6\ \mu s$ and $64.8\ \mu s$.

We now try to write the preceding explanation in the form of an equation. During the time the localization of the deformation is progressing, it is reasonable to assume that material particles near the center of the specimen are deforming plastically. Equation (17) then gives

$$d\gamma_p = \frac{(b^{-1} + \gamma_p)}{m}\left[\frac{ds}{s} + \frac{ad\theta}{1 - a\theta} - \frac{nd\psi}{\psi_0 + \psi}\right].$$

Note that $ds < 0$, $d\theta > 0$ and $d\psi > 0$. Therefore, if the middle term on the right-hand side is not larger than the sum of the magnitudes of the other two terms, $d\gamma_p$ will be negative. If the effect of work hardening is neglected, then the relative temperature rise has to overcome the relative drop in stress for $d\gamma_p$ to be positive.

We note that when the shear stress begins to collapse, the temperature at the center of the band equals 76.9% of the presumed melting temperature of the material. It rises to 96% of the melting temperature within 0.9 μsec and then increases extremely slowly. MARCHAND and DUFFY [1988] estimated the maximum temperature within the shear band to be nearly 75% of the melting temperature of the structural steel tested. Since there is no failure or fracture criterion included herein, our calculations may have been carried too far in time.

One possible way to define the width of a shear band is to equate it to the width of the severely deformed region when the unloading elastic wave emanates outwards from this region. This definition gives the width of the shear band for the material model being studied here to be 0.6 μm which does not compare well with those observed experimentally. The difference between the computed and the observed values could be due to the choice of the values of the material parameters and, or the constitutive relations used. The inclusion of nonlocal effects, as discussed below, does increase the width of the severely deformed region.

III.2 *Dipolar materials*

In Fig. 7 is plotted the evolution of the shear stress s, the dipolar stress σ, the temperature change θ and the plastic strain-rate $\dot{\gamma}_p$ when ℓ is set equal to 0.01. Now the shear stress drops gradually rather than suddenly, and the plastic strain rate does not attain the enormously high values it achieved for nonpolar materials. Also the localization of the deformation is delayed considerably as compared to that for nonpolar materials. At points where the magnitude of the gradient of the dipolar stress is maximum, the shear stress attains minimum values. Since $F \equiv (s - \ell\sigma_{,1})$ acts as a flux for the linear momentum and $s_e \equiv (s^2 + \sigma^2)^{1/2}$ as the effective stress for determining whether the material particle is deforming elastically or plastically, we have plotted these in Fig. 8. As for the nonpolar case, the flux F of the linear momentum stays uniform throughout the block and drops in value first gradually and later on rather sharply. The sharp drop in F is associated with the rapid heating of the material during the final stages of the localization of the deformation. Because of the assumption $\gamma(0, t) = 0$, $s_e = s$ at the center and, therefore, s_e drops noticeably at the center due to the softening of the material caused by the rise in temperature. The negative values of γ imply that λ_m exceeds λ. The

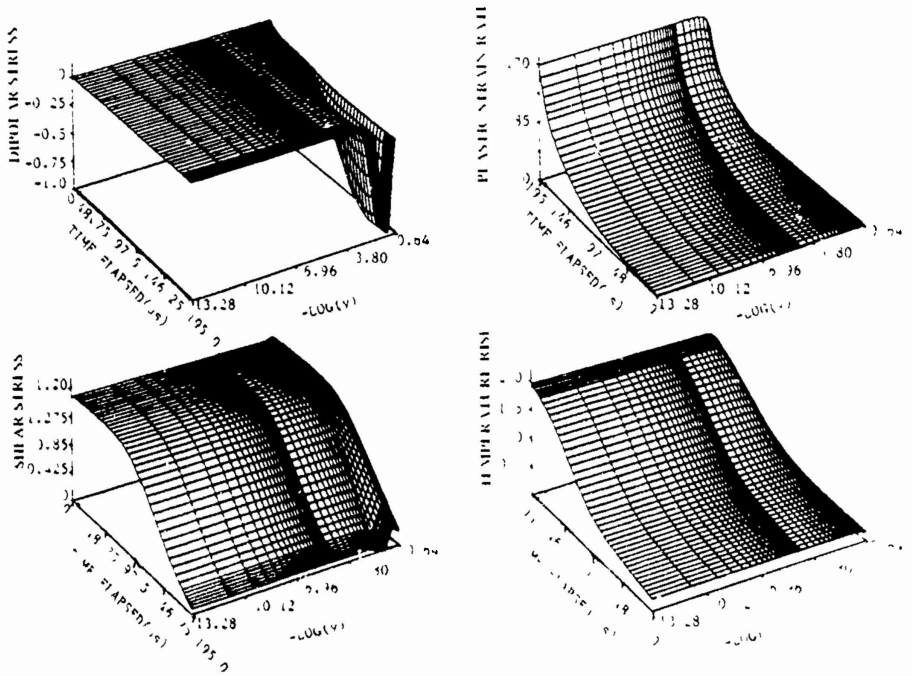

Fig. 7. Evolution of the shear stress, dipolar stress, temperature and plastic strain-rate at points near the center of the specimen for dipolar materials with $\ell = 0.01$

larger values of σ_1 at points away from the center make the effective stress s_e bigger there. The point where s_e assumes maximum values moves towards the center of the block as the deformation proceeds but becomes stationary when the deformation begins to localize severely. In Figs. 9 and 10 we have plotted the distribution of the particle

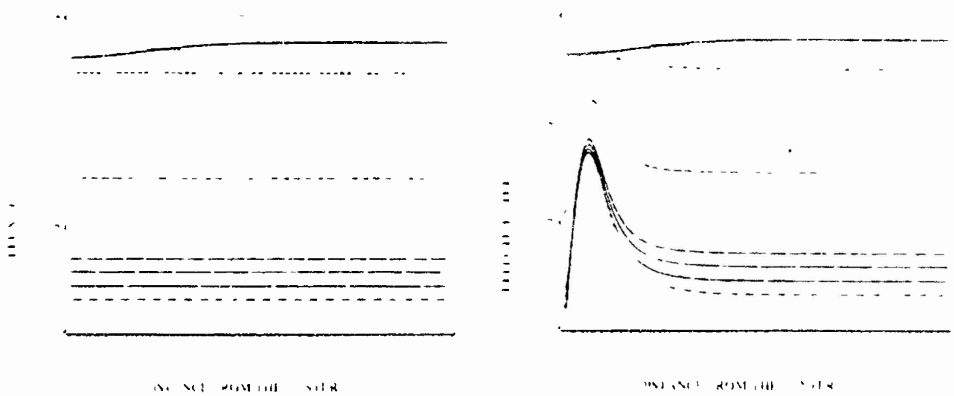

Fig. 8. Distribution of the flux of the linear momentum and the effective stress within the specimen at different times during the localization of the deformation for dipolar materials. Times for the plot of these results are: curve 1, $t = 0.0$ μs; curve 2, $t = 50$ μs; curve 3, $t = 100$ μs; curve 4, $t = 150$ μs; curve 5, $t = 180$ μs; curve 6, $t = 185$ μs; curve 7, $t = 190$ μs; curve 8, $t = 195$ μs.

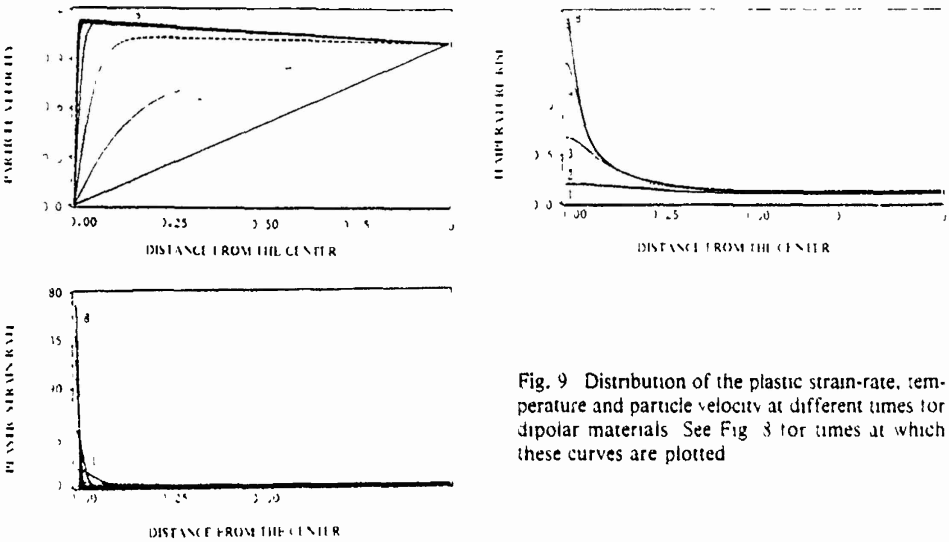

Fig. 9 Distribution of the plastic strain-rate, temperature and particle velocity at different times for dipolar materials See Fig 8 for times at which these curves are plotted

speed, temperature, plastic strain-rate, s and σ within the specimen at different times. It is obvious that there is no unloading wave emanating outwards from the severely deformed region. This is to be expected since the governing equations for $\dot{\ell} \neq 0$ do not have real characteristics. The particle speed increases from the prescribed value of zero at the center of the specimen to 1.14 at the edge of the severely deformed region, and then almost linearly to the prescribed value of 1.0 at the outer boundary of the specimen. The temperature and the plastic strain-rate at the center continue to increase.

In order to decipher the details of the deformation at points near the center of the specimen, we have plotted in Figs. 11 and 12 several field variables within $0 < y < 0.10$ and at different times. These figures show vividly that the temperature and the work-hardening parameter have attained steady values at points for which $0.0175 < y < 0.10$.

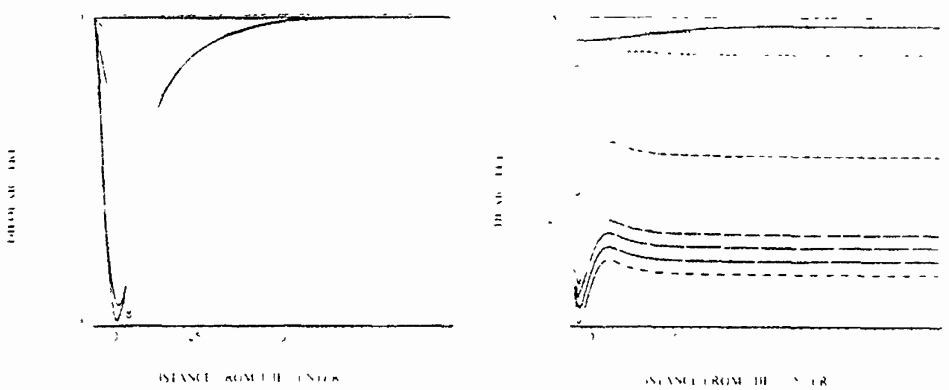

Fig 10 Distribution of the shear stress and the dipolar stress at different times for dipolar materials See Fig 8 for times at which these curves are plotted

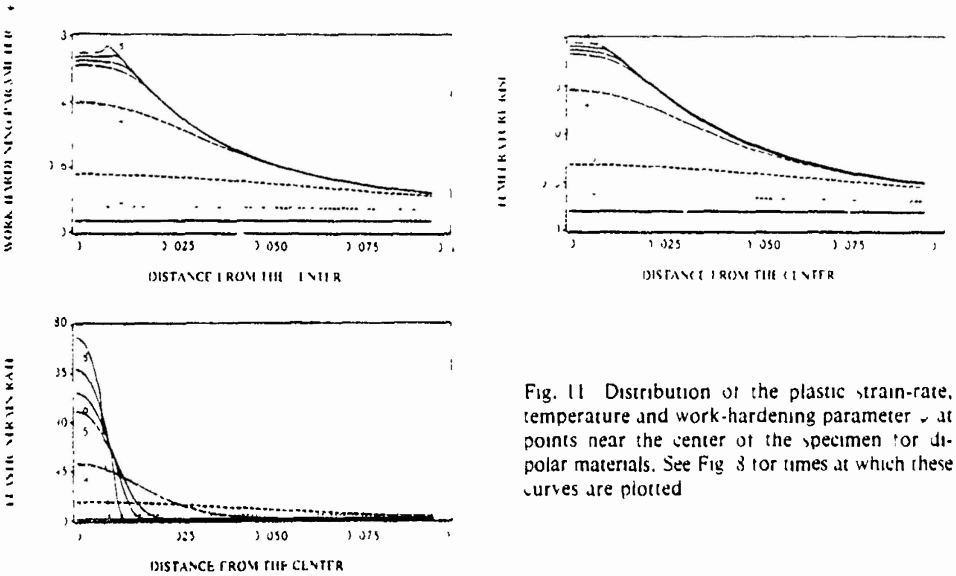

Fig. 11 Distribution of the plastic strain-rate, temperature and work-hardening parameter s at points near the center of the specimen for dipolar materials. See Fig. 8 for times at which these curves are plotted

The shear stress continues to drop and is minimum not at the center but at a point slightly away from it. The temperature at points near the center of the block continues to rise and has essentially uniform values in the region $0 \leq y \leq 0.01$. Even though the shear stress at some points becomes negative for $t \geq 190$ μsec, the flux F of linear momentum is still positive throughout the block. Up to the time these computations have been performed, the peak temperature has not reached the presumed value 2.011 of the melting point of the material. Since the severely deforming region is still narrowing down, it is unclear as to how to define the band width or when to stop the numerical computations for the dipolar case. One possibility is to end the computations when s at any point in the domain becomes zero and regard the width of the severely deformed region as equal to the band width. According to this criterion, the width of the heavily

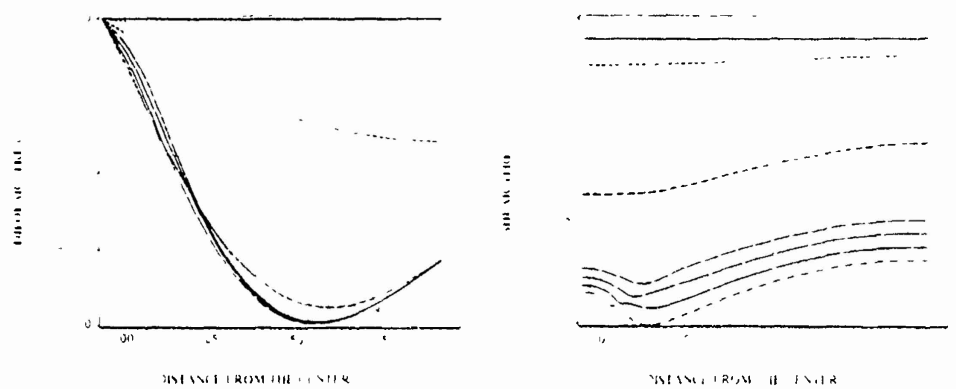

Fig. 12. Distribution of the shear stress and dipolar stress at points near the center of the specimen. See Fig. 8 for times at which these curves are plotted

deformed region, computed for $t = 190\ \mu s$, equals $2 \times 0.0129 \times 2580 = 66.4\ \mu m$. This value is close to those observed experimentally, but the experimentally observed (MARCHAND & DUFFY [1988]) quick drop of the shear stress is not predicted by the dipolar theory. Since the value of ℓ was arbitrarily chosen to be 0.01, there is some room for adjustment. WRIGHT and BATRA [1987] did compute results for $\ell = 0.001$, but the calculations were not carried far enough in time.

BATRA and KIM [1988], using the present material model, have computed results for $\ell = 0.005$, 0.001 and 0.0005. Their computations show that as ℓ is decreased from 0.01 to 0.0005, the computed band width decreases from 66.4 μm to 1.0 μm, the maximum plastic strain-rate at the center increases from 139 to 99,606, and the average strain when the shear stress first becomes zero decreases from 0.1642 to 0.1023. There was no unloading elastic wave observed for any of these three values of the material characteristic length ℓ.

IV. CONCLUSIONS

It is shown that when the uniform temperature field in an elastic, viscoplastic block undergoing simple shearing deformations is perturbed, the deformation localizes. During the localization of the deformation, the stress collapses quickly for nonpolar materials but decreases to zero gradually for dipolar materials. For nonpolar materials, the sharp drop of the shear stress in the narrow region undergoing severe deformations results in an elastic unloading wave to travel outwards from this region to the outer boundaries of the specimen. Both for dipolar and nonpolar materials the temperature and the work hardening parameter continue to increase. Whereas, for dipolar materials, the plastic strain-rate keeps on increasing within the region of the localized deformation; for nonpolar materials, the plastic strain rate oscillates indicating the competing effects of thermal softening and hardening due to plastic strain and plastic strain-rate.

Acknowledgements—R.C. Batra is grateful to Drs. T.W. Wright and John Walter, Jr., of the Ballistic Research Laboratory for helpful discussions on the subject. This work was supported by the U.S. National Science Foundation grant MSM 8715952, and the U.S. Army Research Office Contracts DAAG29-85-K-0238 and DAAL03-88-K-0184 to the University of Missouri-Rolla.

REFERENCES

1944 ZENER, C. and HOLLOMON, J. H., "Effect of Strain Rate on Plastic Flow of Steel," J. Appl. Phys. 15, 22.
1968 GREEN, A. E., MCINNIS, B. C. and NAGHDI, P. M., "Elastic-Plastic Continua with Simple Force Dipole," Int. J. Eng. Sci. 6, 373.
1971 GEAR, C. W., "Numerical Initial Value Problems in Ordinary Differential Equations," Prentice-Hall, Englewood Cliffs, New Jersey.
1977 LITONSKI, J., "Plastic Flow of a Tube Under Adiabatic Torsion," Bull. Acad. Pol. Sci. 25.
1979 ROGERS, H. C., "Adiabatic Plastic Deformation," Ann. Rev. Mat. Sci., 9, 23.
1983 HINDMARSH, A. C., "ODEPACK, A Systematized Collection of ODE Solvers," in STEPLEMAN, R. S. *et al.* (Ed.), Scientific Computing, North-Holland, Amsterdam, pp. 55–64.
1983 ROGERS, H.C., "Adiabatic Shearing—General Nature and Material Aspects," in MEXALL, J. and WEISS, V. (Eds.) Material Behavior Under High Stress and Ultrahigh Loading Rates, Plenum Press, New York, pp. 101–118.
1984 CLIFTON, R. J., DUFFY, J., HARTLEY, K. A., and SHAWKI, T. G., "On Critical Conditions for Shear Band Formation at High Strain Rates," Scripta Metallurgica, 18, 443.
1984 MALVERN, L. in HARDING, J. (Ed.) Mechanical Properties at High Rates of Strain, Inst. Physics Bristol and London, pp. 1–20.
1985 COLEMAN, B. D. and HODGDON, M. L., "On Shear Bands in Ductile Materials," Arch. Rational Mech. Anal., 90, 219.

1985 WRIGHT, T.W. and BATRA, R.C., "The Initiation and Growth of Adiabatic Shear Bands," Int. J. Plasticity, 1, 205

1987 BATRA, R.C., "The Initiation and Growth of, and the Interaction Among, Adiabatic Shear Bands in Simple and Dipolar Materials," Int. J. Plasticity, 3, 75

1987 WRIGHT, T.W. and BATRA, R.C., "Adiabatic Shear Bands in Simple and Dipolar Plastic Materials" in KAWATA, K. and SHIOIRI, J. (Eds.) Proc. IUTAM Symposium on Macro- and Micro-Mechanics of High Velocity Deformation and Fracture, Springer-Verlag, Berlin-Heidelberg-New York, pp. 189–201

1987 WRIGHT, T.W. and WALTER, J.W., "On Stress Collapse in Adiabatic Shear Bands," J. Mech. Phys. Solids, **35**, 701

1988 BATRA, R.C. and KIM, C.H., "Effect of Material Characteristic Length on the Initiation, Growth, and Band Width of Adiabatic Shear Bands in Dipolar Materials," J. de Physique, **49**(C3), 41

1988 MARCHAND, A. and DUFFY, J., "An Experimental Study of the Formation of Adiabatic Shear Bands in a Structural Steel," J. Mech. Phys. Solids, **36**, 251.

Department of Mechanical and Aerospace Engineering and Engineering Mechanics
University of Missouri-Rolla
Rolla, MO 65401-0249

(*Received* 22 *June* 1988; *in final revised form* 29 *October* 1988)

International Journal of Plasticity, Vol 6 pp 231-246, 1990
Printed in the U S A

0749-6419/90 $3 00 + 00

ADIABATIC SHEAR BANDING IN DYNAMIC PLANE STRAIN COMPRESSION OF A VISCOPLASTIC MATERIAL

R.C. Batra and De-Shin Liu

University of Missouri-Rolla

Abstract—Dynamic plane strain thermomechanical deformations of a thermally softening viscoplastic body subjected to compressive loads on the top and bottom faces are studied with the objective of exploring the effect of (a) modeling the material inhomogeneity by introducing a temperature perturbation or assuming the existence of a weak material within the block, (b) introducing two defects symmetrically placed on the vertical axis of the block The effect of setting the thermal conductivity equal to zero is also studied in the latter case. It is found that, irrespective of the way the material inhomogeneity is modeled, a shear band initiates from the site of the defect and propagates in the direction of maximum shearing stress. The value of the average strain at the instant of the initiation of the band depends upon the strength of the material defect introduced. Once the shear band reaches the boundaries of the block it is reflected back, the angle of reflection being nearly equal to the angle of incidence

1. INTRODUCTION

Adiabatic shear banding refers to the localization of the deformation into thin narrow bands of intense plastic deformation that usually form during high-rate plastic deformation. These bands often precede shear fractures. The experimental work in this area is due to Zener and Hollomon [1944], Costin *et al.* [1980], Moss [1981], Lindholm and Johnson [1983], Hartley, Duffy and Hawley [1987], and Marchand and Duffy [1988]. Hartley *et al.* [1987], and Marchand and Duffy [1988], have given a detailed history of the temperature and strain fields within a band formed in a thin steel tube deformed in simple torsion.

During the last ten years, there have been numerous studies aimed at analyzing the initiation and growth of shear bands in the one-dimensional simple shearing problem. For example, Clifton [1980] and Bai [1981] analyzed the growth of infinitesimal periodic perturbations superimposed on a body deformed by a finite amount in simple shear. Burns [1985] used a dual asymptotic expansion to account for the time dependence of the homogeneous solution in the analysis of the growth of superimposed periodic perturbations. Other works include those of Merzer [1983], Wu and Freund [1984], Clifton *et al.* [1984], Coleman and Hodgdon [1985], Wright and Batra [1985], Wright and Walter [1987], Batra [1987a,1987b], Zbib and Aifantis [1988], and Batra and Kim [1990]. We note that Rogers [1979,1983] and Timothy [1987] have reviewed various aspects of shear banding, and Anand *et al.* [1988] have generalized one-dimensional stability analysis of Clifton [1980] to three-dimensional problems.

Recently Lemonds and Needleman [1986a,1986b], Anand *et al.* [1988], Needleman [1989], Batra and Liu [1989], and Shuttle and Smith [1988] have studied the initiation and growth of shear bands in plane strain deformations of a softening material. Except for Needleman, and Batra and Liu, these works neglected the effect of inertia forces Batra and Liu studied the coupled thermomechanical deformations of a thermally softening viscoplastic solid and modeled the material inhomogeneity by

introducing a temperature bump at the center of the block whose boundaries were taken to be perfectly insulated. Two different loadings, namely, those corresponding to simple shearing and simple compression of the block, were considered. Here, we examine the effect of (a) modeling the material inhomogeneity in two different ways, namely, introducing a temperature perturbation and assuming the existence of a weak material, (b) introducing two defects placed symmetrically on the vertical axis of the block, (c) varying the reduction in the flow stress of the weak material, and (d) two different sets of initial conditions.

II. FORMULATION OF THE PROBLEM

We use an updated Lagrangian description (e.g., see BATHE [1982]) to analyze the plane strain thermomechanical deformations of the viscoplastic body. That is, in order to solve for the deformations of the body at time $(t + \Delta t)$, the configuration at time t is taken as the reference configuration. However, it is not assumed that the deformations of the body from time t to time $(t + \Delta t)$ are infinitesimal. With respect to a fixed set of rectangular Cartesian coordinate axes, we denote the position of a material particle in the configuration at time t by X_α and in the configuration at time $(t + \Delta t)$ by x_i. In terms of the referential description the governing equations are

$$(\rho J)^{\cdot} = 0, \tag{2.1}$$

$$\rho_0 \dot{v}_i = T_{i\alpha,\alpha}, \tag{2.2}$$

$$\rho_0 \dot{e} = -Q_{\alpha,\alpha} + T_{i\alpha} \dot{v}_{i,\alpha}, \tag{2.3}$$

supplemented by appropriate constitutive relations, and initial and boundary conditions. Equations (2.1), (2.2), and (2.3) express, respectively, the balance of mass, the balance of linear momentum, and the balance of internal energy. Here ρ is the mass density of a material particle in the current configuration at time $t + \Delta t$, ρ_0 its mass density in the reference configuration; a superimposed dot indicates a material time derivative; $J = \rho_0/\rho$ equals the determinant of the deformation gradient $F_{i\alpha} \equiv x_{i,\alpha}$, v_i is the velocity of a material particle in the x_i-direction, $T_{i\alpha}$ is the first Piola-Kirchoff stress tensor; a comma followed by $\alpha(i)$ implies partial differentiation with respect to $X_\alpha(x_i)$; a repeated index signifies summation over the range of the index; e is the internal energy per unit mass; and Q_α is the heat flux. We assume that plane strain deformations occur in the $X_1 - X_2$ plane, so that $x_3 = X_3$ and the indices i and α range over 1,2.

We note that even when the applied overall strain-rate is kept fixed, different material particles undergo deformations at varying strain-rates. During the course of a loading process in which a shear band forms, the temperature of a material particle may also increase considerably. A constitutive relation that can model the material response over changes in plastic strain-rate and temperature of several orders of magnitude is needed to properly analyze the shear band problem. HARTLEY *et al.* [1987], and MARCHAND and DUFFY [1988], have proposed a power law that seems to describe adequately the simple shearing deformations of the steels tested. However, a constitutive relation applicable to more general deformations is not readily available in the open literature

Here we assume that the following constitutive relations describe adequately the material response:

$$\sigma_{ij} = -p(\rho)\delta_{ij} + 2\mu D_{ij},$$

$$T_{i\alpha} \equiv (\rho_0/\rho)X_{\alpha,j}\sigma_{ij}, \tag{2.4}$$

$$2\mu = \left[\sigma_o/(\sqrt{3}I)\right](1 - \nu\theta)(1 + bI)^m,$$

$$2D_{ij} = v_{i,j} + v_{j,i}, \tag{2.5}$$

$$2I^2 = \tilde{D}_{ij}\tilde{D}_{ji}, \quad \tilde{D}_{ij} = D_{ij} - (1/3)D_{kk}\delta_{ij}, \tag{2.6}$$

$$p(\rho) = B(\rho/\rho_r - 1), \tag{2.7}$$

$$Q_i = -k(\rho_0/\rho)X_{\alpha,i}\theta_{,\alpha}, \tag{2.8}$$

$$\rho_0 e = \rho_0 c\theta + \rho_0 \rho p(\rho)/\rho^2. \tag{2.9}$$

Here, σ_{ij} is the Cauchy stress tensor, σ_o is the yield stress in a quasi-static simple tension or compression test, ν is the coefficient of thermal softening, $\tilde{D}_{ij}$ is the deviatoric strain-rate tensor, D_{ij} is the strain-rate tensor, δ_{ij} is the Kronecker delta, B may be interpreted as the bulk modulus, ρ_r is the mass density in the stress free reference configurations, c is the specific heat, k is the thermal conductivity, and parameters b and m describe the strain-rate sensitivity of the material. The material parameters b, m, B, k, and c are taken to be independent of the temperature. Equation (2.8) is the Fourier law of heat conduction, and eqn (2.4)$_1$ may be interpreted as a constitutive relation for a non-Newtonian fluid whose viscosity μ depends upon the temperature and the strain-rate. Alternatively, defining s_{ij} by

$$s_{ij} = \sigma_{ij} + [p - (2/3)\mu D_{kk}]\delta_{ij} \tag{2.10}$$

$$= 2\mu\tilde{D}_{ij}, \tag{2.11}$$

we can write eqns (2.4) and (2.5) as

$$[(1/2)(s_{ij}s_{ij})]^{1/2} = \left[\sigma_o/\sqrt{3}\right](1 - \nu\theta)(1 + bI)^m \tag{2.12}$$

which can be viewed as a generalized von Mises yield surface when the flow stress (given by the right-hand side of (2.12)) at a material particle depends upon its strain-rate and temperature. That the flow stress decreases linearly with the temperature rise has been observed by BELL [1968], LINDHOLM and JOHNSON [1983], and LIN and WAGONER [1986]. The range of temperatures examined by these investigators is not as large as that expected to occur in the shear band problem. However, constitutive relations akin to eqn (2.4) have been used by ZIENKIEWICZ *et al* [1981] for analyzing the extrusion problem, by BATRA [1988] in studying the steady-state penetration of a viscoplastic target by a rigid cylindrical penetrator, and by BATRA and LIU [1989] for studying the shear band problem.

In terms of the nondimensional variables

$$\tilde{\sigma} = \sigma/\sigma_o, \quad \tilde{p} = p/\sigma_o, \quad \tilde{s} = s/\sigma_o, \quad \tilde{v} = v/v_o,$$

$$\tilde{t} = tv_o/H, \quad \tilde{T} = T/\sigma_o,$$

$$\tilde{x} = x/H, \quad \tilde{\theta} = \theta/\theta_o, \quad \tilde{b} = b(v_o/H), \quad \tilde{v} = v\theta_o, \tag{2.13}$$

$$\tilde{\rho} = \rho/\rho_r, \quad \tilde{\rho} = \rho_o/\rho_r, \quad \tilde{X} = X/H,$$

$$\delta = \rho_r v_o^2/\sigma_o, \quad \beta = k/(\rho_r c v_o H),$$

$$\theta_o = \sigma_o/(\rho_r c), \quad \tilde{B} = B/\sigma_o,$$

the governing equations can be written as

$$\rho + \rho v_{i,i} = 0, \tag{2.14}$$

$$\delta\rho v_i = T_{i\alpha,\alpha}, \tag{2.15}$$

$$\tilde{\rho}\theta = \beta\theta_{,ii} + (\tilde{\rho}/\rho_r)[1/(\sqrt{3}I)](1 + bI)^m(1 - v\theta)\tilde{D}_{ij}\tilde{D}_{ij}, \tag{2.16}$$

$$\sigma_{ij} = -B(\rho - 1)\delta_{ij} + [1/\sqrt{3}I)](1 + bI)^m(1 - v\theta)D_{ij}, \tag{2.17}$$

where we have dropped the superimposed bars. In eqns (2.13) $2H$ is the height of the block and v_o the imposed velocity on the top and bottom surfaces. In eqns (2.14)-(2.16) all of the differentiations are with respect to nondimensional variables. We note that in eqn (2.16) all, rather than 90–95% as stated by TAYLOR and QUINNEY [1934], of the plastic working is assumed to be converted into heat.

For the viscoplastic block being deformed in simple compression we study only those deformations that remain symmetric about the horizontal and vertical planes passing through the center of the block. Thus we analyze the deformations of the material in the first quadrant. With the origin of the coordinate axes situated at the center of the undeformed block (cf. Fig. 1), we can write the pertinent boundary conditions as follows

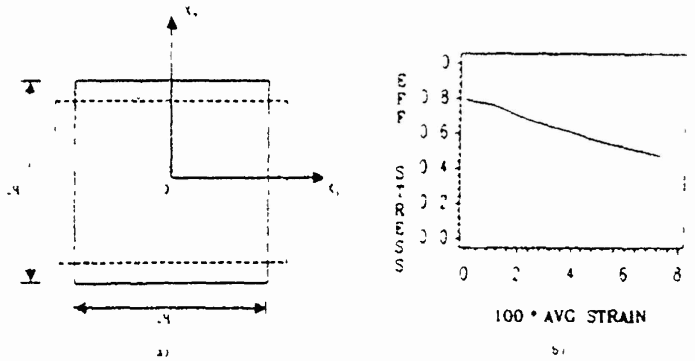

Fig. (a) The problem studied, (b) Stress-strain curve in simple compression for the material studied

$$
\begin{gathered}
v_1 = 0, \quad T_{21} = 0, \quad Q_1 = 0 \text{ at } x_1 = X_1 = 0, \\
v_2 = 0, \quad T_{12} = 0, \quad Q_2 = 0 \text{ at } x_2 = X_2 = 0, \\
T_{i\alpha} N_\alpha = 0, \quad Q_\alpha N_\alpha = 0 \text{ on the right face,} \\
v_2 = -U(t), \quad T_{12} = 0, \quad Q_2 = 0 \text{ on the top surface.}
\end{gathered} \tag{2.18}
$$

That is, boundary conditions resulting from the assumed symmetry of deformations are applied to the left and bottom faces, the right face of the block is taken to be traction free, and a prescribed normal velocity and zero tangential tractions are applied on the top face. Note that the initially flat top surface is assumed to stay flat throughout the deformations of the block. All four sides of the block are assumed to be perfectly insulated.

We consider two different sets of initial conditions. First we take

$$
\rho(\mathbf{X},0) = 1.0, \quad v_1(\mathbf{X},0) = 0, \quad v_2(\mathbf{X},0) = 0, \quad \theta(\mathbf{X},0) = 0, \tag{2.19}
$$

and model a material inhomogeneity/flaw by assuming that

$$
\mu = [1 - \epsilon(1 - r^2)^9 \exp(-5r^2)]\,[[(1 + bI)^m/(\sqrt{3}I)]\,(1 - \nu\theta)] \tag{2.20}
$$

$$
r^2 = (X_1 - X_1^0)^2 + (X_2 - X_2^0)^2. \tag{2.21}
$$

That is, the material around the point $\mathbf{X}^0$ is weaker than the surrounding material. In this case we took

$$
\begin{aligned}
U(t) &= t/0.005, \quad 0 \le t \le 0.005 \\
&= 1 \qquad\quad t \ge 0.005.
\end{aligned} \tag{2.22}
$$

Another set of initial conditions studied involved perturbing the steady state solution corresponding to

$$
v_1 = 0.37x_1, \quad v_2 = -x_2 \tag{2.23}
$$

for an average applied strain-rate of 5,000 sec^{-1} by superposing on it a temperature perturbation given by

$$
\Delta\theta = \epsilon(1 - r^2)^9 \exp(-5r^2). \tag{2.24}
$$

The velocity field (2.23) and the temperature distribution (2.24) were taken as the initial conditions, and $U(t)$ was set equal to 1.0 for $t \ge 0$. We note that the value of ϵ in eqns (2.20) and (2.24) models, in some sense, the strength of the defect.

We refer the reader to BATRA and LIU [1989] for details of seeking an approximate solution of the problem numerically

III. COMPUTATION AND DISCUSSION OF RESULTS

In order to compute numerical results we assigned following values to various material and geometric parameters.

$$b = 10{,}000 \text{ sec}, \quad \nu = 0.0222°\text{C}^{-1}, \quad \sigma_o = 333 \text{ MPa},$$
$$k = 49.22W \text{ m}^{-1} \text{ °C}^{-1}, \quad c = 473J \text{ kg}^{-1} \text{ °C}^{-1}, \tag{3.1}$$
$$\rho_o = 7{,}800 \text{ kg m}^{-3}, \quad B = 128 \text{ GPa}, \quad H = 5 \text{ mm},$$
$$v_o = 25 \ m \text{ sec}^{-1}, \quad m = 0.025.$$

Except for the value of the thermal softening coefficient ν, these values are for a typical hard steel. We assigned a rather large value to ν to reduce the CPU time required to solve the problem. For the values given in (3.1), $\theta_o = 89.6°\text{C}$, the nondimensional melting temperature equals 0.5027, and the average applied strain-rate equals 5,000 sec^{-1}. Figure 1b depicts the effective stress s_e, defined as the left-hand side of eqn (2.12), versus the average strain. The presumed high value of the thermal softening coefficient results in material softening due to the heating of the material overcoming the material hardening due to strain-rate effects right from the beginning.

III.1. *Results with initial temperature perturbation*

Figure 2a depicts the isotherms for the initial temperature distribution (2.24) with $\epsilon = 0.2$ centered around the point (0.0, 0.375). In this case the initial velocity field is assumed to be given by (2.23) and $U(t) = 1.0$ for $t \geq 0$. The peak temperature θ_{max} of 0.2 occurs at the center of perturbation. The isotherms look elliptical because of the different scales along the horizontal and vertical axes. Since the boundaries of the block are taken to be perfectly insulated the heat generated due to plastic working raises the temperature of every material point. The isotherms at five different values of the average strain are plotted in Figs. 2b through 2e. These suggest that material points along lines passing through the center of perturbation and inclined at $\pm 45°$ with the horizontal axis are heated more than other particles. Also contours of successively higher temperatures seem to originate from (0.0, 0.375) and propagate in the direction of maximum shearing stress. They get arrested temporarily at the boundaries of the block and when the material at the boundary where these contours meet it gets heated up, these start propagating into the material as if the incident contours were reflected back into the body, the angle of reflection being almost equal to the angle of incidence. This phenomenon becomes more evident from the plots in Fig. 3 of the contours of the second invariant I of the deviatoric strain-rate tensor. In Figs. 3a through 3f the contours of I are plotted at successively higher values of the average strain γ_{ave}. In each case the peak value I_{max} of I occurs at the point (0.0, 0.375) where the temperature is maximum. At an average strain of 0.04, $I_{max} = 11.44$ implying thereby that the material surrounding it is deforming at a strain-rate greater than 50,000 sec^{-1}. For $\gamma_{ave} = 0.04$, $\theta_{max} = 0.341$ occurs at (0.0, 0.375) and equals 68.2% of the presumed melting temperature of the material. We note that when the temperature perturbation was introduced at (0.0, 0.0) (BATRA & LIU [1989]), I_{max} and θ_{max} at $\gamma_{ave} = 0.04$ equalled 8.73 and 0.313, respectively. For the problem being currently analyzed, the contours

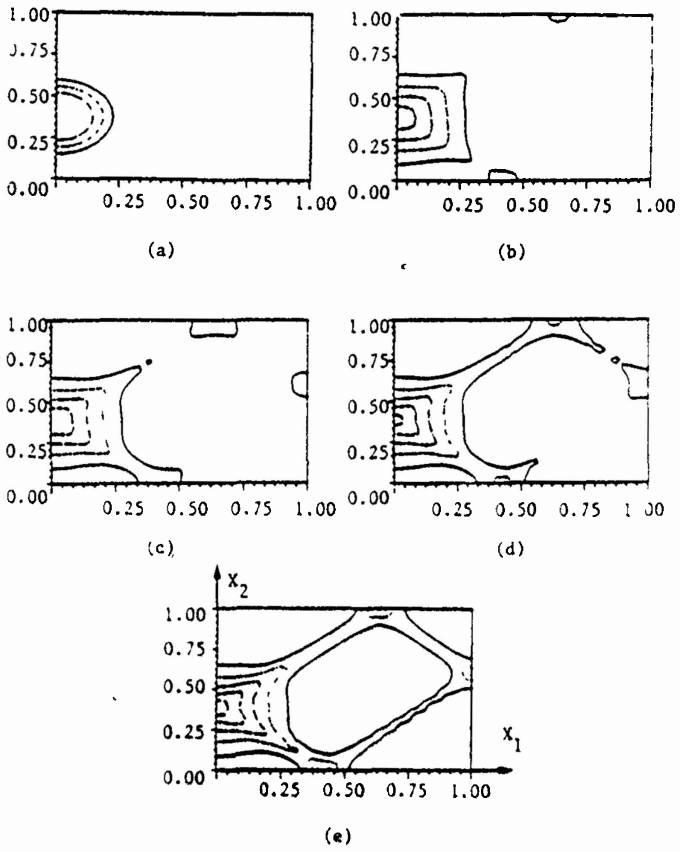

Fig. 2. Isotherms plotted in the reference configuration at different values of the average strain when the material defect is modeled by introducing a temperature perturbation
(a) $\gamma_{avg} = 0.0$, $\vartheta_{max} = 0.2$; ___ 0.10, 0.125, _ _ _ 0.150
(b) $\gamma_{avg} = 0.03$, $\vartheta_{max} = 0.28$; ___ 0.10, 0.15, _ _ _ 0.20, _ _ _ _ 0.25
(c) $\gamma_{avg} = 0.035$, $\vartheta_{max} = 0.304$; ___ 0.10, 0.15, _ _ _ 0.20 _ _ _ _ 0.25
(d) $\gamma_{avg} = 0.0375$, $\vartheta_{max} = 0.3213$, ___ 0.10, 0.15, _ _ _ 0.20, ____ 0.25, _ _ _ 0.30
(e) $\gamma_{avg} = 0.04$, $\vartheta_{max} = 0.341$, ___ 0.10, 0.15 _ _ _ 0.20 ____ 0.25, _ _ _ 0.30

of I originate at (0.0, 0.375) and then fan out along the direction of maximum shearing. There appear to be sources of energy building up at (0.0, 0.375) and three other points on the boundary where the parallelogram through (0.0, 0.375) with adjacent sides making angles of $\pm 45°$ with the horizontal axis intersect it. When there is sufficient energy built up at these points contours of successively higher values of I originate from these points and propagate along the direction of maximum shearing stress. Also as the deformation of the block progresses, these contours become narrower implying thereby that severe deformations are localizing into thin bands.

Figures 4a through 4c depict the velocity field in the X_1 and X_2 direction for $\gamma_{avg} = 0.0$, 0.035 and 0.040. The velocity field at $\gamma_{avg} = 0.0$ is a graphical representation of eqns (2.23) and corresponds to a homogeneous deformation of the block. Once the deformation localizes the velocity field within the material adjoining the sides of the parallelogram stated above varies sharply, and it varies almost linearly within the

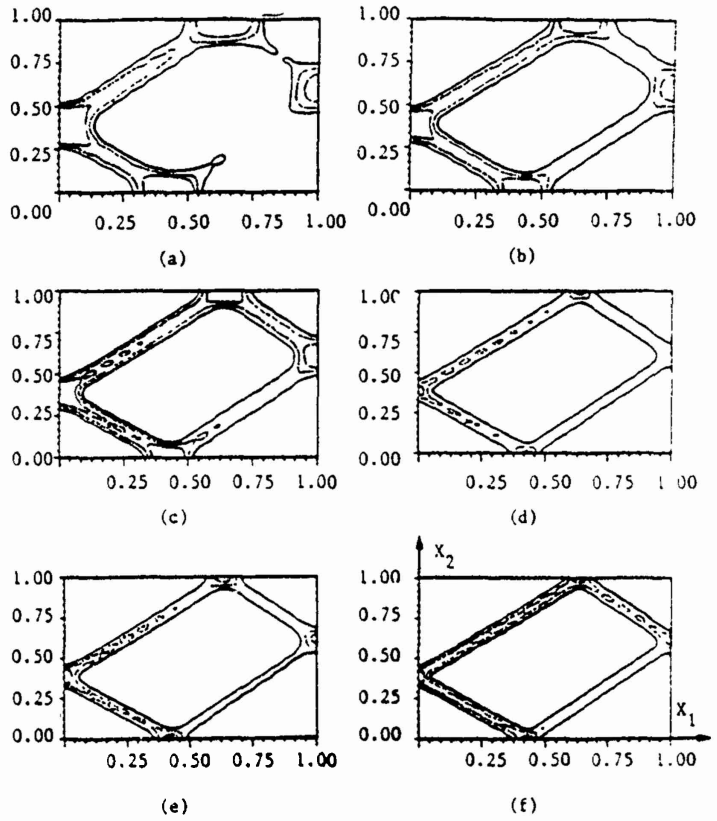

Fig. 3 Contours of the second invariant I of the deviatoric strain-rate tensor at different values of the average strain when the material defect is modeled by a temperature perturbation.
(a) $\gamma_{avg} = 0.02$, $I_{max} = 3.5$, ___ 1.50, 1.75, _ _ _ 2.0.
(b) $\gamma_{avg} = 0.025$, $I_{max} = 4.51$; ___ 1.50, 2.0, _ _ _ 2.5.
(c) $\gamma_{avg} = 0.030$, $I_{max} = 4.83$; ___ 1.50, 2.0, _ _ _ 2.5
(d) $\gamma_{avg} = 0.035$, $I_{max} = 7.91$; ___ 2.50, 3.75, _ _ _ 5.0
(e) $\gamma_{avg} = 0.0375$, $I_{max} = 10.51$; ___ 2.50, 5.0, _ _ _ 7.5
(f) $\gamma_{avg} = 0.040$, $I_{max} = 11.44$; ___ 2.50, 5.0, _ _ _ 7.5

remainder of the material. This contrast between the velocity field in separate regions becomes sharper (e.g. see Fig. 4c) as the deformation becomes more localized.

The variation of the effective stress s_e, defined as being equal to the left-hand side of eqn (2.12), within the block at $\gamma_{avg} = 0.0$, 0.035, 0.0375 and 0.040 is plotted in Figs. 5a through 5d. Initially the effective stress is lower within the material surrounding the center of temperature perturbation because it is computed from the prescribed velocity and temperature fields. Since s_e satisfies eqn (2.12), the initially higher temperature around (0.0, 0.375) reduces the flow stress needed there to deform the material plastically. Even though the values of both the temperature and I are higher within the band as compared to those in the surrounding material, the effect of thermal softening exceeds the material hardening due to strain-rate effects, and the effective stress within the band is lower than that in the rest of the material. The plots of s_e and the velocity field suggest that the band first forms along the shorter side of the parallelogram that passes through the center of the temperature bump. Also the magnitude of the deformation within the band along the four sides of the parallelogram is not the same.

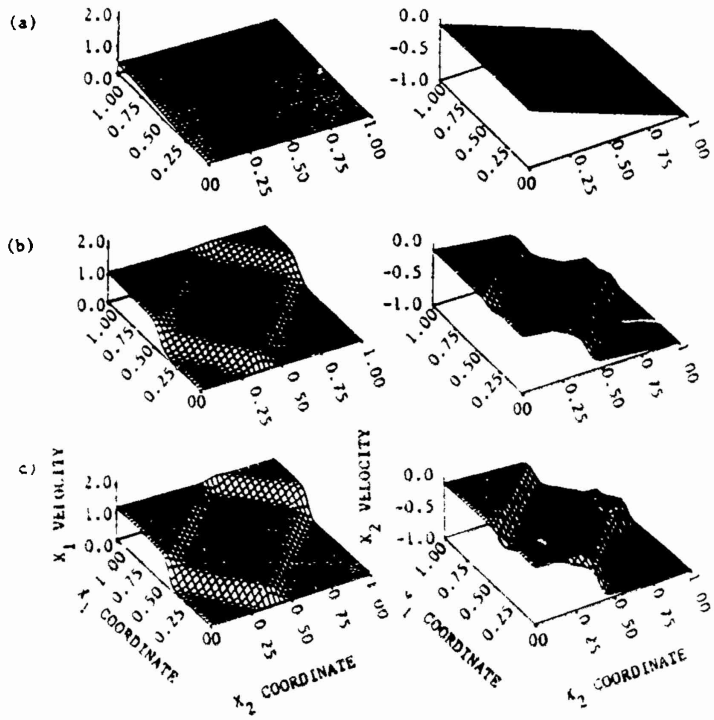

Fig. 4 Velocity field within the block at different values of the average strain with the material defect modeled by a temperature perturabation. (a) $\gamma_{ave} = 0.0$, (b) $\gamma_{ave} = 0.035$, (c) $\gamma_{ave} = 0.040$

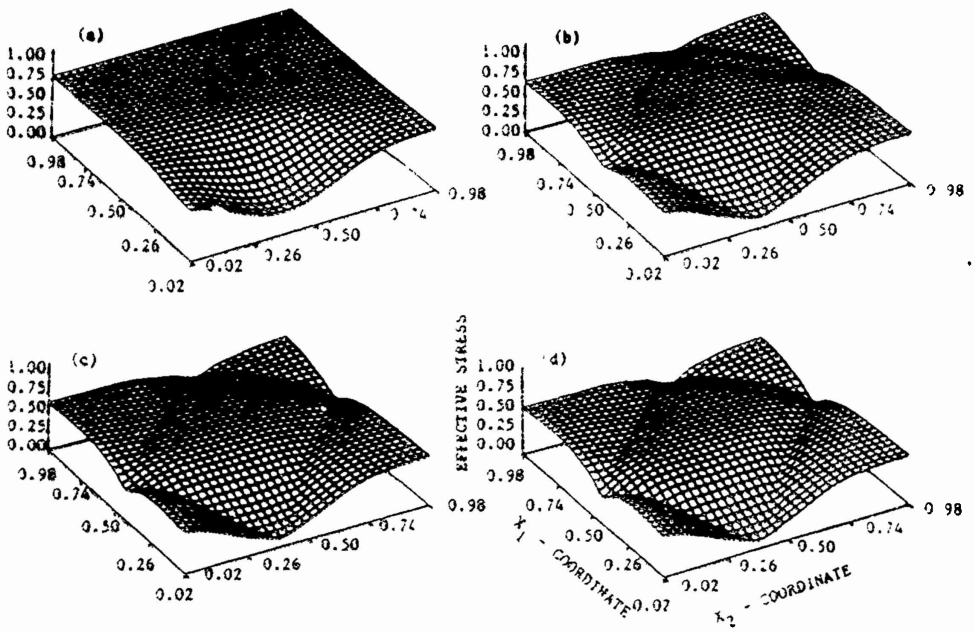

Fig. 5 Distribution of the effective stress within the block at different values of the average strain with the material defect modeled by a temperature perturbation. (a) $\gamma_{ave} = 0.0$, (b) $\gamma_{ave} = 0.035$, (c) $\gamma_{ave} = 0.0375$, (d) $\gamma_{ave} = 0.040$

III.2 *Results with material inhomogeneity modeled by a weak material*

We now assume that the initial velocity field is given by (2.23), $\theta(X,0) = 0$, and the material parameter μ is represented by eqn (2.20) with $\epsilon = 0.1$. That is, the material surrounding the point (0.0, 0.375) is weaker than the rest of the material. In Fig. 6 we have plotted the contours of I and θ at different values of γ_{avg}. A comparison of these results with those in Figs. 2 and 3 reveals that the pattern of the shear band development is identical to that when the material defect was modeled by a temperature perturbation. In this case it takes a little longer for the shear band to form and the maximum value 10.76 computed for I is comparable to that (11.44) obtained for the temperature perturbation. However, the maximum temperature rise of 0.141 computed with the temperature perturbation is lower than the maximum temperature change of 0.2435 obtained in this case. This is to be expected since with the material defect modeled by a weak material a band forms at a higher value of the average strain.

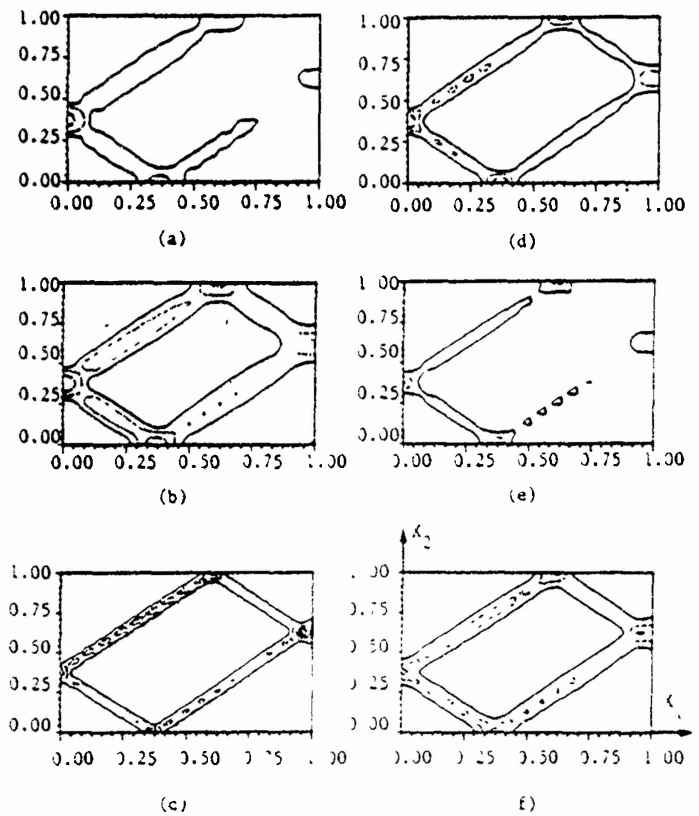

Fig. 6. Contours of the second invariant I of the deviatoric strain-rate tensor and the temperature change θ at different values of the average strain when the material defect is modeled by lowering the flow stress of the material at (0.0, 0.375) by 10%.

(a) $\gamma_{avg} = 0.02$, $I_{max} = 1.938$, ___ 1.2, _ _ _ 1.5, _ _ _ _ 1.8
(b) $\gamma_{avg} = 0.035$, $I_{max} = 3.297$, ___ 1.5, _ _ _ 2.0, _ _ _ _ 2.5
(c) $\gamma_{avg} = 0.0545$, $I_{max} = 10.75$, ___ 2.5, _ _ _ 5.0, _ _ _ _ 7.5, _ _ _ _ 10.0
(d) $\gamma_{avg} = 0.035$, $\theta_{max} = 0.0943$, ___ 0.06, _ _ _ 0.07, _ _ _ _ 0.08
(e) $\gamma_{avg} = 0.045$, $\theta_{max} = 0.154$, ___ 0.10, _ _ _ 0.125, _ _ _ _ 0.150
(f) $\gamma_{avg} = 0.0545$, $\theta_{max} = 0.2435$, ___ 0.10, _ _ _ 0.15, _ _ _ _ 0.20

The plots of the velocity field and the effective stress look similar to those shown in Figs. 4 and 5, and are therefore omitted.

The determination of the equivalent amplitudes of the temperature perturbation and the weakness in the material parameter μ in the sense that the two will result in the formation of the shear band at the same value of the average strain is laborious and has not been attempted here.

III.3 *Effect of the reduction in the strength of the weak material*

For the one-dimensional problem BATRA [1988] found that the temperature perturbation with the higher amplitude hastened the initiation of the shear band. Here we examine the effect of introducing near the center of the block a weak material with flow stress reduced by either 5% or 10%. In each case the initial velocity field given by eqn (2.23) was assumed. Figures 7 and 8 show, respectively, the contours of I and θ for the two cases at various values of the average strain. As expected, the existence of a stronger defect enhances the initiation and development of the shear band. In each case the band forms essentially along the main diagonal, the slight offset is possibly due to the singular nature of the deformations near the top right corner. When the reduction in the flow stress of the material near the center is small the singularity in the deformations near the top right corner may cause a shear band to initiate from this point. With the 5% reduction in the flow stress, I_{max} at $\gamma_{avg} = 0.06$ equals 5.32; and it equals 17.79 for the same value of γ_{avg} but with a 10% reduction in the flow stress. The higher value of I increases the temperature of the material within the band faster which, in turn, reduces the effective stress required to deform the material plastically. The cumulative effect builds upon itself and enhances the growth of the shear band. Whereas a shear band has practically formed at $\gamma_{avg} = 0.06$ for the 10% reduction in the flow stress, it forms at $\gamma_{avg} = 0.0825$ when the flow stress for the material near the center is reduced by 5%. The maximum temperature computed in the two cases equals 0.343 and 0.398, respectively. We note that, except for the delay in the formation of the shear band with the 5% reduction in strength, the results for I and θ, as well as those for the velocity field and the effective stress field, are similar in the two cases.

A comparison of these results with those reported by BATRA and LIU [1989] who introduced the temperature perturbation (2.24) with $\epsilon = 0.2$ at the center of the specimen reveals that the results agree qualitatively with each other. With the temperature perturbation the maximum values of I and the temperature rise $\Delta\theta$ at $\gamma_{avg} = 0.059$ were computed to be 20.7 and 0.249, respectively. At $\gamma_{avg} = 0.06$ and with a 10% reduction in the flow stress at the center of the block, I_{max} and $\Delta\theta_{max}$ equal 17.79 and 0.308, respectively. And these equal 5.324 and 0.167, respectively, with a 5% reduction in the flow stress.

III.4 *Results with zero initial conditions*

The results presented above were obtained by perturbing a steady state solution. We now examine the effect of initial conditions, if any, on the initiation and growth of a shear band. Figure 9 depicts the contours of the second invariant I of the deviatoric strain-rate tensor and the temperature rise when zero initial conditions (i.e., those given by eqn (2.19)), and the boundary velocity field $\zeta(t)$ defined by (2.22) were applied. Also, in this case the thermal conductivity was set equal to zero. The material defect

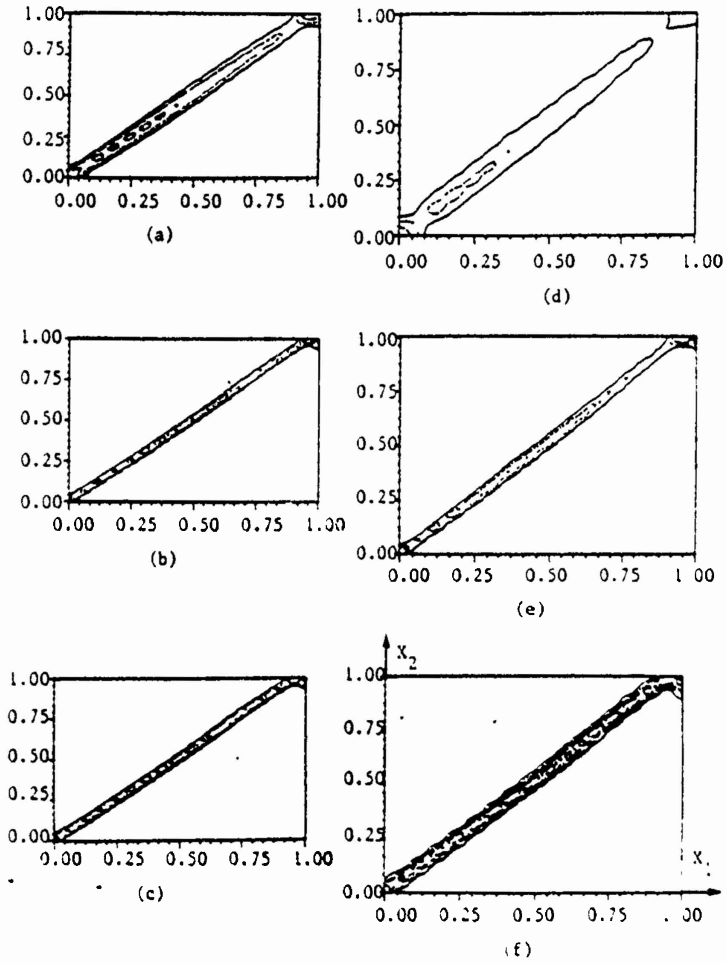

Fig. 7. Contours of the second invariant I of the deviatoric strain-rate tensor at different values of the average strain when the material defect is modeled by reducing the flow stress of the material near the center of the block by either 10% (Figs. 7a–7c) or 5% (Figs. 7d–7f).

(a) $\gamma_{ave} = 0.04$, $I_{max} = 4.21$, ___ 1.5, 2.0, _ _ _ _ 2.5
(b) $\gamma_{ave} = 0.06$, $I_{max} = 17.79$; ___ 5.0, 7.5, _ _ _ _ 10.0
(c) $\gamma_{ave} = 0.064$, $I_{max} = 22.08$, ___ 5.0, 7.5, _ _ _ _ 10.0
(d) $\gamma_{ave} = 0.04$, $I_{max} = 2.0$, ___ 1.25, 1.50, _ _ _ _ 1.75
(e) $\gamma_{ave} = 0.06$, $I_{max} = 5.324$ ___ 2.5, 3.0, _ _ _ _ 3.5
(f) $\gamma_{ave} = 0.0825$, $I_{max} = 19.04$, ___ 2.5, 5.0, _ _ _ _ 7.5, _ _ _ _ 10.0

was modeled by eqn (2.20) with $\epsilon = 0.1$ and $\mathbf{X}^0 = (0.0, 0.375)$, viz. the flow stress of the material surrounding the point (0.0, 0.375), was presumed to be lower than that of the remaining material. A comparison of these results with those shown in Fig. 6 shows that the precise values of initial conditions do not affect the qualitative nature of results. However, quantitatively the results are affected by the choice of initial data. As expected, the values of I_{max} computed for the same value of γ_{ave} is higher when the steady state solution is taken as the initial data as compared to that computed with zero initial conditions. One reason for this difference is that, in both cases, γ_{ave} is

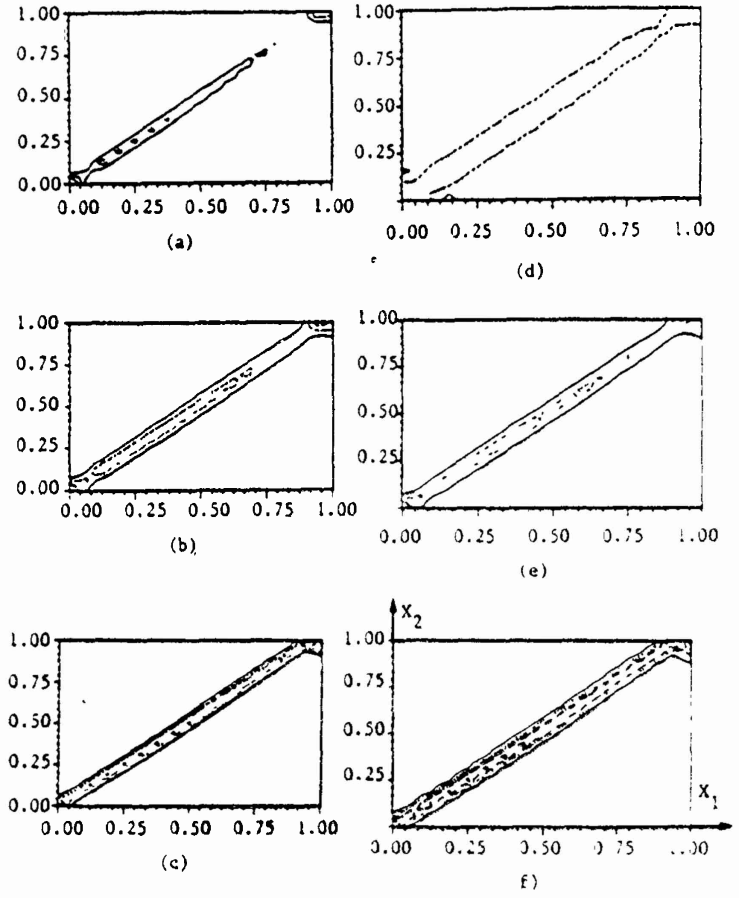

Fig. 8. Contours of the temperature rise θ at different values of the average strain when the material defect is modeled by reducing the flow stress of the material near the center of the block by either 10% (Figs. 8a–8c) or 5% (Figs. 8d–8f)

(a) $\gamma_{ave} = 0.045$, $\theta_{max} = 0.149$; ___ 0.10, _ _ _ 0.1125, _ _ _ _ 0.1250
(b) $\gamma_{ave} = 0.05$, $\theta_{max} = 0.192$, ___ 0.10, _ _ _ 0.125, _ _ _ _ 0.150
(c) $\gamma_{ave} = 0.063$, $\theta_{max} = 0.343$, ___ 0.15, _ _ _ 0.20, _ _ _ _ 0.25, _ _ _ _ _ 0.30
(d) $\gamma_{ave} = 0.045$, $\theta_{max} = 0.099$; ___ _ _ 0.08
(e) $\gamma_{ave} = 0.065$, $\theta_{max} = 0.2113$, ___ 0.125, _ _ _ 0.150, _ _ _ _ 0.175
(f) $\gamma_{ave} = 0.0825$, $\theta_{max} = 0.3984$, ___ 0.15, _ _ _ 0.20, _ _ _ _ 0.25, _ _ _ _ _ 0.30

taken to be zero at time $t = 0$. The difference is reduced somewhat because of neglecting the heat transfer due to conduction. Setting $\kappa = 0$ should result in a slightly higher temperature locally than would be obtained if κ were positive. The higher temperature softens the material more which, in turn, results in higher values of I. What effect the thermal conductivity has on the computed results has not yet been ascertained. For the one-dimensional simple shearing problem, BATRA [1987b] used a constitutive relation similar to eqn (2.4) and found that the thermal conductivity had very little effect on the initiation of the shear band. However, MERZER [1983] used BODNER and PARTOM's [1975] constitutive relation and found that the thermal conductivity significantly affects the width of the shear band.

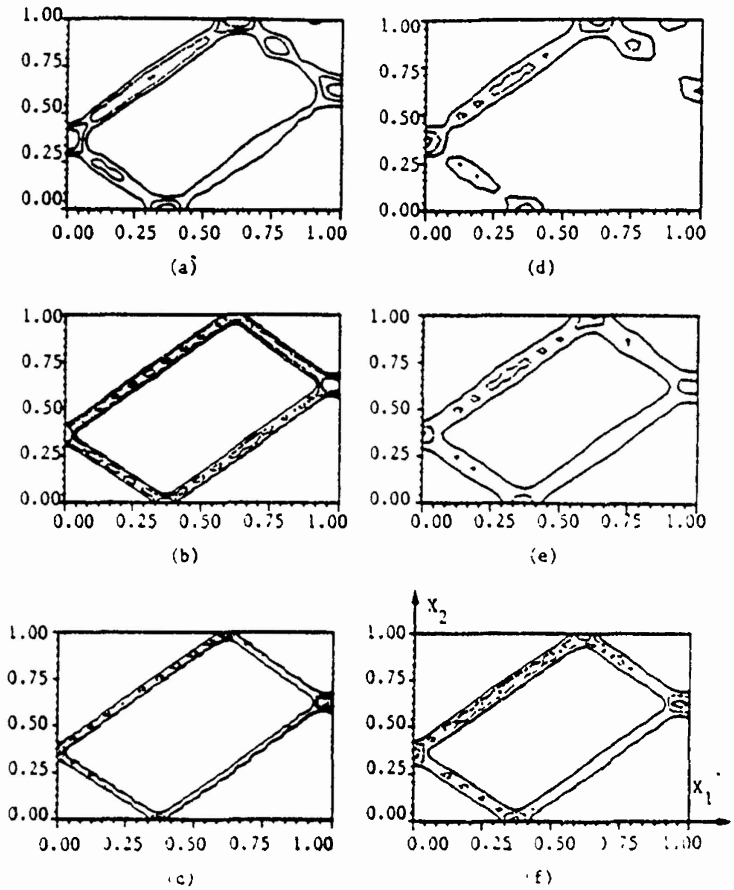

Fig. 9. Contours of the second invariant I of the deviatoric strain-rate tensor and the temperature change θ at different values of the average strain when the material defect is modeled by reducing the flow stress of the material by 10%, taking zero initial conditions and setting the thermal conductivity $k = 0$.

(a) $\gamma_{ave} = 0.035$, $I_{max} = 2.39$; ——— 1.25, 1.50, _ _ _ 1.75
(b) $\gamma_{ave} = 0.055$, $I_{max} = 9.68$, ——— 2.50, 3.75, _ _ _ 5.00
(c) $\gamma_{ave} = 0.065$, $I_{max} = 12.47$, ——— 5.0, 7.5, _ _ _ 10.0
(d) $\gamma_{ave} = 0.04$, $\theta_{max} = 0.1$, ——— 0.075 0.085, _ _ _ 0.095
(e) $\gamma_{ave} = 0.055$ $\theta_{max} = 0.211$ ——— 0.10, 0.15 _ _ _ 0.20
(f) $\gamma_{ave} = 0.065$, $\theta_{max} = 0.310$ ——— 0.15 0.20, _ _ _ 0.25

III.5 *Material damage as a softening mechanism*

The results presented thus far have considered the material softening caused by the rise in its temperature. Another possible softening mechanism is the nucleation, coalescence and growth of voids and/or cracks in the body. One way to model this is to introduce an internal parameter ω whose rate of evolution $\dot{\omega}$ is a function of the history of deformation and/or plastic working. If we assume that ω is a function of the plastic working and the material softening caused by ω can be adequately represented by lowering the flow stress by $(1 - \hat{\omega}\omega)$ where $\hat{\omega}$ is a material parameter, then we may write

$$\Phi = \lambda(1 - \hat{v}\Phi)\tilde{D}_{ij}\tilde{D}_{ij}(1 + bI)^m/(\rho_r\sqrt{3}I), \tag{4.2}$$

$$\sigma_{ij} = -\vartheta(\rho - 1)\delta_{ij} + (1/\sqrt{3}I)(1 + bI)^m(1 - \hat{v}\Phi)D_{ij}, \tag{4.3}$$

where λ is a constant. In this case the results of section 4.4 may be thought of as representing the dynamic development of an adiabatic shear band in plane strain compression of a viscoplastic block when the material softening mechanism is the internal damage caused by plastic working.

IV CONCLUSIONS

The development of a shear band in plane strain compression of a block made of a thermally softening viscoplastic material being deformed at an overall strain-rate of 5,000 sec^{-1} has been studied. The results computed when the material defect is modeled by perturbing the steady-state solution for a homogeneous body (a) with a superimposed temperature bump, and (b) with the introduction of a weaker material agree with each other qualitatively. The qualitative nature of the results remains unchanged even when zero initial conditions are assumed and the transient problem solved.

When the material defect is on the vertical axis of symmetry and away from the center of the block, a shear band initiates from the site of the defect, it propagates along the direction of maximum shearing and is reflected back from the boundaries, the angle of reflection being nearly equal to the angle of incidence. The shear stress within the band is considerably lower than that in the surrounding material. The eventual development of the band along the sides of the parallelogram divides the block into five regions. The velocity field within each region varies linearly and sharp gradients in the velocity field occur at the sides of the parallelogram.

We add that the conclusions drawn above are strictly valid for the constitutive model used herein. However, similar results were obtained by NEEDLEMAN [1989], LEMONDS and NEEDLEMAN [1986a,1986b] and ANAND *et al.* [1988] who used different constitutive relations and the latter two papers ignored the effect of inertia forces. Possibly sharper results could be obtained by using a finer mesh and/or a different space of trial solutions and test functions.

Acknowledgments—This work was supported by the U.S. National Science Foundation grant MSM-8715952 and the U.S. Army Research Office Contract DAAL03-88K-0184 to the University of Missouri-Rolla.

REFERENCES

1934 TAYLOR, G.I. and QUINNEY, H. "The Latent Energy Remaining in a Metal After Cold Working." Proc. Roy. Soc. A 413, 307.
1944 ZENER, C. and HOLLOMON, J.H. "Effect of Strain Rate on Plastic Flow of Steel." J. Appl. Phys. 15, 22.
1968 BELL, J.F. Physics of Large Deformations of Crystalline Solids. Springer-Verlag, New York.
1975 BODNER, S.R. and PARTOM, Y. "Constitutive Equations for Elastic-Viscoplastic Strain Hardening Materials." J. Appl. Mechs. 42, 385.
1979 ROGERS, H.C. "Adiabatic Plastic Deformation." Ann. Rev. Mat. Sci. 9, 23.
1980 CLIFTON, R.J. "Material Response to Ultra High Loading Rates." NRC National Material Advisory Board (U.S.) Report 356.
1980 COSTIN, L.S., CRISMAN, E.E., HAWLEY, R.H. and DUFFY, J. "On the Localization of Plastic Flow in Mild Steel Tubes Under Dynamic Torsional Loading." In HARDING, J. (ed.), Mechanical Properties at High Rates of Strain, Proc. 2nd Oxford Conf. Inst. Phys., London 90–100.

1981 BAI, Y.L., "A Criterion for Thermoplastic Shear Instability," in MEYERS, M.A. and MURR, L.E. (eds.), Shock Waves and High Strain Rate Phenomenon in Metals, Plenum Press, New York, 277-283
1981 MOSS, G.L., "Shear Strain, Strain Rates, and Temperature Changes in Adiabatic Shear Bands," in MEYERS, M.A. and MURR, L.E. (eds.), Shock Waves and High Strain Rate Phenomenon in Metals, Plenum Press, New York, 229-312.
1981 ZIENKIEWICZ, O.C., ORATE, E. and HEINRICH, J.C., "A General Formulation for Coupled Thermal Flow of Metals using Finite Elements," Int. J. Num. Meth. Engng., 17, 1497
1982 BATHE, K.J., Finite Element Procedures in Engineering Analysis, Prentice Hall, Inc., Englewood, N.J.
1983 LINDHOLM, U.S. and JOHNSON, G.R., "Strain-Rate Effects in Metals at Large Strain-Rates," in MESCALL, J. and WEISS, V. (eds.), Material Behavior Under High Stress and Ultrahigh Loading Rates, Plenum Press, New York, 61-79.
1983 MERZER, A.M., "Modelling of Adiabatic Shear Band from Small Imperfections," J. Mech. Phys. Solids, 30, 323.
1983 ROGERS, H.C., "A Review of Adiabatic Shearing," in MESCALL, J. and WEISS, V. (eds.), Material Behavior Under High Stress and Ultrahigh Loading Rates, Plenum Press, New York, 101-118
1984 CLIFTON, R.J., DUFFY, J., HARTLEY, K.A., and SHAWKI, T.G., "On Critical Conditions for Shear Band Formation at High Strain Rates," Scripta Metall., 18, 443
1984 WU, F.H. and FREUND, L.B., "Deformation Trapping due to Thermoplastic Instability in One-Dimensional Wave Propagation," J. Mech. Phys. Sol., 32, 119
1985 BURNS, T.J., "Approximate Linear Stability Analysis of a Model of Adiabatic Shear Band Formation," Quart. Appl. Math., 43, 65
1985 COLEMAN, B.D. and HODGDON, M.L., "On Shear Bands in Ductile Materials," Arch. Rat'l. Mech. Anal., 90, 219
1985 WRIGHT, T.W. and BATRA, R.C., "Adiabatic Shear Bands in Simple and Dipolar Plastic Materials," in Proc. IUTAM Symp. On Macro- and Micro-Mechanics of High Velocity Deformation and Fracture, Aug. 1985, Kawata, K. and Shiori, J. (eds.), Springer-Verlag, NY, 1987, 189-201
1986a LEMONDS, J. and NEEDLEMAN, A., "Finite Element Analysis of Shear Localization in Rate and Temperature Dependent Solids," Mechs. Materials, 5, 339
1986b LEMONDS, J. and NEEDLEMAN, A., "An Analysis of Shear Band Development Incorporating Heat Conduction," Mechs. Materials, 5, 363.
1986 LIN, M.R. and WAGONER, R.H., "Effect of Temperature, Strain, and Strain-Rate on the Tensile Flow Stress of I.F. Steel and Stainless Steel Type 310," Scripta Metall., 20, 143
1987a BATRA, R.C., "The Initiation and Growth of, and the Interaction Among Adiabatic Shear Bands in Simple and Dipolar Materials," Int. J. Plast., 3, 75
1987b BATRA, R.C., "Effect of Material Parameters on the Initiation and Growth of Adiabatic Shear Bands," Int. J. Solids Structures, 23, 1435
1987 HARTLEY, K.A., DUFFY, J., and HAWLEY, R.H., "Measurement of the Temperature Profile During Shear Band Formation in Steels Deforming at High Strain Rates," J. Mech. Phys. Solids, 35, 283
1987 TIMOTHY, S.P., "The Structure of Adiabatic Shear Bands in Metals. A Critical Review," Acta Metall., 35, 301
1987 WRIGHT, T.W. and WALTER, J., "On Stress Collapse in Adiabatic Shear Bands," J. Mech. Phys. Sol., 35, 701
1988 BATRA, R.C., "Steady State Penetration of Thermoviscoplastic Targets," Comp. Mechs., 3, 1
1988 MARCHAND, A. and DUFFY, J., "An Experimental Study of the Formation of Adiabatic Shear Bands in a Structural Steel," J. Mech. Phys. Solids, 36, 251
1988 ANAND, L., LUSH, A.M., and KIM, K.H., "Thermal Aspects of Shear Localization in Viscoplastic Solids," in ATTIA, M.H. and KOPS, L. (eds.), Thermal Aspects in Manufacturing, ASME-PED-Vol. 30, 89-103
1988 SHUTTLE, D.A. and SMITH, I.M., "Numerical Simulation of Shear Band Formation in Soils," Int. J. Num. Analyt. Methods Geomechanics, 12, 611
1988 ZBIB, H.M. and AIFANTIS, E.C., "On the Structure and Width of Shear Bands," Scripta Metall., 22, 703
1989 BATRA, R.C. and LIU, DE-SHIN, "Adiabatic Shear Banding in Plane Strain Problems," J. Appl. Mechs., 56, 527
1989 NEEDLEMAN, A., "Dynamic Shear Band Development in Plane Strain," J. Appl. Mechs., 56
1990 BATRA, R.C. and KIM, C.H., "Adiabatic Shear Banding in Elastic-Viscoplastic Nonpolar and Dipolar Materials," Int. J. Plast., 6, 127-141

Department of Mechanical and Aerospace Engineering and Engineering Mechanics
University of Missouri-Rolla
Rolla, MO 65401, USA

Received 6 February 1989; in Final revised form 6 June 1989

Computers & Structures Vol 39, No 5, pp 459–472, 1991
Printed in Great Britain

0045-7949/91 $3.00 + 0.00

SHEAR BAND DEVELOPMENT IN A THERMALLY SOFTENING VISCOPLASTIC BODY

Z. G ZHU and R. C BATRA

Department of Mechanical and Aerospace Engineering and Engineering Mechanics, University of Missouri-Rolla, Rolla, MO 65401-0249, U S A

(*Received* 20 *March* 1990)

Abstract—Plane strain thermomechanical deformations of a thermally softening viscoplastic body containing a rigid non-heat-conducting circular inclusion at the center are studied. The body is deformed in compression at a nominal strain rate of 5000 sec^{-1}. The flow stress of the material of the body is assumed to decrease linearly with the rise in its temperature. Two different values of the thermal softening coefficient are considered. The rigid inclusion simulates the presence of second phase particles such as oxides or carbides in a steel and serves as a nucleus for the initiation of a shear band.

It is found that the matrix material adjoining the rigid inclusion undergoes severe deformations. The strains in the matrix material near the inclusion surface and adjoining the horizontal axis are larger than that in the matrix material close to the vertical axis. Eventually, only bands along the main diagonals of the cross-section emerge. The speed of propagation of the contours of constant maximum principal logarithmic strain is found to vary from 11 to 420 m/sec.

1. INTRODUCTION

Johnson [1] has recently pointed out that the study of shear bands dates back to 1878 when Henry Tresca [2] observed hot lines, now called shear bands, in the form of a cross during the hot forging of a platinum bar. Massey [3] observed these hot lines in 1921 during the hot forging of a metal and noted that "when diagonal 'slipping' takes place there is great friction between the particles and a considerable amount of heat is generated." Zener and Hollomon [4] stated that shear bands initiate when thermal softening overcomes the hardening due to strain and strain rate effects. They reported 32-μm-wide shear bands during the punching of a hole in a steel plate. A similar experiment was performed by Moss [5] who computed strain rates within the band to be of the order of 10^5 sec^{-1}. The experimental observations of Costin *et al.* [6], Hartley *et al.* [7], Giovanola [8] and Marchand and Duffy [9] involving torsional deformations of thin-wall steel tubes have contributed significantly to our understanding of the initiation and growth of shear bands in steels deformed at strain rates of 500 sec^{-1} to 3000 sec^{-1}.

Most of the analytical [10–18] and numerical [19–28] studies have analyzed overall simple shearing deformations of a viscoplastic block. Different constitutive relations have been used to model the thermomechanical response of the material. A material defect has been modeled by introducing (i) a temperature perturbation, (ii) a geometric defect such as a notch or a smooth variation in the thickness of the specimen, (iii) a perturbation in the strain rate, or (iv) assuming that the material at the site of the defect is weaker than the surrounding material. The focus of these studies has been to delineate factors that enhance or inhibit the initiation and growth of shear bands. Nearly all of the two-dimensional studies [29–36] have assumed that a plane strain state of deformation prevails in the body. These works have employed different constitutive relations and also accounted for varying softening mechanisms.

Here we solve numerically the coupled nonlinear equations, expressing the balance of mass, linear momentum and internal energy, subjected to a suitable set of initial and boundary conditions. It is assumed that a plane strain state of deformation prevails and the body softens because of its being heated up due to the plastic working. A material defect or inhomogeneity is modeled by introducing a perfectly insulated rigid non-heat-conducting circular inclusion at the center of the body. The inclusion can be viewed as precipitates or second phase particles in an alloy. These particles, such as oxides or carbides, are usually very strong relative to the surrounding material, and their deformations can be neglected. Here we take them to be non-heat conducting too. Results are computed for two different values of the thermal softening coefficient and emphasis is placed on finding the speed of propagation of a shear band.

2. FORMULATION OF THE PROBLEM

We use rectangular Cartesian coordinates to study plane strain deformations of a prismatic body with a square cross-section and containing a circular rigid non-heat-conducting inclusion at the center. A cross-section of the body is depicted in Fig. 1. We presume that its deformations are symmetrical about the horizontal and vertical axes passing through the centroid and analyze deformations of the material in

the first quadrant. Equations governing the deformations of the body are

$$\rho + \rho v_{i,i} = 0 \tag{1}$$

$$\rho \ddot{v}_i = \sigma_{ij,j} \tag{2}$$

$$\rho \dot{\theta} = \beta \theta_{,ii} + Q \tag{3}$$

$$\sigma_{ij} = -B(\rho - 1)\delta_{ij} + 2\mu D_{ij} \tag{4}$$

$$2\mu = (1/\sqrt{3}I)(1 + bI)^m(1 - v\theta) \tag{5}$$

$$D_{ij} = (v_{i,j} + v_{j,i})/2$$

$$\bar{D}_{ij} = D_{ij} - \tfrac{1}{3} D_{kk}\delta_{ij} \tag{6}$$

$$2I^2 = \bar{D}_{ij}\bar{D}_{ij} \tag{7}$$

$$Q = 2\mu \bar{D}_{ij}\bar{D}_{ij}. \tag{8}$$

These equations are written in terms of non-dimensional variables which are related to their dimensional counterparts, denoted below by a superimposed bar, as follows:

$$\begin{aligned}
\hat{\sigma} &= \sigma\sigma_0 \\
\hat{B} &= B\sigma_0 \\
\bar{t} &= tA/v_0 \\
\bar{b} &= bA/v_0 \\
\theta_0 &= \sigma_0/(\rho_0 c) \\
\hat{\theta} &= \theta\theta_0 \\
\hat{v} &= v/\theta_0 \\
\hat{\rho} &= \rho\rho_0 \\
\alpha &= \rho_0 v_0^2/\sigma_0 \\
\beta &= \bar{k}/(\rho_0 c v_0 A) \\
\bar{x} &= xA.
\end{aligned} \tag{9}$$

Equations (1), (2) and (3) express, respectively the balance of mass, balance of linear momentum and the balance of internal energy. Equation (4) with μ given by eqn (5) is the constitutive relation for the material of the body. When written as

$$(1/2s_{ij}s_{ij})^{1/2} = (1 + bI)^m(1 - v\theta)/\sqrt{3} \tag{10}$$

$$s_{ij} = \sigma_{ij} - B(\rho - 1)\delta_{ij} - (2\mu/3)D_{kk}\delta_{ij}, \tag{11}$$

it can be viewed as expressing the generalized von Mises yield criterion with the flow stress at a material particle increasing with its strain rate but decreasing with the rise in the temperature of the material particle. Also, it has been assumed that the material obeys Fourier's law of heat conduction with constant thermal conductivity $\bar{k}$. In eqns (1) through (11), ρ is the present mass density and ρ_0 the mass density in the undeformed and unstressed reference configuration, v is the velocity of the material particle in the direction x_i, θ is the temperature rise at a material particle, θ_0 the reference temperature, c the specific heat, β the non-dimensional thermal diffusivity, and σ_0 is the yield stress for the material of the body in a quasi-static simple compression test. Furthermore, $\boldsymbol{\sigma}$ is the Cauchy stress tensor, $\mathbf{s}$ is the deviatoric stress tensor, parameters b and m characterize the strain rate hardening of the material and v delineates its thermal softening. The quantity Q given by eqn (8) equals the heat produced per unit volume due to plastic working, $\mathbf{D}$ is the strain rate tensor and $\bar{\mathbf{D}}$ denotes its deviatoric part. Here we have assumed that all of the plastic working rather than 90–95% of it, as asserted by Farren and Taylor [37], is converted into heat. The non-dimensional numbers α and β in eqns (2) and (3) give, respectively, the magnitude of inertia forces relative to the flow stress of the material and the length over which heat conduction effects are important. A superimposed dot stands for the material time derivative and $v_{i,x} = \partial v_i/\partial x$.

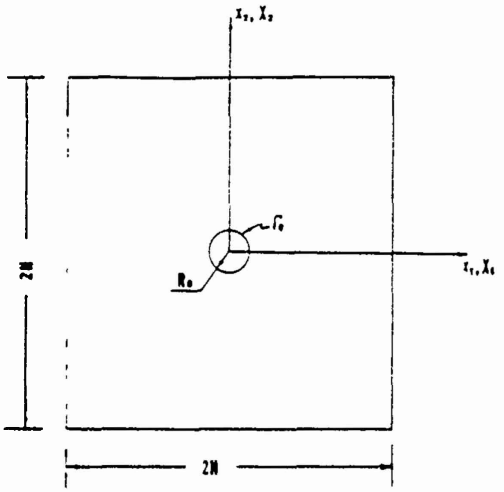

Fig. 1 Cross-section of the prismatic body studied

With the non-deformable and non-heat-conducting inclusion, the boundary conditions for the material in the first quadrant are

$$v_1 = 0 \quad \sigma_{21} = 0, \quad q_1 = 0 \quad \text{on } x_1 = X_1 = 0 \tag{12.1}$$

$$v_2 = 0, \quad \sigma_{12} = 0, \quad q_2 = 0 \quad \text{on } x_2 = Y_2 = 0 \tag{12.2}$$

$$\boldsymbol{\sigma}\mathbf{n} = 0 \quad q_i n_i = 0 \quad \text{on the right surface} \tag{12.3}$$
$$v_2 = -V(t),$$

$$\sigma_{22} = 0 \quad q_2 = 0 \quad \text{on the top surface} \tag{12.4}$$

$$v_i = 0 \quad v_2 = 0, \quad \boldsymbol{\sigma}\mathbf{n} = 0 \quad \text{at the interface } \Gamma \text{ between the inclusion and the matrix} \tag{12.5}$$

That is, all of the bounding surfaces of the block are taken to be perfectly insulated. The boundary

conditions (12.1) and (12.2) follow from the assumed symmetry of the deformations. The boundary condition (12.3) states that the right surface of the block is traction-free. Here $\mathbf{n}$ is an outward unit normal to the surface. The function $U(t)$ in condition (12.4) gives the variation of the prescribed normal velocity with time on the top surface. The contact between the loading device and the top surface is taken to be smooth. The boundary condition (12.5) states that the inclusion is rigid and non-heat-conducting and there is no sliding of the matrix material on the common interface Γ_0 between the matrix and the inclusion. The interface Γ_0 has the parametric representation

$$X_1^2 + X_2^2 = R_0^2$$

or

$$x_1^2 + x_2^2 = R_0^2, \tag{13}$$

where R_0 is the radius of the circular inclusion. The loading function $U(t)$ is taken to be

$$U(t) = \begin{cases} t/0.005 & 0 \leqslant t \leqslant 0.005 \\ 1 & t \geqslant 0.005. \end{cases} \tag{14}$$

For the initial conditions we take

$$\rho(x, 0) = 1.0$$
$$v_1(x, 0) = 0$$
$$v_2(x, 0) = 0$$
$$\theta(x, 0) = 0. \tag{15}$$

The governing equations (1) through (8) are coupled and highly nonlinear. It is difficult to prove the existence and uniqueness of a solution of these equations. Herein we seek an approximate solution of these equations by the finite element method. The Galerkin approximation [38] of the governing equations and the boundary conditions gives a set of coupled nonlinear ordinary differential equations which are integrated with respect to time t by using the backward difference Adams method included in the subroutine LSODE [39]. The subroutine adjusts the time step adaptively until it can compute a solution of the ordinary differential equations within the prescribed tolerance. We use four-noded isoparametric quadrilateral elements to discretize the domain and the lumped mass matrix.

3. COMPUTATION AND DISCUSSION OF RESULTS

In order to compute numerical results, we took the following values of various material and geometric parameters. The values of material parameters are representative of a typical hard steel.

$$\bar{b} = 10{,}000 \text{ sec}$$
$$\sigma_0 = 333 \text{ MPa}$$
$$\bar{k} = 49.22 \text{ Wm}^{-1}\,^{\circ}\text{C}$$
$$m = 0.025$$
$$\bar{c} = 473 \text{ J/kg C}$$
$$\rho_0 = 7800 \text{ kg/m}^3$$
$$B = 128 \text{ GPa}$$
$$\bar{H} = 5 \text{ mm}$$
$$v_0 = 25 \text{ m/sec}$$
$$R_0 = 0.05 \text{ mm}$$
$$\nu = 0.00185\,^{\circ}\text{C}^{-1} \text{ or } 0.01\,^{\circ}\text{C}^{-1} \tag{16}$$

For these values of material parameters, $\theta_0 = 89.6^{\circ}C$, $\alpha = 0.015$ and $\beta = 1.66 \times 10^{-4}$. The presumed values of the thermal softening coefficient are taken to be large so as to reduce the computational resources required to solve the problem. A comparison of the results for two values of ν should enable us to delineate the effect, if any, of the value of the thermal softening coefficient upon the development of a shear band. The finite element mesh used to compute results is shown in Fig. 2. The mesh is very fine in the region surrounding the inclusion and gradually becomes coarse as we move away from it. No attempt was made to align the element sides so that they are parallel to the direction of maximum shearing at the time of the initiation of a shear band. We note that Needleman [31] has suggested that such a mesh will resolve better the sharp gradients of the deformation within and near the band.

3.1. *Results for* $\nu = 0.00185/^{\circ}C$

Since the effective stress at matrix points abutting the rigid inclusion is non-uniform and is expected to be higher than that at matrix points far away from the inclusion, it is not immediately clear where the band will initiate first. Accordingly we have plotted in Figs 3a through 3c the evolution of the maximum principal logarithmic strain ε, the temperature rise and the effective stress at points A(0.0159, 0.00124), B(0.0209, 0.00124), C(0.0259, 0.00124), E(0.0110, 0.0110), F(0.0142, 0.0142) and G(0.501, 0.00202). The logarithmic strain ε is defined as

$$\varepsilon = \ln \lambda_1 \simeq -\ln \lambda_2, \tag{17}$$

where λ_1^2 and λ_2^2 are the eigenvalues of the right (or left) Cauchy–Green tensor. The second relation in eqn (17) follows from the observation that the deformations are nearly isochoric. Note that the point G is far away from the inclusion, and points A, B, C are on the same horizontal line with A being closest to the inclusion surface. Points E and F are on the line that makes an angle of 45° with the horizontal. The evolution of the maximum principal logarithmic strain ε, the temperature rise and the effective stress at points P(0.00124, 0.0170), Q(0.00124, 0.021), R(0.00124, 0.0260), T(0.00624, 0.0210), U(0.00478, 0.0245) and V(0.00142, 0.501) are depicted in Figs 4a

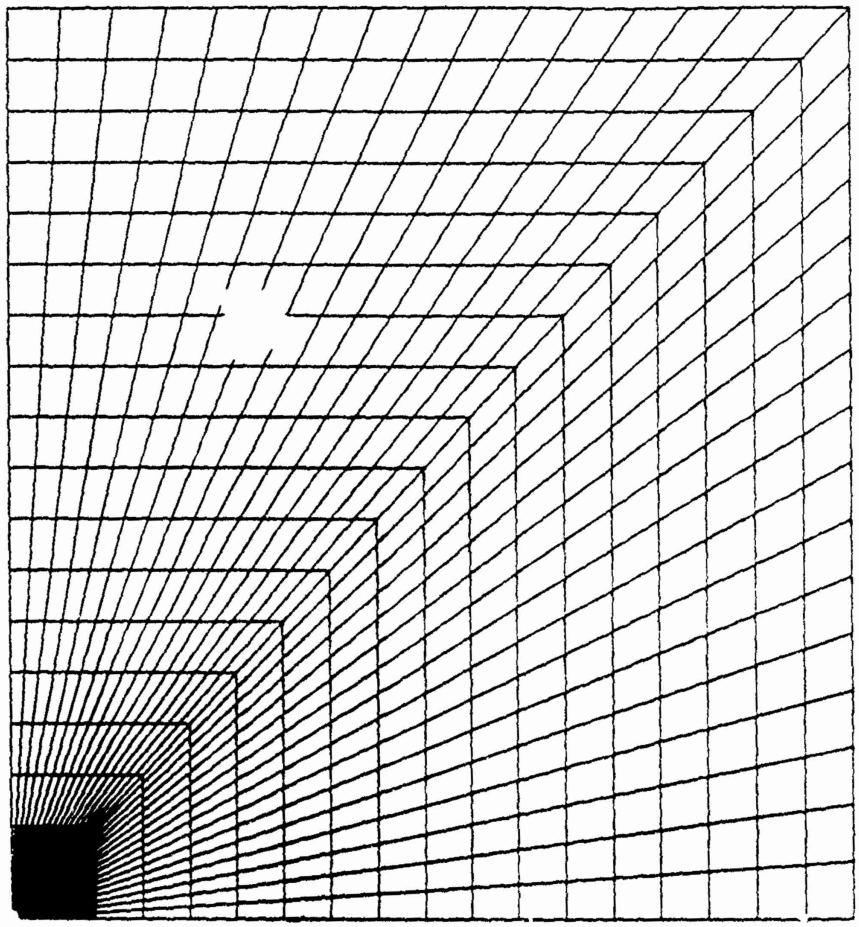

Fig. 2. Finite element discretization of the domain.

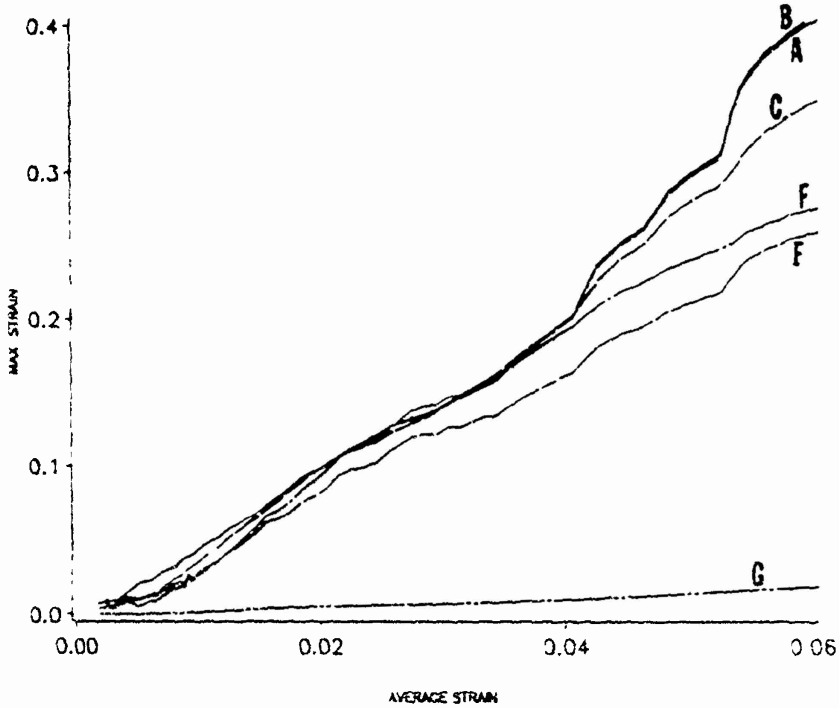

Fig. 3a. Evolution of the maximum principal logarithmic strain at points A(0.0159, 0.00124), B(0.0209, 0.00124), C(0.0259, 0.00124), E(0.0110, 0.0110), F(0.0142, 0.0142) and G(0.501, 0.00202) ($v = 0.00185$ C)

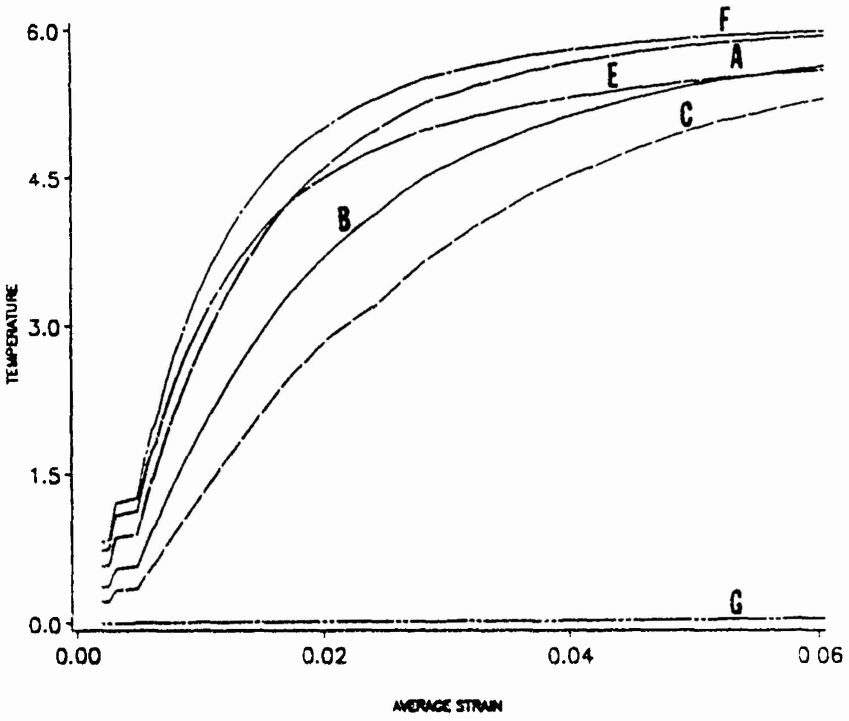

Fig. 3b. Evolution of the temperature rise at points A, B, C, E, F and G ($\nu = 0.00185/°C$)

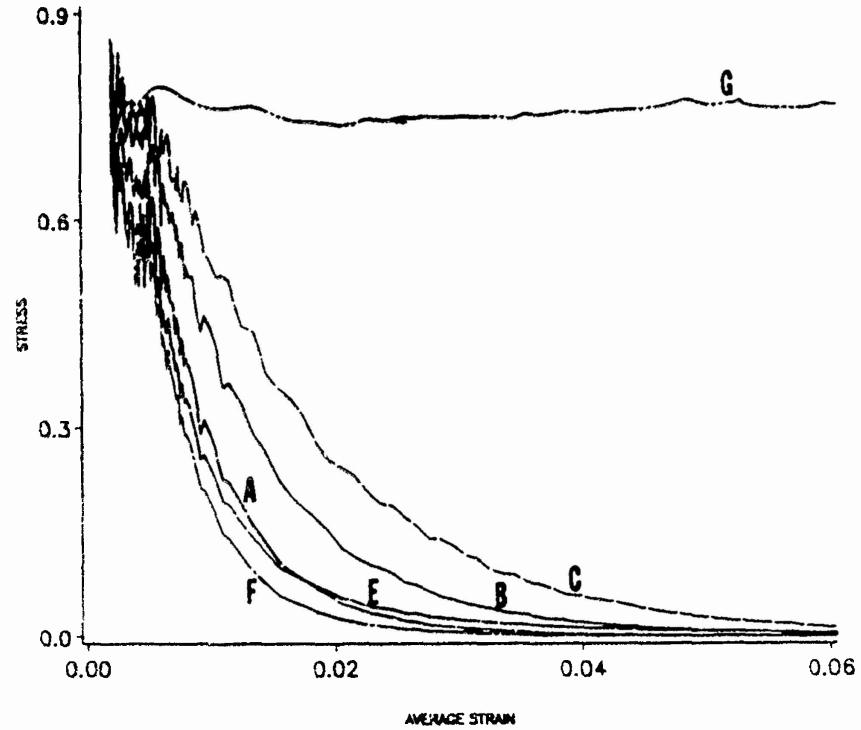

Fig. 3c. Evolution of the effective stress at points A, B, C, E, F and G ($\nu = 0.00185/°C$)

through 4c. Note that points P, Q and R are on the same vertical line, with P being nearest to the inclusion surface. The point V is near the vertical axis but far removed from the inclusion and the top loading surface.

The plots of the maximum principal logarithmic strain at these points reveal that the deformation in the matrix is rather miniscule but that at points close to the inclusion surface it is quite large. The rates of evolution of ε at points G and V, which are far

removed from the inclusion and are near the horizontal and vertical axis, respectively, are nearly the same. At each instant, the value of ε at point A is much higher than that at point P, suggesting thereby that the material surrounding point A is deforming more severely than that adjoining point P. Since the values of ε at points A and B are essentially the same and these are slightly more than that at point C, one is tempted to conclude that the band initiates at point A and propagates from A to C. The rather significant values of ε at points E and F which are higher than the values of ε at points P and Q suggest that the band

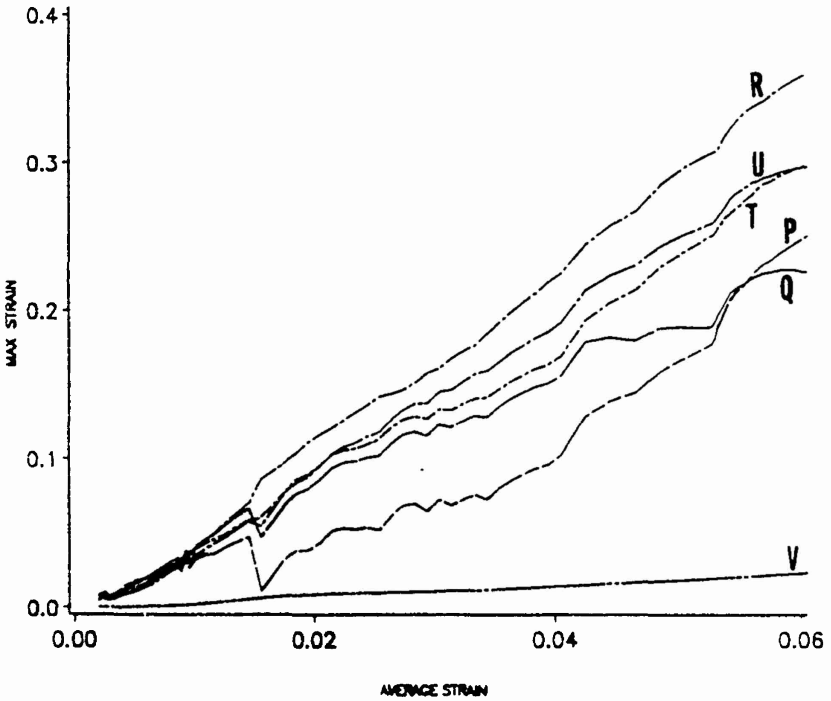

Fig. 4a. Evolution of the maximum principal logarithmic strain at points P(0.00124, 0.0170), Q(0.00124, 0.0210), R(0.00124, 0.0260), T(0.00624, 0.0210), U(0.00478, 0.0245) and V(0.00142, 0.0201) ($v = 0.00185$/°C).

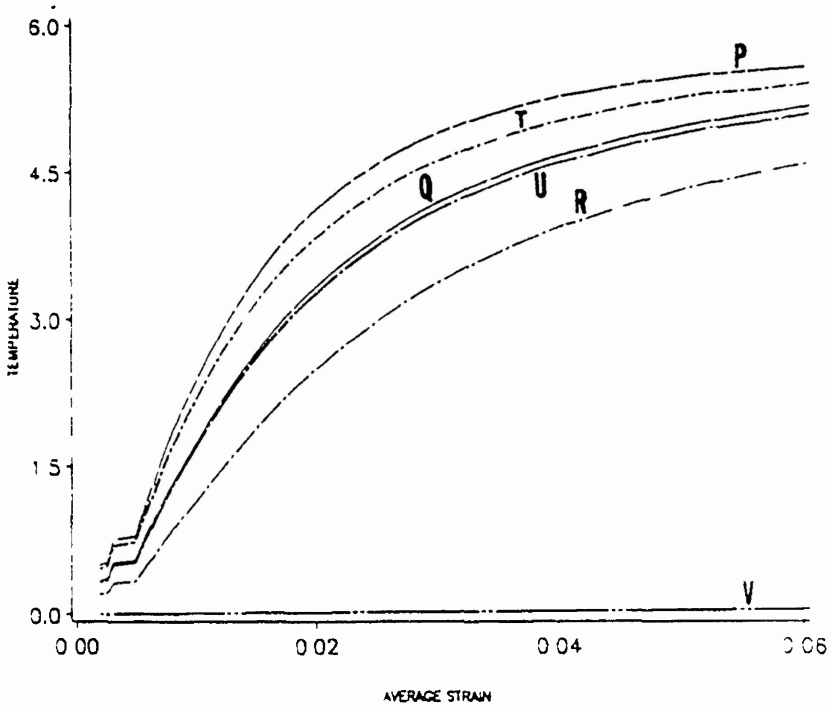

Fig. 4b. Evolution of the temperature rise at points P, Q, R, T, U and V ($v = 0.00185$/°C)

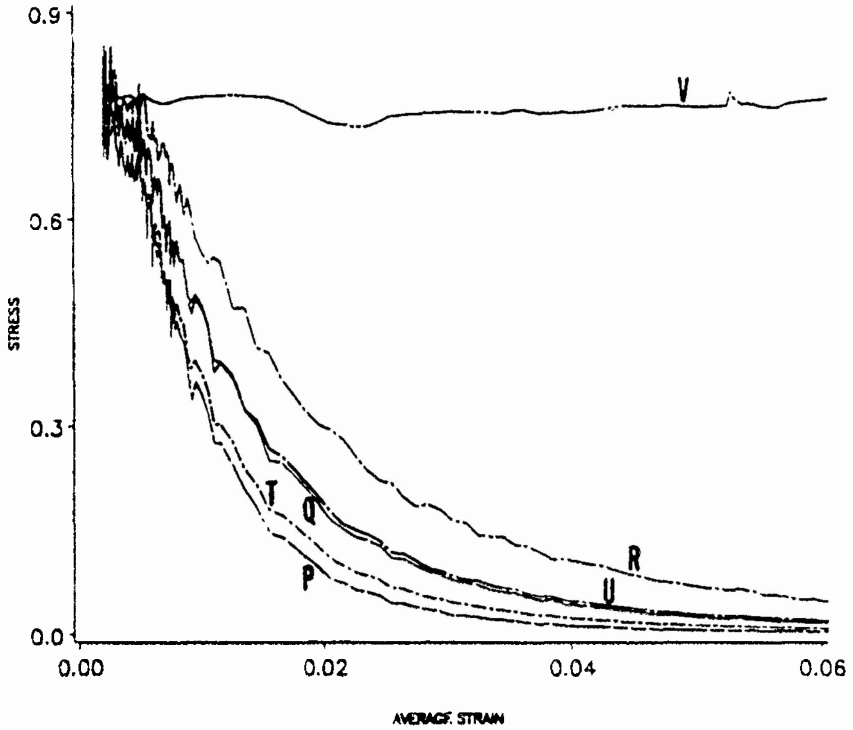

Fig. 4c Evolution of the effective stress at points P, Q, R, T, U and V ($\nu = 0.00185/°C$)

initiating from point A also propagates towards points E and F. The contours of ε plotted in Fig. 5 suggest that the localization of deformation initiating at points P, Q, and R propagates towards points E and F. The band originating from the region enclosing points A and B merges with the band initiating from the region surrounding points P, Q, and R and eventually the two propagate as a single band along the diagonal of the block. We note that for the rigid non-heat-conducting ellipsoidal inclusion [35], a band initiated from its vertex on the major axis and propagated into the matrix in the direction of the maximum shearing. A possible explanation for the value of ε at point R being higher than that at points E, F, P, and Q is that the band originating from the region surrounding points A and B and propagating towards E and F influences the deformations of the region around point R. Also, different components of the stress and strain tensors exhibit singularities of different orders [40] in regions surrounding points A and P. Thus plastic working which equals $tr(\sigma \mathbf{D})$ need not be maximum at the point where the peak value of ε occurs. The computed values of the temperature rise at point R indicate that $tr(\sigma \mathbf{D})$ is lower at R as compared to its value at other neighboring points considered. The computed values of the effective stress plotted in Figs 3c and 4c support the view that, as the temperature at a material point rises, it becomes softer and requires less effective stress for it to deform plastically. The effective stress at points far away from the inclusion surface essentially stays constant whereas that at points near the inclusion surface drops to very low values.

After having determined that a shear band propagates along the main diagonal, we find its speed of propagation as follows. We fix two points in its path and determine the values of the time when a contour of the maximum principal logarithmic strain ε arrives at these two points. The computed speed of propagation is found to depend upon the pair of points used and the value of ε. The results are summarized in Table 1.

Note that the values of the temperature rise and the logarithmic strain at these observation points are not the same, implying thereby that the speed of propagation of an ε-contour at a point depends upon the state of deformation at that point. Batra and Zhang [36], who used the constitutive relation (4) to study the development of shear bands at void tips in a viscoplastic cylinder loaded internally by an impact load, found that contours of $\varepsilon = 0.2524$ and 0.437 propagated at speeds of 115.2 and 14 m/sec, respectively. Needleman [31] who studied plane strain deformations of a viscoplastic block deformed in simple compression and used a quite different constitutive relation, found that contours of constant values of ε propagated at speeds ranging from 590 to 2500 m/sec.

3.2. *Results for* $\nu = 0.01/°C$

Figures 6a, 6b and 6c depict, respectively, the evolution of the maximum principal logarithmic strain ε, the temperature rise, and the effective stress at points A, B, C, D, E and F (0.0177, 0.0177). A comparison of these with the results plotted in Figs 3a through 3c reveals that it is now easy to decipher when a shear band initiates. At a nominal strain of

approximately 0.0105, the values of ε at points A and B begin to increase sharply. A similar behavior occurs at other points considered, except point G, which is far removed from the inclusion surface. The temperature rise and the effective stress exhibit trends similar to those observed for $\nu = 0.00185/°C$. As expected, the localization of the deformation occurs sooner for the larger value of ν. The evolution of ε, the temperature rise and the effective stress at points P, Q, R, T, U and V shown in Figs 7a, 7b and 7c, respectively, also indicate that it is easier to delineate the initiation of a shear band from the ε versus average strain

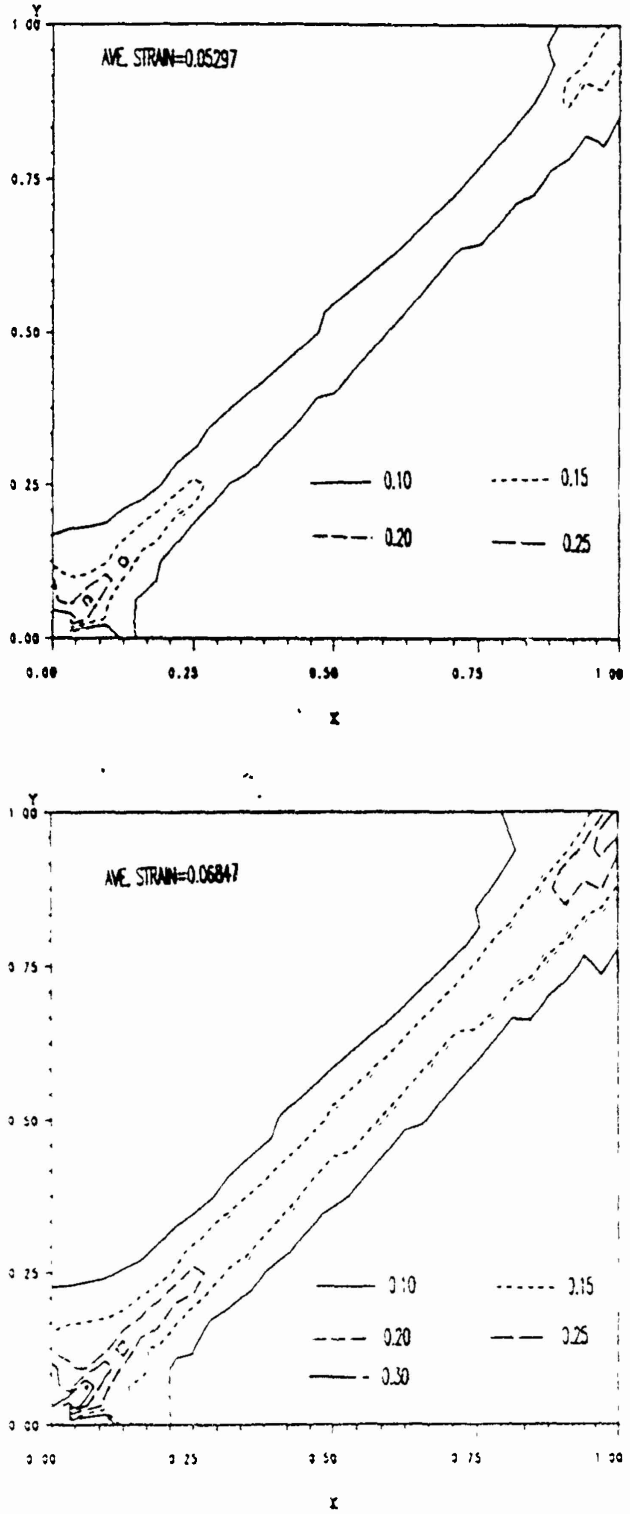

Fig. 7. Contours of the maximum principal logarithmic strain at different times ($\nu = 0.00185$ °C

Table 1.

ε	Co-ordinates of points used	Computed speed (m/sec)
0 025	(0.0623, 0.0625), (0.0994, 0 0997)	34 97
	(0.350, 0.349), (0.470, 0 471)	170 78
	(0 470, 0 226), (0.679, 0 699)	160 84
0 050	(0 227, 0 226), (0.336, 0 335)	51 63
	(0 454, 0 453), (0 660, 0 658)	96 64
	(0 649, 0 628), (0 660, 0 658)	52 57
0 10	(0 339, 0 338), (0 460, 0 459)	42 69
	(0.460, 0 459), (0.544, 0.543)	59 57
0.150	(0.235, 0 234), (0 353, 0.352)	19 62
	(0 353, 0.352), (0 460, 0 459)	43.12
0.20	(0 099, 0.0994), (0.227, 0.226)	11 97
	(0.227, 0.226), (0 303, 0.302)	12 61
0.25	(0 0647, 0.0649), (0.0997, 0.0994)	10 93
	(0.0997, 0 0994), (0.150, 0 151)	42 29

curve. For the larger value of ν, the values of ε at points P, Q and T are higher than those at points R and U. However, ε assumed larger values at points R and S as compared to those at points P, Q and T for the smaller value of ν The curves of the temperature rise and the effective stress are similar for the two cases.

As for $\nu = 0.00185/$ C, only a single band eventually developed along the main diagonal. The speeds of propagation of contours of constant ε, found by the method stated above, are listed in Table 2. We note that these are average speeds for a contour of constant ε to propagate from one point to another point. For points that are very near to each other, the average speed will be close to the instantaneous speed of propagation of the contour of constant ε

In each case studied above, the computations were stopped when a material point melted. In Fig. 8, the average load versus average strain curve is plotted for the two values of ν In each case, the solid curve corresponds to the case when there is a rigid inclusion present in the block. The average compressive force F_v is defined as

$$F_v = -\int_0^1 \sigma_{22}(x_1, 1.0)\, dx_1. \tag{18}$$

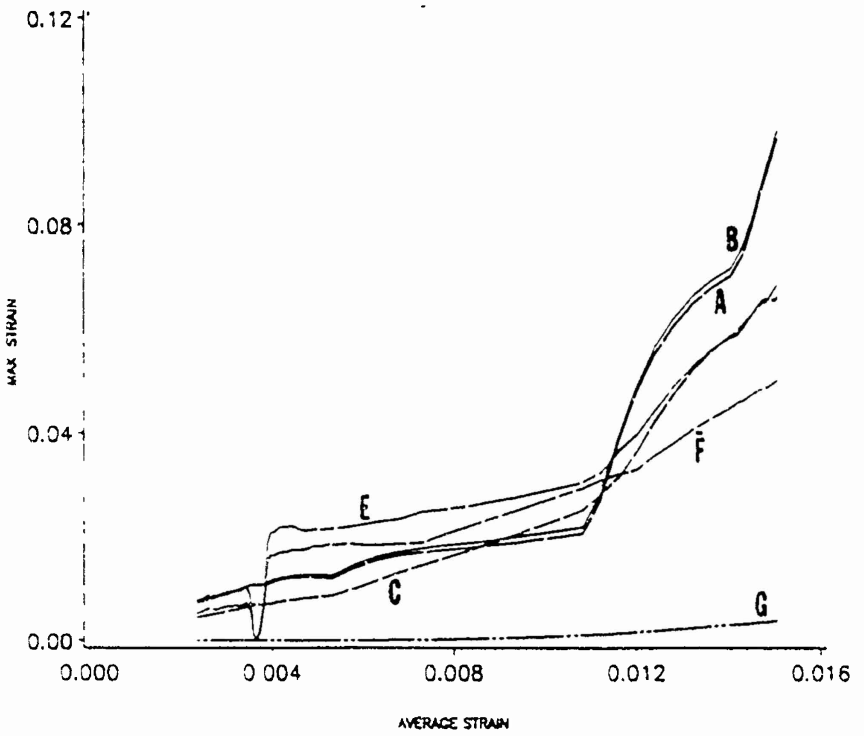

Fig 6a Evolution of the maximum principal logarithmic strain at points A, B, C, E, $\bar{F}$(0 0177, 0 0177) and G ($\nu = 0\,01/$ C)

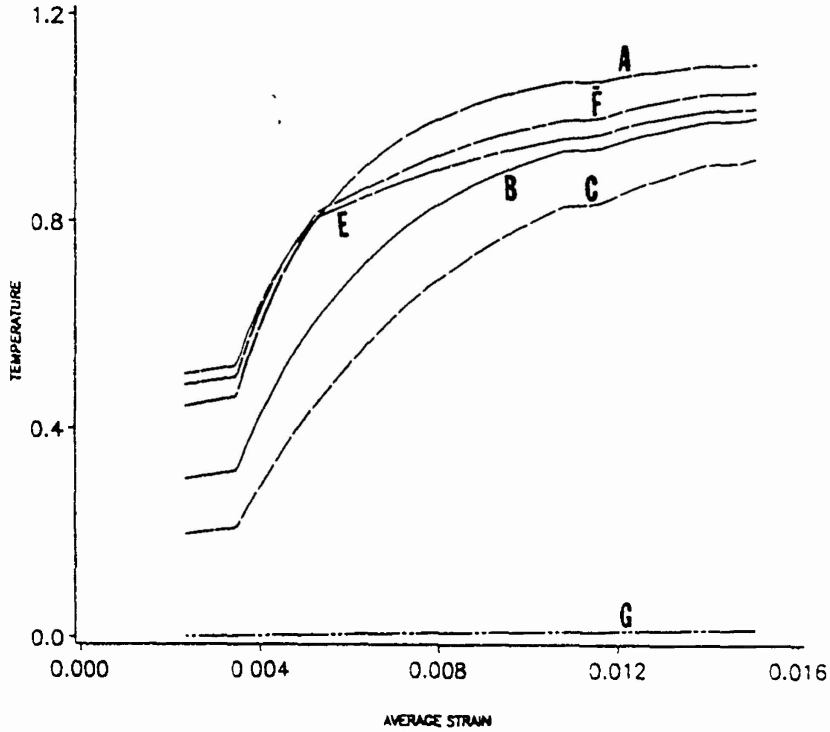

Fig. 6b. Evolution of the temperature rise at points A, B, C, E, $\bar{F}$ and G ($v = 0.01$/°C)

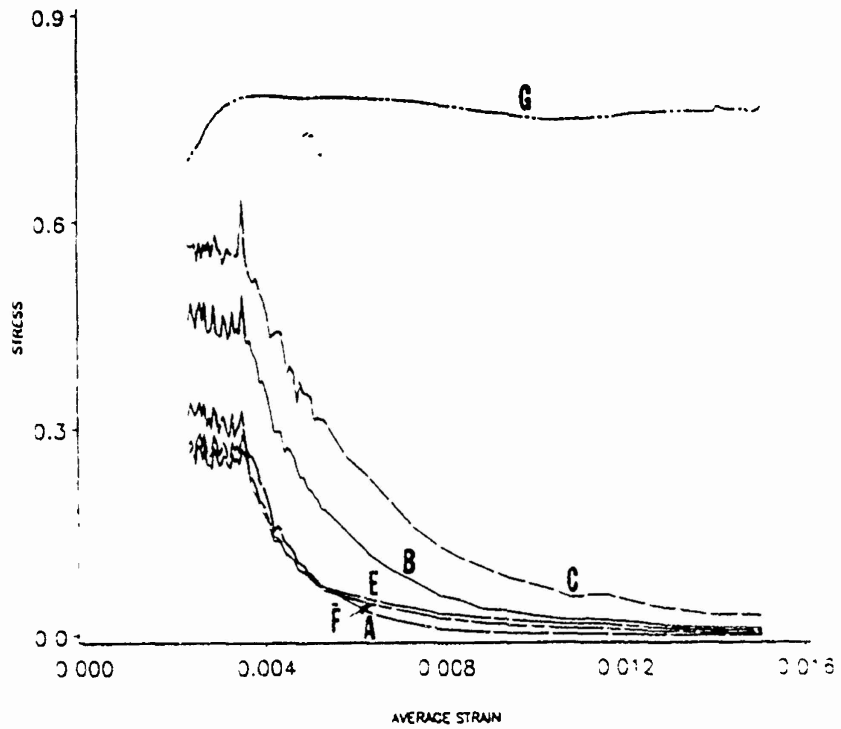

Fig. 6c. Evolution of the effective stress at points A, B, C, E, $\bar{F}$ and G ($v = 0.01$ C)

The integral in eqn (18) is evaluated numerically by using values of σ_{zz} at quadrature points on the top loading surface. The initial almost linear increase of the load is due to the linear increase of the applied velocity field. Due to the heating of the block caused by its plastic deformations, the material softens and the load required to deform it decreases. The decrease in the load is more for the block containing a rigid inclusion because of the nucleation of a shear band in it. Once a band has nucleated the load required to deform it stays lower than that for the homogeneous block signifying the lower

load carrying capacity of the member once a shear band develops in it. The oscillations in the applied load are possibly due to the inhomogeneous deformation of the top rows of elements and the computation of tractions at the boundary points is less accurate than that in the interior of the block. Note that contours of different values of ε arrive at elements in the top row at different times and affect the stress distribution in these elements.

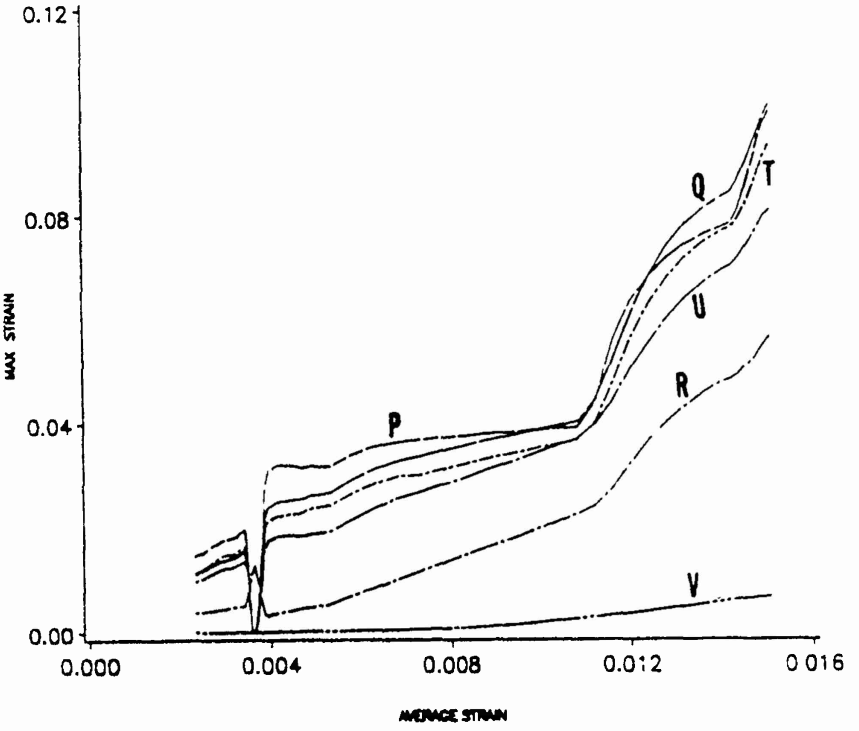

Fig. 7a. Evolution of the maximum principal logarithmic strain at points P, Q, R, T, U and V ($\nu = 0.01$/°C)

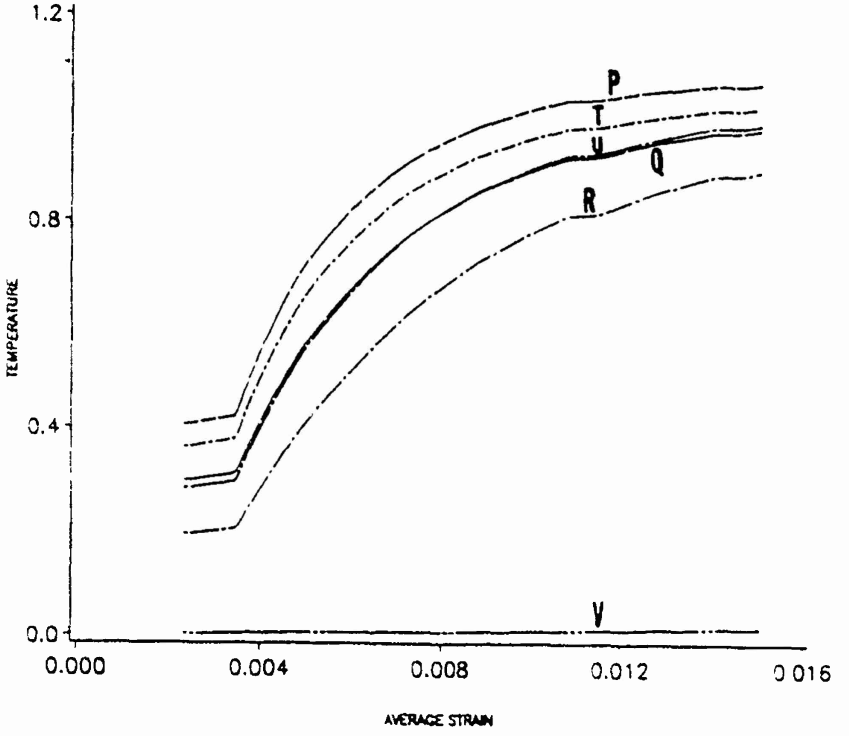

Fig. 7b Evolution of the temperature rise at points P, Q, R, T, U and V ($\nu = 0.01$ C)

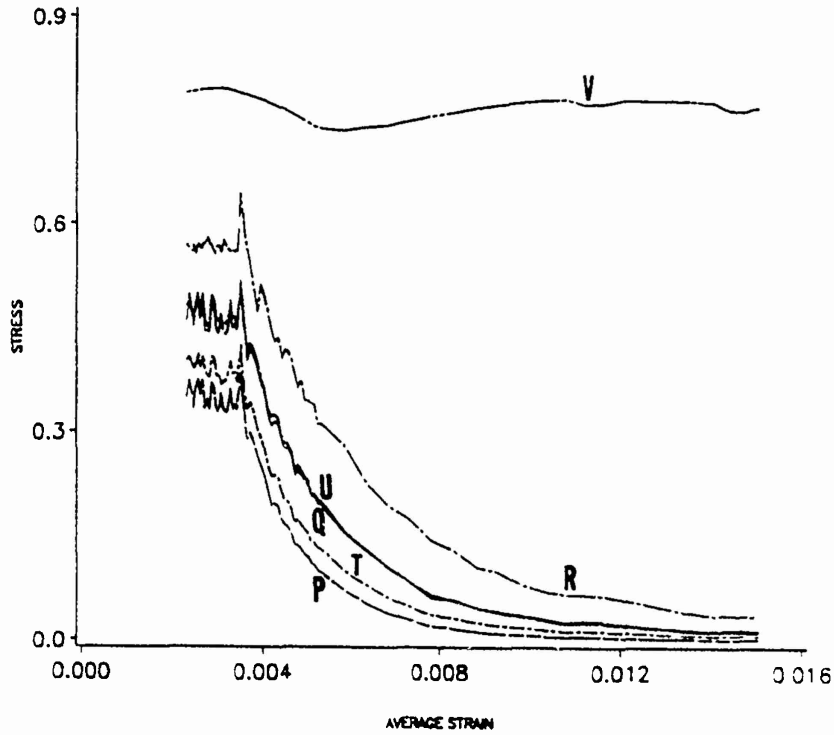

Fig. 7c. Evolution of the effective stress at points P, Q, R, T, U and V ($v = 0.01/^\circ C$)

Table 2.

ε	Co-ordinates of points used	Computed speed (m/sec)
0.020	(0.0609, 0.0611), (0.0965, 0.0962)	33.35
	(0.301, 0.322), (0.508, 0.506)	425.86
	(0.609, 0.611), (0.564, 0.603)	109.58
0.025	(0.0550, 0.0548), (0.0953, 0.0950)	38.0
	(0.225, 0.241), (0.280, 0.30)	109.24

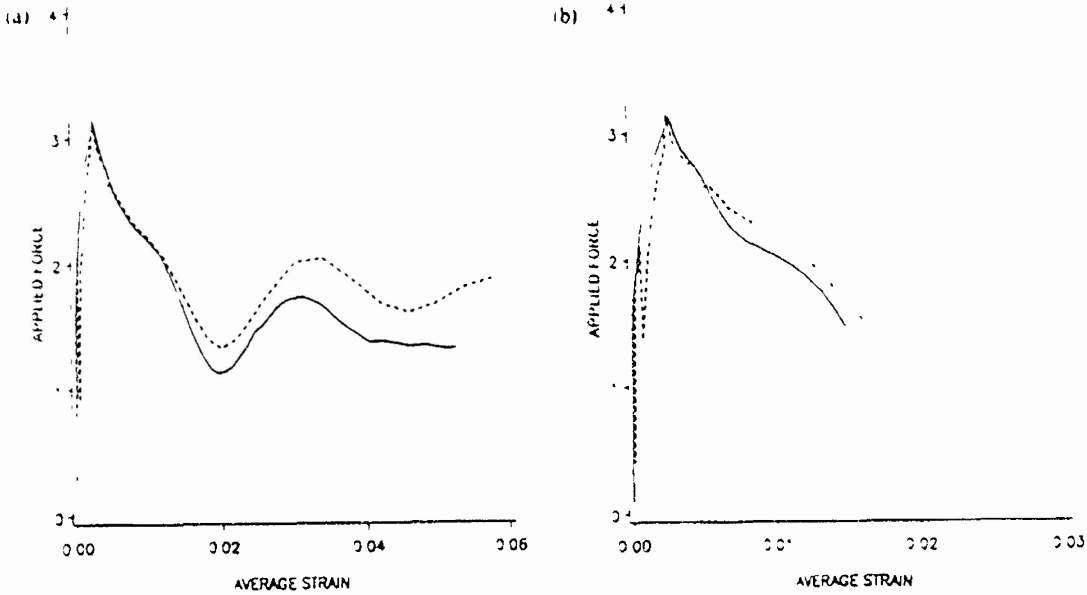

Fig. 8. Compressive force versus average strain (a) $v = 0.00185/^\circ C$ (b) $v = 0.01/^\circ C$ - - - Homogeneous block —— Block with the inclusion

4. CONCLUSIONS

We have studied the problem of the initiation and growth of a shear band in a viscoplastic block containing a rigid circular inclusion and being deformed in plane strain compression at a nominal strain of 5000 sec^{-1} Results have been computed for two values of the thermal softening coefficient In each case the matrix material adjoining the surface of the rigid non-heat-conducting inclusion undergoes severe deformations; that near the horizontal axis deforms more intensely as compared to the one along the vertical axis of the block. Eventually a shear band develops along the diagonals of the block. A narrow zone of material surrounding the inclusion continues to deform severely The speed of propagation of the contours of the constant maximum principal logarithmic strain ε is found to vary from 11 to 420 m/sec. The speed depends upon ε as well as the points in the path of the shear band used to compute the speed. At the time of the initiation of the shear band, the rate of increase of ε at a point is greater for the higher value of the thermal softening coefficient than that for the lower value of the coefficient of thermal softening. Also, contours of constant ε propagate faster when the value of the coefficient of thermal softening is increased.

Acknowledgements—This work was supported by the National Science Foundation Grant MSM 8715952 and the U.S. Army Research Office Contract DAAL03-88-K-0184 to the University of Missouri-Rolla. Some of the computations were performed on the NSF sponsored supercomputer center at the Cornell University, Ithaca.

REFERENCES

1. W. Johnson, Henri Tresca as the originator of adiabatic heat lines. *Int. J mech. Sci.* **29**, 301–305 (1987).
2. H. Tresca, On further application of the flow of solids. *Proc Inst. mech. Engrs* **30**, 301 (1878).
3. H F Massey, The flow of metal during forging. *Proc. Manchester Ass. Engrs* 21–26 (1921). Reprinted by the National Machinery Co., Tiffon, OH (1946)
4. C Zener and J. H. Hollomon, Effect of strain rate on thermoplastic flow of steel. *J. appl. Phys* **14**, 22–32 (1944)
5. G. L. Moss, Shear strain, strain rate and temperature changes in adiabatic shear band. In *Shock Waves and High Strain Rate Phenomenon in Metals* (Edited by M. A Meyer and L. E. Murr), pp. 299–312. Plenum, New York (1981).
6. L. S Costin, E. E. Crisman, R. H Hawley and J Duffy, On the localization of plastic flow in mild steel tubes under dynamic torsional loading. *Int. Phys. Conf. Ser* **47**, 90–100 (1979).
7. K. A. Hartley, J. Duffy and R. H Hawley, Measurement of the temperature profile during shear band formation in steels deforming at high strain rates. *J Mech. Phys. Solids* **35**, 283–301 (1987)
8. J H. Giovanola, Adiabatic shear banding under pure shear loading. *Mech. Materials* **7**, 59–71 (1988)
9. A. Marchand and J. Duffy, An experimental study of the formation process of adiabatic shear bands in a structural steel *J Mech. Phys Solids* **36**, 251–283 (1988)
10. M. R. Staker, The relation between adiabatic shear instability strain and material properties *Acta Metall* **29**, 683–689 (1981).
11. R J Clifton, Material response to ultra high loading rates, NRC National Material Advisory Board (U S) Report 356 (1980).
12. R J Clifton and A. Molinari, Analytic characterization of shear localization in thermoviscoplastic materials *J appl. Mech.* **54**, 806–812 (1987)
13. T J Burns, Approximate linear stability analysis of a model of adiabatic shear band formation *Q appl Math* **43**, 65–83 (1985).
14. T. W Wright, Steady shearing in a viscoplastic solid *J Mech Phys Solids* **35**, 269–282 (1987)
15. L. Anand, K. H. Kim and T G Shawki, Onset of shear localization in viscoplastic solids. Massachusetts Institute of Technology Report, Cambridge, MA (1986)
16. Y L. Bai, A criterion for thermoplastic shear instability In *Shock Waves and High Strain Rate Phenomenon in Metals* (Edited by M. A. Meyer and L. E Murr), pp 277–283 Plenum, New York (1981)
17. B D. Coleman and M L Hodgdon, On shear bands in ductile materials *Archs ration Mech Analysis* **90**, 219–247 (1985)
18. R. F Recht, Catastrophic thermoplastic shear *J appl Mech.* **31**, 189–193 (1964)
19. R. J Clifton, J. Duffy, K. S Hartley and T G Shawki On critical conditions for shear band formation at high strain rates. *Scr metall.* **18**, 443 (1984)
20. A. M. Merzer, Modeling of adiabatic shear band development from small imperfections. *J. Mech. Phys Solids* **30**, 323–338 (1982).
21. F H. Wu and L. B. Freund, Deformation trapping due to thermoplastic instability in one-dimensional wave propagation. *J. Mech. Phys. Solids* **32**, 119–132 (1984).
22. T W Wright and R. C. Batra, The initiation and growth of adiabatic shear bands. *Int. J Plasticity* 1, 205–212 (1985).
23. T. W Wright and R. C. Batra, Adiabatic shear bands in simple and dipolar plastic materials In *Proc IUTAM Symposium on Macro- and Micro-Mechanics of High Velocity Deformation and Fracture* (Edited by K Kawata and J. Shiori), pp. 189–201 Springer, Berlin (1987)
24. T. W. Wright and J. W Walter, On stress collapse in adiabatic shear bands. *J Mech. Phys. Solids* **35**, 701–720 (1987).
25. R C. Batra, The initiation and growth of, and the interaction among adiabatic shear bands in simple and dipolar materials. *Int J. Plasticity* 3, 75–89 (1987)
26. R C. Batra, Effect of material parameters on the initiation and growth of adiabatic shear bands *Int J Solids Struct* **23**, 1435–1446 (1987).
27. R C. Batra, Effect of nominal strain-rate on the initiation and growth of adiabatic shear bands *J appl Mech.* **55**, 229–230 (1988)
28. C Fressengeas, Adiabatic shear morphology at very high strain rates. *Int. J Impact Engng* **8**, 141–158 (1989).
29. J LeMonds and A. Needleman, Finite element analyses of shear localization in rate and temperature dependent solids. *Mech. Materials* **5**, 339–361 (1986).
30. J LeMonds and A. Needleman, An analysis of shear band development incorporating heat conduction *Mech. Materials* **5**, 363–373 (1986).
31. A Needleman, Dynamic shear band development in plane strain. *J appl. Mech* **56**, 1–8 (1989)
32. R C Batra and D S. Liu, Adiabatic shear banding in plane strain problems *J appl. Mech.* **56**, 527–534 (1989).
33. R. C. Batra and D. S. Liu, Adiabatic shear banding in dynamic plane strain compression of a viscoplastic material *Int J Plasticity* 6, 231–246 (1990)

34. L. Anand, A. M. Lush and K. H. Kim. Thermal aspects of shear localization in viscoplastic solids. In. *Thermal Aspects in Manufacturing* (Edited by M H. Attia and L. Kops), pp. 89–103. ASME-PED-Vol 30. New York (1988).
35. Z. G. Zhu and R. C. Batra, Dynamic shear band development in plane strain compression of a viscoplastic body containing a rigid inclusion *Acta mech.* **84**, 89–107 (1990).
36. R. C. Batra and X.-T Zhang, Shear band development in dynamic loading of a viscoplastic cylinder containing two voids. *Acta mech.* **85**, 221–234 (1990).
37 W S. Farren and G. I. Taylor, The heat developed during plastic extrusion of metal. *Proc. R. Soc.* **A107**, 422 (1925).
38. T. J R. Hughes, *The Finite Element Method. Linear Static and Dynamic Finite Element Analysis.* Prentice-Hall, Englewood Cliffs, NJ (1987)
39. A C Hindmarsh, ODEPACK, a systematized collection of ODE solvers In *Scientific Computing* (Edited by R S. Stepleman *et al.*), pp. 55–64 North-Holland, Amsterdam (1983).
40 Z. G Zhu, Micromechanics of time-dependent deformation in polycrystalline metals and composites. Ph.D. dissertation, Rutgers University, New Jersey (1988).

MECHANICS RESEARCH COMMUNICATIONS Vol. 17 (2), 81-91, 1990. Printed in the USA.
0093-6413/90 $3.00 + 00

AN ADAPTIVE MESH REFINEMENT TECHNIQUE FOR THE ANALYSIS OF ADIABATIC SHEAR BANDING

R C Batra and C H. Kim
Department of Mechanical and Aerospace Engineering and
Engineering Mechanics, University of Missouri-Rolla,
Rolla, MO 65401-0249

(Received 30 June1989; accepted for print 5 December 1989)

Abstract

Adiabatic shear bands are narrow regions in which the shear strain is several orders of magnitude higher than that in the adjoining regions. Because of the steep gradients of deformation within and near these bands, a properly graded mesh is required for a satisfactory resolution of the details of the deformation field. Here we use the scaled residuals in the equations expressing the balance of linear momentum and the balance of internal energy to refine the mesh adaptively. The computed results show that the two balance laws generally require refinement of the mesh in different regions.

1 Introduction

Adiabatic shear banding refers to the localization phenomenon that occurs during many high-rate plastic deformation processes such as machining, shock impact loading, ballistic penetration, and metal forming. As shear bands are believed to be precursors to material fracture, a knowledge of factors that inhibit or enhance their initiation and growth, is essential to the production of durable materials and the design of optimum processing environment and conditions.

The interest in adiabatic shear banding seems to have started with the work of Zener and Hollomon[1] who observed 32 μm wide shear bands in a steel plate punched by a standard die and estimated the maximum strain in the band to be 100. Analytical studies aimed at finding critical conditions necessary for the initiation and growth of adiabatic shear bands include the work of Clifton[2], Bai[3], Staker[4], Burns[5], Anand et al.[6], and Wright[7] Experimental investigations have been carried out, among others, by Costin et al [8], Moss[9], Lindholm and Jonnson[10], and Marchand and Duffy[11] Of these, Marchand and Duffy[11] have provided a detailed history of the temperature and strain field during the initiation and development of a shear band. Numerical computations of Clifton et al.[12], Wright and Batra[13], Wright and Walter[14], Batra[15], and Batra and Kim[16] have revealed some interesting aspects of adiabatic shear banding. Whereas these investigations involved analyzing simple shearing deformations of a viscoplastic block, recently, Needleman[17], and Batra and Liu[18] studied the initiation of shear bands in plane-strain

deformations of viscoplastic solids. All of the numerical studies referred to above have used a fixed finite element or finite difference mesh. In general, the computed results depend upon the mesh used. Needleman[19] has discussed this aspect in considerable detail. A robust code should have a properly graded mesh and should be able to compute results with the least usage of the CPU time.

Drew and Flaherty[20] have used the moving grid method to develop an adaptive finite element code that automatically locates regions with large gradients and concentrates finite elements there in order to minimize approximately the discretization error per time step. Pervaiz and Baron[21] have discussed an adaptive technique which refines the spatial and/or temporal grid whenever preselected gradients exceed the threshold levels and have applied it to study quasi-one-dimensional unsteady flow problems involving finite rate chemistry. Herein we use the local refinement method to develop an adaptive mesh refinement technique that makes the scaled residuals uniformly distributed within the domain. The technique is applied to study the simple shearing deformations of a viscoplastic block whose material exhibits strain and strain-rate hardening and thermal softening. Results computed with a fixed mesh and an adaptively refined mesh differ quantitatively only after the deformations have started to localize. Also it is found that the residuals in the balance of the linear momentum and the balance of internal energy are generally not high in the same region. Thus different regions need to be refined to lower the residuals in the two equations.

2. Governing Equations

Equations governing the overall adiabatic thermomechanical deformations of a viscoplastic block bounded within the planes $y = \pm 1$ and undergoing simple shearing deformations are[13,15]

$$v = (1/\rho)\, s_{,y}, \tag{2.1}$$

$$\dot{\theta} = k\theta_{,yy} + s\dot{\gamma}_p , \tag{2.2}$$

$$\dot{s} = \mu(v_{,y} - \dot{\gamma}_p) , \tag{2.3}$$

$$\dot{\psi} = s\dot{\gamma}_p/(1 + \psi/\psi_o)^n , \tag{2.4}$$

$$\dot{\gamma}_p = \max\left[0,\ \frac{1}{b}\left(\left(\frac{s}{(1 + \frac{\psi}{\psi_o})^n(1 - \alpha\theta)}\right)^{1/m} - 1\right)\right] , \tag{2.5}$$

with boundary conditions

$$v(\pm 1, t) = \pm 1 , \quad \theta_{,y}(\pm 1, t) = 0 \tag{2.6}$$

and a suitable set of initial conditions. These equations are

written in terms of nondimensional variables related to their dimensional counterparts, indicated below by a superimposed bar, as follows:

$$y = \bar{y}/H,\ v = \bar{v}/v_o,\ t = \bar{t}\ v_o/H,\ s = \bar{s}/s_o\ ,$$

$$\theta = \bar{\theta}/\theta_o,\ \theta_o = s_o/\bar{\rho}c,\ \rho = \bar{\rho}\ v_o^2/s_o,\ k = \bar{k}/(\bar{\rho}cv_oH)\ , \qquad (2.7)$$

$$\psi = \bar{\psi}\ ,\ \alpha = \bar{\alpha}\theta_o,\ b = \bar{b}\ v_o/H.$$

Here v_o is the velocity imposed on the top and bottom surfaces of the block of height 2H and s_o is the flow stress in a quasistatic simple shear test. Equations (2.1) and (2.2) express, respectively, the balance of linear momentum and the balance of internal energy. In these equations ρ is the mass density, θ the temperature change of a material particle from that in the reference configuration, κ the thermal diffusivity, γ_p the plastic strain-rate, μ the shear modulus, ψ_o and n characterize the work hardening of the material, parameters b and m describe its strain-rate hardening and α the thermal softening. Furthermore, a superimposed dot indicates the material time derivative and a comma followed by y stands for partial differentiation with respect to y. In writing eqn. (2.3) we have assumed that the strain-rate γ has an additive decomposition into elastic γ_e and plastic parts γ_p, i.e.

$$\dot{\gamma} = \dot{\gamma}_e + \dot{\gamma}_p. \qquad (2.8)$$

The internal variable ψ rather than the plastic strain γ_p is used to describe the work-hardening of the material and accounts approximately for the history of the deformation. The rate of evolution of ψ is assumed to be given by equation (2.4). Equation (2.5) states that the plastic strain-rate vanishes whenever

$$s \le (1 + \frac{\psi}{\psi_o})^n(1 - \alpha\theta); \qquad (2.9)$$

otherwise it is computed by solving the equation

$$s = (1 + \frac{\psi}{\psi_o})^n(1 - \alpha\theta)\ (1 + b\ \gamma_p)^m \qquad (2.10)$$

which is a slight generalization of the Litonski equation. A detailed discussion of constitutive assumptions (2.4), (2.5), (2.9) and (2.10) is given in Refs. 13 and 16. The boundary conditions (2.6) imply that the body is placed in a hard perfectly insulated loading device in the sense that the tangential velocity is prescribed on its top and bottom faces which do not exchange heat with their surroundings.

For the initial conditions we take

$$v(y,0) = y,\ \psi(y,0) = 0\ ,$$

$$\theta(y,0) = 0.1 + 0.1\ (1 - y^2)^9\ \exp(-5y^2), \qquad (2\ 11)$$

$$s(y,0) = (1 - \alpha\theta(y,0))(1+b)^m\ ,$$

and seek solutions which exhibit the properties

$$v(-y\ ,\ = -v(y,t),\ s(-y,t) = s(y,t),\ \theta(-y,t) = \theta(y,t) \qquad (2\ 12)$$

Thus the problem needs to be solved on the domain $0 \le y \le 1$ with the boundary conditions (2.6) replaced by

$$v(1,t) = 1,\ \theta_{,y}(1,t) = 0,\ v(0,t) = 0,\ \theta_{,y}(0,t) = 0 \qquad (2\ 13)$$

The initial conditions (2.11) imply that the transients have died out. The second term on the right-hand side of $(2.11)_2$ gives the temperature perturbation which simulates a material inhomogeneity or defect in the body. The size and shape of the temperature perturbation is supposed to model the strength and distribution of the material defect. The final width of the shear band should not depend upon the assumed form of $(2.11)_2$ which was also used in Refs. 13-16. The body is initially taken to be heated to a temperature of 0.10 to reduce the CPU time required to solve the problem. Our aim here is to see how the residuals in the balance of linear momentum and balance of internal energy are distributed, refine the mesh accordingly, and see if the mesh refinements lead to superior results.

We use Galerkin's approximation[22] and piecewise linear finite element basis functions to derive a semi-discrete formulation of the problem defined by equations (2.1) - (2.5), (2.11) and (2.12), and the Crank-Nicolson method to integrate the resulting nonlinear coupled ordinary differential equations. The details of obtaining the nonlinear algebraic equations from (2 1) - (2.5), (2 11) and (2 12) are given in Ref. 15

3 An Adaptive Mesh Refinement Technique

We employ the method of scaled residuals, similar to that outlined by Carey and Oden[23], to selectively refine the mesh in appropriate subregions of the domain Thus it is tacitly assumed that a large scaled residual in a subregion implies that the solution is inaccurate there. Other refinement criteria such as the gradient of a solution variable exceeding a preassigned value could have been employed. What is the most appropriate rule for the problem at hand is an open question No a priori estimates are available because of the strong nonlinearities present in the problem. We have used the following procedure to refine the mesh adaptively in the spatial domain

1 Define an initial mesh M^0 and find an approximate solution of equations (2.1) - (2 6) and (2 11) until the time the mesh is to be checked for possible refinement

2. Using the solution computed in step 1, calculate the scaled element residual

$$R_\alpha^e = \frac{1}{\ell_e} \left(\int_{\Omega_e} r_\alpha^2 \, dy \right)^{1/2} , \quad \alpha = 1,2 \tag{3.1}$$

Here ℓ_e is the length of element Ω_e, and

$$r_1 = \dot{v}^h - \frac{1}{\rho} s^h_{,y} , \tag{3.2}$$

$$r_2 = \dot{\theta}^h - k \, \theta^h_{,yy} - s^h \gamma^h_{,} \tag{3.3}$$

the superscript h indicates that the corresponding field variable is computed from the approximate solution. We note that r_1 and r_2 equal, respectively, the errors in satisfying the balance of linear momentum and the balance of internal energy We have used 4-point Gauss quadrature rule to evaluate numerically the integral in equation (3.1).

3 Find the mean $\bar{R}_\alpha$ (M^o) and the standard deviation σ_α (M^o) of the set

(R_α^e) of scaled element residuals.

4. Cycle over the elements. If in an element either

$$C_1 = (R_1^e - \bar{R}_1)/\sigma_1 \geq 1.0 , \tag{3.4}$$

or

$$C_2 = (R_2^e - R_2)/\sigma_2 \geq 1.0 , \tag{3.5}$$

subdivide the element into two equal elements At the newly introduced nodes the variables are assigned values obtained by linear interpolation of the solution computed in step 1

5 The mesh M^o is replaced by this new mesh, and we repeat steps 1 through 4

Results for a Sample Problem

We illustrate the aforementioned adaptive mesh refinement tech-

nique by computing results for a sample problem and assign values to various material and geometric parameters as follows:

$$\rho = 3.928 \times 10^{-5},\ k = 3.978 \times 10^{-3},\ \mu = 240.3,\ m = 0.025, \qquad (4.1)$$

$$n = 0.09,\ \psi_o = 0.017,\ \alpha = 0.4973,\ b = 5 \times 10^{6},\ \gamma_o = v_o/H = 500\ \text{sec}^{-1}$$

These values, except for α, are for a typical steel. We chose a rather high value for α, equal to seven times that for a typical steel, to cut down on the GPU time required to solve the problem. Not knowing in advance at what values of time t to refine the mesh, we tried the following three alternatives:

1. Refine the mesh at t = 2 μs, 20 μs, 40 μs, 60 μs, 80 μs, 100 μs, 120 μs, 140 μs, 160 μs, and 180 μs
2. Refine the mesh at t = 2 μs, 70 μs, 80 μs, 90 μs, 100 μs, 110 μs, 120 μs, 130 μs, 155 μs, and 180 μs
3. Refine the mesh at t = 2 μs, 60 μs, 120 μs, 130 μs, 140 μs, 150 μs, 160 μs, 170 μs, 180 μs, and 185 μs.

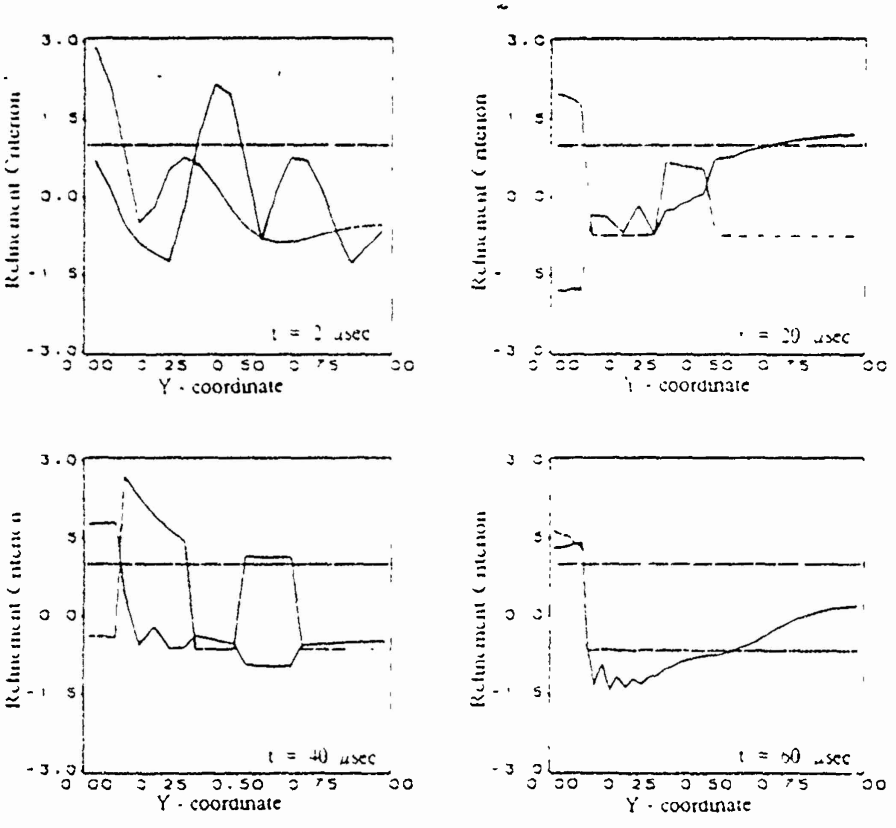

Figure 1. Distribution of the refinement criterion ζ_1 and ζ_2 at t = 2 μs, 20 μs, 40 μs and 60 μs. (Solid Line: Linear Momentum; Dotted Line: Internal Energy)

For each one of these choices, different meshes were computed for t = 140 μs but the results were virtually indistinguishable up to and including t = 140 μs. Also the deformation had localized prior to the next refinement of the mesh. We took the solution at t = 120 μs as the initial data and restarted the job with the mesh to be refined at every 4 μs interval until t = 140 μs. The mesh was not refined subsequently. The initial mesh at t = 0 had 20 uniform elements. The final mesh at t = 140 μs had 458 non-uniform elements of which 423 were located between 0 and 0.10.

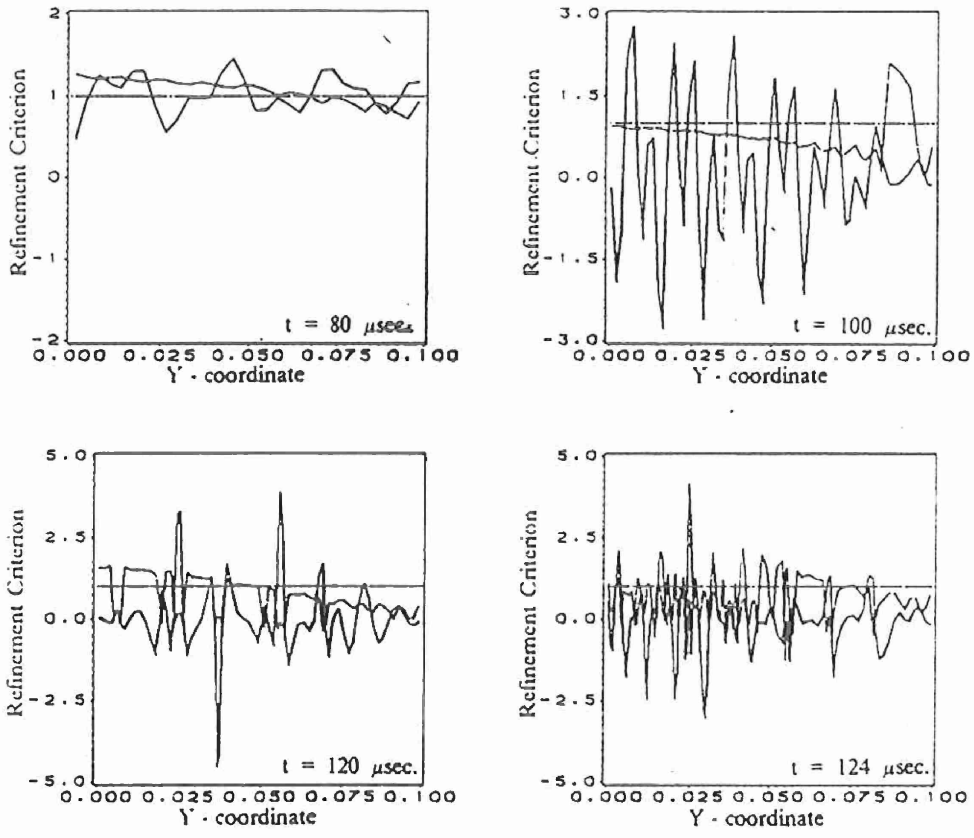

Figure 2. Distribution of the refinement criterion C_1 and C_2 at t = 80 μs, 100 μs, 120 μs, 124 μs. (Solid Line: Linear Momentum; Dotted Line: Internal Energy)

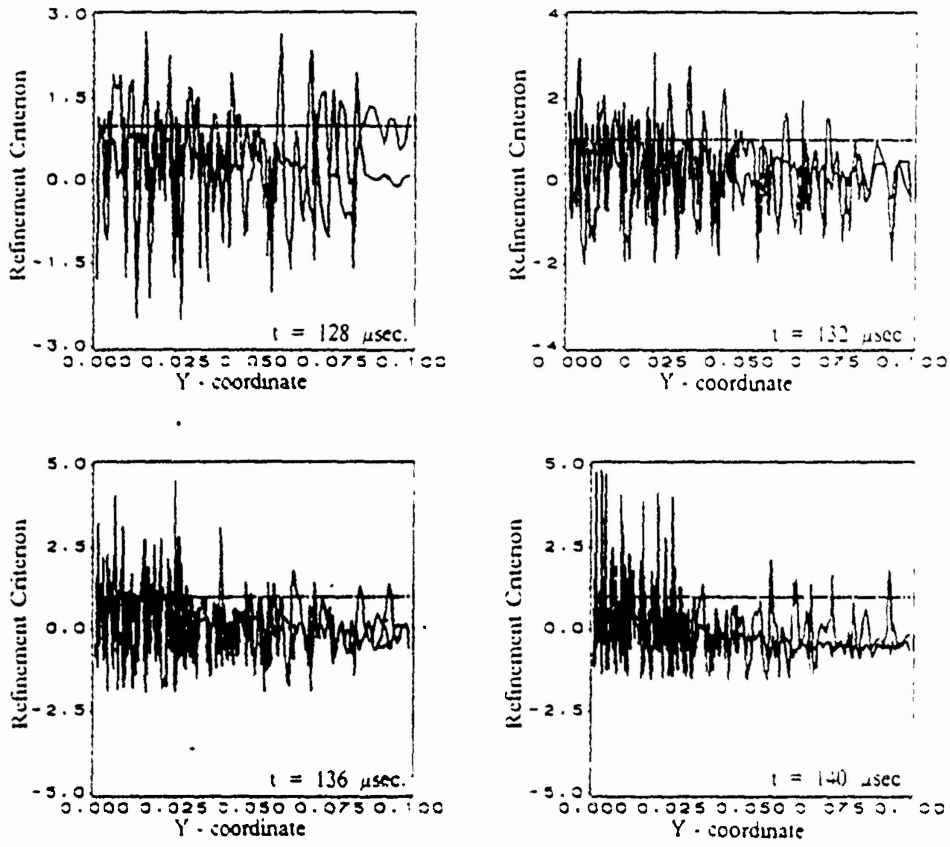

Figure 3. Distribution of the refinement criterion C_1 and C_2 at t = 128 μs, 132 μs, 136 μs, 140 μs. (Solid Line: Linear Momentum; Dotted Line: Internal Energy)

Figure 1 depicts the distribution of the refinement criteria C_1 and C_2 at t = 2 μs, 20 μs, 40 μs and 60 μs. Initially the distribution of scaled residuals in equations expressing the balance of linear momentum and the balance of internal energy require refinement of the mesh in different regions. However, for t ≥ 60 μs the scaled residuals in both equations are relatively high only near the center of the block. Thus, we have plotted in Figures 2 and 3 the distribution of C_1 and C_2 within $0 \le y \le 0.10$ at t = 80 μs, 100 μs, 120 μs, 124 μs, 128 μs, 132 μs, 136 μs and 140 μs. The values of C_1 and C_2 were less than 1.0 for y > 0.10 at the discrete values of t listed in the preceding sentence. For t = 80 μs, 100 μs, 120 μs and 124 μs C_2 varies smoothly and its magnitude does not change a great deal. Starting at t = 100 μs the values of C_1 oscillate quite a bit but are generally less than 1.0. This may be an indication of the initiation of the localization of the deformation. At t = 128 μs, 132 μs, 136 μs and 140 μs, the region where C_1 and C_2 undergo severe oscillations progressively narrows down to that near y = 0. At t = 136 μs and 140 μs both C_1 and C_2 are generally less than 1.0 for y ≥

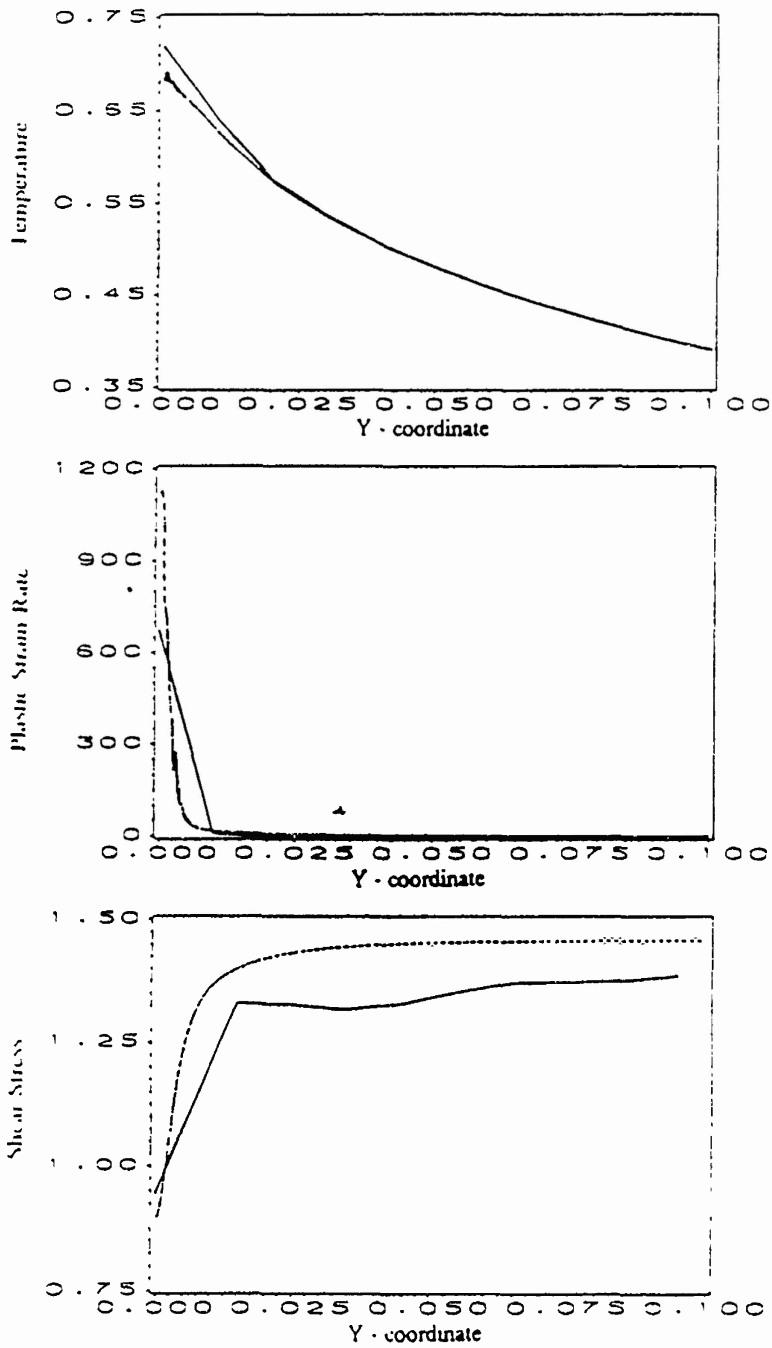

Figure 4. Spatial distribution of the temperature, shear stress and plastic strain at $\gamma_{avg} = 0.142$. (Solid Line: Uniform Mesh; Dotted Line: Refined Mesh)

0.025 implying thereby that some of the nodes could possibly be removed from this region. We are now in the process of adding to our code the capability to combine two or more elements into one and dividing one element into two or more elements depending upon the magnitude and sign of $(C_1 - 1.0)$ and $(C_2 - 1.0)$.

In order to see the improvement, if any, in the results computed with a mesh refined adaptively as compared to those computed with a uniform 100-element mesh we have plotted in Fig. 4 the spatial variation of the temperature, plastic strain-rate and the shear stress. These results confirm the expectation that the adaptively refined mesh can resolve sharp gradients of the deformation fields within the region of localization. From the distribution of the plastic strain-rate it is transparent that the width of the shear band as computed from the adaptively refined mesh is very small as compared to that with the uniform mesh. With the latter mesh it equals the size of one element cle indicating that the mesh is too coarse. Also with the uniform me oscillations in the value of the shear stress from node to node .. very large as compared to those with the adaptively refined mesh. The data plotted represents the average of the values at two consecutive nodes. These oscillations in the shear stress are probably due to the propagation of an unloading elastic shear wave out of the region of localization. The propagation of the wave is not clearly resolved because of the time integration scheme used herein.

5 Discussion and Conclusions

The use of an adaptive mesh refinement technique based on distributing the scaled residuals uniformly throughout the domain for solving the adiabatic shear band problem has enabled us to resolve adequately the sharp gradients of the deformation field within the region of localization. Initially, refinements of the mesh are required by the scaled residuals in the equations expressing the balance of internal energy and the balance of linear momentum. As the deformation begins to localize near the center of the block, the scaled residuals in the energy equation stay essentially equally distributed except when the localization is in progress earnestly However, the scaled residuals in the linear momentum equation oscillate and do necessitate the refinement of the mesh in several regions.

The computed results indicate that the mesh can be refined less frequently prior to the onset of the localization but ought to be refined very frequently subsequent to the initiation of the localization of the deformation. We are now working on the adaptive refinement of the mesh in the time domain

Acknowledgements This work was supported by the U.S National Science Foundation grant MSM-8715952, the U.S. Army Research Office Contract DAAL 03-88-K-0184, and the University of Missouri Weldon Spring Fund.

REFERENCES

1. C. Zener and J. H. Hollomon, J. Appl. Phys., 14, 22-32 (1944).
2. R. J. Clifton, U.S. NRC National Material Advisory Board Report NMAB-356, Herman, W., et al. eds. (1980).
3. Y. L. Bai, In: Shock Waves and High Strain - Rate Phenomena in Metals, Meyers, M. A , and Murr, L. E., eds., Plenum Press, New York (1981)
4. M. R. Staker, Acta Metall., 29, 683 (1981).
5. T. J. Burns, Q. Appl. Math., 43, 65-84 (1985).
6. L. Anand, K. H. Kim, and T. G. Shawki, J. Mechs. Phys. Solids, 35, 407-429 (1987).
7. T. W. Wright, J. Mechs. Phys. Solids, 35, 269-282 (1987).
8. L. S. Costin, E. E. Crisman, R. H. Hawley, and J. Duffy, Inst. Phys. Conf. Ser., 47, 90-100 (1979).
9. G. L. Moss, In: Shock Waves and High Strain-Rate Phenomenon in Metals, Meyers, M. A. and Murr, L. E., eds., Plenum Press, New York, pp. 299-312 (1981).
10. U. S. Lindholm and G. R. Johnson, In: Material Behavior Under High Stresses and Ultrahigh Loading Rates, Mescal, J. and Weiss, V , eds., 61-79 (1983).
11. A. Marchand and J Duffy, J. Mech. Phys. Solids, 36, 251-283 (1988).
12. R. J. Clifton, J Duffy, K. A. Hartley, and T. G. Shawki, Scripta Metall , 18 443 - 448 (1984).
13. T. W. Wright and R C. Batra, Int. J. Plasticity, 1, 205-212 (1985).
14. T. W. Wright and J Walter, J. Mech. Phys. Solids, 35, 701-716 (1987)
15. R. C. Batra, Int. J. Plasticity, 3, 75-89 (1987).
16. R. C. Batra, and C. H. Kim, Int. J. Plasticity, (in press).
17. A. Needleman, J. Appl. Mechs., 56, 1-9 (1989).
18. R. C. Batra and De-Shin Liu, J. Appl. Mechs., 56, 527-534 (1989).
19. A. Needleman, Comp. Meth. Appl. Mech. Eng., 67, 69-85 (1988).
20. D. A. Drew and J. E. Flaherty, In: Phase Transformations and Material Instabilities in Solids, M. E. Gurtin, ed., Academic Press, pp. 37-60 (1984).
21. M. M. Pervaiz and J R. Baron, Comm. Appl. Num. Meth., 4, 97-111 (1988).
22. T. J. R. Hughes, The Finite Element Method, Linear Static and Dynamic Finite Element Analysis, Prentice Hall, Englewood Cliffs (1987)
23. G. F. Carey and J T Oden, Finite Elements, Computational Aspects, Vol 3, Prentice Hall, Englewood Cliffs (1984)

J. Mech. Phys. Solids Vol. 38, No. 6, pp. 859–874, 1990
Printed in Great Britain

0022-5096/90 $3.00 + 0.00

EFFECT OF VISCOPLASTIC FLOW RULES ON THE INITIATION AND GROWTH OF SHEAR BANDS AT HIGH STRAIN RATES

R. C. BATRA and C. H. KIM

Department of Mechanical and Aerospace Engineering and Engineering Mechanics, University of Missouri-Rolla, Rolla, MO 65401-0249, U.S.A.

(*Received* 3 *July* 1989; *in revised form* 30 *October* 1989)

ABSTRACT

MARCHAND and Duffy have reported detailed measurements of the temperature and strain as a shear band develops in a HY-100 steel. Assuming their torsional tests in thin-wall tubes can be adequately modeled by a viscoplastic block undergoing overall adiabatic simple shearing deformations, we investigate the effect of modeling the viscoplastic response of the material by a power law, and flow rules proposed by Litonski, Bodner and Partom, and Johnson and Cook. Each of these flow rules is first calibrated by using the test data at a nominal strain-rate of 3300 s^{-1}. Then predictions from the use of these flow rules at nominal strain-rates of 1400 s^{-1} and 1600 s^{-1} are compared with the experimental findings. It is found that the Bodner–Partom law and the dipolar theory proposed by Wright and Batra predict reasonably well the main features of the shear band formation in a HY-100 steel.

1. INTRODUCTION

THE DEVELOPMENT of shear bands in metals undergoing plastic deformations at high strain-rates usually precedes shear fractures. For this and other reasons their study has received considerable attention during the last ten years. ROGERS (1983) and TIMOTHY (1987) have surveyed various aspects of shear banding. BAI (1981), CLIFTON (1980) and BURNS (1985) among others have investigated conditions which will lead to the growth or decay of perturbations superimposed on a viscoplastic body deformed homogeneously in simple shear. MOLINARI and CLIFTON (1987), TZAVARAS (1987) and WRIGHT (1990) have studied the problem in greater detail. For rigid perfectly plastic materials, WRIGHT (1990) has developed a criterion that ranks materials according to their tendency to form adiabatic shear bands.

The numerical study of shear banding has been conducted, among others, by SHAWKI *et al.* (1983), WRIGHT and BATRA (1985), BATRA (1987), BATRA and KIM (1990), ANAND *et al.* (1988), NEEDLEMAN (1989), LEMONDS and NEEDLEMAN (1986a, 1986b), and BATRA and LIU (1989). These works have employed different viscoplastic flow rules and have examined, qualitatively, different aspects of shear banding in simple shearing and plane-strain compression problems. A material inhomogeneity or defect has been simulated by either introducing a temperature perturbation or assuming the existence of weak material at the site of the defect.

Most of the earlier experimental work (e.g. Zener and Hollomon, 1944, Moss, 1981, Costin *et al.*, 1980) has reported observations made after the shear band had formed. Recently Hartley *et al.* (1987), Giovanola (1987), and Marchand and Duffy (1988) have given histories of the temperature and strain within a band as it develops. This facilitates a detailed comparison of the numerical and experimental results undertaken here. We presume that the torsional experiments of Marchand and Duffy (1988) on thin-wall steel tubes can be analysed by studying the thermomechanical deformations of a viscoplastic block undergoing overall adiabatic simple shearing deformations. We consider four different flow rules, namely the power law (e.g. see Shawki *et al.*, 1983), and those due to Litonski (1977), Bodner and Partom (1975), and Johnson and Cook (1983). Also, because of the presence of steep strain gradients near the edges of the shear band, we consider the effect of including strain gradients and the corresponding dipolar stresses in the analysis. We note that Wright and Batra (1987), Coleman and Hodgdon (1985), and Zbib and Aifantis (1988) have considered the effect of strain gradients in their works. Dillon and Kratochvil (1970) motivated the consideration of strain gradients and dipolar stresses as one way to account for the interaction among dislocations.

The computed results show that the dipolar theory predicts, quantitatively, various experimentally observed features of shear banding very well. The Bodner–Partom law for nonpolar materials also predicts well the initial growth of the shear band. Other flow rules fail to predict, in a noticeable way, one or more aspects of experimental results. This should not be taken as the final word for these viscoplastic laws since our calibration technique used to find values of various material parameters involves solving a nonlinear coupled thermomechanical initial-boundary-value problem and we may get the same stress–strain curve for different combinations of the values of material parameters. Nevertheless, the computed results do favor exploring further refinements of the dipolar theory and the Bodner–Partom law.

2 Formulation of the Problem

A realistic modeling of Marchand and Duffy's (1988) experiments on the twisting of thin-wall tubes requires analysing three-dimensional thermomechanical dynamic deformations of a viscoplastic body. Postponing this ultimate goal and striving to find the most appropriate viscoplastic flow rule, we study here dynamic thermomechanical deformations of a viscoplastic block undergoing overall adiabatic simple shearing deformations. In terms of non-dimensional variables, the governing equations can be written as (e.g. see Batra, 1987)

$$\rho v = (s - l\sigma)_{,Y}, \quad 0 < Y < 1, \tag{2.1}$$

$$\theta = k\theta_{,YY} - s\dot{\gamma}_p - l\sigma\dot{d}_p, \quad 0 < Y < 1, \tag{2.2}$$

$$s = \mu(v_{,Y} - \dot{\gamma}_p), \tag{2.3}$$

$$\sigma = \mu l(v_{,YY} - \dot{d}_p), \tag{2.4}$$

$$\dot{\gamma}_p = g(s, \sigma, \gamma_p, d_p, \theta, l), \tag{2.5}$$

$$d_p = lh(s, \sigma, \gamma_p, d_p, \theta, l). \tag{2.6}$$

These equations, written for dipolar materials, reduce to those for nonpolar materials when l is set equal to zero. Here ρ is the mass density, v is the velocity of a material particle in the direction of shearing, a superimposed dot indicates the material time derivative, s is the shearing stress, l a material characteristic length, σ the dipolar stress, and a comma followed by y signifies partial differentiation with respect to y. Furthermore, k is the thermal conductivity, γ_p is the plastic strain-rate, d_p the dipolar plastic strain-rate, μ the shear modulus, and θ is the temperature change from that in the reference configuration. Whereas (2.1) expresses the balance of linear momentum and (2.2) the balance of internal energy, (2.3)–(2.6) are constitutive relations. The different viscoplastic flow rules differ in the functional forms of g and h and are discussed below in the next section.

For the initial conditions we take

$$v(y, 0) = 0, s(y, 0) = 0, \sigma(y, 0) = 0,$$

$$\theta(y, 0) = a(1 - y^2)^n e^{-y^2/\varepsilon^2} \tag{2.7}$$

That is, in the initial rest state of the block, it is taken to be stress free. The initial temperature distribution simulates the defect or inhomogeneity in the block assumed to be present near the point $y = 0$; the value of ε represents the strength of the defect.

We presume that the overall deformations of the block are adiabatic and the lower surface is at rest while the upper surface is assigned a velocity that increases linearly from 0 to 1 in time t_r and then stays at the constant value of 1.0. Thus,

$$\theta_{,y}(0, t) = 0, \theta_{,y}(1, t) = 0, v(0, t) = 0, \tag{2.8}$$

$$v(1, t) = t/t_r, \quad 0 \leqslant t \leqslant t_r,$$

$$= 1, \quad t \geqslant t_r \tag{2.9}$$

and for dipolar materials, we also assume that

$$\sigma(0, t) = 0, \quad \sigma(1, t) = 0 \tag{2.10}$$

Computations for the domain $-1 \leqslant y \leqslant 1$ and with boundary conditions $\sigma(-1, t) = 0$, $\sigma(1, t) = 0$ have given $\sigma(0, t) = 0$.

3 Viscoplastic Flow Rules

3.1 *Litonski's law for nonpolar and dipolar materials*

Wright and Batra (1987) generalized the constitutive relation proposed by Litonski (1977) to be applicable to nonpolar and dipolar materials. They assumed that

$$\gamma_p = \lambda s, \quad d_p = \frac{\lambda}{l}\sigma \tag{3.1}$$

and postulated that

$$\Lambda = \max\left[0, \left\{\left(\frac{s_e}{(1-\chi\theta)\left(1+\frac{\psi}{\psi_0}\right)^n}\right)^m - 1\right\}\frac{1}{bs_e}\right], \tag{3.2}$$

$$s_e = (s^2+\sigma^2)^{1/2}, \tag{3.3}$$

$$\dot{\psi} = \Lambda s_e^2 \left(1+\frac{\psi}{\psi_0}\right)^n. \tag{3.4}$$

Here ψ may be viewed as an internal variable that describes the work hardening of the material. Its evolution is given by (3.4). In (3.2), $(1-\chi\theta)$ describes the softening of the material due to its heating, b and m characterize its strain-rate hardening, and ψ_0 and n its work hardening. Note that the rate of growth of ψ is proportional to the plastic working. Besides the yield stress in a quasistatic simple shearing test which has been used to non-dimensionalize stress-like quantities, there are five material parameters χ, b, m, ψ_0 and n. For dipolar materials, we also need to specify l.

In (3.2)–(3.4) it is implicitly assumed that

$$s_e = (1-\chi\theta)\left(1+\frac{\psi}{\psi_0}\right)^n \tag{3.5}$$

describes the loading surface, and if the local state given by $(s, \sigma, \psi, \theta)$ lies inside or on this surface, the plastic strain-rate and the dipolar plastic strain-rate vanish.

3.2. *Power law*

For nonpolar materials, COSTIN *et al.* (1980) and MARCHAND and DUFFY (1988) have described the dynamic stress–strain curve for steels as

$$s = \left(\frac{\gamma}{\gamma_0}\right)^n \left(\frac{\dot{\gamma}}{\dot{\gamma}_0}\right)^m \left(\frac{\theta}{\theta_0}\right)^\nu. \tag{3.6}$$

Here γ_0 is the strain at yield in a quasistatic simple shear test for which $\dot{\gamma}_0 = 10^{-3}$ s^{-1}, θ_0 is the reference temperature and θ the current temperature of a material particle in degrees Kelvin. In order to use the power law, we assumed that there is no loading surface and that

$$\dot{\gamma} = \dot{\gamma}_0 \left(\frac{\gamma}{\gamma_0}\right)^{n/m} \left(\frac{\theta}{\theta_0}\right)^{\nu/m}. \tag{3.7}$$

Thus in addition to the yield stress in a quasistatic simple shear test, there are five material parameters $\dot{\gamma}_0$, θ_0, m, n and ν.

3.3. *Bodner–Partom law*

For nonpolar materials undergoing simple shearing deformations, the constitutive relation proposed by BODNER and PARTOM (1975) can be written as

$$\dot{\gamma}_p = D_0 \exp\left[-\frac{1}{2}\left(\frac{K^2}{3s^2}\right)^n\right], \quad n = \frac{a}{\theta} + b, \tag{3.8}$$

$$K = K_1 - (K_1 - K_0)\exp(-mW_p) \tag{3.9}$$

Here θ is the absolute temperature of a material particle, W_p is the plastic work done, and K may be considered as an internal variable. D_0 is the limiting value of the plastic strain-rate and is generally set equal to $10^8\ s^{-1}$. Besides D_0, we need to specify a, K_1, K_0, m and b to characterize the material. We note that there is no loading or yield surface assumed in this case also.

3.4. *Johnson–Cook law*

JOHNSON and COOK (1983) tested several materials in simple shear and compression at different strain-rates and found that

$$\dot{\gamma}_p = \exp\left[\left\{\frac{1}{(A + B\dot{\gamma}_p^n)(1 - T^x)} - 1.0\right\}\frac{1}{c}\right], \tag{3.10}$$

$$T = (\theta - \theta_0)/(\theta_m - \theta_0), \tag{3.11}$$

describe well the test data. Here A, B, n, x, c and θ_m are to be determined experimentally. For θ_m equal to the melting temperature of the material and θ_0 equal to the ambient temperature, they tabulated values of other parameters for several materials. The relation (3.10) is valid for nonpolar materials and presumes that there is no loading surface.

4. CALIBRATION PROCEDURE

4.1. *Determination of material parameters*

For HY-100 structural steel, MARCHAND and DUFFY (1988) have given the dynamic and quasistatic shear stress–shear strain curves found at strain-rates of $3300\ s^{-1}$ and $10^{-4}\ s^{-1}$ respectively. They also reported the values of the exponents m, n and ν for the power law

In order to calibrate the various flow rules against the same test data we solved, numerically, the initial-boundary value problem outline in Section 2 with

$$v(Y,0) = 1.0, \quad \dot{\gamma}_p(Y,0) = 0.012, \quad v(1,t) = V, \quad \theta(1,0) = 0\ C, \quad = 0,$$

$$v(1,t) = 1.0, \quad \dot{\gamma}(0,t) = 0, \quad \theta\ (0,t) = 0, \quad \theta\ (1,t) = 0, \quad \rho = 7860\ kg\ m$$

$$c = 473\ J/kg\ C, \quad k = 49.73\ W\ m^{-1}\ C, \quad H = 2.5\ mm, \quad = 3300\ s$$

Here H is the height of the block and $$ is the average applied strain-rate. With no initial temperature perturbation, the block deforms uniformly and homogeneously and the dipolar effects vanish identically. In order to keep to a minimum the number of parameters to be varied, we kept, as far as possible, the values of the strain-hardening exponent and the strain-rate hardening exponent equal to those given by

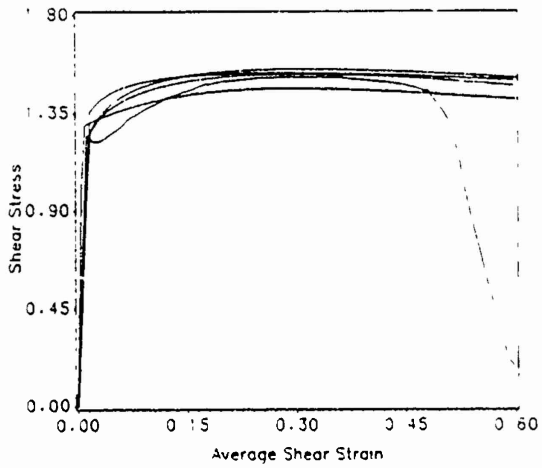

FIG. 1. A comparison of the shear stress–shear strain curves computed by solving an initial-boundary value problem with different flow rules with the experimental stress–strain curve of Marchand and Duffy at a nominal strain-rate of 3300 s^{-1} for a HY-100 structural steel. ——— experimental, – – Bodner–Partom, Litonski (non-polar), – – Litonski (dipolar), — – — Power, — – – Johnson–Cook.

MARCHAND and DUFFY (1988), and adjusted the values of parameters describing the thermal softening of the material till the computed stress–strain curve came out close to that given by Marchand and Duffy. For curves depicted in Fig. 1, we used the following values of various material parameters. Note that these curves approximate closely the experimental curve well beyond the value of the nominal strain at which the peak in the stress occurs.

(a) Litonski law for nonpolar and dipolar materials.

$$\alpha = 0.00185 \text{ C}, \quad \psi_0 = 0.012, \quad n = 0.107, \quad m = 0.0117, \quad b = 10^{-4}\text{ s}, \quad \gamma = 0.005$$

(b) Power law

$$\dot{\varepsilon}_0 = 10^{-4}\text{ s}^{-1}, \quad \varepsilon_0 = 0.012, \quad \theta_0 = 300\text{K}, \quad m = 0.0117, \quad n = 0.107, \quad \gamma = -0.75$$

(c) Bodner–Partom law

$$a = 1200\text{K}, \; b = 0, \; K_1 = 3.95, \; K_0 = 3.21, \; m = 5.0, \; D_1 = 10^4\text{ s}^{-1}$$

(d) Johnson–Cook law

$$A = 0.45, \; B = 1.433, \; n = 0.107, \; \theta_m - \theta_0 = 1200\text{ C}, \; \alpha = 0.7, \; \dot{\varepsilon}_0 = 0.0277$$

We note that the computed curves mimic reasonably well the experimental one till the shear stress begins to drop catastrophically. This rapid drop of the shear stress with increasing shear strain starting with an average strain of 0.50 in the experimental stress–strain curve is due to the initiation and growth of a shear band. We need to simulate a defect in the specimen in order to reproduce this part of the curve.

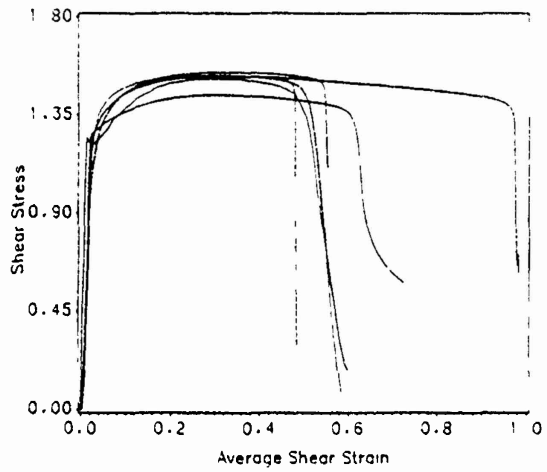

FIG. 2. Shear stress–shear strain curves computed with different flow rules but with the same initial temperature perturbation. See Fig. 1 for the description of various curves.

4.2. *Determination of the size of the perturbation*

MARCHAND and DUFFY (1988) found that the thickness of their specimens was uniform in the circumferential direction but varied from 5–10% in the axial direction. This and possibly the slight variation in the material properties served as the triggering mechanism for the initiation of a shear band. Here we model the cumulative effect of these inhomogeneities by assuming a nonuniform initial temperature distribution as given by Eq. (2.7). BATRA and LIU (1990) have shown that different ways of modeling a material inhomogeneity give similar results.

Ideally, the same value of a in (2.7) when used with different flow rules should initiate a shear band, as indicated by the rapid drop of the shear stress, at the value of the nominal strain observed experimentally. Unfortunately, as shown in Fig. 2, for $a = 1$ C, different flow rules predict shear band initiation at widely different values of the nominal strain. No value of a could be found that will cause the shear band to initiate at the same value of the nominal strain with the different flow rules. We thus have the following two choices. One, to use different values of a with the various flow rules and the other, to fix a and find the values of material parameters so as to match the computed stress–strain curves with and without the temperature perturbation with the corresponding experimental ones. This would necessitate changing the values of the strain hardening exponent and or strain-rate hardening exponent also. This program, though feasible, is very arduous and could be interpreted as manipulating parameters to obtain the desired results. We note in passing that for presumably the same experimental data, HARTLEY *et al.* (1987), KLEPACZKO *et al.* (1987) and MOLINARI and CLIFTON (1987), have given different values of the strain hardening exponent, strain-rate hardening exponent and the thermal softening exponent in the power law. This alludes to the difficulty in obtaining values of various material parameters. Here we adopt the first approach and find a so that different flow rules

cause the band to initiate at approximately the same value of the nominal strain This is justifiable because we compare computed results with experimental findings mostly during the growth of the localization process, i.e. post initiation period. Also, we note that the calibration is done at a nominal strain-rate of 3300 s^{-1}, and the comparison of results is made for deformations occurring at nominal strains of 1600 s^{-1} and 1400 s^{-1} For an assigned value of α, the initial-boundary value problem outlined in Section 2 with $t_r = 0.033$ was solved by the finite element method. Values of α equal to 1 C, 2 C, 5 C and 9 C for the Litonski law for nonpolar and dipolar materials, power law, the Bodner–Partom law and the Johnson–Cook law, respectively, result in stress–strain curves shown in Fig. 3. Subsequently, these values of α for the various flow rules were used.

5 Comparison of Numerical Results with Experimental Findings

The curves plotted in Fig. 3 vividly reveal that until the time the shear stress begins to drop rapidly, all of the flow rules considered predict material behavior in reasonable agreement with the experimental observations For nonpolar materials Litonski's law, the power law and the Johnson–Cook law give essentially a catastrophic drop in the shear stress with virtually no increase in the nominal shear strain. This does not agree with the experimental data since Marchand and Duffy observed that during the drop of the shear stress, the nominal strain increases by approximately 5%. The Litonski law for dipolar materials and the Bodner-Partom law for nonpolar materials do predict the gradual drop in the shear stress in agreement with the experimental data. However, for the Bodner–Partom law the shear stress does not drop as much as it

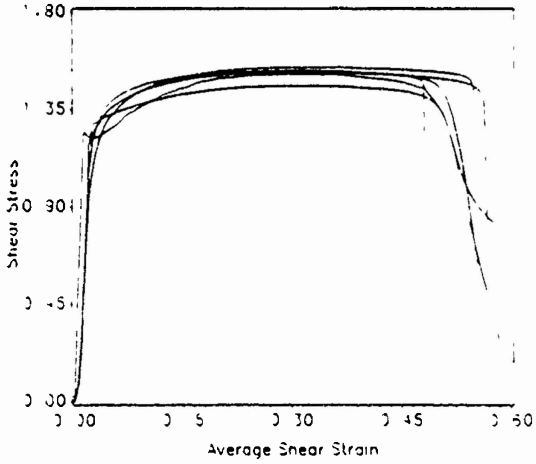

Fig. 3 Shear stress–shear strain curves computed with different flow rules and with different initial temperature perturbation The objective is to find the size of the initial temperature perturbation in order to initiate a rapid drop of the shear stress at an average strain close to that found experimentally See Fig 1 for the description of various curves

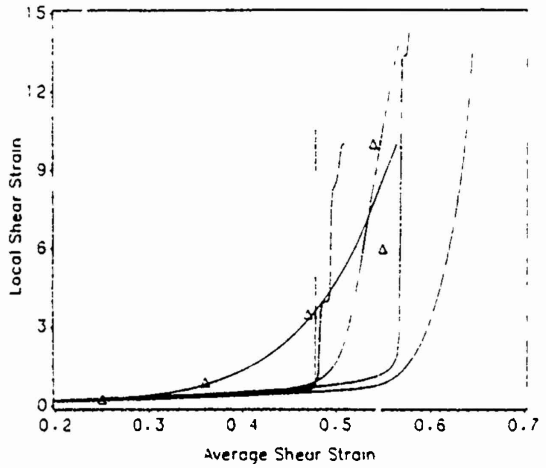

FIG. 4. Growth of the local shear strain within the band as the specimen deforms. See Fig. 1 for the description of various curves. The experimental data points are denoted by a Δ.

does during the tests. The computed value of the shear stress reaches a plateau. Since curves plotted in Fig. 3 were for calibration purposes, these remarks should be regarded as general observations rather than a test of the validity of any of the flow rules.

For a nominal strain-rate of 1600 s^{-1}, Marchand and Duffy have also given values of the shear strain within the band at five different values of the nominal strain. We note that each data point was obtained in a different test and that explains the rather noticeable difference in the values of the local strain within the band for essentially the same value of the nominal strain for the last two data points. These and the corresponding numerically computed results with the different flow rules are plotted in Fig. 4. Whereas the Litonski law, the power law and the Johnson–Cook law give a rapid increase in the local strain once a shear band initiates, the Bodner–Partom law and the Litonski law for dipolar materials give general trends in agreement with the experimental data. We should add that the values of the material parameters and the size of the temperature perturbation were those found earlier and outlined in the preceding section. Also, the computed local strain equals the strain at the center.

With the power law and the Johnson–Cook law, the plastic strain started to oscillate during the time the shear stress was dropping. This was earlier pointed out by BATRA and KIM (1990) and has also been noticed by WRIGHT and WALTER (1989). A possible explanation for this is the interplay between the material hardening due to the strain and strain-rate effects and the thermal softening. This explains the discontinuities in the curves computed with these two flow rules.

The experimental data points plotted in Fig. 5 were taken from the data given in table 4 of Marchand and Duffy's paper. Each data point represents a different test performed at an average strain-rate of approximately 1600 s^{-1}. Since the nominal strain γ^*_{ave} at which the shear stress attained the maximum value τ_{max} is different in each test we have plotted in Fig. 5 $\gamma_{ave}/\gamma^*_{ave}$ vs τ/τ_{max} during the time the shear stress is

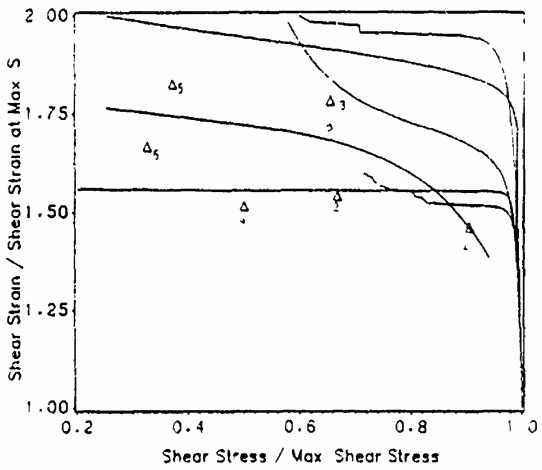

FIG. 5. Plot of normalized shear strain vs the normalized shear stress during the time shear stress is dropping with increasing strain. See Fig. 1 for the description of various curves.

dropping. There is too much scatter in the experimental data to draw any conclusions. Since test points 2 and 3 have abscissa values 0.6667 and 0.6546, we take the midpoint P on the line joining these two points as representing the average of the results for these two tests. If we take the smooth curve passing through the test point 1, point P and the midpoint of the line joining points 5 and 6, we obtain a curve essentially parallel to that computed with the Bodner–Partom law and the Litonski law for dipolar materials. The scarcity of the available experimental data makes a better comparison difficult at this time.

Figures 6–8 depict, respectively, the spatial variation of the plastic strain, the temperature and the flux of linear momentum when $s = s_{max} = 0.667$ and $t_{ave} = 1600$ s. We note that the flux of linear momentum equals the shear stress for nonpolar materials and $(s - l\sigma')$ for dipolar materials. By the time the momentum flux drops to two-thirds of its maximum value, the shear band should have well developed. In order to highlight the variation of the shear strain, temperature and the shear stress within and near the region of localization of the deformation, we have plotted these quantities on an expanded scale in the region around the shear band center. Both the Johnson–Cook law and the Litonski law for nonpolar materials predict a rather sharp drop in the shear strain at the edges of the band. The Litonski law for dipolar materials gives nearly constant values of the temperature and shear strain within the band. The power law and the Bodner–Partom law give a rather gradual drop of the shear strain and the temperature with the distance from the center of the band. With the dipolar theory the momentum flux takes on the least value at the band center and increases rapidly as we move away from the center and then decreases and stays constant through most of the specimen. The Johnson–Cook law gives a slightly higher value of the shear stress at the center of the band as compared to that at the specimen boundary and the rate of change of the shear stress is constant. With the other flow rules the computed values of the shear stress came out to be essentially constant throughout the specimen.

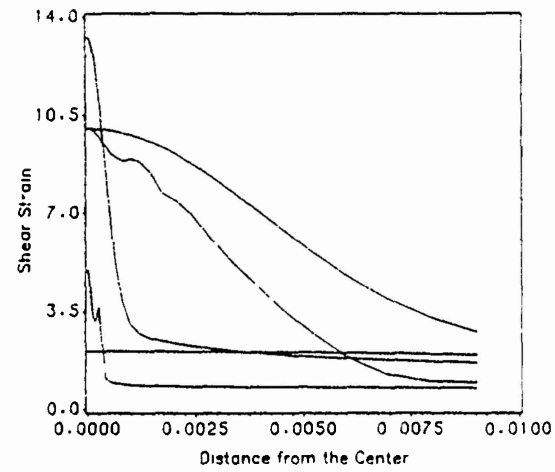

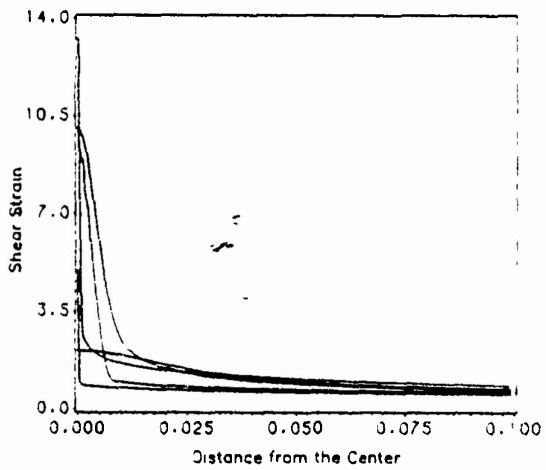

FIG. 6. Spatial variation of the plastic strain when $\gamma/\gamma_{max} \approx 0.667$. See Fig. 1 for the description of various curves.

Defining the band width as the width of the region over which the plastic shear strain varies by no more than 5% of its value at the center, the computed bandwidth with the Litonski law, the power law, the Bodner–Partom law, the Johnson–Cook law, and the Litonski law for dipolar materials is found to be 2 μm, 14 μm, 14 μm, 6 μm and 51 μm respectively. For $\gamma/\gamma_{max} = 0.66$, Marchand and Duffy found the bandwidth to be between 20 μm and 55 μm depending upon the point of observation around the circumference of the tube. This comparison favors the Bodner–Partom law, the power law and the Litonski law for dipolar materials over the other two flow rules.

In another series of tests on HY-100 steel conducted at a nominal strain-rate of approximately 1400 s^{-1}, Marchand and Duffy measured the temperature within the

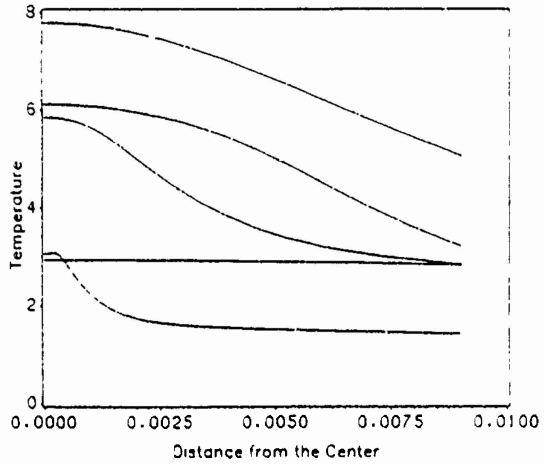

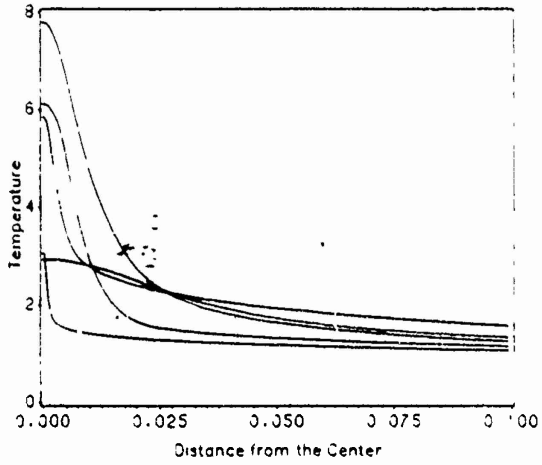

FIG. 7. Spatial variation of the temperature when $\gamma_{max} \simeq 0.667$. See Fig. 1 for the description of various curves. The temperature in °C is obtained by multiplying the nondimensional value by 1089.

band. The data taken from table 5 of their paper is plotted in Fig. 9 along with the computed results for $\dot{\gamma}_0 = 1400\ s^{-1}$. They measured the temperature over a spot width of 35 μm which is larger than the band width. In plotting their data, we have assumed that the reported temperature in the band occurred at the maximum value of the nominal strain in a test. In order to minimize the variation in the results among different tests we have plotted the measured maximum temperature in the band vs $\dot{\gamma}_{ave}/\dot{\gamma}_{ave}^*$. Even though it is hard to draw a smooth curve through the test data, the detector output plotted in fig. 19 of Marchand and Duffy's paper reveals that the temperature rises during the last stage of the localization process when the shear stress is dropping and that the increase in the average strain during the time temperature rises is about 8%. This observation is in closer agreement with the results computed

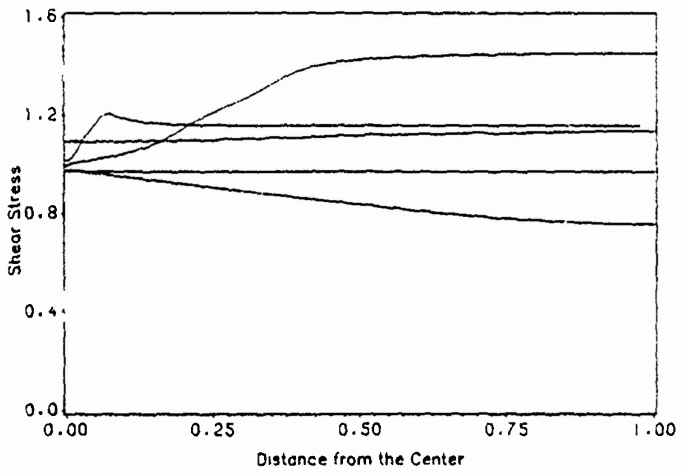

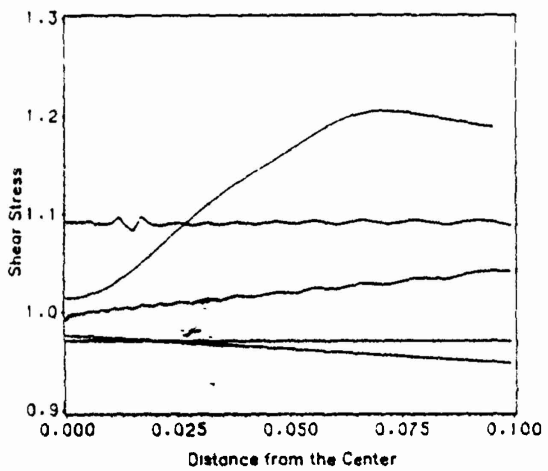

FIG. . Spatial description of the flux of linear momentum when $s/s_{max} \simeq 0.667$ See Fig 1 for the description of various curves

with the Litonski law for dipolar materials. Also the computed temperature rise of 539 C with this flow rule when $\tau_e/\tau_e^* = 1.91$ agrees well with the average value of 475 C found in the eight tests. We should note that the computed temperature within the band of 50 μm width came out to be nearly uniform. Marchand and Duffy estimated that the maximum temperature in the band reached a little over 900 C. Since we do not have any failure criterion included in our work, it is hard to decide when to stop the computations and thus estimate the maximum temperature rise.

Figure 10 shows how the temperature at the center increases after the peak in the shear stress has been attained. It is interesting to note that the temperature, when the shear stress attains the maximum value, is essentially the same for all flow rules. However, the rate of rise of temperature with the drop in the shear stress for the

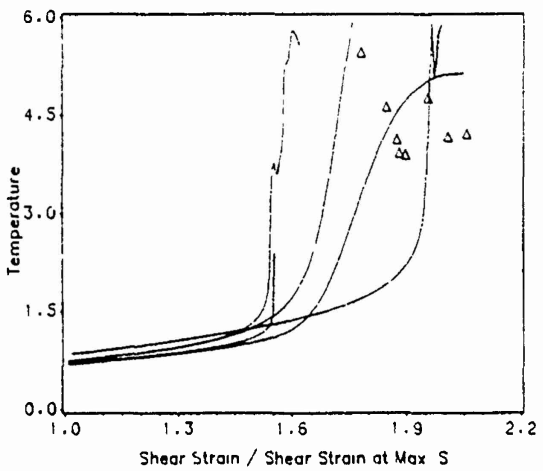

FIG. 9. Temperature at the center vs the normalized shear strain. The experimental data points are denoted by a Δ. See Fig. 1 for the description of various curves.

Johnson–Cook law, the power law and the Bodner–Partom law is nearly the same but differs significantly from that for the Litonski law for nonpolar and dipolar materials. The transition in the slope of the curves near $\gamma/\gamma_{max} = 1.0$ indicates the point when the rapid drop in the shear stress occurs and the plastic strain rate rises sharply. Thus, the computed temperature rise will depend upon the point when the material is taken to have failed. As pointed out by Marchand and Duffy, once the shear stress begins to collapse, the load carrying capacity of the member is drastically reduced and the material has failed.

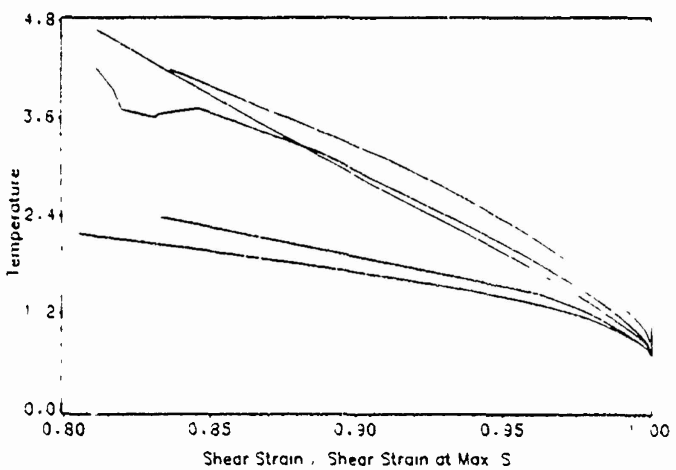

FIG. 10. The evolution of the temperature at the center vs the normalized shear strain during the time the shear stress is dropping. See Fig. 1 for the description of various curves.

6. Conclusions

We have modeled the dynamic torsional tests of Marchand and Duffy on thin-wall steel tubes by analysing the dynamic deformations of a viscoplastic block undergoing overall simple shearing deformations. A material defect or inhomogeneity has been represented by an initial nonuniform temperature distribution. The focus of the work has been to compare predictions of the various flow rules with the experimental findings during the growth of a shear band. For this purpose, we have also used a dipolar theory and Litonski's flow rule as modified by Wright and Batra and studied extensively by Batra and his coworkers. Whereas it maybe premature to draw definitive conclusions, the Bodner–Partom law and the dipolar theory predict many features of shear banding that are in closer agreement with the experimental observations than the predictions from the power law, the Johnson–Cook law and the Litonski law for nonpolar materials. We note that when finding the values of material parameters for different flow rules, we kept the value of the strain hardening exponent and the strain-rate hardening exponent as close to the test value as possible and varied the parameter describing the thermal softening of the material till the computed stress–strain curve essentially replicated the corresponding experimental curve for nominal strain-rate equal to 3300 s^{-1}. With values of material parameters kept unchanged, computed results for nominal strains equal to 1600 s^{-1} and 1400 s^{-1} were compared with the corresponding experimental findings.

Acknowledgements

This work was supported by the U.S. National Science Foundation Grant No. MSM8715952 and the Army Research Office Contract DAAL03-88-K-0184 to the University of Missouri-Rolla. The computations were performed on the IBM 3090-160 vector machine in Columbia, MO under the IBM trial program.

References

Anand, L., Lush, A. M. and Kim, K. H. 1988 In *Thermal Aspects in Manufacturing* (edited by M. H. Attia and L. Kops) ASME-PED-Vol. 30, 89.

Bai, Y. L. 1981 In *Shock Waves and High Strain-Rate Phenomenon in Metals* p. 277 (edited by M. A. Meyers and L. E. Murr) Plenum Press, New York.

Batra, R. C. 1987 *Int. J. Plasticity* **3**, 75.

Batra, R. C. and Kim, C. H. 1990 *Int. J. Plasticity* **6**, 127.

Batra, R. C. and Liu, Di-Shin 1989 *J. appl. Mech.* **56**, 527.

Batra, R. C. and Liu, De-Shin 1990 *Int. J. Plasticity* **6**, 231.

Bodner, S. R. and Partom, Y. 1975 *J. appl. Mech.* **42**, 385.

Burns, T. J. 1985 *Q. appl. Math.* **43**, 65.

Clifton, R. J. 1980 Adiabatic shear in material response to ultrahigh loading rates. U.S. NRC National Material Advisory Board Report NMAB-356 (edited by W. Herrman *et al.*).

Coleman, B. D. and Hodgdon, M. L. 1985 *Arch. ration. Mech. Anal.* **90**, 219.

COSTIN, L. S., CRISMAN, E. E., HAWLEY, R. H. and DUFFY, J	1980	In *Mechanical Properties at High Strain Rates* p 90 (edited by J HARDING) Proc 2nd Oxford Conf. Inst. Phys., London
DILLON, O W and KRATOCHVIL, J.	1970	*Int J. Solids Struct* **6**, 1513
GIOVANOLA, J.	1987	Proc. Impact Loading and Dynamic Behavior of Materials, Bremen, F R.G.
HARTLEY, K. A., DUFFY, J. and HAWLEY, R. H.	1987	*J. Mech Phys Solids* **35**, 283
JOHNSON, G. R. and COOK, W. H.	1983	In *Proc 7th Int. Symp Ballistics*, The Hague, The Netherlands, p 1
KLEPACZKO, J. R., LIPINSKI, P and MOLINARI, A.	1987	In *Proc Impact Loading and Dynamic Behaviour of Materials*, p 695 (edited by C Y CHIEM, H. D KUNZE and L. W MEYER). Informationsgesellschaft, Bremen, F R G., 1987
LEMONDS, J. and NEEDLEMAN, A.	1986a	*Mech. Mater* **5**, 339
LEMONDS, J. and NEEDLEMAN, A	1986b	*Mech. Mater* **5**, 363
LITONSKI, J	1977	In *Bulletin de l'Académie Polonaise des Sciences*, Sciences Tech., Vol 25, 7
MARCHAND, A. and DUFFY, J	1988	*J Mech Phys Solids* **36**, 251
MOLINARI, A. and CLIFTON, R J	1987	*J appl Mech.* **54**, 806
MOSS, G L.	1981	In *Shock Waves and High Strain Rate Phenomenon in Metals*, p. 229 (edited by M A MEYERS and L. E. MURR). Plenum Press, New York
NEEDLEMAN, A.	1989	*J appl Mech.* **56**, 1
ROGERS, H. C.	1983	In *Material Behavior Under High Stress and Ultrahigh Loading Rates*, p 101 (edited by J MESCALL and V WEISS). Plenum Press, New York.
SHAWKI, T G., CLIFTON, R. J and MAJDA, G.	1983	Analysis of shear strain localization in thermal visco-plastic materials, Brown Univ Report ARO DAAG29-81-K-0121 3
TIMOTHY, S. P	1987	*Acta Metall.* **35**, 301
TZAVARAS, A. E.	1987	*Archs ration. Mech Anal.* **99**, 349
WRIGHT, T W	1990	*J Mech Phys Solids* **38**, 515
WRIGHT, T W and BATRA, R. C	1985	*Int J Plasticity* **1**, 205
WRIGHT, T W and BATRA, R C	1987	In *Proc Macro- and Micro-Mechanics of High Velocity Deformation and fracture*, IUTAM Symp., Tokyo Aug 1985 p 189
WRIGHT, T W and WALTER, J W	1989	Adiabatic shear bands in one-dimension, Ballistic Research Laboratory Report BRL-MR-3759
ZBIB, H M and AIFANTIS, E C	1988	*Scripta Metall* **20**, 703
ZENER, C and HOLLOMON, J H	1944	*J appl Phys* **15**, 22

Acta Mechanica 84, 89—107 (1990)

ACTA MECHANICA

Dynamic shear band development in plane strain compression of a viscoplastic body containing a rigid inclusion

Z. G. Zhu and R. C. Batra, Rolla, Missouri

(Received October 18, 1989; revised January 3, 1990)

Summary. We study the plane strain thermomechanical deformations of a viscoplastic body containing a rigid non-heat-conducting ellipsoidal inclusion at the center. Two different problems, one in which the major axis of the inclusion is parallel to the axis of compression and the other in which it is perpendicular to the loading axis are considered. In each case the deformations are presumed to be symmetric about the two centroidal axes and consequently deformations of a quarter of the block are analyzed. The material of the block is assumed to exhibit strain-rate hardening, but thermal softening. The applied load is such as to cause deformations of the block at an overall strain-rate of 5000 sec^{-1}. The rigid inclusion simulates the presence of second phase particles such as oxides or carbides in a steel and acts as a nucleus for the shear band.

It is found that a shear band initiates near the tip of the inclusion and propagates along a line inclined at 45° to the horizontal axis. At a nominal strain of 0.25, the peak temperature rise near the tip of the vertically aligned inclusion equals 75% of that for the horizontally placed inclusion. The precipitous drop in the effective stress near the inclusion tip is followed somewhat later by a rapid rise in the maximum principal logarithmic strain there.

1 Introduction

A phenomenon which is commonly observed during high strain rate inelastic deformation of metals is the formation of narrow bands of intense shear strain usually called adiabatic shear bands. These shear bands form during high speed material processing, metal forming, and ballistic penetration. This is an important mode of deformation as these shear zones often become the sites for eventual failure of the material.

Since the time Zener and Hollomon [1] recognized the destabilizing effect of thermal softening in reducing the slope of the stress-strain curve in nearly adiabatic deformations, there have been many analytical (e.g. Recht [2], Staker [3], Clifton [4], Clifton and Molinari [5], Burns [6], Wright [7], Anand et al. [8], Bai [9], Coleman and Hodgdon [10]), experimental (e.g. Moss [11], Costin et al. [12], Marchand and Duffy [13]) and numerical (e.g. Clifton et al. [14], Merzer [15], Wu and Freund [16], Wright and Batra [17], [18], Wright and Walter [19], Batra [20]—[22], LeMonds and Needleman [23], [24], Needleman [25], Batra and Liu [26], [27], Anand et al. [28]) studies aimed at understanding the factors that enhance or inhibit the shear strain localization.

Although it is well recognized that dynamic fracture is significantly influenced by grain boundaries, precipitates and inclusions, inherent voids and flaws, texture, substructure, and impurities [29], very little is known about how such microstructural features influence shear band nucleation and growth. Most computational shear band models are

based on the relative ability of a material to work harden and thermal soften, and metallurgical influences are taken into account only implicitly as they influence the stress-strain and strength-temperature curves. The presence of a material defect has usually been modeled by introducing either a temperature perturbation [19]—[22], [26]—28] or assuming that the material at the site of the defect is weaker than the surrounding material [25], [27]. Of the numerical studies cited above, LeMonds and Needleman [23], [24], Needleman [25], Batra and Liu [26], [27] and Anand et al. [28] have analyzed the development of a shear band in plane strain problems. Of these, only Needleman and Batra and Liu have considered the effect of inertia forces. Whereas Batra and Liu assumed that the material softens because of its being heated up, Needleman studied a mechanical problem and accounted for softening mechanisms through the use of an internal variable.

In this paper, we study the thermomechanical plane strain deformations of a thermally softening viscoplastic solid and model the material inhomogeneity by introducing a rigid perfectly insulated cylindrical inclusion at the center of the block. The inclusion can be viewed as precipitates or second phase particles in an alloy. These particles, such as oxides or carbides, are usually very strong relative to the surrounding material, and their deformations can be neglected. Here we also take the inclusion to be non-heat conducting. Whereas Batra and Liu [26], [27] modeled the thermal softening of the material by a linear relation, we assume that the flow stress decreases exponentially with a rise in temperature. Thus, the material never looses its strength entirely even though it becomes quite small at very high temperatures. The problem formulation incorporates the effect of inertia forces, strain-rate sensitivity and heat conduction. The coupled nonlinear equations expressing the balance of mass, linear momentum and internal energy are solved numerically for a prescribed set of initial and boundary conditions.

2 Formulation of the problem

We study plane strain thermomechanical deformations of a cylindrical body having a square cross-section and presume that there is a rigid inclusion whose centroidal axis coincides with that of the body. The cross-section of the inclusion is taken to be elliptical with the major axis either parallel to or perpendicular to the axis of loading.

We use an updated Lagrangian description [30], where in order to solve for the deformations of the body at time $(t + \Delta t)$, the configuration at time t is taken as the reference configuration. However, the deformations of the body from time t to time $(t + \Delta t)$ could be finite. With respect to a fixed set of rectangular Cartesian coordinates axes, we denote the position of a material particle in the configuration at time t by X_i, and in the configuration at time $(t + \Delta t)$ by x_i. In terms of the referential description, the governing equations for the deformable matrix can be written as

$$(\rho J)^{\cdot} = 0, \tag{2.1}$$

$$\rho_0 \ddot{x}_i = T_{ij,j}, \tag{2.2}$$

$$\rho_0 \dot{e} = -q_{i,i} + T_{ij} l_{i,j}, \tag{2.3}$$

which ought to be supplemented by appropriate constitutive relations and initial and boundary conditions. Equations (2.1), (2.2), and (2.3) express, respectively, the balance of mass, the balance of linear momentum, and the balance of internal energy. Here ρ is the

mass density of a material particle in the current configuration at time t — [illegible], ρ_0 its mass density in the reference configuration at time t, a superimposed dot expresses a material time derivative, $J = \rho_0/\rho$ equals the determinant of the deformation gradient $F_{i\alpha} = x_{i,\alpha}$, v_i is the velocity of a material particle in the x_i-direction, $T_{i\alpha}$ is the first Piola-Kirchhoff stress tensor, a comma followed by $\alpha(i)$ implies partial differentiation with respect to $X_\alpha(x_i)$, the usual summation convention over repeated indices has been used, e is the specific internal energy, and Q_α is the heat flux measured per unit area in the reference configuration. In plane strain deformations in the $x_1 - x_2$ plane, the subscripts α and i range over 1 and 2.

The following constitutive equations are employed to describe the matrix response:

$$\sigma_{ij} = -p(\rho)\,\delta_{ij} - 2\mu D_{ij}, \tag{2.4}$$

$$T_{i\alpha} \equiv (\rho_0/\rho)\, X_{\alpha,j}\sigma_{ij}, \tag{2.5}$$

$$2\mu = \left[\sigma_0/\left(\sqrt{3}\, I\right)\right] e^{-\nu\theta}(1 - bI)^m, \tag{2.6}$$

$$Q_\alpha = -(\rho_0/\rho)\, k X_{\alpha,j}\theta_{,j}, \tag{2.7}$$

$$2D_{ij} = v_{i,j} - v_{j,i}, \tag{2.8}$$

$$2I^2 = \tilde{D}_{ij}\tilde{D}_{ij}, \qquad \tilde{D}_{ij} = D_{ij} - \frac{1}{3} D_{kk}\delta_{ij}, \tag{2.9}$$

$$p(\rho) = B(\rho/\rho_r - 1), \tag{2.10}$$

$$\rho_0\dot{e} = \rho_0 c\dot{\theta} - \rho_0\dot{\rho}\, p(\rho)/\rho^2, \tag{2.11}$$

where σ_{ij} is the Cauchy stress tensor, σ_0 is the stress in a quasi-static simple tension or compression test, ν is the coefficient of thermal softening, $\tilde{D}_{ij}$ is the deviatoric strain rate tensor, D_{ij} is the strain-rate tensor, δ_{ij} is the Kronecker delta, B may be interpreted as the bulk modulus, ρ_r is the mass density in the stress free reference configuration, c is the specific heat, k the thermal conductivity, and parameters b and m describe the strain-rate sensitivity of the material. Here ν, σ_0, k, c, b and m are taken to be independent of the temperature. Equation (2.7) is the Fourier law of heat conduction, referred to the reference configuration.

Introducing non-dimensional variables

$$\begin{aligned}
&\bar{\sigma} = \sigma/\sigma_0, && \bar{p} = p/\sigma_0, && \bar{\mathbf{s}} = \mathbf{s}/\sigma_0, && \bar{\mathbf{v}} = \mathbf{v}/v_0, \\
&\bar{t} = tv_0/H, && \bar{\mathbf{T}} = \mathbf{T}/\sigma_0, && \bar{\mathbf{x}} = \mathbf{x}/H, && \bar{\theta} = \theta/\theta_r, \\
&\bar{b} = bv_0/H, && \bar{\nu} = \nu\theta_r, && \bar{\rho} = \rho/\rho_r, && \bar{\rho}_0 = \rho_0/\rho_r, && \bar{X} = X/H \\
&\delta = \rho_r v_0^2/\sigma_0, && \beta = k/(\rho_r c v_0 H), && \theta_r = \sigma_0/(\rho_r c), && \bar{B} = B/\sigma_0,
\end{aligned} \tag{2.12}$$

the governing equations become

$$\dot{\bar{\rho}} + \bar{\rho}\bar{v}_{i,i} = 0, \tag{2.13}$$

$$\delta\bar{\rho}_0\dot{\bar{v}}_i = \bar{T}_{i\alpha,\alpha}, \tag{2.14}$$

$$\bar{\rho}_0\dot{\bar{\theta}} = -\bar{Q}_{\alpha,\alpha} + (\bar{\rho}_0/\bar{\rho})\left[1/\left(\sqrt{3}\,\bar{I}\right)\right](1 + \bar{b}\bar{I})^m e^{-\bar{\nu}\bar{\theta}}\tilde{D}_{ij}\tilde{D}_{ij}, \tag{2.15}$$

$$\bar{Q}_\alpha = -\frac{\beta}{\bar{\rho}}\,\bar{\rho}_0\bar{X}_{\alpha,j}\bar{\theta}_{,j}, \tag{2.16}$$

$$\bar{\sigma}_{ij} = -\bar{B}(\bar{\rho} - 1)\delta_{ij} + \left[1/\left(\sqrt{3}\,\bar{I}\right)\right](1 + \bar{b}\bar{I})^m e^{-\bar{\nu}\bar{\theta}}\tilde{D}_{ij}, \tag{2.17}$$

where the superimposed bars have been dropped. In Eq. (2.12), $2H$ is the height of the block and v_0 the imposed velocity on the top and bottom surfaces. In Eqs. (2.13)–(2.17) all of the differentiations are with respect to non-dimensional variables.

For the simple compression problem, we restrict ourselves to deformations that remain symmetrical about both $X_1 = 0$ and $X_2 = 0$. With the nondeformable and non-heat-conducting inclusion, the boundary conditions for the material in the first quadrant are:

$$
\begin{aligned}
&v_1 = 0, \quad T_{21} = 0, \quad Q_1 = 0 && \text{at } x_1 = X_1 = 0,\\
&v_2 = 0, \quad T_{12} = 0, \quad Q_2 = 0 && \text{at } x_2 = X_2 = 0,\\
&T_{ia}N_a = 0, \quad Q_aN_a = 0 && \text{on the right surface,}\\
&v_2 = -U(t), \quad T_{12} = 0, \quad Q_2 = 0 && \text{on the top face,}\\
&v_1 = 0, \quad v_2 = 0, \quad Q_aN_a = 0 && \text{at the interface } \Gamma_0 \text{ between the inclusion and the matrix.}
\end{aligned}
\tag{2.18}
$$

That is, boundary conditions resulting from the assumed symmetry of deformations are applied on the left and bottom faces, the right face of the block is taken to be traction free, and a prescribed normal velocity and zero tangential tractions are applied on the top face. All four sides of the block are assumed to be perfectly insulated. The zero velocity and the zero heat flux at interface Γ_0 implies that the second phase particle is rigid and non-heat-conducting.

The interface Γ_0 between the inclusion and the matrix has the parametric representation

$$
\frac{X_1^2}{a^2} - \frac{X_2^2}{b^2} = 1 \quad \text{or} \quad \frac{x_1^2}{a^2} - \frac{x_2^2}{b^2} = 1, \tag{2.19}
$$

where $2a$ and $2b$ are the major and minor axes of the ellipse respectively.

For the initial conditions we take

$$
\varrho(\mathbf{X}, 0) = 1.0, \quad v_1(\mathbf{X}, 0) = 0, \quad v_2(\mathbf{X}, 0) = 0, \quad \theta(\mathbf{X}, 0) = 0, \tag{2.20}
$$

and the loading path is

$$
U(t) = \begin{cases} t/0.005 & 0 \leqq t \leqq 0.005, \\ 1 & t \geqq 0.005 \end{cases} \tag{2.21}
$$

3 Finite element formulation of the problem

Because of our inability to solve the coupled nonlinear partial differential equations (2.13) to (2.16) analytically, we seek an approximate numerical solution of the problem by the finite element method. By using the Galerkin method and the lumped mass matrix (e.g. see Hughes [31]), we obtain the following semi-discrete formulation of the problem from Eqs. (2.13) – (2.16), boundary conditions (2.18), and initial conditions (2.20)

$$
\dot{\boldsymbol{d}} = F(\boldsymbol{d}, \alpha, \beta, b, m, r), \tag{3.1}
$$

$$
\boldsymbol{d}(0) = \boldsymbol{d}_0. \tag{3.2}
$$

Here $\boldsymbol{d}$ is the vector of nodal values of the mass density, two components of the velocity and the temperature. The number of nonlinear ordinary differential equations (3.1) equals

four times the number of nodes. These differential equations are solved by using the backward difference Adams method included in the IMSL subroutine LSODE. The subroutine adjusts the time increment adaptively until it can compute a solution of (3.1) and (3.2) to the prescribed accuracy.

Batra and Liu [26], [27] initially used 9-noded quadrilateral elements. Their subsequent work [32] revealed that 4-noded quadrilateral elements provide a better resolution of the intense deformation within the region of localization. Thus, we use here 4-noded quadrilateral elements. The finite element code developed by Batra and Liu [26] was modified to include the exponential thermal softening of the material.

4 Numerical results

The following values of material and geometric parameters used in the calculations are representative of a typical hard steel.

$$
\begin{aligned}
&b = 10{,}000\ \text{sec}, \quad \sigma_0 = 333\ \text{MPa}, \quad k = 49.22\ \text{Wm}^{-1}\text{°C}^{-1}, \quad m = 0.025,\\
&c = 473\ \text{J Kg}^{-1}\text{°C}^{-1}, \quad \varrho_r = 7{,}860\ \text{Kg m}^{-3}, \quad B = 128\ \text{GPa},\\
&H = 5\ \text{mm}, \quad v_0 = 25\ \text{msec}^{-1}, \quad \nu = 0.0025\ \text{°C}^{-1},\\
&a = 0.2, \quad b = 0.02 \quad \text{or} \quad a = 0.02 \quad \text{and} \quad b = 0.2.
\end{aligned}
\tag{4.1}
$$

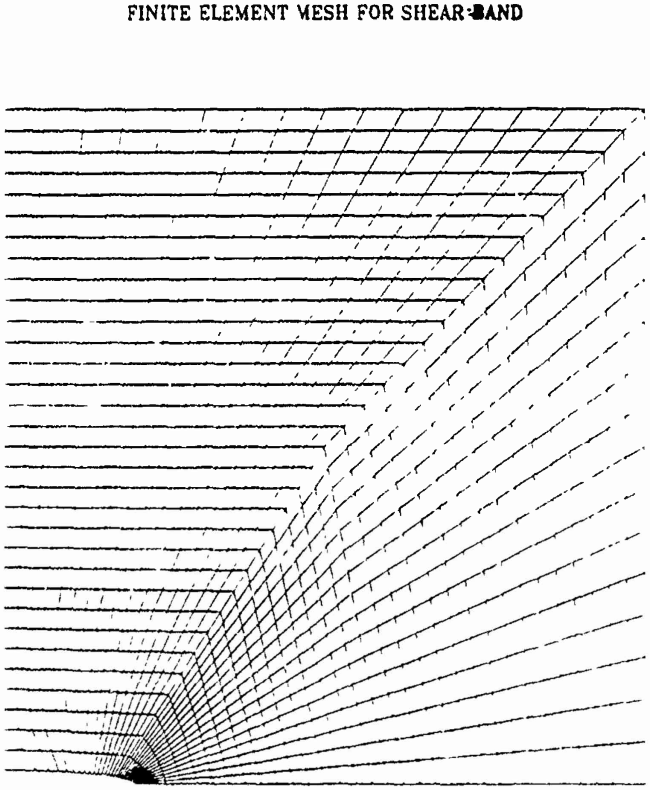

Fig. 1. The finite element mesh used for the analysis of the problem when the rigid elliptic inclusion is placed horizontally

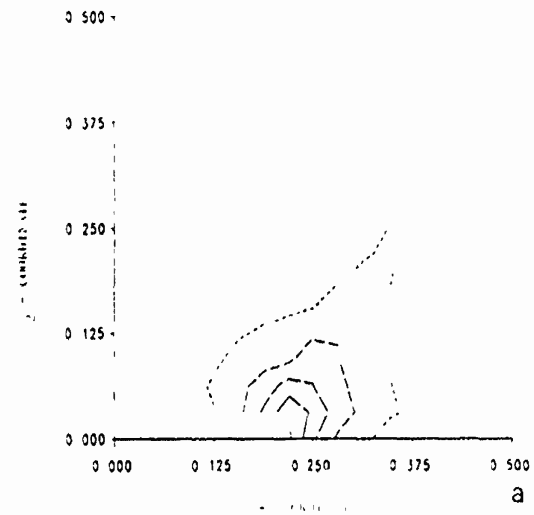
0.500
0.375
0.250
0.125
0.000
0.000
0.125
0.250
0.375
0.500
a

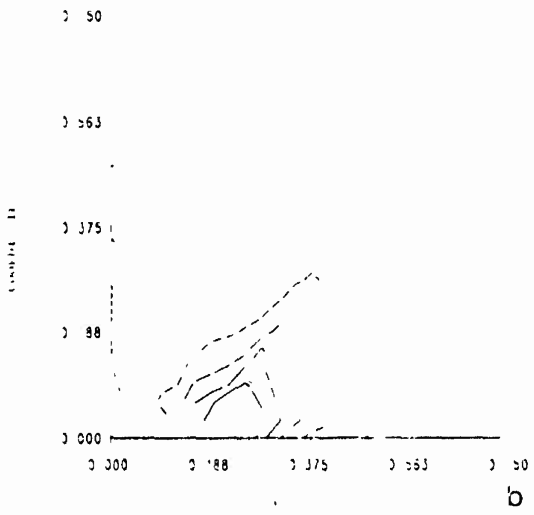
0.50
0.375
0.000
b

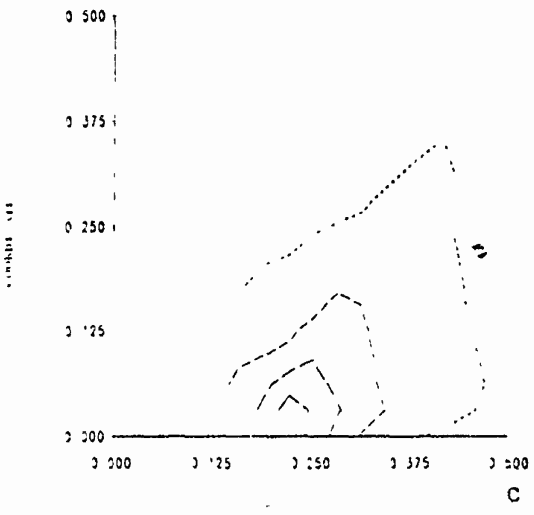
0.500
0.375
0.250
0.000
0.000
0.125
0.250
0.375
0.500
c

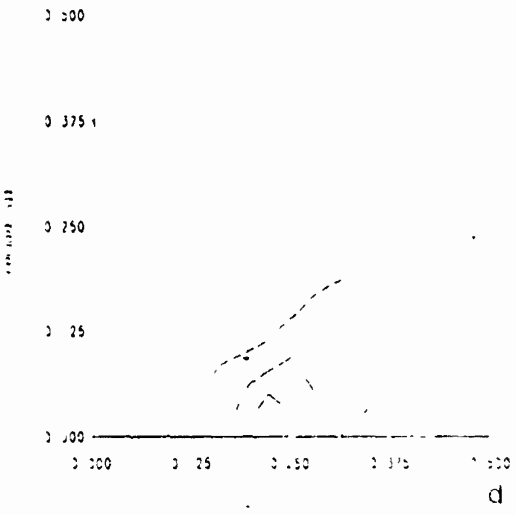
0.375
0.250
0.000
d

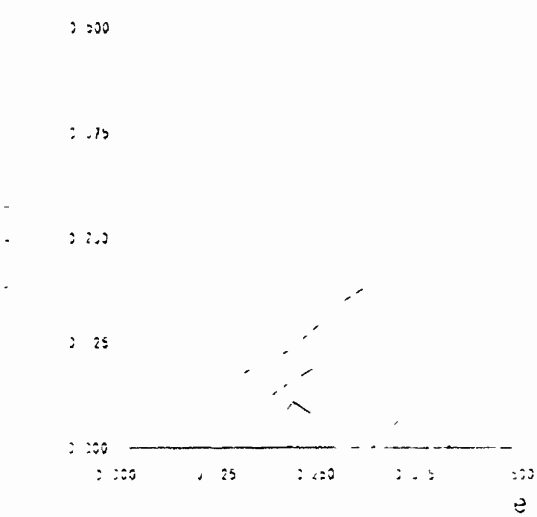
e

For values given in (4.1), $\theta_0 = 89.6\,^{\circ}\mathrm{C}$ and the average applied strain-rate equals 5000 $\sec^{-1}$. Figure 1 depicts the finite element mesh used in the computations when the major axis of the elliptic inclusion is along the x_1-axis. The aspect ratio of the elliptical inclusion is taken to be large so as to increase the stress concentration near the vertex of the major axis and reduce the CPU time required to solve the problem. The finite element mesh used is very fine in the region surrounding the edge of the inclusion and gradually becomes coarser as we move away from it. A similar mesh is used when the major axis of the inclusion is vertical. We note that we have not made any attempt to align the element sides along the direction of maximum shearing. Needleman [25] has used a mesh with the element sides aligned along the expected direction of development of the shear band.

The isotherms at five different values of the average strain are plotted in Figs. 2a through 2e for the horizontally placed elliptic inclusion, and Figs. 3a through 3e for the vertically oriented elliptic inclusion. Due to the high stress concentration at the tip of the inclusion, the material near the tip is severely deformed and gets heated up faster than the rest of the block. The built up heat makes the material softer but the softer material cannot deform very rapidly because of the constraints imposed on it by the surrounding material. Also the heat slowly conducts out of this relatively warmer region. With continued further straining of the block, the material near the inclusion tip becomes sufficiently hot that thermal softening effect exceeds the hardening due to the straining of the material. Even though the material point near the inclusion tip may become unstable, a shear band need not initiate at this time. For example, the one-dimensional numerical studies [19]—[22] make it clear that a shear band usually initiates at a value of nominal strain far in excess of the value at which the shear stress attains its peak value. Once a shear band initiates, the material within the band gets heated up very fast. As the shear band grows, the rate of temperature rise at the inclusion tip slows down. We have plotted in Figs. 4a and 4b the temperature rise at six points within the deforming region as a function of the average strain for each of the two cases considered. In each case, the temperature rises at a point near the inclusion tip much faster than that at points away from it. The rate of temperature rise at points near the inclusion tip decreases gradually and eventually attains a constant value. At points far removed from the inclusion tip, the rate of temperature increase is essentially uniform implying thereby that the small regions surrounding these points are deforming homogeneously. Even though the results for the horizontally and vertically aligned inclusions are similar in nature the temperature rise near the inclusion tip for the vertically aligned inclusion is considerably less as compared to that for the horizontally placed inclusion. In each case, the contours of constant temperature propagate along lines inclined at 45° to the horizontal axis. In the absence of an inclusion, this will be the direction of the maximum shearing stress.

The variation of the effective stress s_e, defined by

$$s_e^2 = \frac{1}{2} S_{ij} S_{ij}, \qquad S_{ij} = \sigma_{ij} - \left(p - \frac{2}{3}\mu D_{kk}\right)\delta_{ij}, \tag{4.2}$$

Fig. 2. Isotherms plotted in the reference configuration at different values of the average strain with the horizontally placed inclusion

(a) $\gamma_{avg} = 0.0536$, $\theta_{max} = 5.17$ ···· 1, - - - - 2, — — — 3; ——— 4; ——— 5.
(b) $\gamma_{avg} = 0.1486$, $\theta_{max} = 8.63$. See part (a) for values of θ corresponding to different curves.
(c) $\gamma_{avg} = 0.1887$, $\theta_{max} = 9.62$. ···· 2, - - - - 4, — — — 6; ——— 8; ——— 10
(d) $\gamma_{avg} = 0.2008$, $\theta_{max} = 9.82$. See part (c) for values of θ corresponding to different curves
(e) $\gamma_{avg} = 0.2478$ $\theta_{max} = 10.46$. See part (c) for values of θ corresponding to different curves

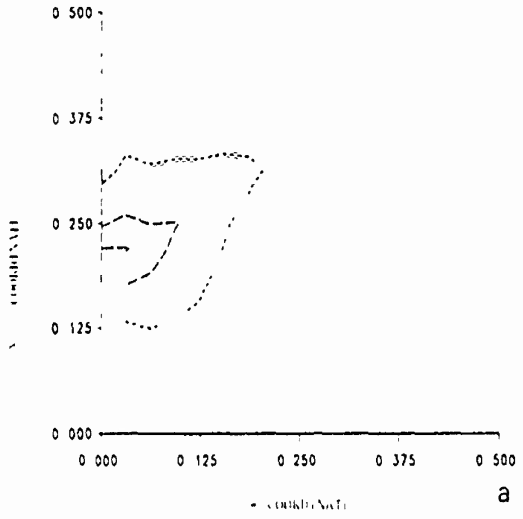
0.500
0.375
0.250
0.125
0.000
0.000
0.125
0.250
0.375
0.500
a

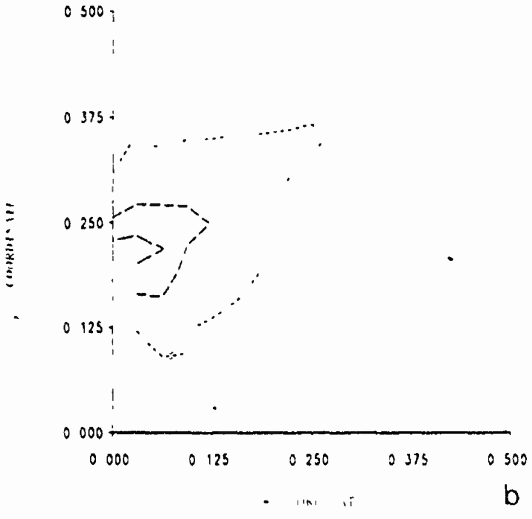
0.500
0.375
0.250
0.125
0.000
0.000
0.125
0.250
0.375
0.500
b

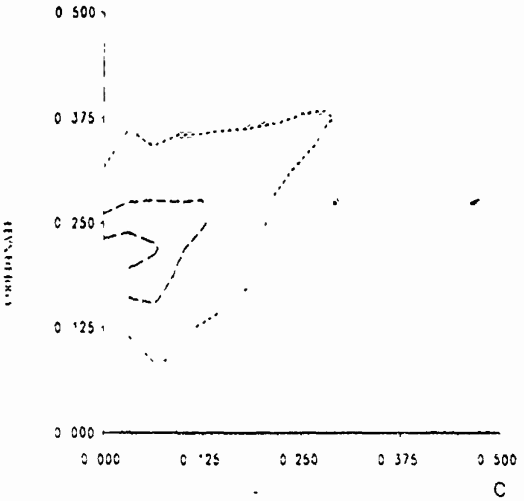
0.500
0.375
0.250
0.125
0.000
0.000
0.125
0.250
0.375
0.500
c

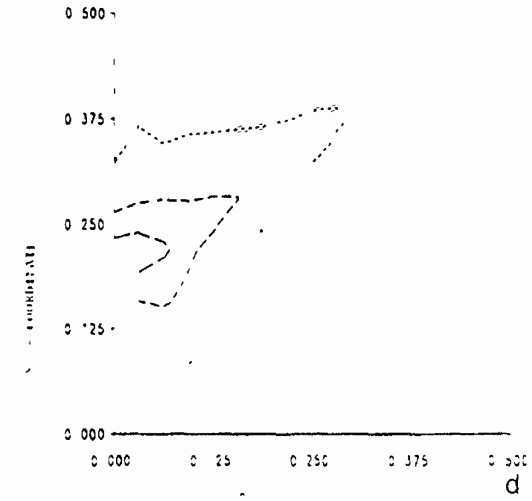
0.500
0.375
0.250
0.125
0.000
0.000
0.125
0.250
0.375
0.500
d

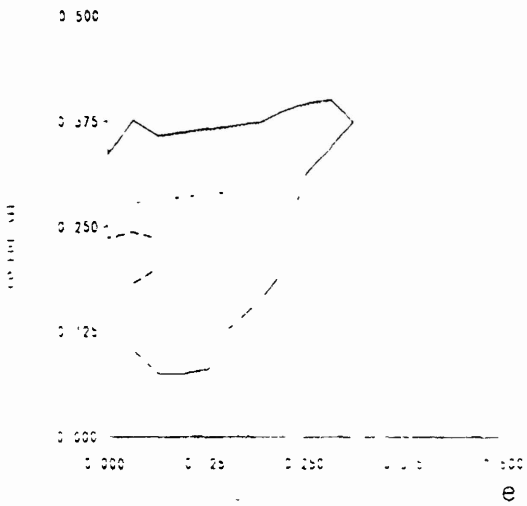
0.500
0.375
0.250
0.125
0.000
0.000
0.125
0.250
0.375
0.500
e

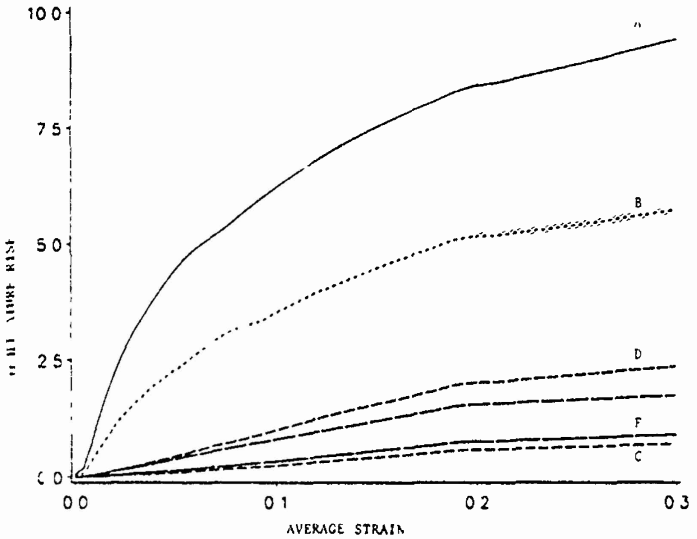

Fig. 4a. Variation of the temperature rise with the average strain at six different points for the horizontally aligned inclusion. Coordinates of these points in the reference configuration are: A (0.2052, 0.000218), B (0.1782, 0.01625), C (0.009525, 0.02621), D (0.4044, 0.00345), E (0.0951, 0.2952), F (0.006907, 0.04353)

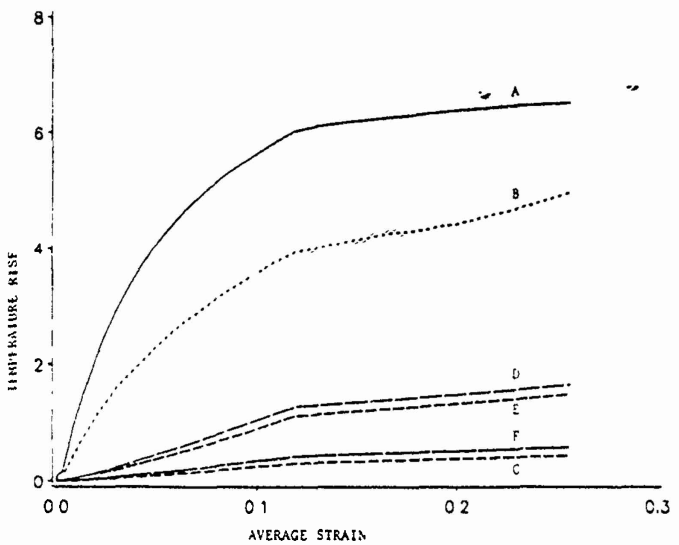

Fig. 4b. Variation of the temperature rise with the average strain at six different points for the vertically aligned inclusion. Coordinates of these points in the reference configuration are: A (0.000217 6, 0.20523), B (0.01625, 0.17824), C (0.02621, 0.009525), D (0.00345, 0.4044), E (0.2952, 0.09511), F (0.04353, 0.006907)

Fig. 3. Isotherms plotted in the reference configuration at different values of the average strain with the vertically placed inclusion

(a) $\gamma_{avg} = 0.095$, $\theta_{max} = 6.11$, ···· 2, — — — 4, ——— 6
(b) $\gamma_{avg} = 0.131$, $\theta_{max} = 6.85$. See part (a) for values of θ corresponding to different curves.
(c) $\gamma_{avg} = 0.167$, $\theta_{max} = 7.14$. See part (a) for values of θ corresponding to different curves
(d) $\gamma_{avg} = 0.193$, $\theta_{max} = 7.24$. See part (a) for values of θ corresponding to different curves
(e) $\gamma_{avg} = 0.248$, $\theta_{max} = 7.74$. ——— 2, ···· 4; — — — 6

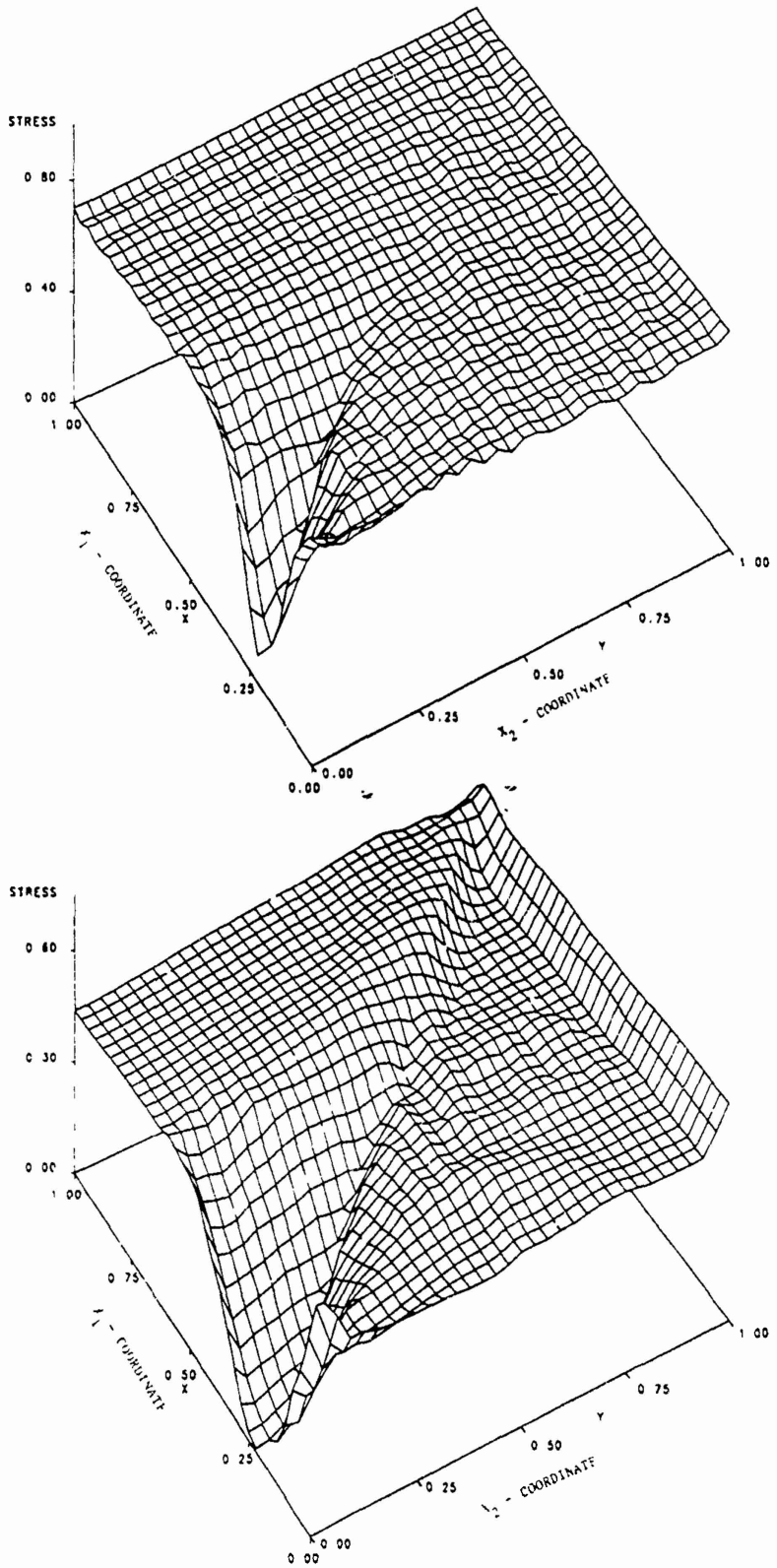

Fig. 5. Distribution of the effective stress within the body at two different values of the average strain with the inclusion aligned along the x_1-axis. (a) $\gamma_{avg} = 0.0536$, (b) $\gamma_{avg} = 0.2479$

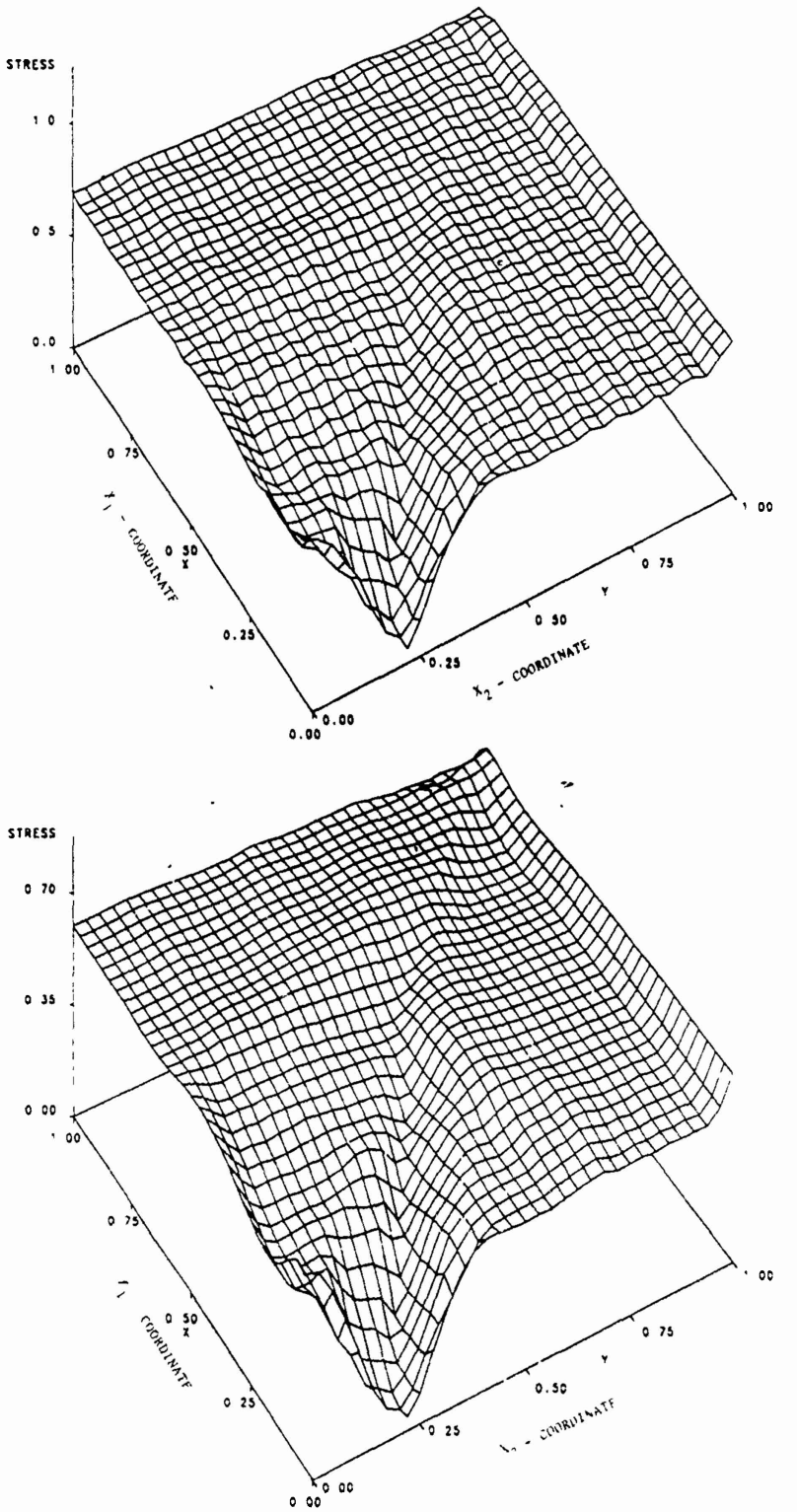

Fig. 6. Distribution of the stress within the body at two different values of the average strain with the inclusion aligned along the x_2-axis (a) $\gamma_{avg} = 0.095$, (b) $\gamma_{avg} = 0.2479$

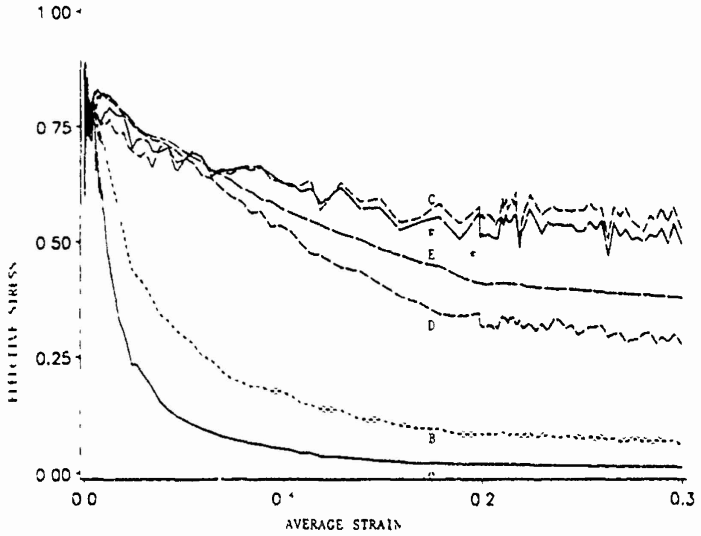

Fig. 7a. Variation of the effective stress with the average strain at six different points for the horizontally aligned inclusion. See Fig. 4a for the coordinates of the six points

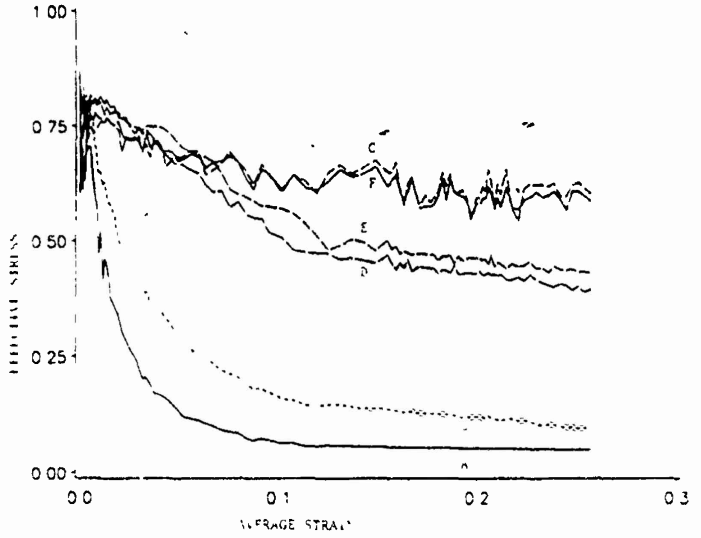

Fig. 7b. Variation of the effective stress with the average strain at six different points for the vertically aligned inclusion. See Fig. 4b for the coordinates of six points

is plotted in Figs. 5a and 5b, and Figs. 6a and 6b for the horizontally and vertically placed inclusions, respectively. In both cases, the stress drops noticeably near the tip of the inclusion and as the band propagates along the 45° direction, the shear stress drops. The rather small drop of the shear stress near the other extremity of the 45° line indicates that the deformation there has not localized as much as it has near the inclusion tip. Batra and Liu [26], [27] used linear thermal softening law with a rather large value of the thermal softening coefficient and found that once the deformation localized near the site of the defect, it propagated quickly along the 45° direction to the other edge. Here the thermal softening is represented by an exponential function and the band propagates slowly leading one to conjecture that the speed of propagation of the shear band is strongly influenced by

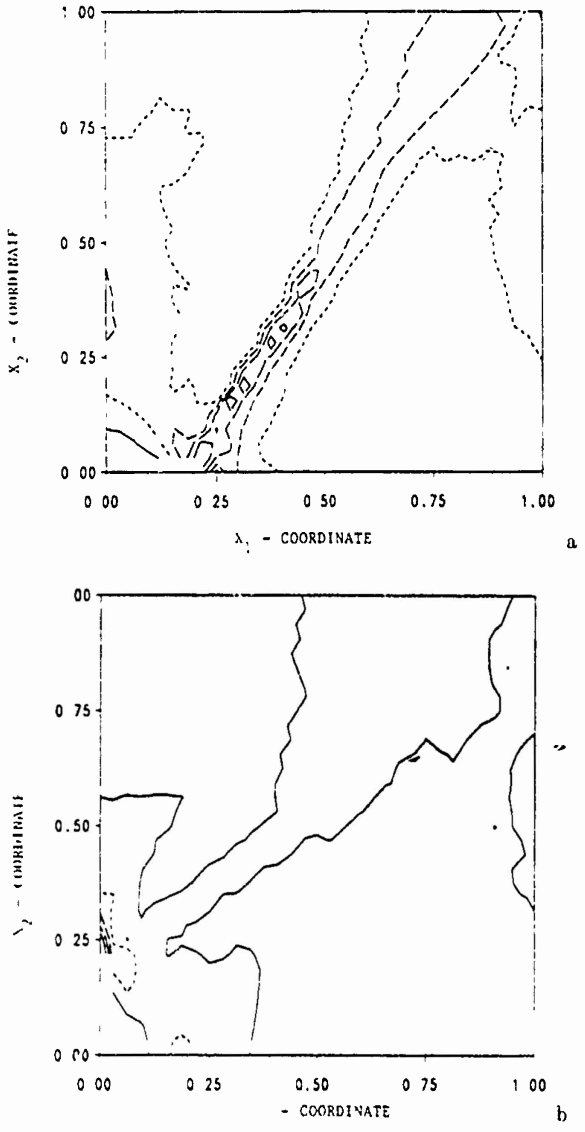

Fig. 5. Contours of the maximum principal logarithmic strain (a) horizontally aligned inclusion, $\gamma_{avg} = 0.344$; ——— 0.2, ···· 0.4, – – – – 0.6, ——— — 0.8, —·— 1.0, (b) vertically aligned inclusion, $\gamma_{avg} = 0.248$; ——— 0.3, ···· 0.5, – – – 0.7, ——— — 0.9, —·— 1.1

the thermal softening law and the value of the thermal softening coefficient used. In Figs 7a and 7b, we have plotted the variation of the effective stress with the average strain at six points for the horizontally and vertically aligned inclusions We note that the temperature rise at these points was plotted in Fig 4. As for the one-dimensional case, the initiation and development of a shear band is accompanied by a rapid drop of the effective stress The stress drop at the inclusion tip is significantly more than that at the adjoining point considered At points far removed from the inclusion tip, the stress drops only slightly The oscillations in the value of the effective stress at points far away from the inclusion tip is possibly due to the fact that the rate of deformation there is small and the stress computations involve the division of one small number by another small number For each case studied, the effective stress near the inclusion tip reaches a plateau after the rapid drop

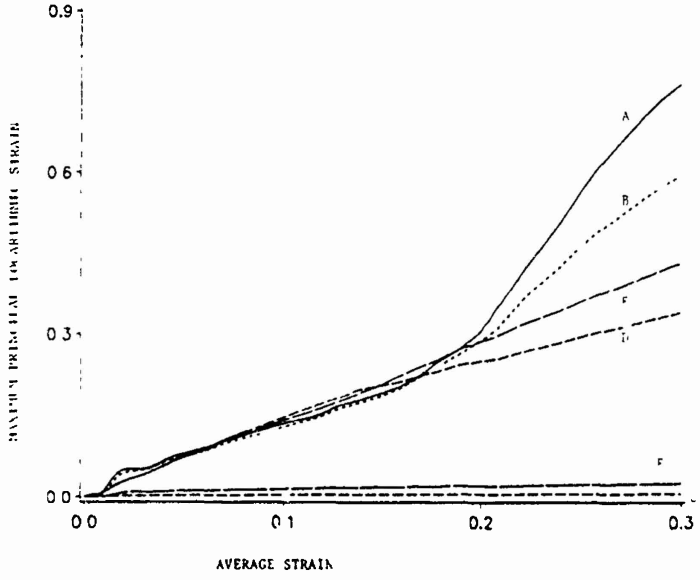

Fig. 9a. Variation of the maximum principal logarithmic strain with the average strain at six different points for the horizontally aligned inclusion. See Fig. 4a for the coordinates of the six points

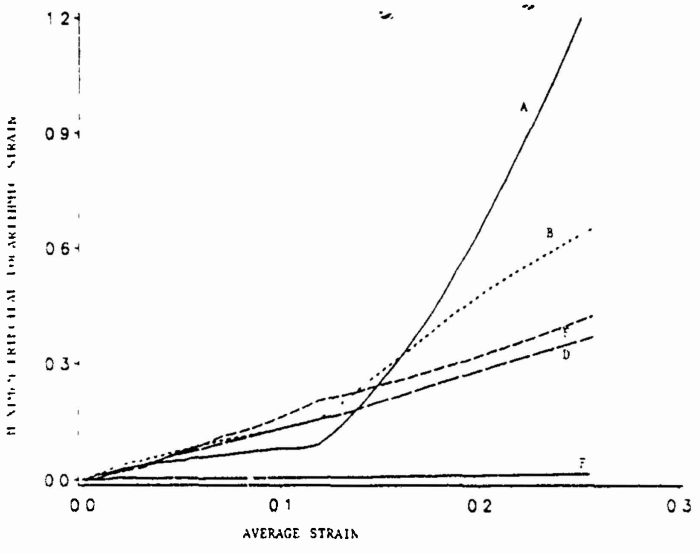

Fig. 9b. Variation of the maximum principal logarithmic strain with the average strain at six different points for the vertically aligned inclusion. See Fig. 4b for the coordinates of the six points

This was not observed in the one-dimensional computations with the linear thermal softening, but was found to be the case [33] when the material behavior was modeled by the Bodner-Partom law

Figures 8a and 8b depict the contours of the maximum principal logarithmic strain

$$\varepsilon = \ln \lambda_1 \tag{4.3}$$

where λ_1^2 is the maximum eigenvalue of the right Cauchy-Green tensor

$$C_{\alpha\beta} = x_{\gamma,\alpha} x_{\gamma,\beta} \tag{4.4}$$

Let λ_2^2 and 1 be the other two eigenvalues of $C_{\alpha\beta}$ Since the deformations are nearly isochoric,

$$\ln \lambda_1 \approx -\ln \lambda_2 \tag{4.5}$$

It is clear from these plots that severe deformations occur in a narrow region For the horizontally aligned inclusion, the shear band is rather well defined For the vertically aligned inclusion, contours of higher values of ε have not propagated farther into the deformable block. Note that the nominal strain at which these results are plotted is different in the two cases. However, the variation of ε with the nominal strain at six points plotted in Figs. 9a and 9b reveal that near the inclusion tip ε attains higher values for the vertically aligned inclusion as compared to that for the horizontally aligned elliptic inclusion For the former case, the curves of ε vs. average strain coincide for points E and F In each case, ε increases slowly first near the inclusion tip. Subsequently, the rate of growth of ε picks up sharply and the region surrounding the inclusion tip is deformed more intensely as compared to the rest of the body. Note that the values of the nominal strain at which s_1 drops sharply and ε increases rapidly at the same point near the inclusion tip are different the stress drop occurs first Thus, even though the material in a small neighborhood of the inclusion tip has weakened, the surrounding material contributes significantly to the load carrying capacity of the member and constrains the weaker small region from deforming severely. Thus, if one adopts the view point that a shear band initiates when the maximum logarithmic strain at a point increases sharply, then the initiation of the shear band in this case occurs considerably after the shear stress has dropped precipitously. This differs from the results of the one-dimensional computations [19], [33] in which the precipitous drop of the shear stress and the sharp increase of the plastic strain at a point occur simultaneously.

Figure 10 depicts the velocity field within the deforming material at an average strain of 25% and when the major axis of the inclusion is along the x_1-axis There is a noticeable change in the velocity field across the 45° line along which a shear band has formed. Johnson [34] has recently pointed out that Tresca [35] and Massey [36] observed shear bands in the form of a cross with sides inclined at $\pm 45^\circ$ to the direction of loading during hot forging of certain metals. They asserted that the tangential velocity is discontinuous across these bands The velocity field plotted in Fig. 10 supports this to some degree We add that the velocity field plotted in Fig. 3 of Batra and Liu's paper [26] vividly demonstrates that the tangential velocity suffers a jump across the shear band. The velocity field for the vertically aligned inclusion exhibits a behavior similar to that shown in Fig 10 and the plots are not included herein.

The average compressive force F_y given by

$$F_y = -\int_0^1 \sigma_{22}\, dx_1 \tag{4.6}$$

versus the nominal strain is plotted for the two cases in Fig 11 The curve of dash lines represents the case when there is no inclusion present The integral in Eq. (4.6) is evaluated by using values of σ_{22} at quadrature points on the top loading surface Initially, the applied force increases almost linearly in each case due to the linear increase of the applied velocity The presence of the inclusion necessitates initially a larger force as compared to that required to deform the homogeneous block Due to the heating of the block caused by the ensuing plastic deformation, the material softens and the load required to deform it decreases. This decrease in the load is more for the block with an inclusion because of the

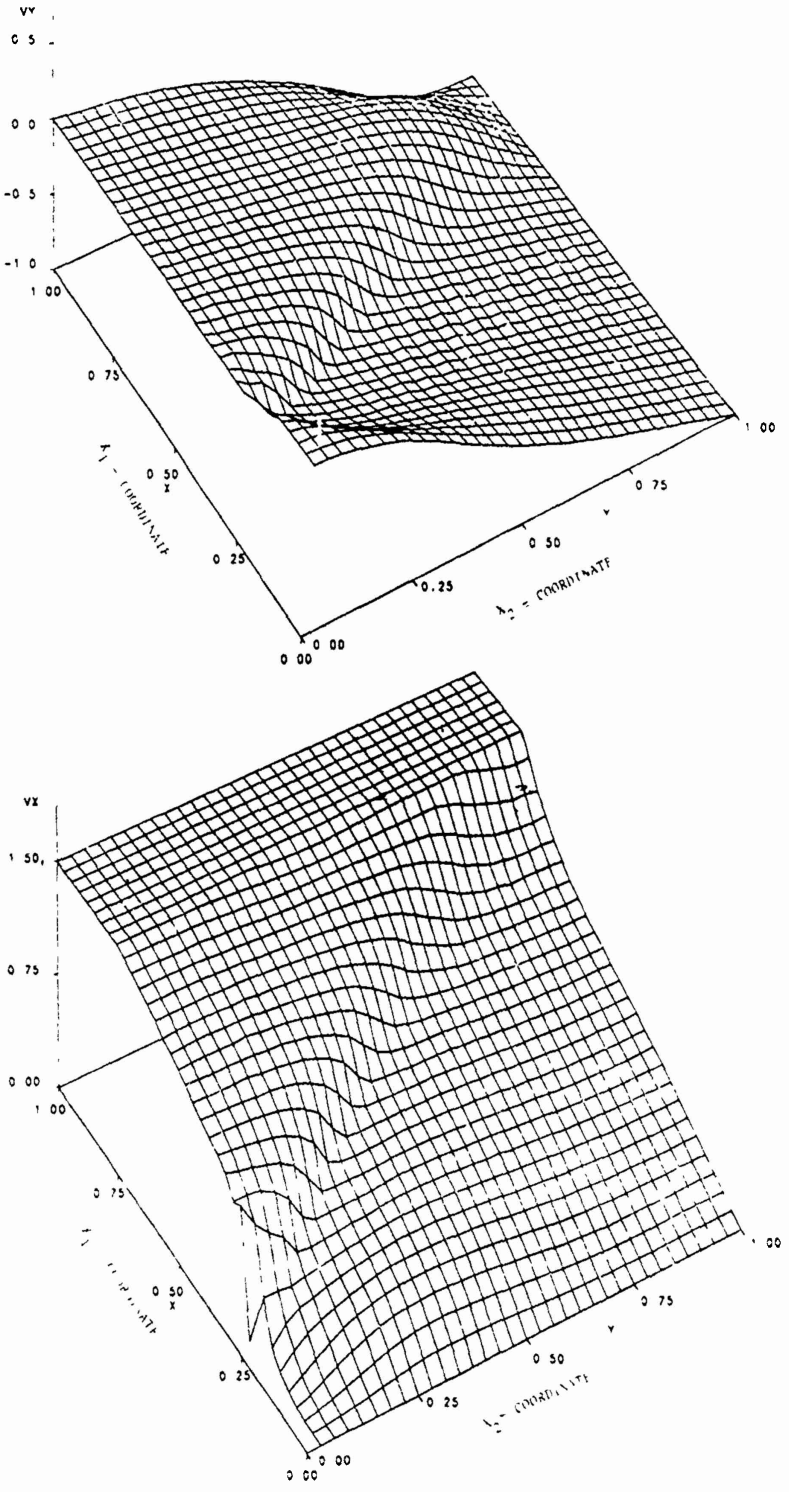

Fig. 10. Velocity distribution within the block for the inclusion along the x_1-axis at an average strain of 0.2478

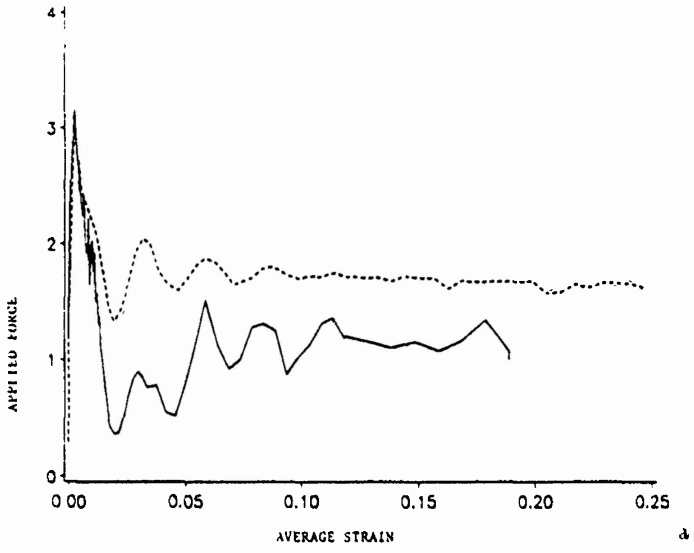

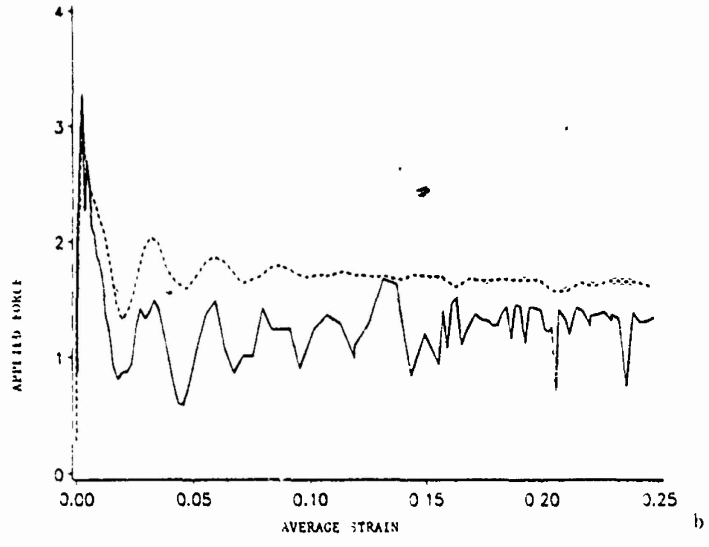

Fig. 11. Load-average strain curves for (a) horizontally aligned inclusion (solid line), (b) vertically aligned inclusion (solid line). The dash line represents the load-displacement curve when there is no inclusion present in the block

nucleation of a shear band near the tip of the inclusion. However, subsequent to the initiation of a shear band, the applied force stays lower than that for the homogeneous block signifying the lower load carrying capacity of the member once a shear band develops in it. The oscillations in the applied force are more for the vertically aligned inclusion. These can be attributed, at least partially, to the fact that the deformation in the top row of elements is not homogeneous and the computations of tractions at the boundary points is less accurate as compared to the solution within the block. Note that contours of different values of ϵ and θ arrive at some elements in the top row at different instants and thus affect the stress distribution in the elements. We believe that the use of a finer mesh would

decrease the oscillations in F_y, but this could not be verified because of the limited computational resources available to us. Also, a finer mesh would improve the resolution of the deformation within the band.

5 Conclusions

The problem of the initiation and subsequent growth of a shear band in plane strain thermomechanical deformations of a viscoplastic block containing an elliptical inclusion has been studied by the finite element method. It is found that a shear band nucleates at the tip of the inclusion and propagates along the direction of maximum shearing. As the strain rate within the band increases, the effective stress in it drops and the temperature continues to increase. The maximum computed temperature when the effective stress had dropped to nearly zero equalled 937 °C. At a point near the inclusion tip the effective stress drops rapidly first. This is followed, much later, by a sharp increase in the maximum principal logarithmic strain at the same point. This delay is possibly due to the constraining effects of the relatively strong material surrounding the weakened material near the inclusion tip.

Acknowledgements

This work was supported by the U.S. National Science Foundation Grant MSM 8715952 and the U.S. Army Research Office Contracts DAAL 03-88-K-0184 and DAAL 03-89-K-0050 to the University of Missouri-Rolla. Some of the computations were performed on the IBM 3090 vector machine in Columbia, MO under the trial program.

References

[1] Zener, C., Hollomon, J. H.: Effect of strain rate on plastic flow of steel. J. Appl. Phys. 14, 22–32 (1944).

[2] Recht, R. F.: Catastrophic thermoplastic shear. ASME J. Appl. Mech. 31, 189–193 (1964).

[3] Staker, M. R.: The relation between adiabatic shear instability strain and material properties. Acta Met. 29, 683–689 (1981).

[4] Clifton, R. J.: Material response to ultra high loading rates. NRC National Material Advisory Board (U.S.) Report 356 (1980).

[5] Molinari, A., Clifton, R. J.: Analytic characterization of shear localization in thermoviscoplastic materials. J. Appl. Mechs. 54, 806–812 (1987).

[6] Burns, T. J.: Approximate linear stability analysis of a model of adiabatic shear band formation. Quart. Appl. Math. 43, 65–83 (1985).

[7] Wright, T. W.: Steady shearing in a viscoplastic solid. J. Mech. Phys. Solids 35, 269–282 (1987).

[8] Anand, L., Kim, K. H., Shawki, T. G.: Onset of shear localization in viscoplastic solids. Massachusetts Institute of Technology Report, 1986.

[9] Bai, Y. L.: A criterion for thermoplastic shear instability. In: Shock waves and high strain rate phenomenon in metals (Meyers, M. A., Murr, L. E., eds.), pp. 277–283. New York: Plenum Press 1981.

[10] Coleman, B. D., Hodgdon, M. L.: On shear bands in ductile materials. Arch. Rat. Mech. Anal. 90, 219–247 (1985).

[11] Moss, G. L.: Shear strain, strain rate and temperature changes in adiabatic shear band. In: Shock waves and high strain rate phenomenon in metals (Meyer, M. A., Murr, L. E., eds.), pp. 299–312. New York: Plenum Press 1981.

[12] Costin, L. S., Crisman, E. E., Hawley, R. H., Duffy, J.: On the localization of plastic flow in mild steel tubes under dynamic torsional loading. Int. Phys. Conf. Ser. No. 47, 90–100 (1979).

[13] Marchand, A., Duffy, J.: An experimental study of the formation process of adiabatic shear bands in a structural steel. J. Mech. Phys. Solids 36, 251–283 (1988).

[14] Clifton, R. J., Duffy, J., Hartley, K. S., Shawki, T. G.: On critical conditions for shear band formation at high strain rates. Scripta Metallurgica 18, 443–450 (1984).
[15] Merzer, A. M.: Modeling of adiabatic shear band development from small imperfections. J. Mech. Phys. Solids 30, 323–338 (1982).
[16] Wu, F. H., Freund, L. B.: Deformation trapping due to thermoplastic instability in one-dimensional wave propagation. J. Mech. Phys. Solids 32, 119–132 (1984).
[17] Wright, T. W., Batra, R. C.: The initiation and growth of adiabatic shear bands. Int. J. Plasticity 1, 205–212 (1985).
[18] Wright, T. W., Batra, R. C.: Adiabatic shear bands in simple and dipolar plastic materials. In: Proc. IUTAM Symposium on macro- and micro-mechanics of high velocity deformation and fracture (Kawata, K., Shioiri, J., eds.), pp. 189–201. Berlin–Heidelberg–New York: Springer 1987.
[19] Wright, T. W., Walter, J. W.: On stress collapse in adiabatic shear bands. J. Mech. Phys. Solids 35, 701–720 (1987).
[20] Batra, R. C.: The initiation and growth of, and the interaction among adiabatic shear bands in simple and dipolar materials. Int. J. Plasticity 3, 75–89 (1987).
[21] Batra, R. C.: Effect of material parameters on the initiation and growth of adiabatic shear bands. Int. J. Solids and Structures 23, 1435–1446 (1987).
[22] Batra, R. C.: Effect of nominal strain-rate on the initiation and growth of adiabatic shear bands. J. Appl. Mechs. 55, 229–230 (1988).
[23] LeMonds, J., Needleman, A.: Finite element analyses of shear localization in rate and temperature dependent solids. Mechs. Materials 5, 339–361 (1986).
[24] LeMonds, J., Needleman, A.: An analysis of shear band development incorporating heat conduction. Mechs. Materials 5, 363–373 (1986).
[25] Needleman, A.: Dynamic shear band development in plane strain. J. Appl. Mechs. 56, 1–8 (1989).
[26] Batra, R. C., Liu, D. S.: Adiabatic shear banding in plane strain problems. J. Appl. Mechs. 56, 527–534 (1989).
[27] Batra, R. C., Liu, D. S.: Adiabatic shear banding in dynamic plane strain compression of a viscoplastic material. Int. J. Plasticity 6, 231–246, 1990.
[28] Anand, L., Lush, A. M., Kim, K. H.: Thermal aspects of shear localization in viscoplastic solids. Thermal aspects in manufacturing. In: ASME-PED-Vol. 30. (ATTIA, M. H., Kops, L., eds.), 89–103 (1988).
[29] Shockey, D. A., Seaman, L., Curran, D. R.: The influence of microstructure features on dynamic fracture. In: Metallurgical effects at high strain rates (Rhode, R. W., Butcher, B. M., Holland, J. R., Karnes, E. H., eds.), p. 473. New York–London: Plenum Press 1973.
[30] Bathe, K. J.: Finite element procedures in engineering analysis. Englewood Cliffs: Prentice-Hall 1982.
[31] Hughes, T. J. R.: The finite element method. Linear static and dynamic finite element analysis. Englewood Cliffs: Prentice Hall 1987.
[32] Batra, R. C., Liu, D. S.: Dynamic shear band development in thermally softening viscoplastic materials. Proc. 2nd Int. Symp. Plasticity and its Current Applications (Khan, Akhtar, S., Tokuda, M., eds.), pp. 435–438. Pergamon Press 1989.
[33] Batra, R. C., Kim, C. H.: Effect of viscoplastic flow rules on the initiation and growth of shear bands at high strain rates. J. Mechs. Phys. Solids (in press).
[34] Jonnson, W.: Henri Tresca as the originator of adiabatic heat lines. Int. J. Mech. Sci. 29, 301–310 (1987).
[35] Tresca, H.: On further application of the flow of solids. Proc. Inst. Mech. Engr. 30, 301–345 (1878).
[36] Massey, H. F.: The flow of metal during forging. Proc. Manchester Assoc. Engineers, pp. 21–26, 1921. Reprinted by the National Machinery Co., Tiffon, Ohio 1946.

Authors' address: Z. G. Zhu and R. C. Batra, Department of Mechanical and Aerospace Engineering and Engineering Mechanics, University of Missouri-Rolla, Rolla, MO 65401-0249, U.S.A.

Made in Germany
Maxim Gorki - Druck GmbH, Carl-v.-Ossietzki-Str. 30/31, 7400 Altenburg

Acta Mechanica 85, 221—234 (1990)

ACTA MECHANICA

Shear band development in dynamic loading of a viscoplastic cylinder containing two voids

R. C. Batra and **X.-T. Zhang**, Rolla, Missouri

(Received January 18, 1990)

Summary. We presume that plane strain state of deformation prevails when the interior of a long gun barrell or a cylindrical pressure vessel is dynamically loaded. The viscoplastic material of the body is taken to exhibit strain-rate hardening and thermal softening. Two thin ellipsoidal voids located symmetrically on the horizontal axis and near the center of the cylinder wall act as nuclei for the initiation of shear bands. We note that deformations of the cylinder are nonhomogeneous even in the absence of the voids. It is therefore interesting to investigate when the bands initiate from the void tips and the interaction, if any, among them.

It is found that shear bands initiate first at void tips closer to the center of the cylinder. These bands propagate faster to the inner surface of the cylinder as compared to those initiating from the other void tips which propagate towards the outer bounding surface of the cylinder. Whereas contours of constant maximum principal logarithmic strain originating from the outer void tips spread out laterally in both directions as they propagate into the cylinder, those originating from the inner void tips spread out in only one lateral direction as they propagate into the body.

1 Introduction

Johnson [1] has recently pointed out that Tresca [2] observed hot lines during the forging of platinum in 1878. Tresca stated that these were the lines of greatest sliding, and also therefore the zones of greatest development of heat. Subsequently, these hot lines were also observed by Massey [3] in 1921. He stated that "when diagonal 'slipping' takes place there is great friction between particles and a considerable amount of heat is generated". These hot lines are now referred to as adiabatic shear bands. Zener and Hollomon [4] observed 32 μm wide shear bands during the punching of a hole in a steel plate. They added that heating caused by the plastic deformation of the material made it softer and the material became unstable when this thermal softening equalled the combined effects of strain and strain-rate hardening. Since then there have been numerous analytical [5]—[13], numerical [14]—[30] and experimental [31]—[34] studies aimed at understanding the physics and factors that enhance or inhibit the initiation and development of shear bands. Most of the analytical and numerical works have studied the simple shearing deformations of a viscoplastic body and modeled a material defect by introducing (i) a perturbation in temperature or strain-rate, (ii) a geometric defect such as a notch or a smooth variation in the thickness of the specimen, (iii) a weaker material at the site of the defect, (iv) a void, or (v) a rigid inclusion.

The previous two-dimensional studies [24]—[30] have presumed that plane strain state of deformation prevails in the body. Also, the body undergoes homogeneous deformations in the absence of a material defect. Here, we study the initiation and growth of a shear

band originating from the tips of a long narrow elliptic void or crack in a hollow cylindrical vessel whose inner surface is subjected to an impact load. We note that the deformations of the cylindrical pressure vessel are non-homogeneous even in the absence of the void. Also because of the tensile hoop stress, the void never coalesces. It is rather interesting to explore whether or not the bands initiate simultaneously from the void tips, their direction of propagation and the interaction amongst them.

The computed results suggest that the shear bands at the void tips initiate at different times and grow independently of each other. Due to the stress concentration at void tips, the temperature there rises. This is followed by a rapid drop in the effective stress. Soon after the effective stress drops to nearly zero value, the maximum principal logarithmic strain increases sharply. This increased deformation produces more heating which makes the material softer and hence facilitates its subsequent even larger deformations.

2 Formulation of the problem

We use rectangular Cartesian coordinates to analyze the plane strain deformations of a long cylindrical pressure vessel made of a thermally softening viscoplastic material and loaded internally by an impulsive load. The cross-section of the body, shown in Fig. 1, has two narrow ellipsoidal voids situated on the horizontal axis and the deformations of the body are presumed to be symmetrical about the two centroidal axes. Therefore, only the deformations of the material in the first quadrant are analyzed. In terms of non-dimensional

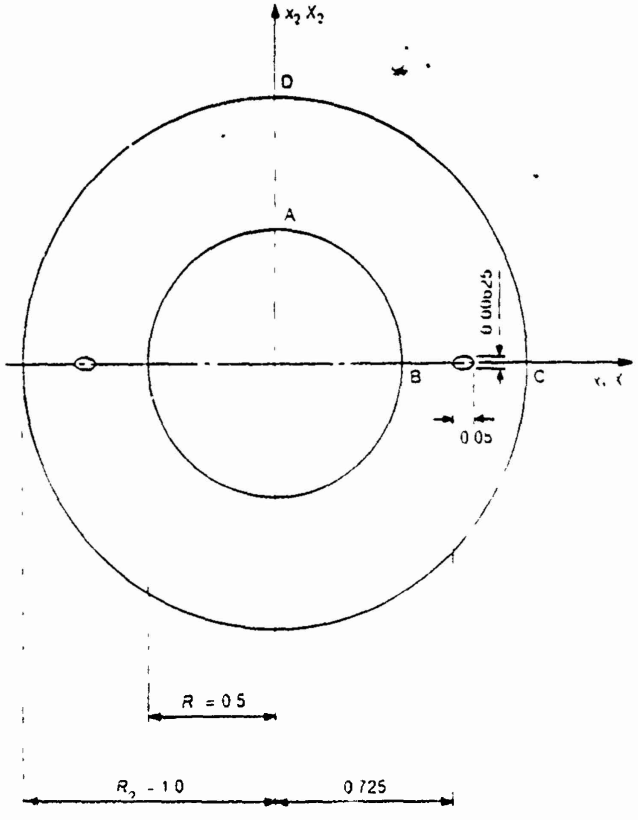

Fig. 1. Cross-section of the cylindrical body studied

variables, equations governing the deformations of the body are [26]:

$$\dot{\varrho} - \varrho v_{i,i} = 0, \tag{2.1}$$

$$\varrho v\dot{v}_i = \sigma_{ij,j}, \tag{2.2}$$

$$\varrho\dot{\theta} = \beta\theta_{,ii} - Q, \tag{2.3}$$

$$\sigma_{ij} = -B(\varrho - 1)\,\delta_{ij} + 2\mu D_{ij}, \tag{2.4}$$

$$2\mu = \frac{1}{\sqrt{3}\,I}(1 - bI)^m(1 - \varkappa\theta), \tag{2.5}$$

$$D_{ij} = (v_{i,j} - v_{j,i})/2, \qquad 2I^2 = \bar{D}_{ij}\bar{D}_{ij}, \qquad \bar{D}_{ij} = D_{ij} - 1/3D_{kk}\delta_{ij}, \tag{2.6}$$

$$Q = 2\mu\bar{D}_{ij}\bar{D}_{ij}. \tag{2.7}$$

Equations (2.1), (2.2) and (2.3) express, respectively, the balance of mass, balance of linear momentum and the balance of internal energy. Equation (2.4) is the presumed constitutive relation for the Cauchy stress σ_{ij} where 2μ is defined by Eq. (2.5). In Eqs. (2.1)—(2.7), ϱ is the mass density, v_i the velocity of a material particle in the direction x_i, θ is the temperature rise at a material particle, β is the non-dimensional diffusivity, σ_0 is the yield stress for the material of the body in a quasistatic simple compression test, B is the bulk modulus, parameters b and m describe the strain-rate hardening of the material, $\varkappa$ characterizes its thermal softening, Q is the rate of heat generated because of the plastic working, a superimposed dot stands for the material time derivative, a comma followed by an index i implies partial differentiation with respect to x_i, and the usual summation convention is used.

The non-dimensional variables are related to their dimensional counterparts, denoted below by a superimposed bar, as follows:

$$\begin{aligned}
&\bar{\sigma} = \sigma\sigma_0, \qquad \bar{t} = t\bar{R}_0/v_0, \qquad \bar{b} = b\bar{R}_0/v_0, \qquad \bar{B} = B\sigma_0,\\
&\theta_0 \equiv \sigma_0/(\varrho_0\bar{c}), \qquad \bar{\theta} = \theta\theta_0, \qquad \bar{x} = x/\theta_0, \qquad \bar{\varrho} = \varrho\varrho_0,\\
&\nu = \varrho_0 v_0^2/\sigma_0, \qquad \beta = \bar{k}/(\varrho_0\bar{c}v_0\bar{R}_0), \qquad \bar{\boldsymbol{x}} = \boldsymbol{x}\bar{R}_0.
\end{aligned} \tag{2.8}$$

Here $\bar{R}_0$ is the outer radius of the cylindrical vessel, v_0 is the final value of the radial velocity imposed on the inner surface, t is the elapsed time, $\bar{c}$ is the constant specific heat, $\bar{k}$ the constant thermal conductivity of the material of the body, and ϱ_0 is the mass density in the undeformed reference configuration of the body. The parameter ν indicates the relative magnitude of the inertia forces as compared to the flow stress.

Define s_{ij} by

$$s_{ij} = \sigma_{ij} - [B(\varrho - 1) - (2\mu/3)\,D_{kk}]\,\delta_{ij} = 2\mu\bar{D}_{ij}, \tag{2.9 1, 2}$$

Thus,

$$(1/2s_{ij}s_{ij})^{1/2} = (1/\sqrt{3})(1 - \varkappa\theta)(1 - bI)^m. \tag{2.10}$$

where we have substituted for 2μ from Eq. (2.5). Equation (2.10) can be regarded as representing a generalized von Mises yield surface with the flow stress, given by the right-hand side of Eq. (2.10), at a material particle depending upon the strain-rate and the temperature rise.

For the initial conditions, we take

$$\varrho(x, 0) = 1, \qquad v(x, 0) = 0, \qquad \theta(x, 0) = 0 \tag{2.11}$$

That is, the body is initially at rest, and has a uniform temperature and a constant mass density. We also assume that the body is initially stress free The boundary conditions for the material in the first quadrant are taken to be

$$v_r = h(t), \quad v_\theta = 0 \quad \text{and} \quad q_r = 0, \quad \text{on the inner surface } AB, \tag{2.12}$$

$$v_2 = 0, \quad \sigma_{12} = 0 \quad \text{and} \quad q_2 = 0 \quad \text{on the bottom surface } BC, \tag{2.13 1}$$

$$\sigma_{ij} n_j = 0, \quad \text{and} \quad \boldsymbol{q} \cdot \boldsymbol{n} = 0 \quad \text{on the void surface}, \tag{2.13.2}$$

$$\sigma_{rr} = 0, \quad \sigma_{\theta r} = 0 \quad \text{and} \quad q_r = 0 \quad \text{on the outer surface } CD, \tag{2.14}$$

$$v_1 = 0, \quad \sigma_{21} = 0 \quad \text{and} \quad q_1 = 0 \quad \text{on the left surface } DA. \tag{2.15}$$

Here $q_i = -\beta\theta_{,i}$ is the heat flux, the subscripts r and θ denote the radial and circumferential components of a quantity. These boundary conditions simulate the case when all bounding surfaces are taken to be perfectly insulated, the conditions imposed by the presumed symmetry of the deformations are applied on the surfaces BC and DA, the outer surface is taken to be traction free, and material particles on the inner surface AB are subjected to zero tangential velocity and time dependent radial velocity This radial velocity simulates approximately the effect of impact loading in the interior of the cylinder. The loading function $h(t)$ is taken to be

$$\begin{aligned} h(t) &= t/0.005, \qquad 0 \leqq t \leqq 0.005, \\ &= 1, \qquad\qquad t \geqq 0.005. \end{aligned} \tag{2.16}$$

We note that the governing equations (2.1) through (2.7) are coupled and highly nonlinear. It is rather hard to prove that these equations under the side conditions (2.11) through (2.15) have a solution or that the solution is unique. We seek an approximate solution of these equations by the finite element method. By using the Galerkin approximation [35], we first obtain from Eqs. (2.1) through (2.3) a set of coupled nonlinear ordinary differential equations. The number of these equations equals four times the number of nodes in the finite element discretization of the domain. We use four noded isoparametric quadrilateral elements to discretize the domain and use the lumped mass matrix. These ordinary differential equations are integrated with respect to time by using the Adams method included in the subroutine LSODE [36]. The computer code developed by Batra and Liu [27] was suitably modified to solve the present problem.

3 Computation and discussion of results

Assuming that the gun barrell or the cylindrical pressure vessel is made of a typical steel, we took the following values for various parameters.

$$\begin{aligned} &\bar{b} = 10{,}000\ \text{sec}, \quad \sigma_0 = 333\ \text{MPa}, \quad \bar{k} = 49.22\ \text{W m}^{-1}\ \text{C}^{-1}, \quad m = 0.025, \\ &\bar{c} = 473\ \text{J kg}^{-1}\ \text{C}^{-1}, \quad \varrho_0 = 7{,}800\ \text{kg m}^{-3}, \quad \bar{B} = 128\ \text{GPa}, \\ &\chi = 0.0025\ \text{C}^{-1}, \quad c_0 = 25\ \text{m sec}^{-1}, \quad \bar{R}_1 = 25\ \text{mm}, \quad \bar{R}_0 = 50\ \text{mm} \end{aligned} \tag{3.1}$$

Here R_1 and R_0 denote, respectively, the inner and the outer radius of the pressure vessel For values given in (3.1), $\theta_0 = 89.6$ C The location and relative dimensions of the void are shown in Fig. 1 The aspect ratio of the elliptical void is taken to be large so as to increase

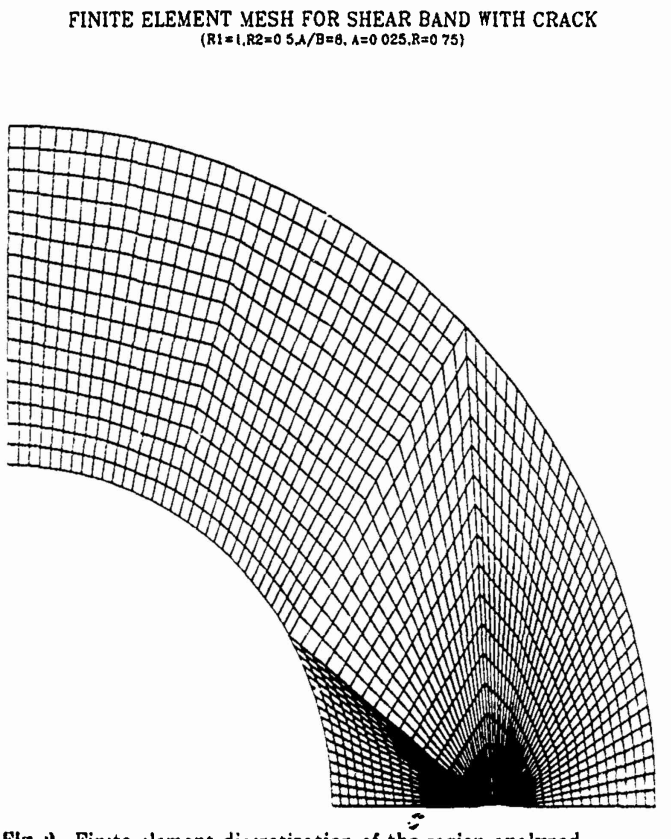

Fig. 2. Finite element discretization of the region analyzed

the stress concentration near the void tips and thereby accelerate the initiation of shear bands. The finite element mesh, depicted in Fig. 2, is very fine in the regions surrounding the void tips and gradually becomes coarser as we move away from them. No attempt has been made to align element sides in any particular direction. Needleman [25] used a mesh with the element sides aligned along the expected direction of the development of the shear band. He pointed out that such a mesh will give a better resolution of the sharp gradients of the deformation within the band.

In Figs. 3a through 3e, we have plotted contours of the temperature rise θ at $t = 0.0129$, 0.0149, 0.0177, 0.0191, 0.0219, and 0.0255 respectively. The temperature rise at a point is essentially proportional to the plastic work done there since for $t = 0.0255$, $t = 51$ μs and the time available for the heat to be conducted away is rather small. In order to decipher these contours clearly, we have focussed on a small region containing the ellipsoidal void. It is clear from these plots that the contours of temperature propagate towards the bounding surfaces of the cylinder as its deformation progresses. Whereas temperature contours surrounding the right tip of the void fan out laterally in both directions, those surrounding the left tip of the void spread out only downward towards the horizontal axis and the upper edge only moves longitudinally towards the inner surface of the cylinder. The distance through which these contours propagate depends upon θ, those for higher values of θ travel through a smaller distance implying thereby that their speeds are less as compared to the speed of propagation of contours of the lower temperature. In order to assess the effect of intense deformations near the void tips on the temperature rise there, we have plotted in Fig. 4 the temperature rise vs. the radial displacement of the inner surface at four different

points situated on the horizontal axis. Two of these points, namely Q and R, are close to the void tips and the other two points, P and S, are near the bounding surfaces. It is clear from the plots of Fig. 4 that the temperature rise at points near the bounding surfaces of the cylinder is miniscule as compared to that near the void tips. Also, the temperature rise near the void tip closer to the inner surface is significantly more than that at the other void tip. We note that the rate of temperature rise at these points is not constant. However, the two curves essentially stay parallel to each other after the initial development of shear bands near the void tips. Computations were stopped when the temperature at any point reached the presumed melting temperature of the material. Unlike the one-dimensional problem, the melting of a material point does not necessarily imply that the load carrying capacity

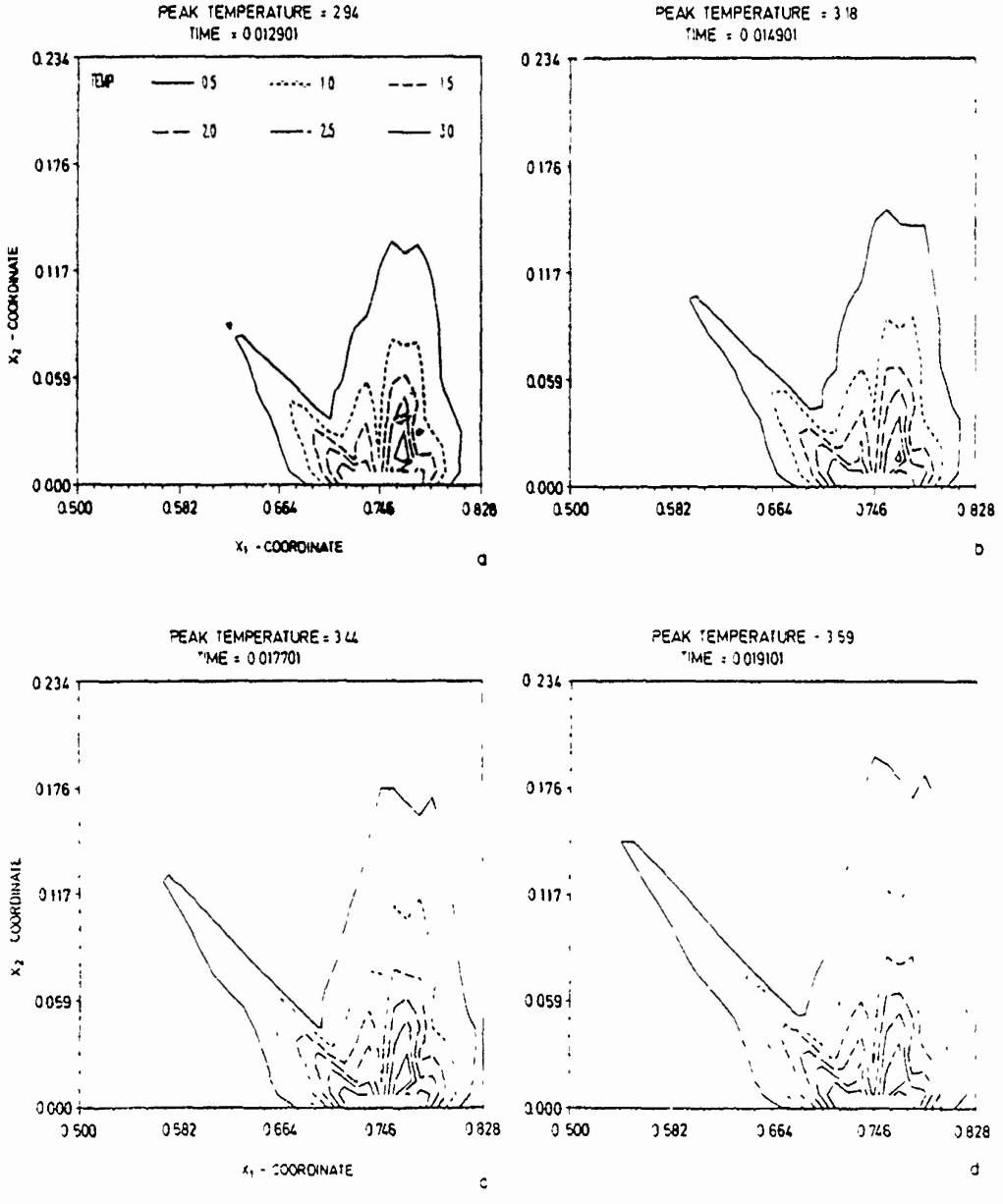

Fig. 3

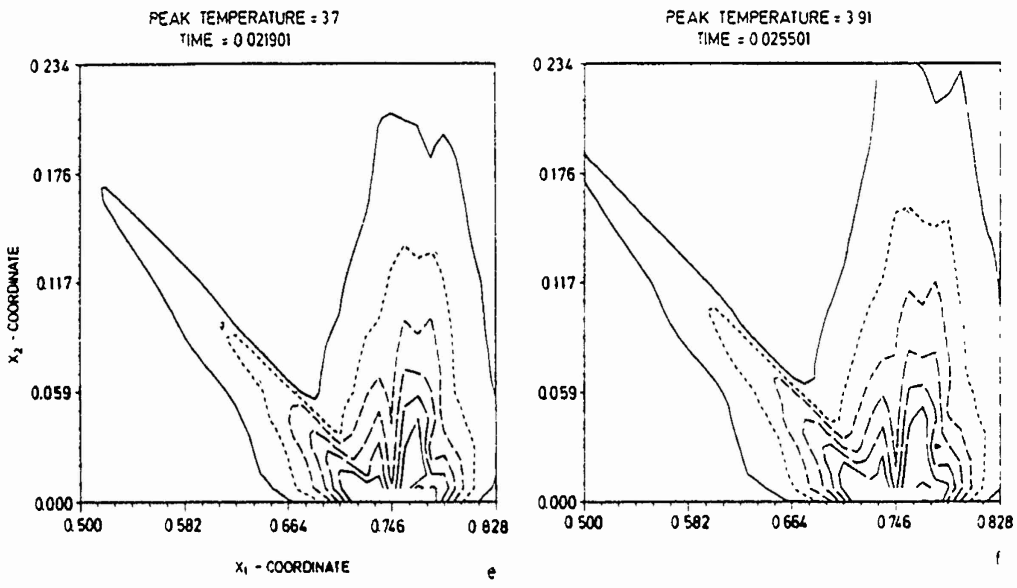

Fig. 3. Contours of the temperature rise θ at different values of elapsed time

a $t = 0.0129$ **b** $t = 0.0149$ **c** $t = 0.0177$
d $t = 0.0191$ **e** $t = 0.0219$ **f** $t = 0.0255$

——— $\theta = 0.5$; $\theta = 1.0$; ---------- $\theta = 1.5$;
——— $\theta = 2.0$; ——— $\theta = 2.5$; ——— 3.0

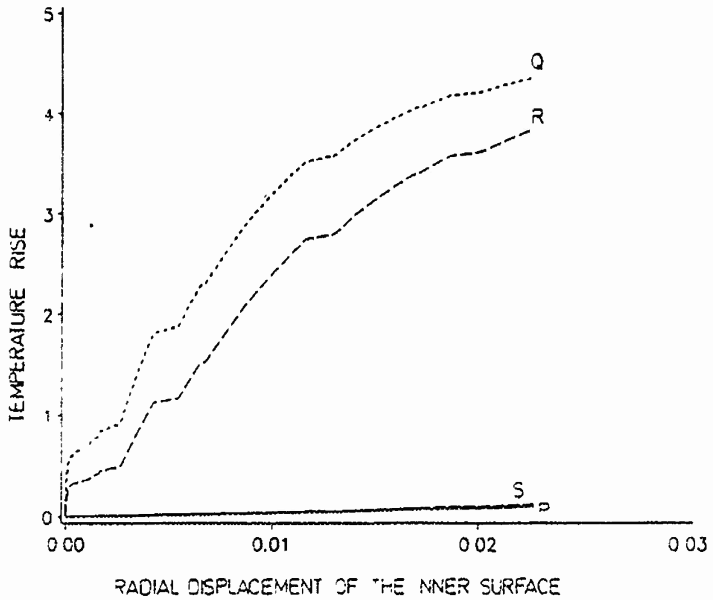

Fig. 4. The temperature rise vs. the radial displacement of the inner surface at four different points in the region. Co-ordinates of points in the stress free reference configuration are P (0.7016, 0.0015), Q(0.7193, 0.0033), R(0.7764, 0.0035) S(0.9984, 0.0027)

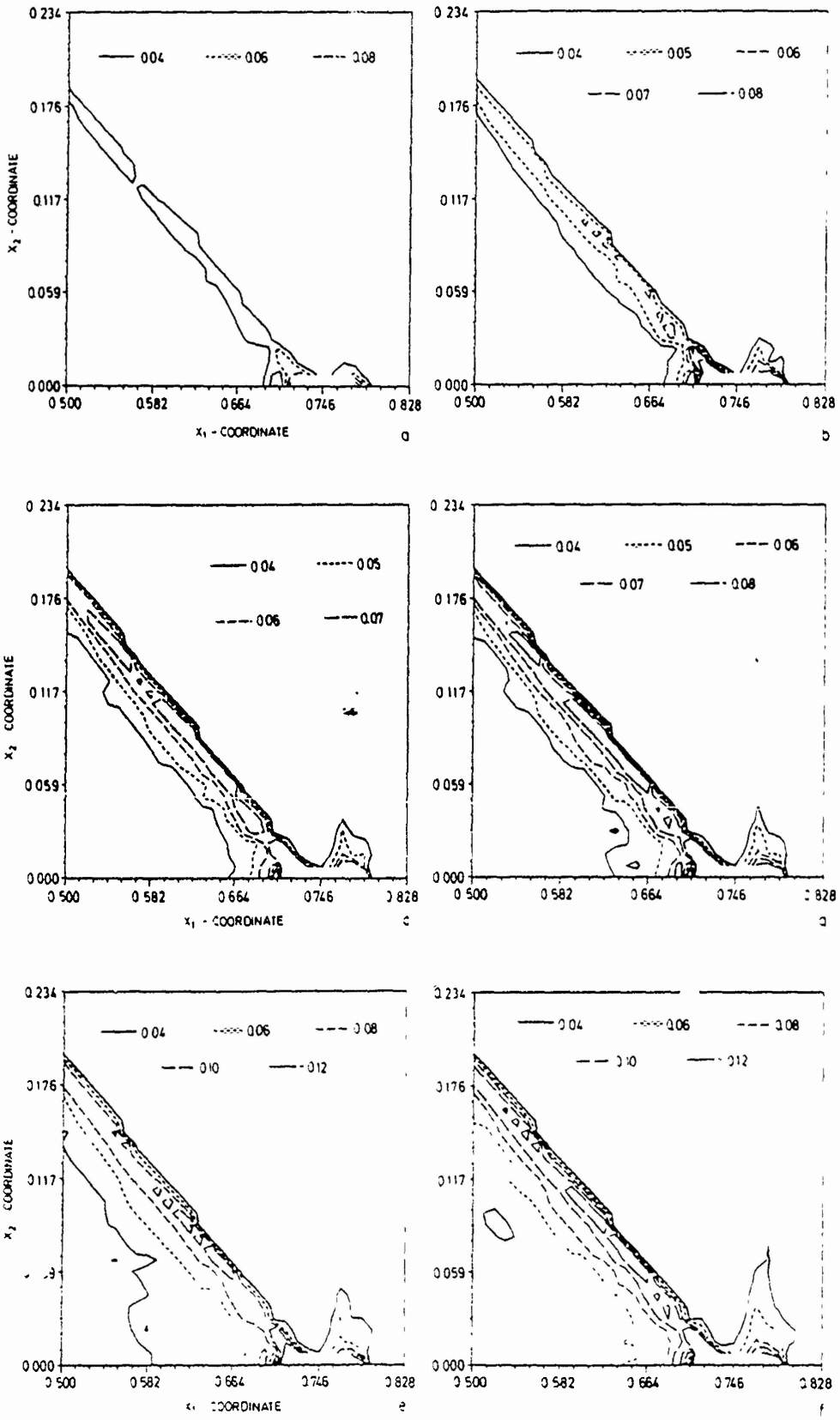
0.234
0.176
0.117
0.059
0.000
0.500
0.582
0.664
0.746
0.828
x_2 - COORDINATE
x_1 - COORDINATE
0.04
0.05
0.06
0.07
0.08
0.10
0.12
a
b
c
d
e
f

of the cylinder has been reduced to zero since the material surrounding the melted part of the body constrains its subsequent deformations. Whereas in the one-dimensional computations [37], subsequent to the formation of a shear band, the rate of temperature rise within the band was a nondecreasing function of time except for the Bodner-Partom law that is not so in the problem being studied herein. Here the rate of the temperature rise at a point near the void tips decreases slowly implying thereby that it will eventually reach a plateau. For the 2-dimensional problem involving the plane strain compression of a viscoplastic block containing a rigid ellipsoidal inclusion studied by Zhu and Batra [29], the rate of temperature rise gradually decreased. Zhu and Batra assumed an exponential thermal softening law. Therefore no material point ever lost its strength completely in their computations.

In order to elucidate how the strain field grows within shear bands and the region surrounding them, we have plotted contours of the maximum principal logarithmic strain ε in Fig. 5a—5e at $t = 0.0129, 0.0149, 0.0177, 0.0191, 0.0219$ and 0.0255 respectively. Note that

$$\varepsilon = \ln \lambda_1 \approx -\ln \lambda_2 \tag{3.2}$$

where λ_1^2, λ_2^2 and 1 are the eigenvalues of the right Cauchy-Green tensor $C_{\alpha\beta}$ defined as

$$C_{\alpha\beta} = x_{i,\alpha} x_{i,\beta}. \tag{3.3}$$

The second relation in Eq. (3.2) follows from the fact that the deformations are nearly isochoric. It is clear that at any instant the shear band initiating from the left void tip has propagated farther into the body than that initiating from the right void tip. A possible reason for this could be that the material to the left of the void undergoes more severe deformations as compared to that lying to the right of the void. The nonhomogeneous deformations of the cylinder, even in the absence of the void, possibly account for the different rate of growth of the two shear bands at the void tips. Like the contours of temperature, as the shear band develops, contours of successively higher values of ε originate from the void tips and propagate into the body. Whereas contours of ε originating from the right void tip fan out laterally in both directions as they propagate into the body those originating at the left void tip spread out only in one lateral direction. The plots in Fig. 6 of ε vs. the radial displacement of the inner surface at six points located near the horizontal axis reveal the intensity of the deformation within the shear bands. We note that points T and U are very close to Q and R respectively. They were chosen so as to lie on the path of the shear bands. It seems that the rapid growth of the strain within the two bands initiates almost simultaneously. However, the rate of growth of the deformation in the band surrounding the left void tip is noticeably higher than that in the band enclosing the right void tip. It is interesting to note that the changes in the rate of development of the two bands occur essentially at the same time and are similar in nature. We note that the maximum value of ε in the left band is more than 100 times the maximum value of ε at any point near the inner or outer surfaces of the cylinder. A comparison of the curves of ε vs. the

Fig. 5. Contours of the maximum principal logarithmic strain ε at different values of the elapsed time

a $t = 0.0129$ b $t = 0.0149$ c $t = 0.0177$
d $t = 0.0191$ e $t = 0.0219$ f $t = 0.0255$

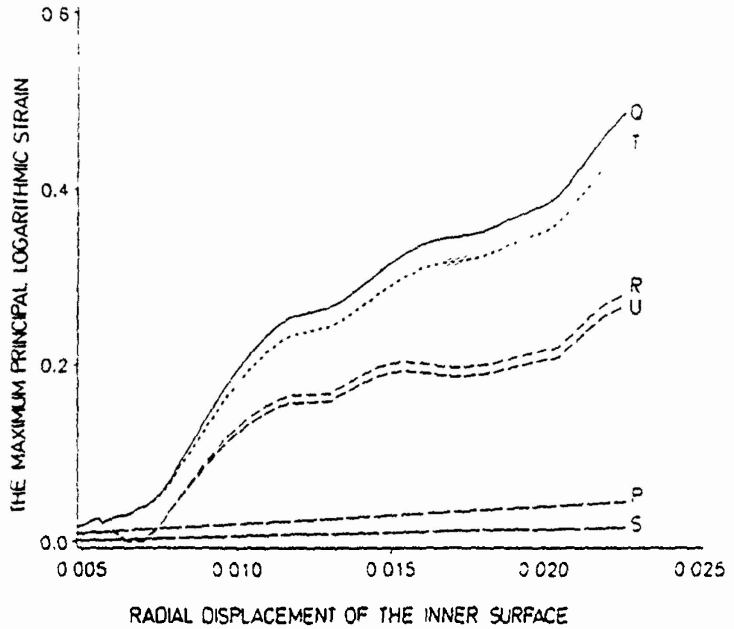

Fig. 6. The maximum principal logarithmic strain vs. the radial displacement of the inner surface at six different points in the region. See Fig. 4 for the co-ordinates of points P, Q, R, S. Co-ordinates of other two points are $T(0.7188, 0.0034)$, $U(0.7764, 0.0037)$

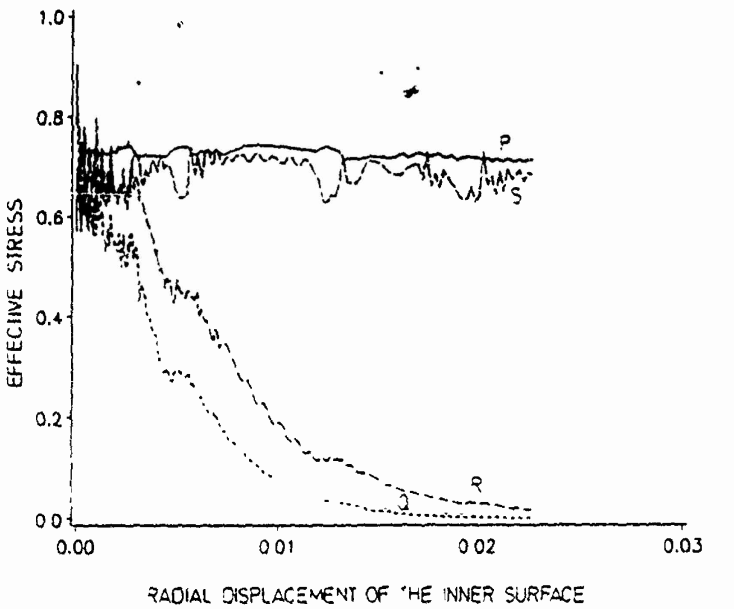

Fig. 7. The effective stress vs. the radial displacement of the inner surface at six different points in the region. See Fig. 6 for the coordinates of points

radial displacement of the inner surface at points Q and T, and R and U reveals that contours of small values of ε propagate much faster than those of large values of ε. For example, the time taken for $\varepsilon = 0.437$ to travel from point Q to point T equals 1.7144 μs and the distance QT equals 0.02405 mm thereby giving the speed of contour of $\varepsilon = 0.437$ as 14 m/sec. A similar exercise gives that the contour of $\varepsilon = 0.2524$ travels between points R and S at a speed of 115.2 m/sec. We note that the state of deformation in the region

surrounding points Q and R for the aforestated values of ε is quite different. Needleman [25], who studied plane strain deformations of a viscoplastic block deformed in simple compression, found that contours of constant values of ε propagated at speeds ranging from 590 m sec to 2500 m/sec depending upon the imposed nominal strain-rate. The constitutive relation used by Needleman is quite different from the one employed herein.

In Fig. 7, we have plotted the evolution of the effective stress s_e, defined as

$$2s_e^2 = s_{ij}s_{ij} \tag{3.4}$$

at points P, Q, R and S previously described. It is evident that the effective stress at points P and S that are close to the inner and outer surfaces, respectively, stays essentially constant after the initial transients have died out. The small oscillations reflect possibly the arrival of the contours of different strain and temperature at different values of the elapsed time. The effective stress within the two bands drops gradually to nearly zero. The effective stress in the left band is always lower than that in the right band which is consistent with the higher values of the temperature in the left band. Recalling the plots of ε vs the radial displacement of the inner surface in Fig. 6, we see that the rapid rise in the values of ε within the bands starts after the effective stress has dropped significantly. Zhu and Batra [29] observed a similar phenomenon in their study of the plane strain compression of a viscoplastic block containing a non-heat-conducting rigid inclusion even though they modeled thermal softening by an exponential function as opposed to the linear function used herein. This is possibly due to the fact that the relatively stronger material surrounding the weaker material within the band constrains the deformations of the latter.

Figure 8 shows how the average pressure

$$p = -2\pi \int_0^{\pi/2} \sigma_{rr}(0.5, \theta)\, d\theta \tag{3.5}$$

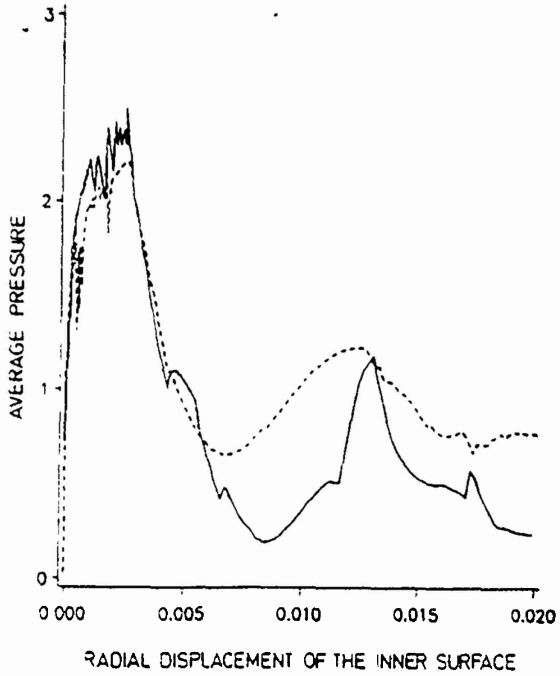

Fig. 8. The average internal pressure vs. radial displacement of the inner surface - — — — homogeneous cylinder; ———— cylinder with voids

on the inner surface varies with its radial displacement. The dashed curve corresponds to the deformations of a homogeneous cylinder and the solid curve to that of the cylinder with two ellipsoidal voids placed symmetrically on the horizontal axis. Note that in the solution of the problem, essential boundary conditions are prescribed on the inner surface of the cylinder. Subsequent to the development of the shear bands at void tips, as signified by the rapid rise of the maximum principal logarithmic strain, the average pressure in the cylinder with the shear bands stays lower than that in the homogeneous cylinder. This reflects the decrease in the load carrying capacity of the cylinder once a shear band has developed in it.

4 Conclusions

We have studied the problem of the initiation and growth of shear bands at void tips during the plane strain deformations of a hollow cylinder subjected to an impact load on the inner surface. Shear bands are found to develop at each void tip. The band forming at the void tip near the inner surface propagates towards the inner surface of the cylinder and that forming at the void tip near the outer surface propagates towards the outer surface of the cylinder. Whereas contours of the maximum principal logarithmic strain and the temperature rise originating at the void tip near the outer surface fan out laterally as they propagate into the body, those originating at the other void tip fan out only in the direction of the major axis of the ellipsoidal void. The shear band at the void tip near the inner surface forms sooner than that at the other void tip.

A review of the results discussed in the previous section gives the following scenario for the development of shear bands at the void tips. First, the temperature in the narrow region surrounding the void tips rises because of the stress concentration there. This is followed by a rapid drop in the effective stress and subsequently by a sharp increase in the values of the maximum principal logarithmic strain. The rate of drop of the effective stress and that of the rise in the maximum principal logarithmic strain depend upon the material parameters and the constitutive relation used to model the material response.

Acknowledgements

This work was supported by the National Science Foundation Grant MSM 8715952 and the U.S. Army Research Office Contract DAAL 03-88-K-0184 to the University of Missouri-Rolla. Some of the computations were performed on the IBM 3090 vector machine in Columbia, MO under the trial program.

References

[1] Johnson, W. Henri Tresca as the originator of adiabatic heat lines. Int. J. Mech. Sci. 29, 301–310 (1987).

[2] Tresca, H. On further application of the flow of solids. Proc. Inst. Mech. Engr. 30, 301 (1878).

[3] Massey, H. F. The flow of metal during forging. Proc. Manchester Assoc. Engineers, pp. 21–26, 1921. Reprinted by the National Machinery Co., Tiffon, Ohio, 1946.

[4] Zener, C., Hollomon, J. H., Effect of strain rate on plastic flow of steel. J. Appl. Phys. 14, 22–32 (1944).

[5] Recht, R. F. Catastrophic thermoplastic shear. J. Appl. Mech. 31, 189–193 (1964).

[6] Staker, M. R.: The relation between adiabatic shear instability strain and material properties. Acta Met. 29, 683–689 (1981).
[7] Clifton, R. J.: Material response to ultra high loading rates. NRC National Material Advisory Board (U.S.) Report 356, 1980.
[8] Molinari, A. Clifton, R. J.,: Analytic characterization of shear localization in thermoviscoplastic materials. J. Appl. Mech. 54, 806–812 (1987).
[9] Burns, T. J.: Approximate linear stability analysis of a model of adiabatic shear band formation. Quart. Appl. Math. 43, 65–83 (1985).
[10] Wright, T. W.: Steady shearing in a viscoplastic solid. J. Mech. Phys. Solids 35, 269–282 (1987).
[11] Anand, L., Kim, K. H., Shawki, T. G.: Onset of shear localization in viscoplastic solids. Massachusetts Institute of Technology Report, 1986.
[12] Bai, Y. L.: A criterion for thermoplastic shear instability. In: Shock waves and high strain rate phenomenon in metals (Meyers, M. A., Murr, L. E., eds.) pp. 277–283. New York: Plenum Press 1981.
[13] Coleman, B. D., Hodgdon, M. L.: On shear bands in ductile materials. Arch. Rat. Mech. Anal. 90, 219–247 (1985).
[14] Clifton, R. J., Duffy, J., Hartley, K. S., Shawki, T. G.: On critical conditions for shear band formation at high strain rates. Scripta Metallurgica 18, 443–448 (1984).
[15] Merzer, A. M.: Modeling of adiabatic shear band development from small imperfections. J. Mech. Phys. Solids 30, 323–338 (1982).
[16] Wu, F. H., Freund, L. B.: Deformation trapping due to thermoplastic instability in one-dimensional wave propagation. J. Mech. Phys. Solids 32, 119–132 (1984).
[17] Wright, T. W., Batra, R. C.: The initiation and growth of adiabatic shear bands. Int. J. Plasticity 1, 205–212 (1985).
[18] Wright, T. W., Batra, R. C.: Adiabatic shear bands in simple and dipolar plastic materials. In: Proc. IUTAM Symposium on macro- and micro-mechanics of high velocity deformation and fracture (Kawata, K., Shioiri, J., eds.) pp. 189–201. Berlin–Heidelberg–New York: Springer 1987.
[19] Wright, T. W., Walter, J. W.: On stress collapse in adiabatic shear bands. J. Mech. Phys. Solids 35, 701–720 (1987).
[20] Batra, R. C.: The initiation and growth of, and the interaction among adiabatic shear bands in simple and dipolar materials. Int. J. Plasticity 3, 75–89 (1987).
[21] Batra, R. C.: Effect of material parameters on the initiation and growth of adiabatic shear bands. Int. J. Solids and Structures, 23, 1435–1446 (1987).
[22] Batra, R. C.: Effect of nominal strain-rate on the initiation and growth of adiabatic shear bands. J. Appl. Mech. 55, 229–230 (1988).
[23] LeMonds, J., Needleman, A.: Finite element analyses of shear localization in rate and temperature dependent solids. Mech. Materials 5, 339–361 (1986).
[24] LeMonds, J., Needleman, A.: An analysis of shear band development incorporating heat conduction. Mech. Materials 5, 363–373 (1986).
[25] Needleman, A.: Dynamic shear band development in plane strain. J. Appl. Mech. 56, 1–9 (1989).
[26] Batra, R. C., Liu, D. S.: Adiabatic shear banding in plane strain problems. J. Appl. Mech. 56, 527–534 (1989).
[27] Batra, R. C., Liu, D. S.: Adiabatic shear banding in dynamic plane strain compression of a viscoplastic material. Int. J. Plasticity 6, 231–246 (1990).
[28] Anand, L., Lush, A. M., Kim, K. H.: Thermal aspects of shear localization in viscoplastic solids. In: Thermal aspects in manufacturing (Attia, M. H., Kops, L., eds.) ASME PED-Vol. 30, 89–103, 1988.
[29] Zhu, Z. G., Batra, R. C.: Dynamic shear band development in plane strain compression of a viscoplastic body containing a rigid inclusion. Acta Mechanica 84, 59–107 (1990).
[30] Fressengeas, C.: Adiabatic shear morphology at very high strain rates. Int. J. Impact Engr. 8, 141–158 (1989).
[31] Moss, G. L.: Shear strain, strain rate and temperature changes in adiabatic shear band. In: Shock waves and high strain rate phenomenon in metals (Meyer, M. A., Murr, L. E., eds.) pp. 299–312. New York: Plenum Press 1981.
[32] Costin, L. S., Crisman, E. E., Hawley, R. H., Duffy, J.: On the localization of plastic flow in mild steel tubes under dynamic torsional loading. Int. Phys. Conf. Ser. 47, 90–100 (1979).

[33] Hartley, K. A., Duffy, J., Hawley, R. H.: Measurement of the temperature profile during shear band formation in steels deforming at high strain rates. J. Mech. Phys. Solids 35, 283–301 (1987).
[34] Marchand, A., Duffy, J.: An experimental study of the formation process of adiabatic shear bands in a structural steel. J. Mech. Phys. Solids 36, 251–283 (1988).
[35] Hughes, T. J. R.: The finite element method. Linear static and dynamic finite element analysis. Englewood Cliffs: Prentice Hall 1987.
[36] Hindmarsh, A. C.: ODEPACK, a systematized collection of ODE solvers. In: Scientific computing (Stepleman R. S. et al., eds) pp. 55–64. Amsterdam: North-Holland 1983.
[37] Batra, R. C., Kim, C. H.: Effect of viscoplastic flow rules on the initiation and growth of shear bands at high strain rates. J. Mech. Phys. Solids (in press).

Authors' address: R. C. Batra and X.-T. Zhang, Department of Mechanical and Aerospace Engineering and Engineering Mechanics, University of Missouri-Rolla, Rolla, MO 65401-0249, U.S.A.

Printed in Germany
Maxim Gorki - Druck GmbH Carl-von-Ossietzky-Str. 30/31, 7400 Altenburg

Acta Mechanica 86, 31—52 (1991)

ACTA MECHANICA

Dynamic shear band development in a thermally softening bimetallic body containing two voids

R. C. Batra and Z. G. Zhu, Rolla, Missouri

(Received May 18, 1990; revised July 12, 1990)

Summary. We study the development of shear bands in a thermally softening viscoplastic prismatic body of square cross-section and containing two symmetrically placed thin layers of a different viscoplastic material and two elliptical voids with their major axes aligned along the vertical centroidal axis of the cross-section. One tip of each elliptical void is abutting the common interface between the layer and the matrix material. Two cases, i.e., when the yield stress of the material of the thin layer in a quasistatic simple compression test equals either five times or one-fifth that of the matrix material are studied. The body is deformed in plane strain compression at an average strain-rate of 5,000 sec^{-1}, and the deformations are assumed to be symmetrical about the centroidal axes.

It is found that in each case shear bands initiate from points on the vertical traction free surfaces where the layer and the matrix materials meet. These bands propagate horizontally into the layer when it is made of a softer material and into the matrix along lines making an angle of $\pm 45°$ with the vertical when the layer material is harder. In the former case, the band in the layer near the upper matrix/layer interface bifurcates into two bands, one propagating horizontally into the layer and the other into the matrix material along the direction of the maximum shear stress. The band in the layer near the lower matrix/layer interface propagates horizontally first into the layer and then into the matrix material along the direction of the maximum shear stress. Irrespective of the value of the yield stress for the layer material, a band also initiates from the void tip abutting the layer/matrix interface. This band propagates initially along the layer/matrix interface and then into the matrix material along a line making an angle of approximately 45° with the vertical.

1 Introduction

Johnson [1] has recently pointed out that Tresca [2] in 1878 and Massey [3] in 1921 observed hot lines, now referred to as shear bands, in the form of a cross during the hot forging of a metal. There has been a surge of activity in this area since the time Zener and Hollomon [4] reported 32 μm wide shear bands during the punching of a hole in a steel plate. They asserted that the heat generated because of the plastic working softened the material and that the material became unstable when thermal softening equalled the combined effects of strain and strain-rate hardening. The experimental observations of Moss [5], Costin et al. [6], Hartley et al. [7], Giovanola [8], and Marchand and Duffy [9] have added enormously to our understanding of the phenomenon of shear strain localization. Marchand and Duffy have pointed out that for thin steel tubes subjected to a pure torque at the ends, the localization of deformation into shear bands consists of three stages. In stage I, the body deforms homogeneously. In stage II, stipulated to initiate when the shear stress at a point attains its maximum value, the deformation becomes non-homogeneous. In stage III, that occurs much later, the shear stress drops precipitously and the deformation localizes into a shear band. These experimental observations agree with the numerical work of Wright and Walter [10], Molinari and Clifton [11], and Batra and Kim [12] to

[15]. We note that there have been numerous other numerical [16]—[24] and analytical studies [25]—[32] aimed at increasing our understanding of factors that affect the initiation and development of shear bands. These works have analysed the simple shearing deformations of a viscoplastic body containing a defect.

Recently, LeMonds and Needleman [33], [34], Needleman [35], Zbib and Aifantis [36], Anand et al. [37], Batra and Liu [38], [39], Zhu and Batra [40], and Batra and Zhang [41] have studied the phenomenon of shear banding in plane strain deformations of a viscoplastic solid. These works have generally used different constitutive relations and have assumed that the entire body or the portion of the body whose deformations were analyzed had only one defect in it. The prismatic body whose plane strain thermomechanical deformations are studied herein is of a square cross-section and has two thin layers made of a viscoplastic material different from that of the body and placed symmetrically about and parallel to the centroidal horizontal axis. These horizontal planes may be thought of as representing planes of chemical inhomogeneity. The material of the layer differs from that of the body only in the value σ_0 of the flow stress in a quasistatic simple compression test. Two cases, namely when σ_0 for the layer material equals five times or one-fifth that of the matrix material are studied. Also, there are two elliptical voids with major axes aligned with the vertical centroidal axis of the square cross-section and with tips touching the layer/matrix interfaces. The other ends of the ellipsoidal voids are towards the center of the cross-section. The points on the free edges where the thin layer and the matrix materials meet as well as the void vertices on the major axes of the ellipsoid act as nuclei for the initiation of shear bands. It thus becomes an interesting excercise to investigate the initiation and propagation of various bands and the interaction amongst them. We add that we do account for the effect of inertia forces, strain-rate sensitivity of the materials, their thermal softening, heat conduction, and the heat generated because of plastic working.

2 Formulation of the problem

The cross-section of the prismatic body containing two ellipsoidal voids and two thin layers of a different viscoplastic material is shown in Fig. 1. The deformations of the body are assumed to be symmetrical about the two centroidal axes. Thus, the deformations of the material in the first quadrant are analyzed. With respect to a fixed set of rectangular Cartesian coordinate axes, equations governing the plane strain thermomechanical deformations of the body are:

$$(\varrho J)^{\cdot} = 0, \tag{2.1}$$

$$\varrho_0 \dot{v}_i = T_{ij,j}, \tag{2.2}$$

$$\varrho_0 \dot{e} = -Q_{i,i} - T_{ij} v_{i,j}, \tag{2.3}$$

$$D_{ij} = (v_{i,j} + v_{j,i})/2, \tag{2.4}$$

$$T_{ij} = (\varrho_0/\varrho)\, \sigma_{ij} x_{i,J}, \qquad \sigma_{ij} = -B(\varrho/\varrho_0 - 1)\, \delta_{ij} + 2\mu D_{ij}, \tag{2.5}$$

$$2\mu = \left[\sigma_0 / \left(\sqrt{3}\, I\right)\right] (1 - bI)^m (1 - \lambda\theta), \tag{2.6}$$

$$I^2 = (1/2)\, \overline{D}_{ij} \overline{D}_{ij}, \tag{2.7}$$

$$\overline{D}_{ij} = D_{ij} - (1/3)\, D_{kk} \delta_{ij}, \tag{2.8}$$

$$Q_i = (\varrho_0/\varrho)\, \eta_i \theta_{,i}, \qquad \eta_i = -k\theta_{,i}, \tag{2.9}$$

$$\dot{e} = c\dot{\theta} - B(\varrho/\varrho_0 - 1)\, \dot{\varrho}/\varrho^2. \tag{2.10}$$

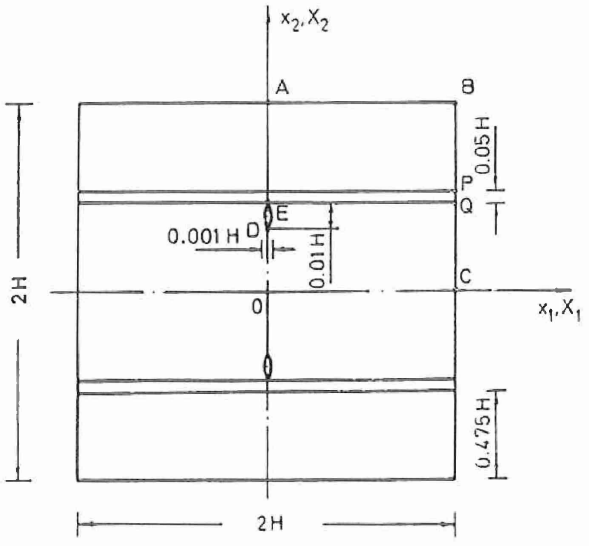

Fig. 1. The cross-section of the prismatic body studied

Equations (2.1), (2.2) and (2.3), written in terms of the referential description of motion, express respectively the balance of mass, balance of linear momentum and the balance of moment of momentum. Equations (2.5), (2.9) and (2.10) are the constitutive assumptions. In these equations x_i gives the position at time t of the material particle X_a, $v_i = \dot{x}_i$ is its velocity in the x_i-direction, ϱ is its present mass density, ϱ_0 its mass density in the reference configuration, $J = \det[x_{i,a}]$, $x_{i,a} = \partial x_i/\partial X_a$, T_{ia} is the first Piola-Kirchhoff stress tensor, e is the specific internal energy, Q_a is the heat flux measured per unit area in the reference configuration, and $\boldsymbol{D}$ is the strain-rate tensor. Furthermore, a superimposed dot indicates material time derivative, a comma followed by index a(j) implies partial differentiation with respect to X_a (x_j), and a repeated index implies summation over the range (1, 2) of the index. In the constitutive relations (2.5), (2.9) and (2.10), the material parameter B may be regarded as the bulk modulus, σ_0 is the yield stress in a quasistatic simple compression test, parameters b and m describe the strain-rate hardening of the material, $\varkappa$ is the thermal softening parameter, θ equals the temperature change of a material particle from that in the reference configuration, k is the thermal conductivity and c is the specific heat. Both k and c are taken to be constants and we have neglected stresses caused by the thermal expansion.

Equations (2.1) through (2.10) hold in the regions occupied by the matrix and the layer, the only difference being either

$$\sigma_0 \text{ layer } = 5\sigma_0 \text{ matrix}, \tag{2.11.1}$$

or

$$\sigma_0 \text{ layer } = (1/5)\,\sigma_0 \text{ matrix}. \tag{2.11.2}$$

The values of other material parameters are the same for the matrix and the layer.

With $\boldsymbol{s}$ defined by

$$\boldsymbol{s} = \boldsymbol{\sigma} + [B(\varrho/\varrho_0 - 1) - (2\mu/3)\,\mathrm{tr}\,\boldsymbol{D}]\,\boldsymbol{1}, \tag{2.12.1}$$

$$= 2\mu\bar{\boldsymbol{D}}, \tag{2.12.2}$$

equations (2.12), (2.5) and (2.6) give

$$(1/2 \text{ tr } \mathbf{s}^2)^{1/2} = \left(\sigma_0/\sqrt{3}\right)(1 - \alpha\theta)(1 - bI)^m . \tag{2.13}$$

This can be viewed as the equation of a generalized von Mises yield surface when the flow stress, given by the right-hand side of (2.13), at a material particle depends upon its strain-rate and temperature.

For the initial conditions we take

$$\varrho(\boldsymbol{x}, 0) = 1, \qquad \boldsymbol{v}(\boldsymbol{x}, 0) = \mathbf{0}, \qquad \theta(\boldsymbol{x}, 0) = 0. \tag{2.14}$$

That is, the body is initially at rest at a uniform temperature and has constant mass density. We also assume that the body is initially stress free. The pertinent boundary conditions for the material analyzed in the first quadrant are

$$v_2 = -h(t), \qquad T_{12} = 0 \quad \text{and} \quad Q_2 = 0, \quad \text{on the top surface } AB. \tag{2.15}$$

$$T_{11} = 0, \qquad T_{21} = 0 \quad \text{and} \quad Q_1 = 0, \quad \text{on the right surface } BC, \tag{2.16}$$

$$v_2 = 0, \qquad T_{12} = 0 \quad \text{and} \quad Q_2 = 0, \quad \text{on the bottom surface } C0, \tag{2.17}$$

$$v_1 = 0, \qquad T_{21} = 0 \quad \text{and} \quad Q_1 = 0, \quad \text{on parts } OD \text{ and } EA \text{ of the left surface } OA, \tag{2.18}$$

$$T_{ia}N_a = 0 \quad \text{and} \quad Q_a N_a = 0, \quad \text{on the surface } DE \text{ of the void}. \tag{2.19}$$

These boundary conditions simulate the situation when the top surface is moving downward with a speed $h(t)$, there is no friction between it and the loading device, the right surface is traction free, the void has not coalesced and the entire boundary is thermally insulated. If during the deformations of the body, any point on the void surface touches the vertical axis, the boundary condition on it is changed to (2.18). The boundary conditions (2.17) and (2.18) are due to the presumed symmetry of the deformations about the x_1 and x_2 axes. For the loading function $h(t)$ we take

$$\begin{aligned} h(t) &= v_0 t/t_r, \qquad 0 \leqq t \leqq t_r, \\ &= v_0, \qquad t > t_r, \end{aligned} \tag{2.20}$$

where $2H$ is the height of the block and v_0 is the steady speed of the top surface. The steady speed is reached in time t_r.

At the common interface between the matrix and the reinforcing layer, the velocity field, surface tractions, the temperature and the normal component of the heat flux are assumed to be continuous.

3 Computational considerations

Substitution for $\boldsymbol{T}$, $\boldsymbol{Q}$ and e from Eqs. (2.5) through (2.10) into the balance laws (2.2) and (2.3) results in coupled nonlinear partial differential equations which along with initial conditions (2.14) and boundary conditions (2.15) through (2.19) are to be solved for ϱ, $\boldsymbol{v}$ and θ. We use the updated Lagrangian method [42] to solve the problem. That is, in order to find the fields of ϱ, $\boldsymbol{v}$ and θ in the body at time $t - \Delta t$, the configuration of the body at time t is taken as the reference configuration. The governing nonlinear partial differential equations are first reduced to a set of coupled nonlinear ordinary differential equations by using the Galerkin approximation [42] and the lumped mass matrix. Figure 2 depicts the

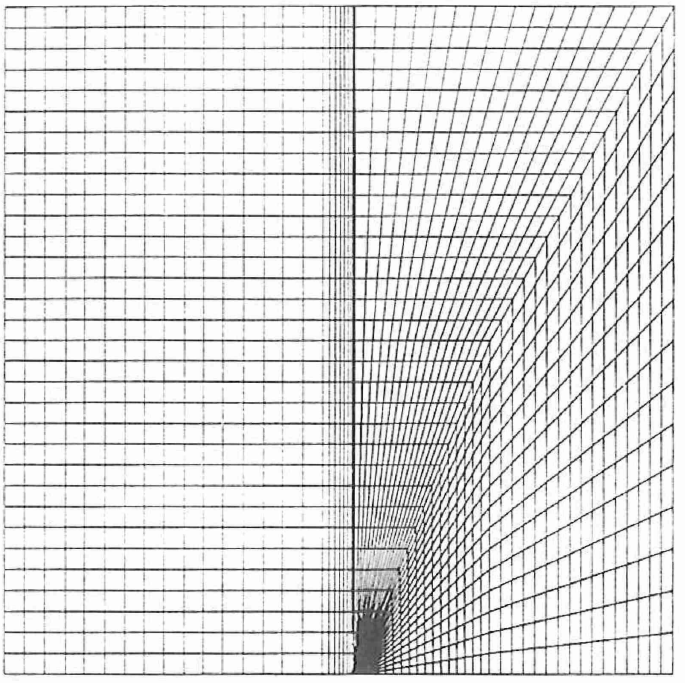

Fig. 2. The finite element discretization of the domain in the stress free reference configuration

discretization of the stress free reference configuration into 4-noded isoparametric quadrilateral elements that has been used to analyze the problem. The mesh is very fine in the region surrounding the void and gradually becomes coarse as we move away from it. The layer as well as a small matrix region adjoining it has been divided into a fine mesh too. We add that the coordinates of the nodes are updated after each time increment. Thus, the spatial domain occupied by the body and the shapes of these elements vary with time. At each node the mass density, two components of the velocity and the temperature are unknown. The coupled nonlinear ordinary differential equations are integrated by using the Gear method [43] for stiff differential equations. We use the subroutine LSODE taken from the package ODEPACK, developed by Hindmarsh [44], and employed the option of using the full Jacobian matrix. The subroutine adjusts the time step adaptively until a solution of the coupled nonlinear ordinary differential equations has been computed to the desired accuracy. The finite element code developed earlier by Batra and Liu [38] was modified to study the present problem.

4 Computation and discussion of results

We used the following values of various material and geometric parameters to compute results that are discussed below:

$$b = 10.000\,\text{sec},\ \sigma_0 = 333\,\text{MPa},\ k = 49.22\,\text{W m}^{-1}\,^{\circ}\text{C}^{-1},\ m = 0.025,$$
$$c = 473\,\text{J kg}^{-1}\,^{\circ}\text{C}^{-1},\ \varrho_0 = 7{,}860\,\text{kg m}^{-3},\ B = 128\,\text{GPa}, \tag{3.1}$$
$$H = 5\,\text{mm},\ v_0 = 25\,\text{msec}^{-1},\ \chi = 0.0025\,^{\circ}\text{C}^{-1}.$$

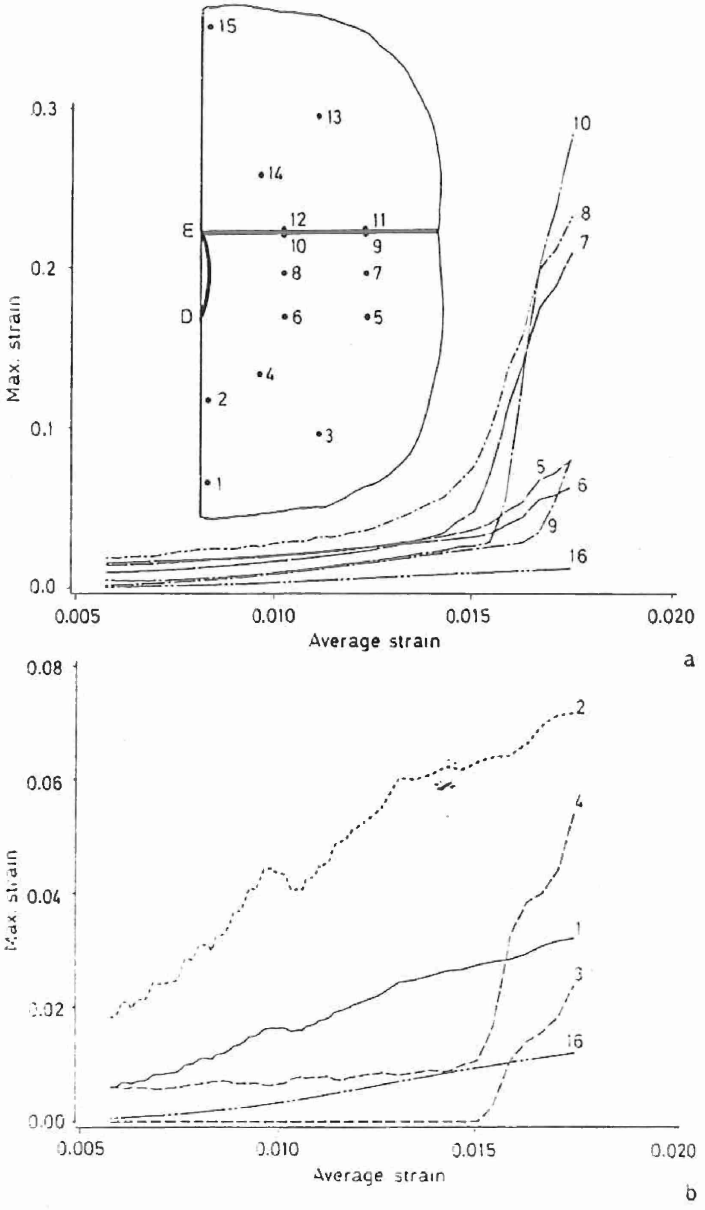

Fig. 3a. The maximum principal logarithmic strain versus the average strain at points 5 through 10 and 16 when the layer material is softer than the matrix material. Coordinates, in the stress free reference configuration, of these points are: 5 (0.0200, 0.4650), 6 (0.010, 0.4650), 7 (0.0200, 0.4700), 8 (0.010, 0.4700), 9 (0.0200, 0.4749), 10 (0.010, 0.4749), 16 (0.010, 0.8000)

Fig. 3b. The maximum principal logarithmic strain versus the average strain at points 1 through 4 and 16 when the layer material is softer than the matrix material. Coordinates, in the stress free reference configuration, of these points are: 1 (0.0010, 0.4450), 2 (0.0010, 0.4550), 3 (0.0141, 0.4509), 4 (0.0071, 0.4579)

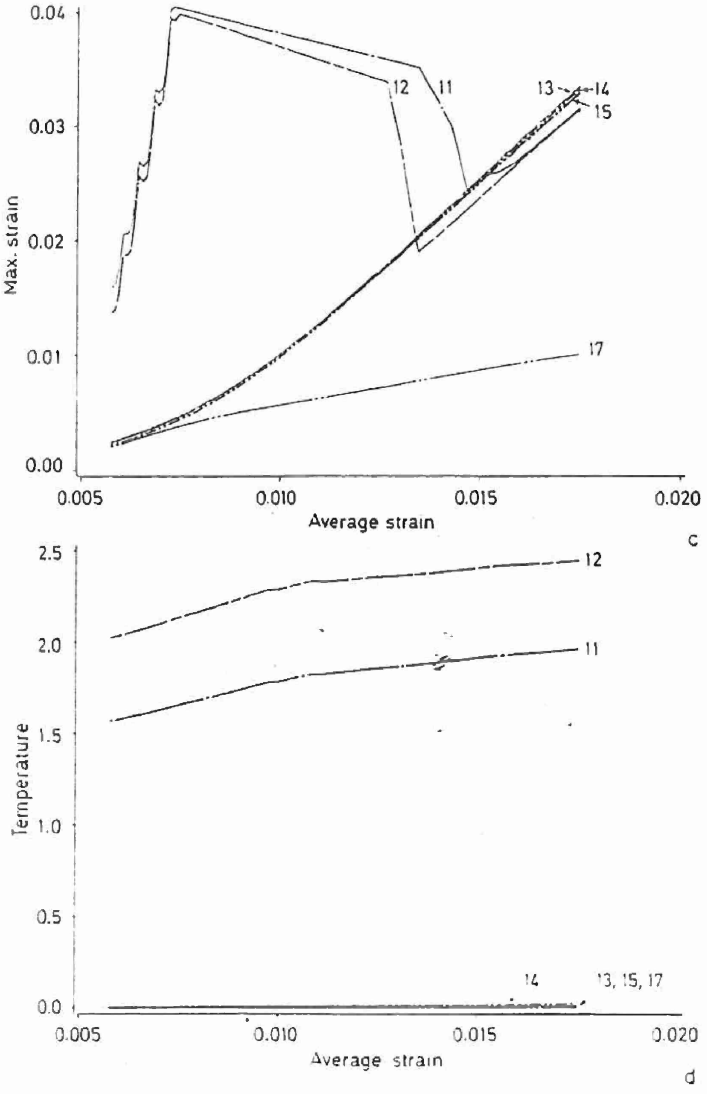

Fig. 3c. The maximum principal logarithmic strain versus the average strain at points 11 through 15 and 17 when the layer material is softer than the matrix material. All of these points are in the soft layer. Coordinates, in the stress free reference configuration, of these points are: 11 (0.0200, 0.4751), 12 (0.0100, 0.4751), 13 (0.01414, 0.4891), 14 (0.0071, 0.4821), 15 (0.0010, 0.5), 17 (0.5, 0.5)

Fig. 3d. The temperature rise versus the average strain at points 11 through 15 and 17 when the layer material is softer than the matrix material

Thus the average applied strain-rate $\dot{\gamma}_{avg}$ equals 5,000 sec^{-1}, $\theta_0 \equiv \sigma_0/(\varrho_0 c) = 89.6\,^{\circ}$C, and $\nu \equiv \varrho_0 v_0^2/\sigma_0 = 0.015$. The nondimensional number ν determines the effect of inertia forces relative to the flow stress of the material. For the simple shearing problem, Batra [21] noted that the inertia forces play a noticeable role when $\nu = 0.004$. Hence, the inertia forces will very likely play a significant role in the present problem.

We discuss below results in terms of the following nondimensional variables indicated by a superimposed bar.

$$\bar{s} = s/\sigma_0, \qquad \bar{\theta} = \theta/\theta_0, \qquad \bar{x} = x/H, \qquad \bar{I} = I/\dot{\gamma}_{avg}. \tag{3.2}$$

Henceforth, we drop the superimposed bars. To measure the deformation at a point, we use the maximum principal logarithmic strain ε given by

$$\varepsilon = \ln \lambda_1 \simeq -\ln \lambda_2, \tag{3.3}$$

where λ_1^2 and λ_2^2 are eigenvalues of the right Cauchy-Green tensor $C_{ij} = x_{i,\alpha}x_{i,\beta}$ or the left Cauchy-Green tensor $B_{ij} = x_{i,\alpha}x_{j,\alpha}$. The second equality in Eq. (3.3) holds because the deformations of the body are nearly isochoric.

4.1 Layer material softer than the matrix material

Recall that one tip of the elliptical void is at the interface between matrix material and the relatively softer layer and the other tip is in the matrix. In order to find out where the shear bands form and their directions of propagation, we plot the evolution of the maximum principal logarithmic strain ε at several points surrounding the void and at points near the common interface between the layer and the matrix material. Figure 3a depicts the growth of ε at points 5 through 10 and point 16. Point 10 in the matrix is near the void tip that touches the common interface, point 9 is near the interface and on a horizontal line through point 10, point 8 is near the midsurface of the void and point 7 on a horizontal line through point 8, point 6 is near the other tip of the void and point 5 on a horizontal line through point 6. Point 16, not shown in the figure, is the near the vertical centroidal axis but is far removed from the void and the layer/matrix interfaces. Coordinates of these points in the stress free reference configuration are given in the figure caption and their approximate locations are shown in Fig. 3a. Results plotted in this figure clearly indicate that at a nominal strain of nearly 0.015, the values of ε at points 7, 8 and 10 increase sharply with the rate of growth of ε at point 10 being higher than that at points 7 and 8. Note that the value of ε at point 16 is very close to the average strain, and the values of ε at points 5, 6 and 9 are higher than that at point 16 but considerably smaller than those at points 7, 8 and 10. Thus the small region containing points 7, 8 and 10 undergoes severe deformations. In Fig. 3b, we have plotted the growth of ε at points 1, 2, 3, 4 and 16. Point 2 is near the void tip D, point 1 is on a vertical line through point 2, and the line joining points D, 4 and 3 makes an angle of 45° with the vertical. At an average strain of approximately 0.015, the values of ε at points 3 and 4 increase sharply. However, the peak values attained at points 1, 2, 3 and 4 are much lower than those at points 7, 8 and 10. Thus in the matrix material surrounding the void, more intense deformations occur near the void tip E at the matrix/layer interface. In an attempt to assess the deformations of the layer, we have plotted ε versus the average strain in Fig. 3c at points 11, 12, 13, 14, 15 and 17 in the layer. Points 11 and 12 are near the matrix/layer interface and correspond respectively to points 9 and 10 in the matrix, the line joining points E, 14 and 13 makes an angle of 45° with the horizontal,

point 15 is near the vertical centroidal axis, and point 17 in the layer is far removed from the void tip. The approximate location of these points is given in Fig. 3a and their coordinates in the stress free reference configuration are given in the figure caption. Even though the values of ε at points 11 and 12 increase sharply in the beginning, they eventually match those at points 13, 14 and 15. Recalling that σ_0 for the layer material equals one—fifth that for the matrix material, we may imagine the void to be in a rigid material as far as the deformations of the layer are concerned. Thus the deformations of the layer near the void tip need not be excessively large as compared to its average deformations. This is borne out by the results plotted in Fig. 3c which show that the peak values of ε at points 13, 14 and 15 are nearly twice the average. Because of the continuity of the displacements and temperatures across the layer/matrix interface, initially points 11 and 12 undergo essentially the same deformations as points 9 and 10. The rise in the temperature at points 11 and 12 makes the material there softer. The surrounding relatively hard layer material results in redistribution of the deformations. Note that points 9, 10, 11 and 12 are a little bit away from the layer/matrix interface. Thus one may conclude that no localization of the deformation into a shear band occurs within the layer material near the void tip. That the temperature rise at points 11 and 12 is much larger than that at points 13, 14, 15 and 17 becomes clear from the results plotted in Fig. 3d. The plots of the temperature rise at other points considered are not included herein. However, we note that the temperature rise at points 7, 8 and 10 where severe deformations of the matrix material occur was considerably more than that at point 16 which is far away from the void.

We now focus on the deformations of the layer and the matrix materials near points P and Q on the right traction free surface. Points P and Q are also on the layer/matrix interfaces. Figure 4a shows the plot of ε versus the average strain at points 18 through 25 near the upper matrix/layer interface. Points 18 through 21 are in the layer and points 22 through 25 are in the matrix. It is clear that deformations of points 18 and 19 are significantly more than the deformations of other points considered in this plot. Also intense deformations of the layer material surrounding point 18 propagate horizontally to point 19. The deformations of points 21 through 25 are very small as compared to the deformations of points 18 and 19. The value of ε at point 20 is nearly four times that at point 21. It is possible that the intense deformations initiating at point 18 propagate to point 20 too. In an attempt to shed some light on what happens to the shear band initiating from point 18, we have plotted in Fig. 4b values of ε versus the average strain at points 24 through 30 in the matrix. Points 20, 24, 27 and 29 are on the same vertical line with points 20 and 24 on the opposite sides of the matrix layer interface. Points 24, 27 and 29 are in the matrix. Points 24, 26 and 25 are on a horizontal line and points 24, 28 and 30 are on the line that makes an angle of 45° with the horizontal. Relatively large values of ε at points 24, 26, 27, 28 and 30 seem to suggest that the region surrounding points 24, 26 and 27 deforms severely and that these severe deformations propagate along the line joining points 24, 28 and 30. Since points 20 and 24 are very near to each other, it is reasonable to conclude that the localization of deformation initiating at point 18 within the soft layer propagates towards point 20 and then along the line joining points 20, 28 and 30. Results plotted at similarly situated points near the other interface between the layer and the matrix reveal that a shear band initiating from point Q propagates horizontally within the layer too and then into the matrix along a line that makes an angle of 45° with the vertical.

The picture of the development of shear bands outlined above is reinforced by the plots of contours of ε shown in Fig. 5 at three values of the average strain. One shear band initiates within the matrix surrounding the void tip near the matrix/layer interface and

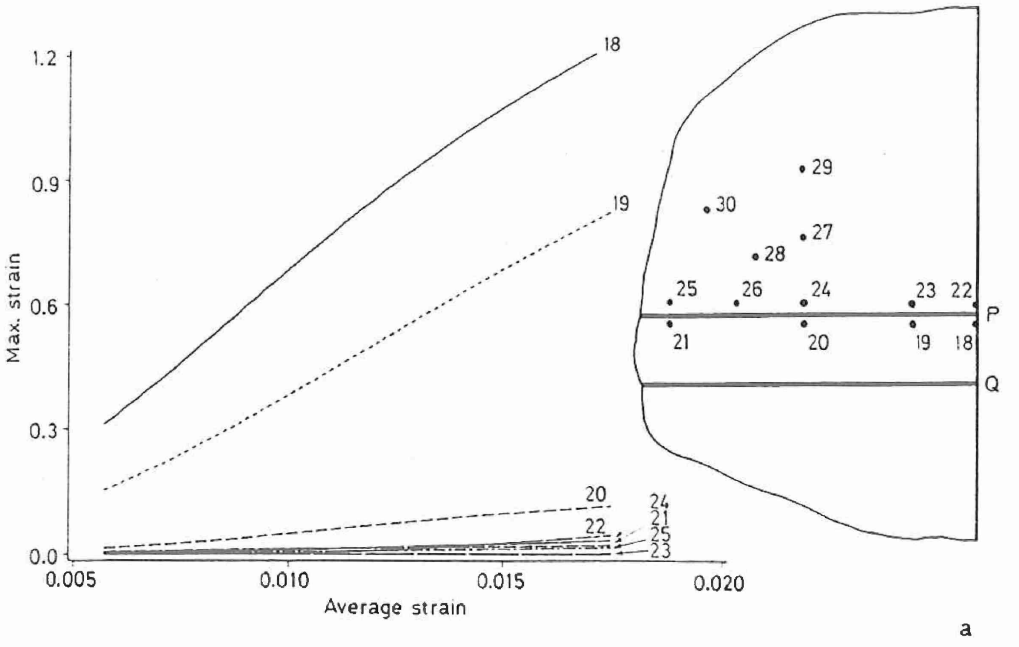

Fig. 4a. The maximum principal logarithmic strain versus the average strain at points 18 through 25 when the layer material is softer than the matrix material. Coordinates of these points in the stress free reference configuration are: 18 (0.999, 0.522), 19 (0.95, 0.522), 20 (0.87, 0.522), 21 (0.77, 0.522), 22 (0.999, 0.532), 23 (0.95, 0.532), 24 (0.87, 0.532), 25 (0.77, 0.532)

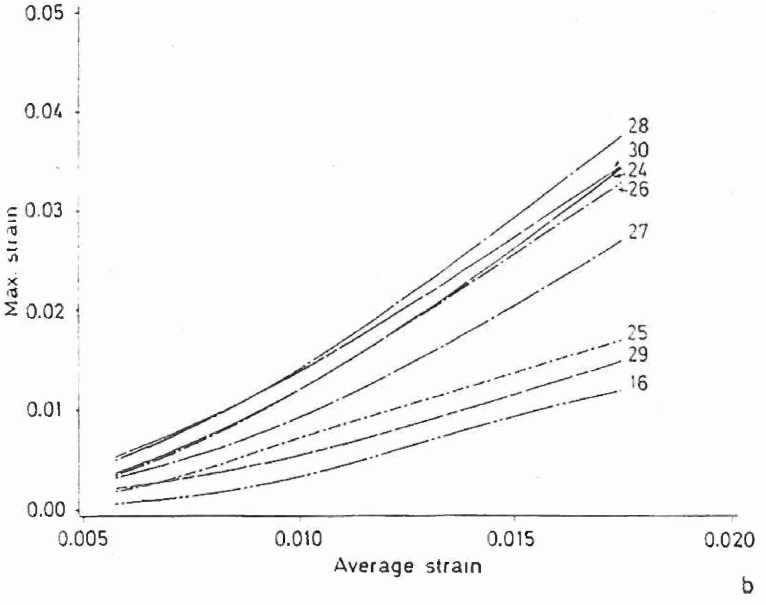

Fig. 4b. The maximum principal logarithmic strain versus the average strain at points 24 through 30 and 16 when the layer material is softer than the matrix material. Coordinates of points not given earlier are: 26 (0.82, 0.532), 27 (0.87, 0.582), 28 (0.8346, 0.5674), 29 (0.87, 0.632), 30 (0.7993, 0.6027)

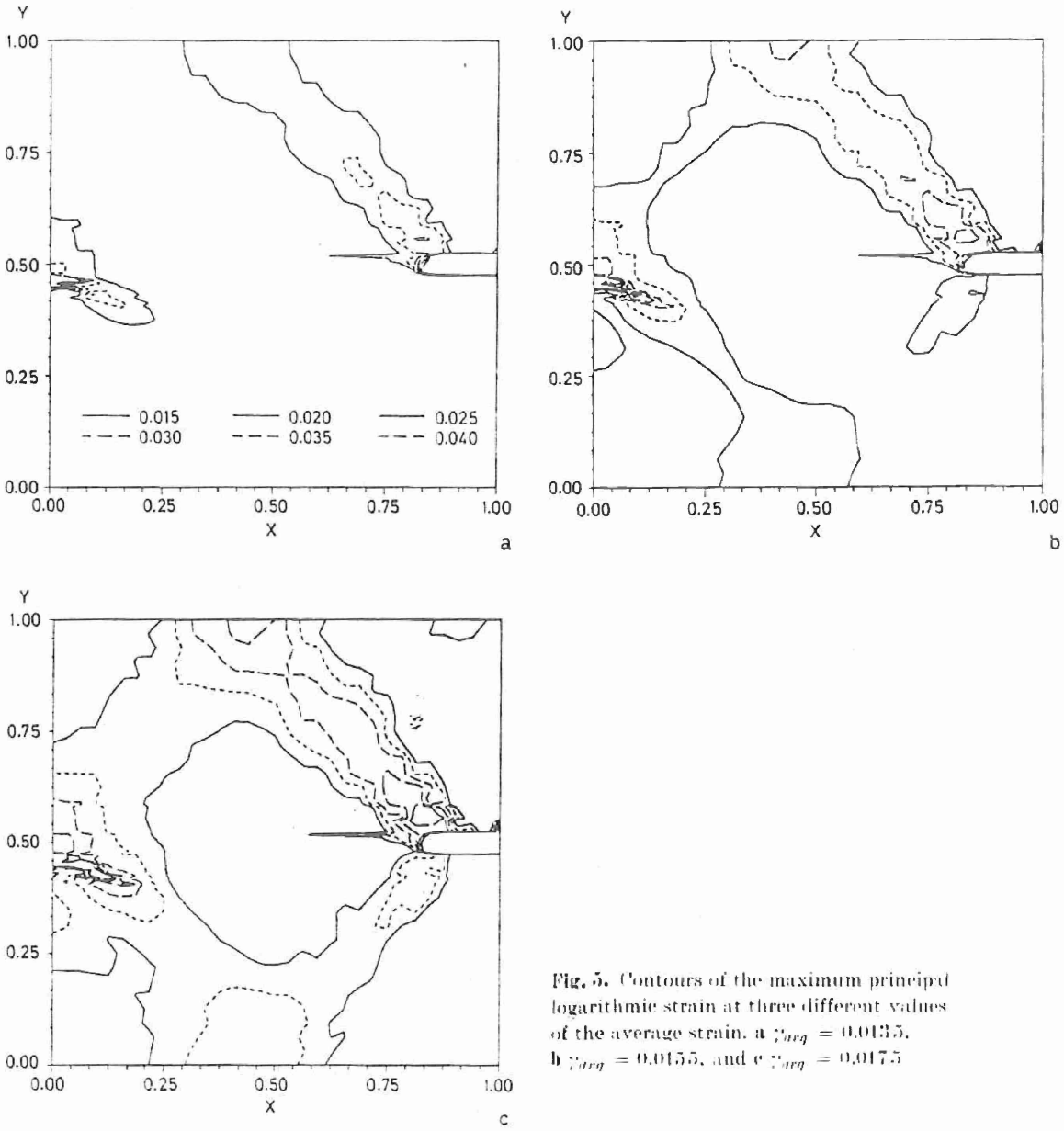

Fig. 5. Contours of the maximum principal logarithmic strain at three different values of the average strain. a $\gamma_{avg} = 0.0135$, b $\gamma_{avg} = 0.0155$, and c $\gamma_{avg} = 0.0175$

propagates into the matrix material below the common interface, the direction of propagation being nearly 45° to the vertical axis. The shear bands initiating at points of intersection of the matrix layer interfaces with the right traction free surface propagate into the soft layer and then bifurcate into the matrix material along lines making an angle of approximately 45° with the vertical. The band in the layer near the upper matrix layer interface bifurcates into the matrix prior to that near the lower interface. Also the band in the layer near the upper matrix/layer interface continues to propagate horizontally into the layer too while that near the lower surface does not. In order to elucidate upon the differences between these two bands within the soft layer, we have plotted in Figs. 6a, 6b and 6c contours of ε and in Figs. 6d, 6e and 6f contours of the temperature rise θ in a

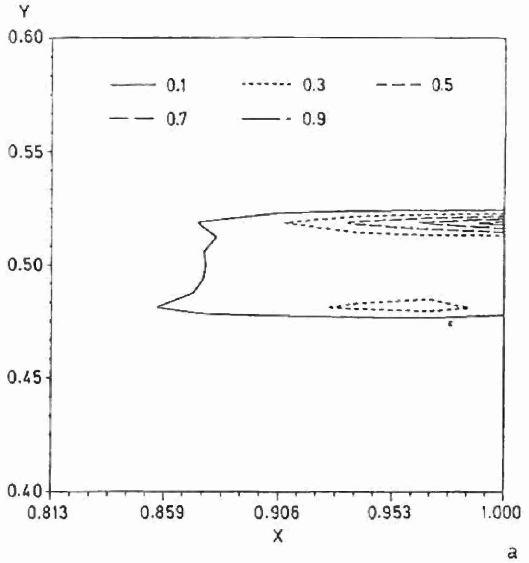
Y
0.60
0.55
0.50
0.45
0.40
0.1
0.3
0.5
0.7
0.9
0.813
0.859
0.906
0.953
1.000
X
a

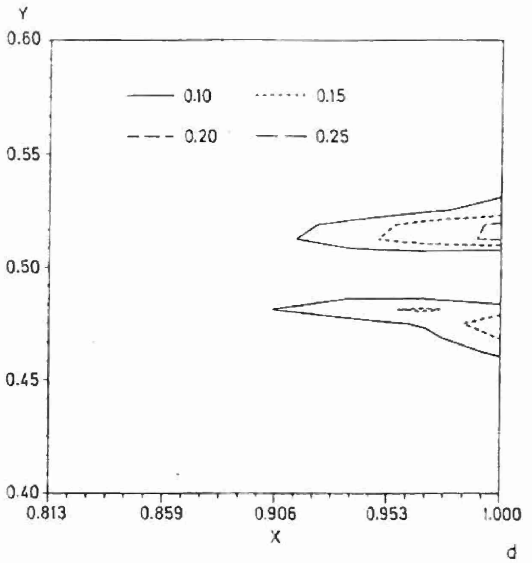
Y
0.60
0.55
0.50
0.45
0.40
0.10
0.15
0.20
0.25
0.813
0.859
0.906
0.953
1.000
X
d

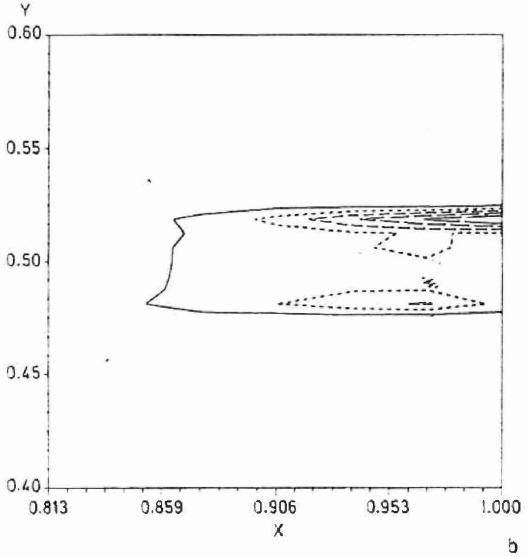
Y
0.60
0.55
0.50
0.45
0.40
0.813
0.859
0.906
0.953
1.000
X
b

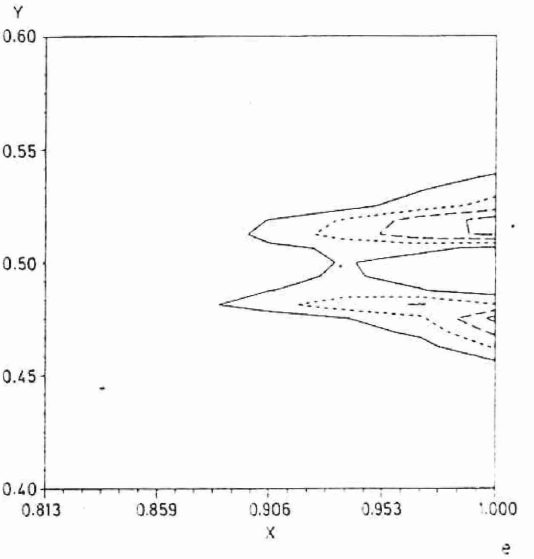
Y
0.60
0.55
0.50
0.45
0.40
0.813
0.859
0.906
0.953
1.000
X
e

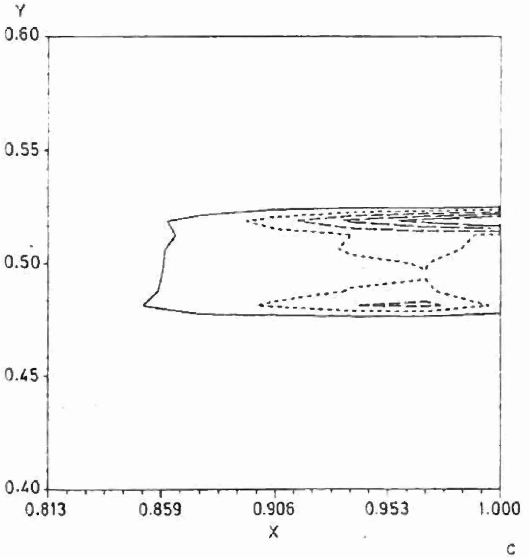
Y
0.60
0.55
0.50
0.45
0.40
0.813
0.859
0.906
0.953
1.000
X
c

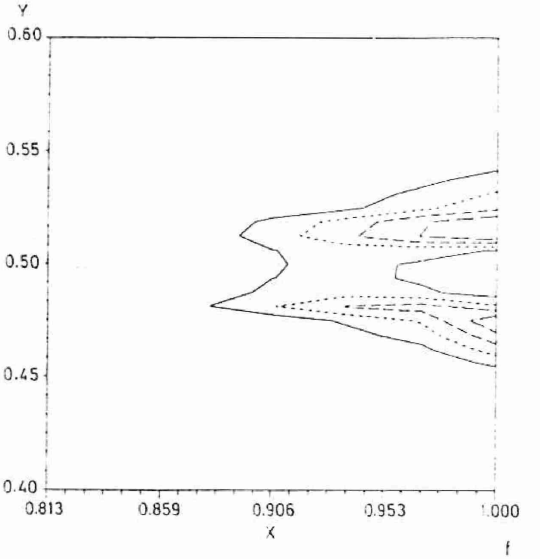
Y
0.60
0.55
0.50
0.45
0.40
0.813
0.859
0.906
0.953
1.000
X
f

small region surrounding the layer and near the right traction-free surface. We note that the layer material near the upper interface undergoes more severe deformations than the layer material near the lower interface. This could be due to the differences in the reflection and refraction of waves at the two interfaces, and the interaction of these waves with the loading wave. The bands near the upper and lower interfaces propagate both horizontally in the layer and laterally towards each other. Had the computations been carried further, it is clear that the two bands will merge with each other. The computations could not be carried further because we had exhausted the computing resources available to us. Because of the stiff equations and the nonuniform mesh, the time step required to integrate the equations is extremely small. The contours of θ indicate that the matrix material is also being heated up. Since the layer is softer than the matrix material, the stress in it is low and higher values of ε in the layer give rise to nearly the same value of the energy dissipated as the lower values of ε in the matrix because the stress in it is higher. The temperature rise makes the matrix material softer and the bands propagating in the layer bifurcate into two, one travels horizontally into the layer and the other into the matrix material along the direction of the maximum shear stress.

Figure 7 shows the distribution of the vertical component of the velocity at an average strain of 0.0175. In our work the velocity field is assumed to be continuous throughout the

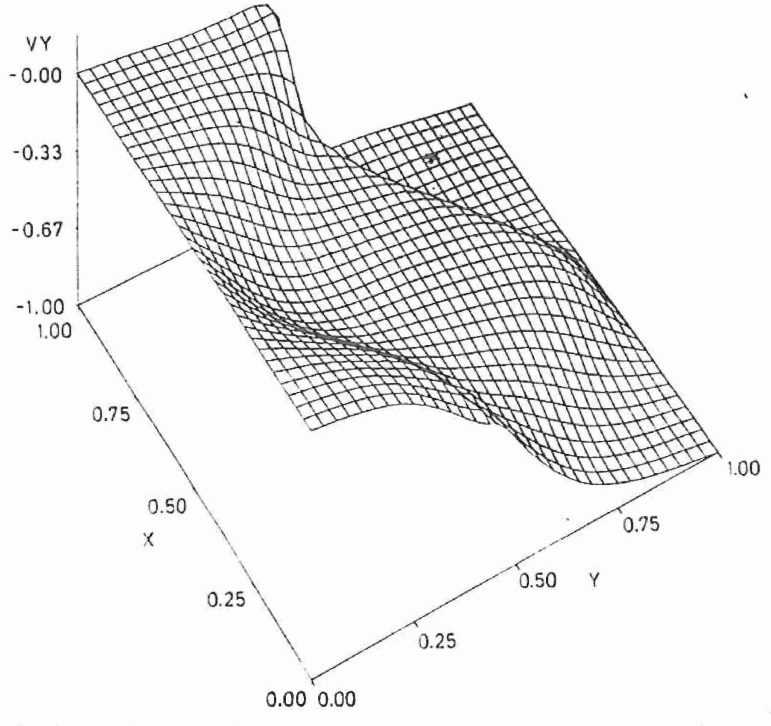

Fig. 7. Distribution of the vertical component of the velocity in the cross-section when the layer material is softer than the matrix material at $\gamma_{avg} = 0.0175$

Fig. 6. Contours of the maximum principal logarithmic strain and temperature rise within a small region enclosing the soft layer near the right traction-free surface at three different values of the average strain. a, d $\gamma_{avg} = 0.0135$, b, e $\gamma_{avg} = 0.0163$, and c, f $\gamma_{avg} = 0.0175$

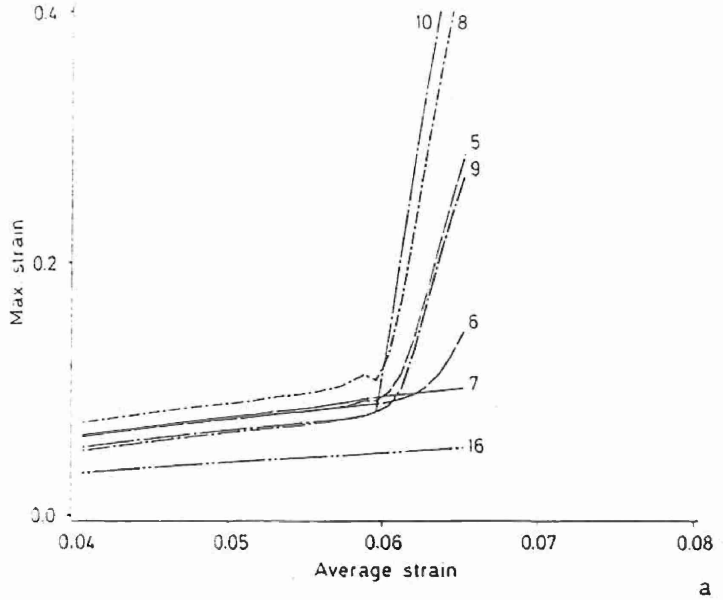

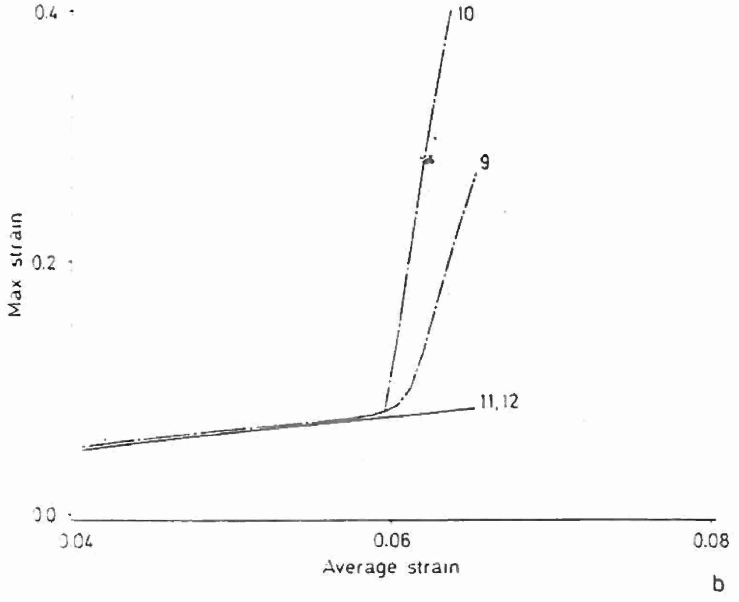

Fig. 8a. The maximum principal logarithmic strain versus the average strain at points 5 through 10 and 16 when the layer material is stronger than the matrix material. Coordinates of these points in the stress free reference configuration are the same as for points in Fig. 3a and are given in the caption of Fig. 3a.

Fig. 8b. The maximum principal logarithmic strain versus the average strain at points 9, 10, 11 and 12 when the layer material is stronger than the matrix material. Coordinates of these points in the stress free reference configuration are given in the captions of Figs. 3a and 3c.

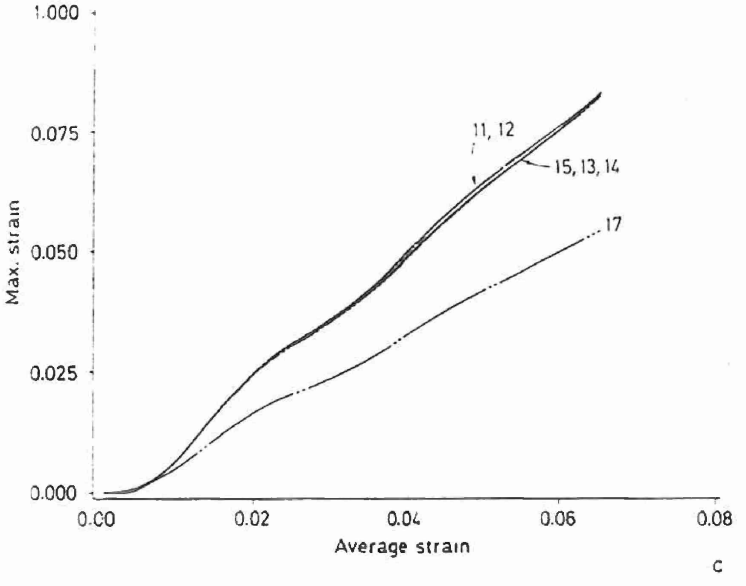

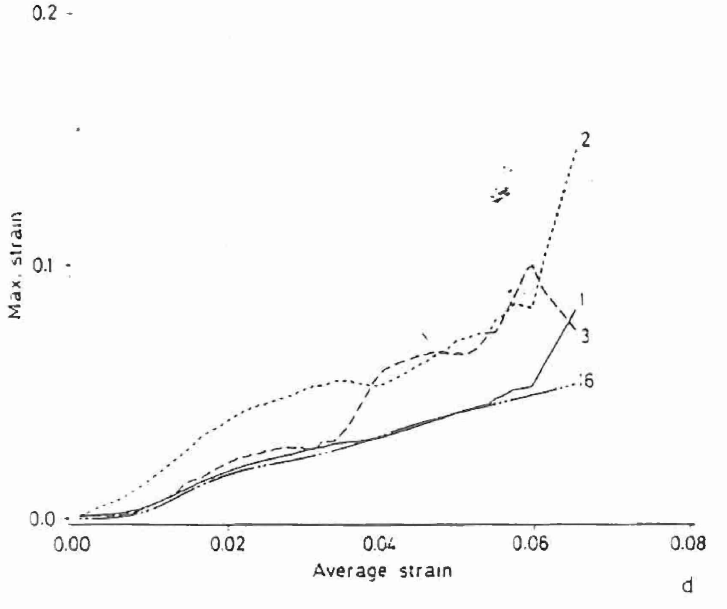

Fig. 8c. The maximum principal logarithmic strain versus the average strain at points 11 through 15 and point 17 when the layer material is stronger than the matrix material. See Figs. 3a and 3c for the coordinates of these points in the stress free reference configuration.

Fig. 8d. The maximum principal logarithmic strain versus the average strain at points 1, 2, 3 and 16 when the layer material is stronger than the matrix material. See Fig. 3a and 3b for the coordinates of these points in the stress free reference configuration.

region. However, the plotted velocity field does show that the value of v_2 increases sharply as one crosses the severely deforming region thus supporting the assertions made by Tresca [2] and Massey [3].

4.2 *Layer material stronger than the matrix material*

Figures 8a, 8b and 8c depict the growth of the maximum principal logarithmic strain ε at several matrix points near the void. The coordinates of these points in the stress free reference configuration are given in the figure captions and their approximate locations are shown in Fig. 3a. Results plotted in Fig. 8a clearly indicate that at a nominal strain of

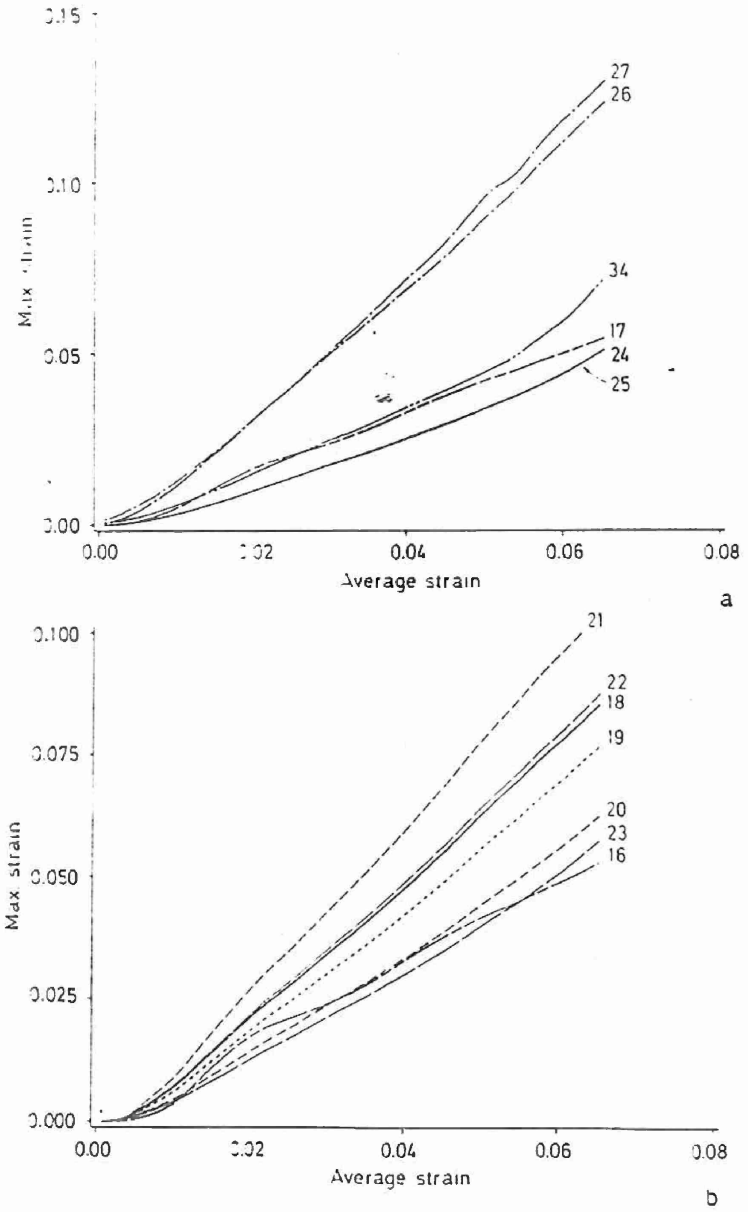

Fig. 9

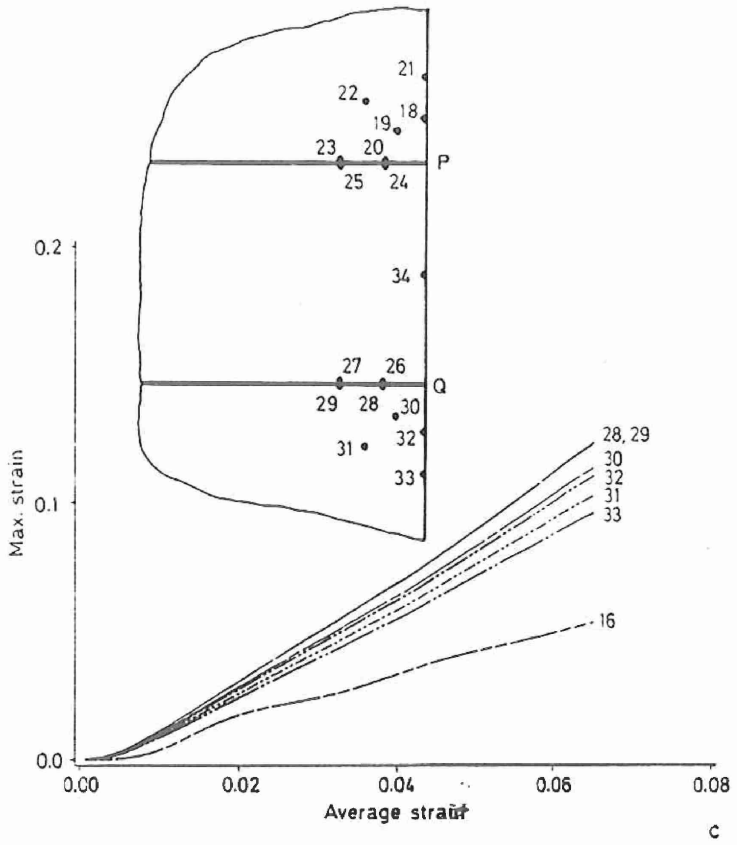

Fig. 9. The maximum principal logarithmic strain versus the average strain at points 18 through 34 when the layer material is stronger than the matrix material. Coordinates of these points in the stress free reference configuration are: 18 (0.999, 0.535), 19 (0.993, 0.5321), 20 (0.990, 0.5251), 21 (0.999, 0.545), 22 (0.9859, 0.5391), 23 (0.980, 0.5251), 24 (0.990, 0.5249), 25 (0.98, 0.5249), 26 (0.99, 0.4751), 27 (0.98, 0.4751), 28 (0.99, 0.4749), 29 (0.98, 0.4749), 30 (0.993, 0.4679), 31 (0.9859, 0.4609), 32 (0.999, 0.465), 33 (0.999, 0.455), 34 (0.999, 0.5)

0.06, the values of ε at points 5, 8, 9 and 10 increase sharply, with the rate of growth of ε at points 8 and 10 being much greater than that at points 5 and 9. Thus the small region containing points 8, 9 and 10 undergoes intense deformations which propagate towards point 5. This will become transparent when we subsequently plot the contours of ε. Recall that point 10 is near the void tip that touches the matrix layer interface, point 9 is near the interface and on a horizontal line through point 10, point 8 is near the midsurface of the void, points 7 and 8 are on a horizontal line, point 6 is near the other void tip, and point 5 on a horizontal line through point 6. Because the layer material is harder than the matrix material, the maximum principal logarithmic strain ε at points 11 and 12 adjoining points 9 and 10 respectively is considerably less than that at points 9 and 10. The values of ε versus the average strain at these four points are shown in Fig. 8b. In Fig. 8c, we have plotted the evolution of ε at points 11 through 17 in the layer. Points 13 and 14 are on a line through the void tip that makes an angle of 45° with the horizontal, point 15 is near the vertical centroidal axis, and point 17 is on the midsurface of the layer but far removed from the void tip. At an average strain of 0.06, the values of ε at points 11 through 15 are nearly 40% higher than that at point 17 and this difference increases

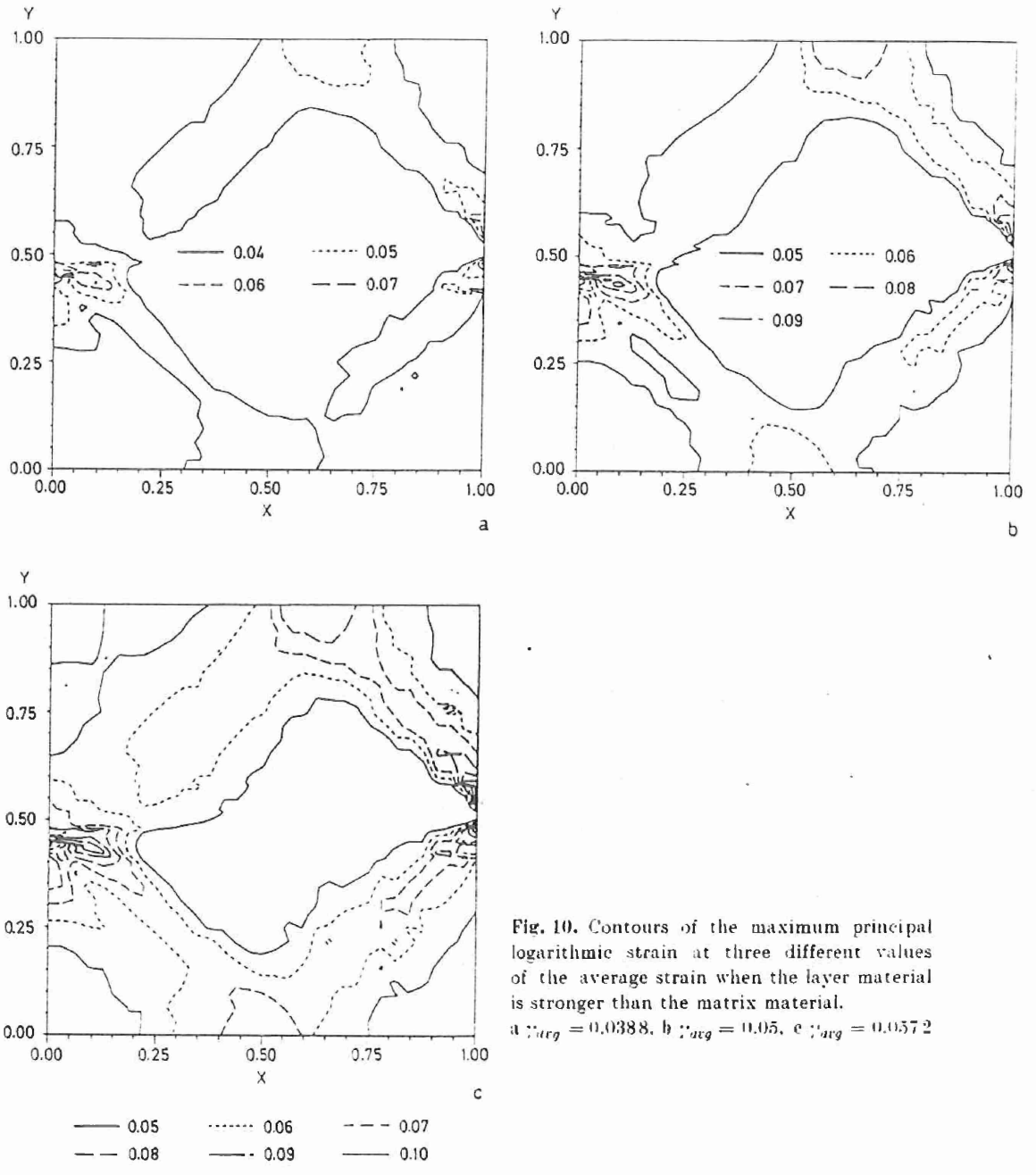

Fig. 10. Contours of the maximum principal logarithmic strain at three different values of the average strain when the layer material is stronger than the matrix material.
a $\gamma_{avg} = 0.0388$, b $\gamma_{avg} = 0.05$, c $\gamma_{avg} = 0.0572$

with increase in the average strain. Since points 11 through 15, distributed in the layer region surrounding the void tip, have undergone the same amount of deformation, it is reasonable to conclude that no localization of deformation has occurred in the layer. The plot of ε versus the average strain at points 1, 2, 3 and 16, depicted in Fig. 8d, reveals that at an average strain of approximately 0.06, the small region surrounding point 2 deforms severely and these deformations propagate towards point 1. We note that point 2 is near the void tip away from the matrix/layer interface, and points 1 and 2 are near the vertical centroidal axis.

In the previous case when the layer material was weaker than the matrix material, a shear band formed at an average strain of 0.016. In that case, the layer material underwent severe deformations. However, because of the small thickness of the layer, the overall deformations of the body stayed small.

We now explore deformations of the layer and matrix materials surrounding points P and Q on the right traction-free edge of the block. The coordinates of the selected points in the stress free reference configuration are given in the figure captions, and their approximate locations are shown in Fig. 9c. Results plotted in Figs. 9a, 9b and 9c reveal that the growth of ε at any one of these points is not phenomenal as compared to the average strain either in the layer (e.g. at point 17), or in the block (e.g. at point 16), or the overall average strain. At an average strain of 0.06, the values of ε at points 26 and 27 in the layer equal 2.5 times that at point 17, but that at layer points 24 and 25 which are near the upper layer interface, are comparable to the value of ε at point 17. The values of ε at matrix points situated below the matrix layer interface are higher than those at similarly situated matrix points above the matrix/layer interface. Thus the shear band initiating from point Q and propagating into the matrix material will involve more severe deformations than that initiating from point P and propagating into the matrix. Unlike the case of the soft layer, the deformations within the layer do not localize into a shear band.

Figure 10 depicts contours of ε at $\gamma_{avg} = 0.0388$, 0.05, and 0.0572. These reveal that a shear band initiating from the void tip abutting the matrix/layer interface propagates initially along the interface and then into the matrix material along a line making an angle of nearly 45° with the vertical. The shear band initiating from the lower void tip also propagates into the matrix material along a line making an angle of approximately 45° with the vertical. Two shear bands also initiate from points P and Q on the right traction free surface and these propagate into the matrix material along lines making an angle of 45° with the vertical. Even though it seems that near the vertical centroidal axis a shear band has propagated into the layer, there is no localization of the deformation occurring in the layer material. This is evidenced by the plots of ε versus the average strain at several points in the layer that are included in Fig. 8c. Even though the strain within the layer is small, the values of stress are not and the total energy dissipated at a layer particle may be comparable to that at a matrix particle. The contours of the temperature rise, not included in the paper, support the picture laid out above for the development of four bands, two from the void tips and two from points on the right traction free surface where the layer and the matrix materials meet.

5 Conclusions

We have studied plane strain thermomechanical deformations of a thermally softening viscoplastic body of square cross-section and containing two elliptical voids and two thin layers placed symmetrically about the horizontal centroidal axis. The major axes of the voids are aligned with the vertical centroidal axis of the cross-section and one tip of each void touches the matrix/layer interface. Two cases, namely when the flow stress in a quasistatic simple compression test for the layer material equals one-fifth or five times that of the matrix material, are studied. When the layer material is weaker than the matrix material, two bands initiate from points on the vertical traction free surfaces where the layer and the matrix materials meet. These bands propagate horizontally into the layer and also spread out laterally towards each other. The band near the upper layer matrix inter-

face is stronger than the one near the lower layer matrix interface in the sense that the peak value of the maximum principal logarithmic strain in it is higher than that in the band near the lower layer matrix interface. These bands eventually cross the interface and propagate into the matrix material along the direction of the maximum shearing stress. The band near the upper layer matrix interface continues to propagate horizontally too. The matrix material surrounding the void tip touching the layer/matrix interface undergoes severe deformations also. This band initially propagates horizontally along the interface for a small distance and then propagates into the matrix material in the direction of the maximum shearing stress.

When the layer material is stronger than the matrix material, two bands initiate from points on the vertical traction free surfaces where the layer/matrix interfaces intersect them. These bands propagate into the matrix along the direction of the maximum shearing stress. Also bands initiate from each of the void tips. The bands initiating from the void tips touching the matrix layer interfaces initially propagate horizontally and then into the matrix material in the direction of the maximum shearing stress. The bands initiating from the other void tips also propagate into the matrix material in the direction of the maximum shearing stress. In this case no localization of deformation occurs within the layer. The average strain at which a shear band forms in this case is nearly four times that in the previous case of softer layer material.

Acknowledgements

This work was supported by the U.S. National Science Foundation Grant MSM 8715952 and the U.S. Army Research Office Contract DAAL03-88-K-0184 to the University of Missouri-Rolla.

References

[1] Johnson, W.: Henri Tresca as the originator of adiabatic heat lines. Int. J. Mech. Sci. 29, 301–310 (1987).

[2] Tresca, H.: On farther application of the flow of solids. Proc. Inst. Mech. Engr. 30, 301–345 (1878).

[3] Massey, H. F.: The flow of metal during forging. Proc. Manchester Assoc. Engineers, pp. 21–26 (1921). Reprinted by the National Machinery Co., Tiffon, Ohio (1946).

[4] Zener, C., Hollomon, J. H.: Effect of strain rate on plastic flow of steel. J. Appl. Phys. 14, 22–32 (1944).

[5] Moss, G. L.: Shear strain, strain rate and temperature changes in an adiabatic shear band. In: Shock waves and high strain rate phenomenon in metals (Meyer, M. A., Murr, L. E., eds.), pp. 299–312. New York: Plenum Press 1981.

[6] Costin, L. S., Crisman, E. E., Hawley, R. H., Duffy, J.: On the localization of plastic flow in mild steel tubes under dynamic torsional loading. Int. Phys. Conf. Ser. No. 47, 90–100 (1979).

[7] Hartley, K. A., Duffy, J., Hawley, R. H.: Measurement of the temperature profile during shear band formation in steels deforming at high strain rates. J. Mech. Phys. Solids 35, 283–301 (1987).

[8] Giovanola, J. H.: Adiabatic shear banding under pure shear loading. Part I. Direct observation of strain localization and energy dissipation measurements. Mech. Materials 7, 59–71 (1988).

[9] Marchand, A., Duffy, J.: An experimental study of the formation process of adiabatic shear bands in a structural steel. J. Mech. Phys. Solids 36, 251–283 (1988).

[10] Wright, T. W., Walter, J. W.: On stress collapse in adiabatic shear bands. J. Mech. Phys. Solids 35, 701–716 (1987).

[11] Molinari, A., Clifton, R. J.: Analytic characterization of shear localization in thermoviscoplastic materials. ASME J. Appl. Mech. 54, 806–812 (1987).

[12] Batra, R. C., Kim, C. H.: Adiabatic shear banding in elastic-viscoplastic nonpolar and dipolar materials. Int. J. Plasticity 6, 127–141 (1990).
[13] Batra, R. C., Kim, C. H.: Effect of viscoplastic flow rules on the initiation and growth of shear bands at high strain rates. J. Mech. Phys. Solids 38 (in press).
[14] Batra, R. C., Kim, C. H.: Analysis of shear banding in six ductile metals. Submitted for publication.
[15] Batra, R. C., Kim, C. H.: Analysis of shear banding in six less ductile metals. Submitted for publication.
[16] Wright, T. W., Batra, R. C.: The initiation and growth of adiabatic shear bands. Int. J. Plasticity 1, 205–212 (1985).
[17] Wright, T. W., Batra, R. C.: Adiabatic shear bands in simple and dipolar plastic materials. In: Proc. IUTAM Symposium on Macro-Micro-Mechanics of High Velocity Deformation and Fracture (Kawata, K., Shioiri, J., eds.), pp. 189–201. Berlin–Heidelberg–New York: Springer 1987.
[18] Clifton, R. J., Duffy, J., Hartley, K. S., Shawki, T. G.: On critical conditions for shear band formation at high strain rates. Scripta Metallurgica 18, 443–448 (1984).
[19] Batra, R. C.: The initiation and growth of, and the interaction among adiabatic shear bands in simple and dipolar materials. Int. J. Plasticity 3, 75–89 (1987).
[20] Batra, R. C.: Effect of material parameters on the initiation and growth of adiabatic shear bands. Int. J. Solids and Structures 23, 1435–1446 (1987).
[21] Batra, R. C.: Effect of nominal strain-rate on the initiation and growth of adiabatic shear bands. ASME J. Appl. Mech. 55, 229–230 (1988).
[22] Merzer, A. M.: Modeling of adiabatic shear band development from small imperfections. J. Mech. Phys. Solids 30, 323–338 (1982).
[23] Wu, F. H., Freund, L. B.: Deformation trapping due to thermoplastic instability in one-dimensional wave propagation. J. Mech. Phys. Solids 32, 119–132 (1984).
[24] Burns, T.: A mechanism for shear band formation in the high strain rate torsion test. J. Appl. Mech. (in press).
[25] Fressengeas, C.: Adiabatic shear morphology at very high strain rates. Int. J. Impact Engr. 8, 141–157 (1989).
[26] Recht, R. F.: Catastrophic thermoplastic shear. ASME J. Appl. Mech. 31, 189–193 (1964).
[27a] Staker, M. R.: The relation between adiabatic shear instability strain and material properties. Acta Met. 29, 683–689 (1981).
[27b] Burns, T. J.: Approximate linear stability analysis of a model of adiabatic shear band formation. Quart. Appl. Math. 43, 65–84 (1985).
[28] Clifton, R. J.: Adiabatic shear banding. In: Material response to ultrahigh loading rates, chapter 8, pp. 129–142. NRC National Material Advisory Board (U.S.) Report No. NMAB-356.
[29] Coleman, B. D., Hodgdon, M. L.: On shear bands in ductile materials. Arch. Rat. Mech. Anal. 90, 219–247 (1985).
[30] Wright, T. W.: Steady shearing in a viscoplastic solid. J. Mech. Phys. Solids 35, 269–282 (1987).
[31] Anand, L., Kim, K. H., Shawki, T. G.: Onset of shear localization in viscoplastic solids. J. Mech. Phys. Solids. 35, 381–399 (1987).
[32] Bai, Y. L.: A criterion for thermoplastic shear instability. In: Shock waves and high strain rate phenomenon in metals (Meyers, M. A., Murr, L. E., eds.) pp. 277–283. New York: Plenum Press 1981.
[33] LeMonds, J., Needleman, A.: Finite element analyses of shear localization in rate and temperature dependent solids. Mech. Materials 5, 339–361 (1986).
[34] LeMonds, J., Needleman, A.: An analysis of shear band development incorporating heat conduction. Mech. Materials 5, 363–373 (1986).
[35] Needleman, A.: Dynamic shear band development in plane strain. ASME J. Appl. Mech. 56, 1–9 (1989).
[36] Zbib, H. M., Aifantis, E. C.: On the localization and postlocalization behavior of plastic deformation. I. On the initiation of shear bands. Res Mechanica 23, 261–277 (1988).
[37] Anand, L., Lush, A. M., Kim, K. H.: Thermal aspects of shear localization in viscoplastic solids. In: Thermal aspects in manufacturing (Attia, M. H., Kops, L., eds.). ASME-PED 30, 89–103 (1988).
[38] Batra, R. C., Liu, D. S.: Adiabatic shear banding in plane strain problems. ASME J. Appl. Mech. 56, 527–534 (1989).

[39] Batra, R. C., Liu, D. S.: Adiabatic shear banding in dynamic plane strain compression of a viscoplastic material. Int. J. Plasticity 6, 231—246 (1990).
[40] Zhu, Z. G., Batra, R. C.: Dynamic shear band development in plane strain compression of a viscoplastic body containing a rigid inclusion. Acta Mechanica 84, 89—107 (1990).
[41] Batra, R. C., Zhang, X.-T.: Shear band development in dynamic loading of a viscoplastic cylinder containing two voids. Acta Mechanica 85, 221—234 (1990).
[42] Bathe, K. J.: Finite element procedures in engineering analysis. Englewood Cliffs: Prentice-Hall 1982.
[43] Gear, C. W.: Numerical initial value problems in ordinary differential equations. Englewood Cliffs: Prentice-Hall 1971.
[44] Hindmarsh, A. C.: ODEPACK. A systematized collection of ODE solvers. In: Scientific computing (Stepleman, R. S. et al., eds.) pp. 55—64. Amsterdam: North-Holland 1983.

Authors' address: R. C. Batra and Z. G. Zhu, Department of Mechanical and Aerospace Engineering and Engineering Mechanics, University of Missouri-Rolla, Rolla, MO 65401-0249, U.S.A.

Printed in Germany
Maxim Gorki - Druck GmbH, Carl-v.-Ossietzky-Str. 30/31, 7400 Altenburg

Int. J. Engng Sci. Vol. 29, No. 8, pp. 949–960, 1991
Printed in Great Britain.

0020–7225/91 $3.00 + 0.00

EFFECT OF THERMAL CONDUCTIVITY ON THE INITIATION, GROWTH AND BANDWIDTH OF ADIABATIC SHEAR BANDS

R. C. BATRA and C. H. KIM

Department of Mechanical and Aerospace Engineering and Engineering Mechanics, University of Missouri–Rolla, Rolla, MO 65401-0249, U.S.A.

Abstract—We ascertain the effect of thermal conductivity on the initiation and growth of shear bands in a structural steel by analyzing the development of shear bands in a block undergoing overall adiabatic simple shearing deformations. The material of the block is assumed to exhibit strain and strain-rate hardening, and thermal softening. Three constitutive relations, namely, the Litonski law, the Bodner–Partom law, and the Johnson–Cook law, have been used to model the thermoviscoplastic response of the material. For each material model, five values of thermal conductivity differing by three orders of magnitude have been used.

It is found that an increase in the value of the thermal conductivity delays the initiation and slows down the subsequent development of the shear band. For the Litonski law and Johnson–Cook law, the band width tends to zero as the thermal conductivity approaches zero. However, for the Bodner–Partom law, the band width is non-zero even when the thermal conductivity is set equal to zero.

1. INTRODUCTION

Adiabatic shear banding refers to the localization phenomenon that occurs during high strain-rate plastic deformation, such as machining, shock impact loading, ballistic penetration, and metal forming processes. As shear bands precede material fracture, the discernment of variables that enhance or retard their initiation and growth will make possible design of materials and manufacturing techniques that are less conducive to the formation of shear bands. Variables that are believed to have a noticeable effect on the development of shear bands include material strain-rate sensitivity, thermal diffusivity, thermal softening, strain hardening, inertia forces, and the initial temperature of the specimen. Here we explore in some detail the effect of the thermal conductivity or the thermal length on the initiation and subsequent growth of shear bands in a viscoplastic block undergoing overall adiabatic simple shearing deformations at an average strain-rate of $3300\,s^{-1}$. The values of material parameters, except for the thermal conductivity, are those for a typical structural steel. Five values of the thermal conductivity, namely, 0, 5, 50, 500, and 5000 W/m °C, have been used to assess its effect on the development of shear bands.

In studying the growth of shear bands in the center of a finite slab after initiation at a small imperfection, Merzer [1] concluded that the final width of the band depends on the thermal diffusivity and the overall strain rate. Wu and Freund [2], in studying the formation of shear bands at a moving boundary, concluded that thermal diffusivity has little influence on the final shape of the band. The detailed geometry and constitutive equations considered in these two papers are different. In both papers, there are two natural length scales, one arising from the rate effect in the constitutive equation, and the other from heat conductivity. In the latter paper, these two scales have been arbitrarily set equal to each other, and in the former paper the relative effect of heat conductivity has been examined parametrically for the Bodner–Partom constitutive relation. Wu and Freund [2] also showed that for linear strain-rate sensitivity the shear layer thickness increased with boundary velocity, but the reverse happened for logarithmic rate sensitive materials. Possible reasons for opposing effects of thermal conductivity reported in these two papers could be (a) different problems studied, and/or (b) different constitutive relations employed. Here we use three constitutive relations, namely, the Litonski law, the Bodner–Partom law, and the Johnson–Cook law, to model the viscoplastic response of the material. It is found that for all three constitutive relations, the computed band width increases with increase in the value of the thermal conductivity, suggesting thereby that

the apparently contradictory results reported in the above-cited two papers are due to the different phenomenon presumed for the occurrence of adiabatic shear bands.

In recent years there have been numerous experimental [3–7], analytical [8–15], and numerical [16–23] investigations aimed at increasing our understanding of the localization of the deformation into shear bands. Shawki and Clifton [24] have reviewed much of the literature dealing with the one-dimensional shear banding problem. Recently, there have been a few studies [25–35] of the phenomenon of shear banding in plane strain deformations of a thermally softening viscoplastic block. Anand *et al.* [12] have extended the one-dimensional perturbation analysis of Clifton and coworkers [36] to three-dimensional problems. They also included the effect of hydrostatic pressure on plastic flow, so as to better model the behavior of polymeric materials. Their analysis predicts that for pressure-sensitive materials, shear bands can initiate in two directions even in simple shear.

2. FORMULATION OF THE PROBLEM

In terms of non-dimensional variables, equations governing the dynamic thermomechanical deformations of a viscoplastic block undergoing overall adiabatic simple shearing deformations are

$$\alpha w\dot{v} = (ws)_{,y}, \qquad 0<y<1, \tag{2.1}$$

$$w\dot{\theta} = \beta(w\theta_{,y})_{,y} + ws\dot{\gamma}_p, \qquad 0<y<1, \tag{2.2}$$

$$\dot{s} = \mu(v_{,y} - \dot{\gamma}_p), \tag{2.3}$$

$$\dot{\gamma}_p = g(s, \gamma_p, \theta). \tag{2.4}$$

Here v, θ, s, γ_p and w represent, respectively, the velocity of a particle in the direction of shearing taken to be along the x-axis, temperature rise, shear stress, plastic strain, and thickness of the block. Furthermore, β is the thermal diffusivity, μ is the shear modulus, α signifies the effect of inertia forces relative to the flow stress of the material, a superimposed dot indicates material time derivative, and a comma followed by y implies partial differentiation with respect to y. Equation (2.1) expresses the balance of linear momentum, equation (2.2) the balance of internal energy, equation (2.3) Hooke's law written in the rate form, and equation (2.4) is a constitutive relation for $\dot{\gamma}_p$. The viscoplastic flow rules differ in the functional forms of g. Fourier's law of heat conduction has been used in equation (2.2). Also, we have assumed that the shear strain-rate has additive decomposition into elastic and plastic parts, and all of the plastic working, given by the second term on the right-hand side of equation (2.2), is converted into heat. We note that Sulijoadikusumo and Dillon [37] and Farren and Taylor [38] found that only 90–95% of the plastic work done is responsible for raising the temperature of the body.

The dimensional variables, indicated below by a superimposed bar, are related to the non-dimensional variables as follows:

$$\bar{y} = yH, \qquad \bar{w} = wH, \qquad \bar{t} = tH/v_0, \qquad \bar{\theta} = \theta\theta_0, \qquad \theta_0 = \sigma_0/\rho c,$$
$$\bar{s} = s\sigma_0, \qquad \alpha = \rho v_0^2/\sigma_0, \qquad \bar{\mu} = \mu\sigma_0, \qquad \beta = k/(\rho c v_0 H),$$
$$\dot{\bar{\gamma}}_p = \dot{\gamma}_p v_0/H. \tag{2.5}$$

In equation (2.5), H is the height of the block, v_0 is the final value of the speed imposed on the top surface of the block, ρ is the mass density, t is the time elapsed, σ_0 is the yield stress in a quasistatic simple shear test, k is the thermal conductivity, and c is the specific heat. Hereafter, we drop the superimposed bars and indicate a dimensional quantity by specifying its units.

For the initial and boundary conditions we take

$$\theta(y, 0) = 0, \qquad v(y, 0) = 0, \qquad s(y, 0) = 0, \qquad \gamma_p(y, 0) = 0,$$
$$\theta_{,y}(0, t) = 0, \qquad \theta_{,y}(1, t) = 0, \qquad v(0, t) = 0,$$
$$v(1, t) = t/0.01, \qquad 0 \le t \le 0.01,$$
$$= 1, \qquad t \ge 0.01. \tag{2.6}$$

That is, the block is initially stress free, is undeformed, is at rest, and has a uniform temperature, normalized to be zero. The overall deformations of the block are taken to be adiabatic and the lower surface is at rest, whereas the upper surface is assigned a velocity that increases from 0 to 1 in a non-dimensional time of 0.01 and then stays equal to 1.0. The block is taken to be thinnest at the center, $y = \frac{1}{2}$, and thickest at the boundary surfaces, $y = 0, 1$, with the thickness variation given by

$$w(y) = w_0\left[1 + \frac{\delta}{2}\sin\left(\frac{1}{2} + 2y\right)\pi\right]. \tag{2.7}$$

We note that Marchand and Duffy [7] reported nearly 10% variation in the thickness of the steel tubes they tested in torsion. Our choice of locating the thinnest section at the center is for convenience only and should not affect the computed results.

3. VISCOPLASTIC FLOW RULES

3.1 *Litonski's law*

Wright and Batra [18] modified the Litonski law to account for elastic unloading of a material point. They postulated that

$$\dot{\gamma}_p = \Lambda s, \tag{3.1}$$

$$\Lambda = \max\left[0, \left(\left(\frac{s}{(1 - v\theta)\left(1 + \frac{\psi}{\psi_0}\right)^n}\right)^{1/m} - 1\right) \Big/ bs\right], \tag{3.2}$$

$$\dot{\psi} = s\dot{\gamma}_p/(1 + \psi/\psi_0)^n. \tag{3.3}$$

We may view ψ as an internal variable that describes the work hardening of the material. Its evolution equation (3.3) implies that the rate of growth of ψ is proportional to the plastic working. In equation (3.2), $(1 - v\theta)$ describes the softening of the material as a result of its heating, b and m characterize its strain-rate sensitivity, and ψ_0 and n its work hardening. Equations (3.1) and (3.2) imply that

$$\dot{\gamma}_p = 0 \quad \text{if} \quad s \le (1 - v\theta)(1 + \psi/\psi_0)^n. \tag{3.4}$$

Thus $s = (1 - v\theta)(1 + \psi/\psi_0)^n$ describes a loading surface, and if the local state given by (s, ψ, θ) lies inside or on this surface, the plastic strain-rate is zero and the material then is deforming elastically. Besides σ_0, which has been used to non-dimensionalize stress-like quantities, five material parameters, v, b, m, ψ_0, and n are needed to specify the viscoplastic response of the material.

3.2 *Bodner–Partom law*

Bodner and Partom [39] assumed that there is no loading surface and that plastic strain-rate $\dot{\gamma}_p$, albeit very small at low values of s, is always non-zero. Their constitutive relation can be written as

$$\dot{\gamma}_p = D_0 \exp\left[-\frac{1}{2}\left(\frac{z^2}{3s^2}\right)^n\right], \qquad n = \frac{a}{T} + b. \tag{3.5}$$

$$z = z_1 - (z_1 - z_0)\exp(-mW_p). \tag{3.6}$$

$$W_p = s\gamma_p. \tag{3.7}$$

Here T is the absolute temperature of a material particle, W_p is the plastic work done, z may be regarded as an internal variable, and D_0 is the limiting value of the plastic strain-rate, usually taken as $10^8\ s^{-1}$. Besides D_0, we need to specify a, z_1, z_0, m, and b to characterize the material

3.3 Johnson–Cook law

Johnson and Cook [40] tested 12 materials in simple shear and compression at different strain-rates and found that

$$\dot{\gamma}_p = \exp\left[\left(\frac{s}{(A + B\gamma_p^n)(1 - \bar{T}^\nu)} - 1.0\right)\Big/ C\right], \tag{3.8}$$

$$\bar{T} = (\theta - \theta_0)/(\theta_m - \theta_0), \tag{3.9}$$

describe well the test data. For θ_m equal to the melting temperature of the material and θ_0 equal to the ambient temperatur- they tabulated values of A, B, n, ν, and C for 12 materials. It should be noted that there is n ding surface assumed in this case, too.

4. RESULTS

4.1 Computational considerations

The governing equations (2.1)–(2.4) with the function g given by one of the flow rules described in the previous section are highly nonlinear, and are difficult to solve analytically under the side conditions (2.5) and (2.6). An approximate solution of these equations has been computed numerically by using the finite element method. The partial differential equations (2.1)–(2.4) are first reduced to a set of coupled nonlinear ordinary differential equations by using the Galerkin approximation. The stiff ordinary differential equations are integrated with respect to time by the Gear method [41]. For this purpose, the subroutine LSODE included in the package ODEPACK developed by Hindmarsh [42] is used. The subroutine adjusts the time increment adaptively until a solution of the stiff ordinary differential equations has been computed to the desired accuracy.

In the computation of results given below, the following values of various material parameters were used: $\rho = 7860\ \text{kg/m}^3$, $\sigma_0 = 405$ MPa, and $c = 473\ \text{J/kg °C}$;

(a) Litonski's law: $\nu = 6 \times 10^{-4}/°\text{K}$, $\psi_0 = 0.012$, $m = 0.01872$, $n = 0.054$, and $b = 10^4$ s;

(b) Bodner–Partom law: $D_0 = 1000$, $z_1 = 3.778$, $z_2 = 3.185$, $m = 2.5$, $a = 1800°\text{K}$, and $b = 0$;

(c) Johnson–Cook law: $A = 0.275$, $B = 1.433$, $C = 36$, $n = 0.054$, $\nu = 0.8$, $\theta_m = 1800°\text{K}$ and $\theta_0 = 300°\text{K}$.

The values of geometric parameters used are $H = 2.5$ mm, $w_0 = 0.38$ mm, and $\delta = 0.05$. The values of the material parameters given above are such that for $k = 50\ \text{W/m °C}$ and average strain-rate of $3300\ \text{s}^{-1}$, the average shear stress s_a versus the average shear strain γ_{avg} curve approximated well the experimental stress–strain curve for HY-100 steel given by Marchand and Duffy [7]. The average shear stress s_a is defined as

$$s_a = \int_0^1 s(y, t)\, dy.$$

For $\gamma_{avg} = 3300\ \text{s}^{-1}$, the inertia effects do not play a noticeable role, and the shear stress depends upon y mainly because of the dependence of w upon y. Subsequently, the values of material parameters and the average strain-rate were kept fixed, and results were computed for $k = 0$, 5, 50, 500, and 5000 W/m °C. These results are identified below as follows.

Curve type	k (W/m °C)
·····	0
———	5
– – –	50
– – – – –	500
— – – — – – — –	5000

For the Litonski law, and for $k = 0$ and 5 W/m °C, results could not be computed satisfactorily once the shear stress began to drop precipitously.

4.2 Numerical results

Figure 1 depicts the average shear stress s_a versus the average shear strain γ_{avg} curves for the three constitutive models and the five values of the thermal conductivity k. For each constitutive relation used, the $s_a-\gamma_{avg}$ curves for $k=0$ and 5 W/m °C are essentially identical with each other. The value of γ_{avg} at which s_a begins to drop increases a little with an increase in the value of the thermal conductivity. However, the rate of stress drop decreases dramatically as the value of k is increased from 50 to 500 W/m °C as compared with that when k is increased from 5 to 50 W/m °C. For each value of k considered, the value of γ_{avg} when the average shear stress s_a becomes maximum is the least for the Johnson–Cook law. The $s_a-\gamma_{avg}$ curves look alike for the Litonski law and the Bodner–Partom law, except that the rate of stress drop is a little less for the Bodner–Partom law than for the Litonski law.

Figure 2 depicts the evolution of the homologous temperature, defined as the ratio of the absolute temperature of a material point to the melting temperature of the material, at the center of the specimen. Because of the non-dimensional variables being used herein, the horizontal scale representing the average strain can also be interpreted as the time elapsed. For each of the three constitutive relations used, the rate of temperature rise is largest for $k=0$ and decreases as the value of k is increased. For $k=0$ and 5 W/m °C, the Johnson–Cook law gives the steepest rise in the temperature at the specimen center. It should be recalled that the shear stress is greatest at the specimen center because the thickness there is the least. For $k=50$ W/m °C, the Litonski law gives the most rapid rate of temperature increase at the center of the specimen. The value of γ_{avg} when the temperature at the specimen center begins to rise sharply is different for the three constitutive relations. For $k=5000$ W/m °C and for

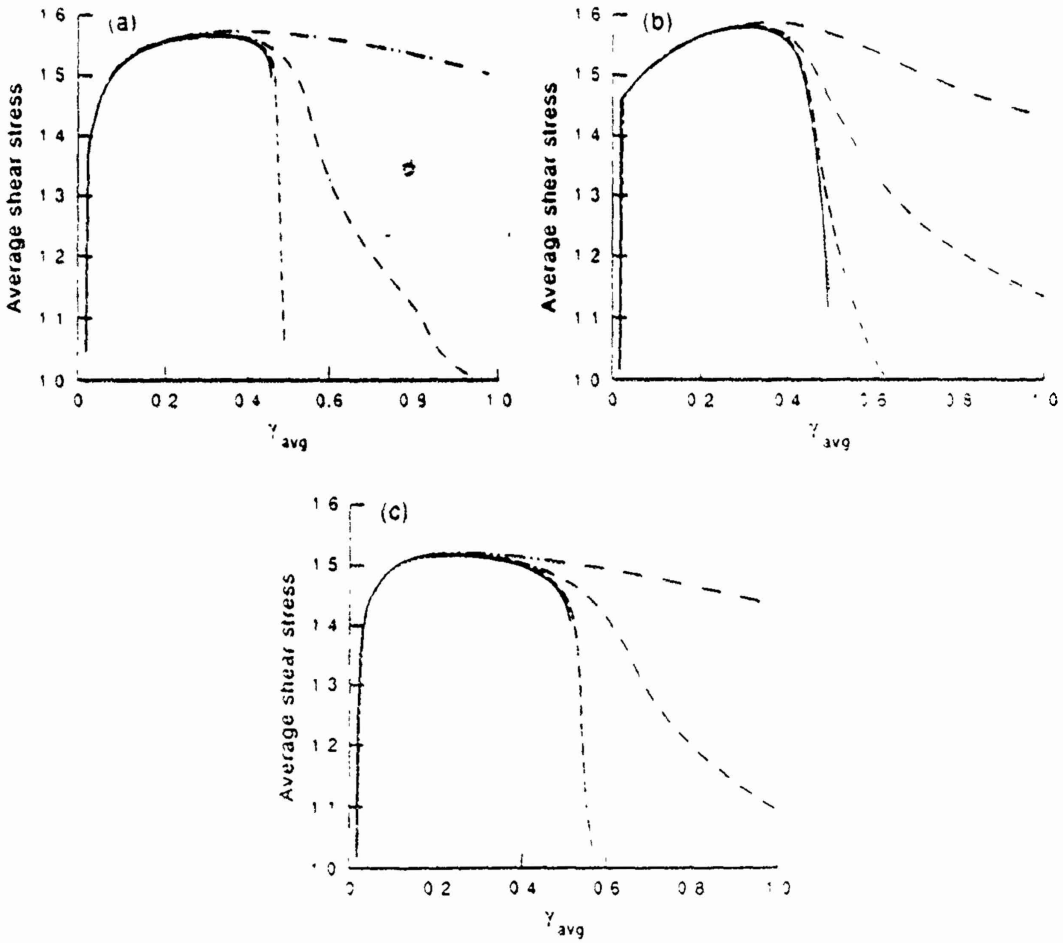

Fig. 1. Average shear stress vs average shear strain for the three constitutive relations and the five values of the thermal conductivity (a) Litonski, (b) Bodner–Partom, (c) Johnson–Cook

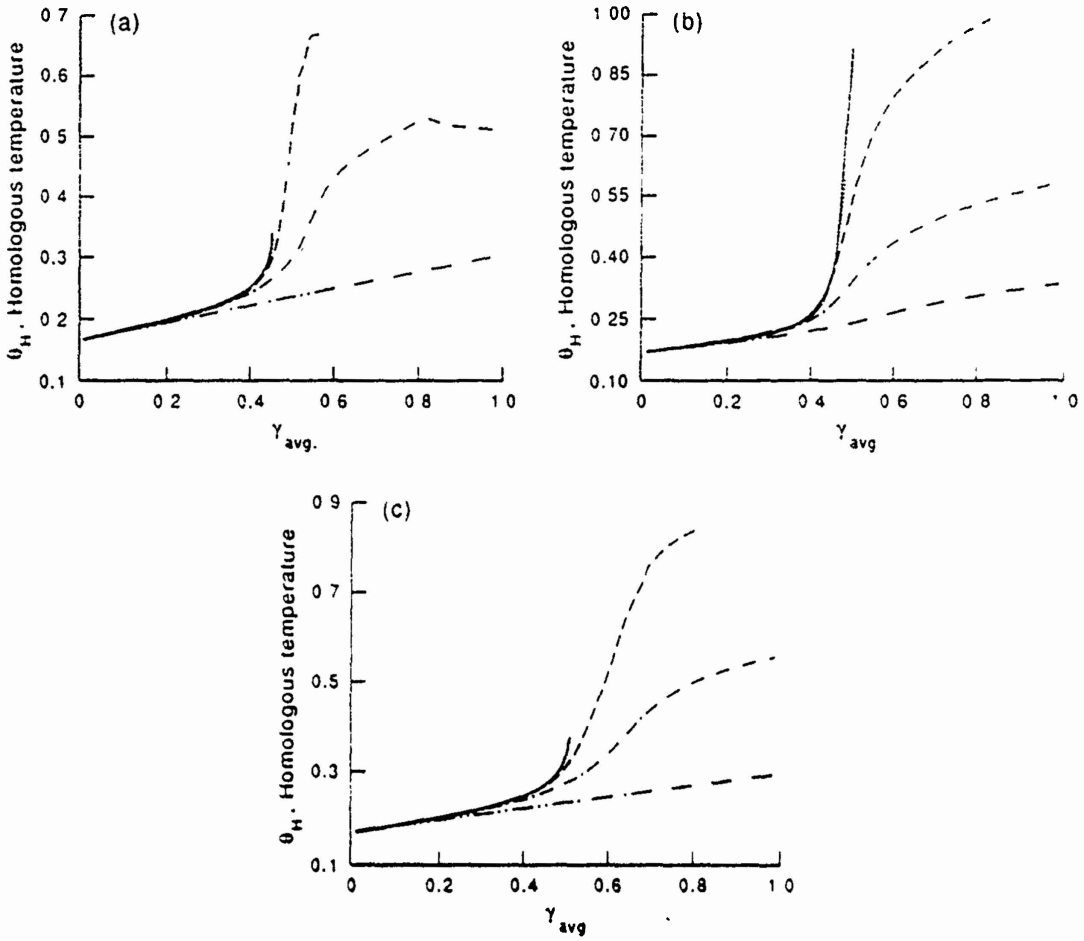

Fig. 2. Evolution of the homologous temperature at the center of the specimen for the three constitutive relations and five values of the thermal conductivity. (a) Litonski. (b) Bodner–Partom. (c) Johnson–Cook.

$0 < \gamma_{avg} < 1$, the temperature at the specimen center increases nearly linearly for each of the three constitutive relations used, except that for the Bodner–Partom law the slope of the θ_H vs. γ_{avg} curve increases at $\gamma_{avg} \simeq 0.4$. As the value of k increases, the heat conducted away from the central hotter region to the outer parts of the specimen increases and the rate of temperature rise at the specimen center decreases. Because of the adiabatic boundary conditions assumed, the temperature everywhere in the specimen increases.

As a significant part of the temperature rise occurs after the shear stress has attained its maximum value, we have plotted in Fig. 3 the homologous temperature θ_H at the specimen center versus s_a/s_{max}. For the Litonski law and the Johnson–Cook law, the θ_H–s_a/s_{max} curve corresponding to $k = 50\,W/m\,°C$ shows a second-order transition at $s_a/s_{max} \simeq 0.945$ and 0.92 respectively. For each of the three constitutive relations studied herein, the value of θ_H, when $s_a/s_{max} = 1.0$, appears to be independent of k. This value of θ_H equals 0.2, 0.21, and 0.214 for the Johnson–Cook law, the Bodner–Partom law, and the Litonski law respectively. For the Bodner–Partom law, the θ_H–s_a/s_{max} curves for the five values of k are essentially straight lines, and the slope of the straight line decreases with an increase in the value of k. It should be noted that for fixed values of k and s_a/s_{max}, the temperature rise at the specimen center depends upon the constitutive relation employed. This is because the three constitutive relations give different rates of stress drop.

Figure 4 shows the shear strain at the specimen center, γ_{loc}, versus the average strain. The curves for the Bodner–Partom law differ from those for the Litonski law and the Johnson–Cook law. For the Bodner–Partom law, with an increase in the value of k, the slope of the

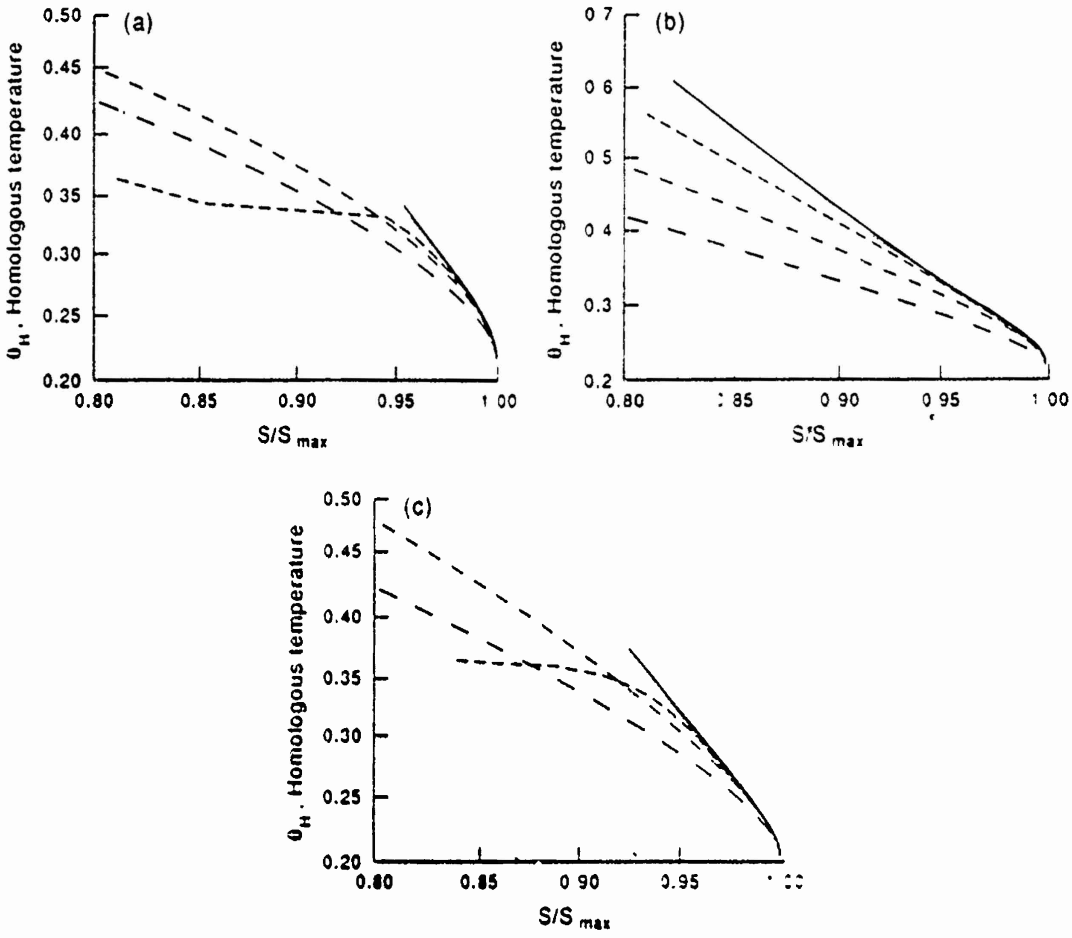

Fig. 3. Homologous temperature at the specimen center vs s_a/s_{max}. (a) Litonski, (b) Bodner–Partom, (c) Johnson–Cook.

γ_{loc}–γ_{avg} curve when $s_a/s_{max} < 1$ decreases. For the Litonski law and the Johnson–Cook law, the γ_{loc}–γ_{avg} curves for $k = 50$ W/m °C show similar qualitative behavior. However, γ_{loc} increases more rapidly for the Litonski law than that for the other two constitutive relations. For $k = 5000$ W/m °C, γ_{loc} increases very slowly, mainly because most of the heat developed near the specimen center due to plastic working is conducted away. For $k = 500$ W/m °C and the Litonski law, the local strain seems to have reached the saturation value at $\gamma_{avg} = 0.82$. A similar behavior was observed for the Johnson–Cook law at $\gamma_{avg} = 1.5$, but not for the Bodner–Partom law up to $\gamma_{avg} = 4.0$.

We recall that the thermal softening is described by essentially similar functions in the Litonski law and the Johnson–Cook law, but by a totally different functional relationship in the Bodner–Partom law. We believe that it is the difference in the thermal softening behavior stipulated in the three constitutive relations that accounts for the difference in the evolution of the temperature and hence the local strain at the specimen center.

A measure of the localization of the deformation at the specimen center is the ratio of the shear strain there to the average strain in the specimen. As localization of the deformation occurs in earnest when the shear stress has started to drop precipitously, we have plotted $\gamma_{loc}/\gamma_{avg}$–$s_a/s_{max}$ in Fig. 5. For the Bodner–Partom law, the curves for $k = 0$, 5, 50, and 500 W/m °C essentially coincide with each other, whereas that for $k = 5000$ W/m °C exhibits a different trend and suggests that $\gamma_{loc}/\gamma_{avg} = 5.5$ for $s_a/s_{max} \leq 0.80$. For $k = 5000$ W/m °C and for $s_a/s_{max} \leq 0.8$, $\gamma_{loc}/\gamma_{avg}$ equals 2.3 for the Johnson–Cook law and 3.1 for the Litonski law. For $k = 50$ W/m °C, the curve for the Litonski law shows a sharp jump in the slope at $s_a/s_{max} \approx 0.85$, indicating the rapid growth of the localization of the deformation at the specimen center. By the time the shear stress drops to 80% of its maximum value, the shear

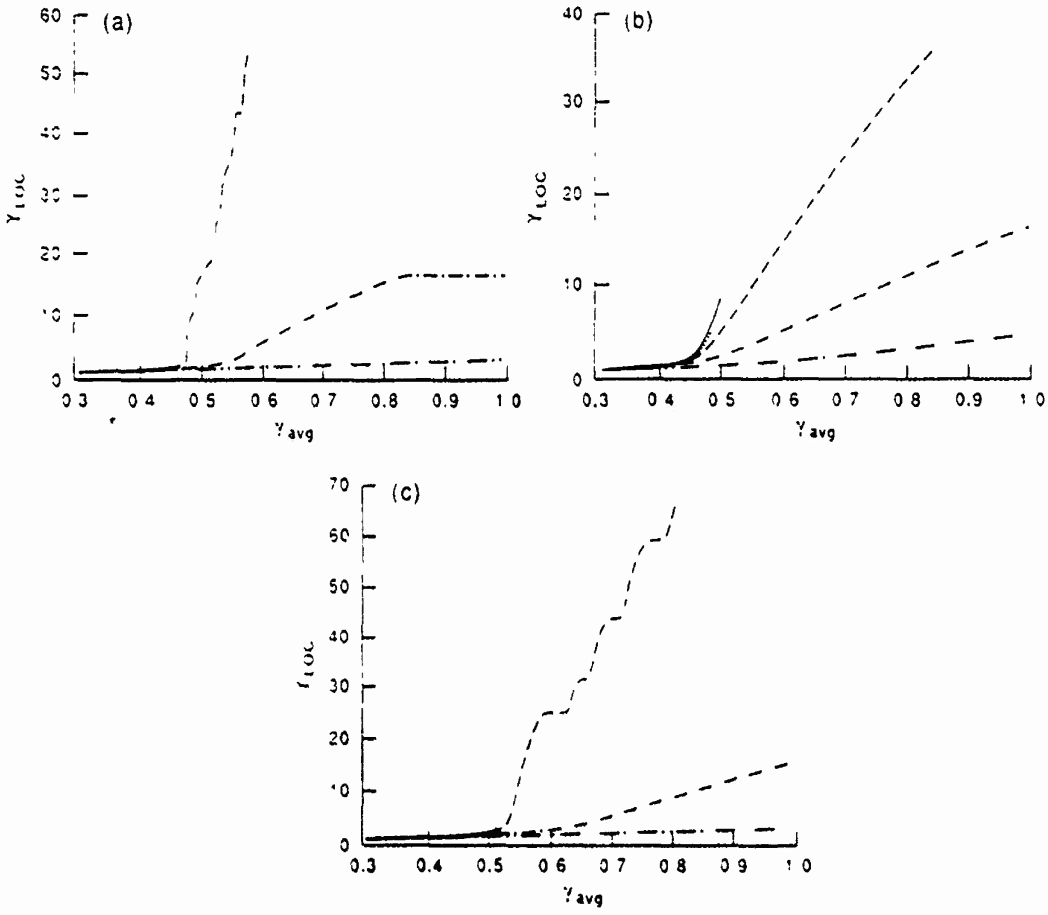

Fig. 4. Evolution of the shear strain at the specimen center for the three constitutive relations and the five values of the thermal conductivity. (a) Litonski, (b) Bodner–Partom, (c) Johnson–Cook.

strain at the specimen center would have increased enormously and the specimen would probably have failed. We recall that Marchand and Duffy [7] observed the maximum shear strain within the band to be about 20. For $k = 500$ W/m °C, $\gamma_{loc}/\gamma_{avg}$ reached a saturation value of 18 for $s_a/s_{max} \leq 0.6$ for the Bodner–Partom law. For the other two constitutive relations used, $\gamma_{loc}/\gamma_{avg}$ reached a maximum value of approximately 18 and 20 at $s_a/s_{max} \simeq 0.7$ and 0.62 for the Litonski law and the Johnson–Cook law respectively. The decrease in the value of $\gamma_{loc}/\gamma_{avg}$ signifies that the growth of the shear strain at the specimen center is less than the increase in the value of γ_{avg}. Thus the width of the severely deformed region must increase.

Marchand and Duffy [7] defined the band width as the width of the region over which the shear strain stays constant. In the problem studied herein, except when $k = 500$ or 5000 W/m °C, the band width so computed will be zero. Therefore, we define the band width as the width of the region over which the shear stain equals or exceeds 95% of its value at the specimen center. As the localization of the deformation depends upon how far the shear stress has dropped from its peak value, we have plotted in Fig. 6 the band width versus the square-root of the non-dimensional thermal conductivity β when $s_a/s_{max} = 0.95$, 0.90, 0.85, 0.80, 0.75, and 0.70. The reason for selecting $(\beta)^{1/2}$ rather than β as abscissa is that Dodd and Bai [43] found the band width to be proportional to $(\beta)^{1/2}$. It is clear that the dependence of the band width upon the thermal conductivity is nonlinear and is different for each of the three constitutive relations used. The band width decreases with a decrease in the value of the thermal conductivity. For the Litonski law and the Johnson–Cook law, the band width tends to zero as the thermal conductivity decreases to zero, but such is not the case for the Bodner–Partom law. For this law and for $k = 0$, the computed band width depends upon how far the shear stress at the specimen center has dropped. We note that the depicted curves were

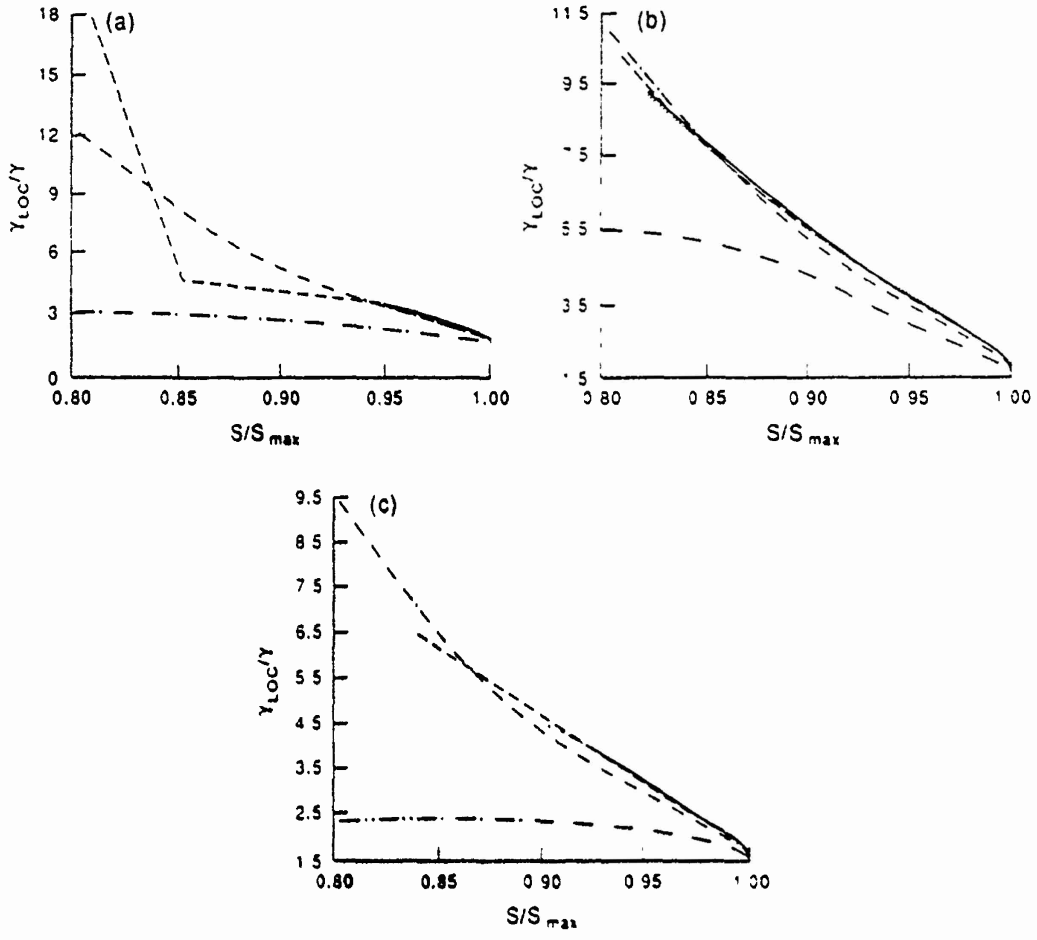

Fig. 5. Localization ratio vs s_a/s_{max}. (a) Litonski. (b) Bodner–Partom. (c) Johnson–Cook.

obtained by joining data points with straight lines rather than fitting a smooth curve through the data points. These curves do not support Dodd and Bai's result that the band width is proportional to $(\beta)^{1/2}$.

In Fig. 7 we have plotted the band width as a function of s_a/s_{max} for the five values of the thermal conductivity and the three constitutive relations used. For $k = 50$ and 500 W/m °C, the band width does seem to reach a stable value as the shear stress at the specimen center drops. For the Litonski law, and for $k = 0$ and 5 W/m °C, satisfactory results could not be computed for $s_a/s_{max} \leq 0.95$. For the same values of k, and with the Johnson–Cook law, satisfactory results could not be obtained for $s_a/s_{max} \leq 0.90$. For each of the constitutive relations used, and for $k = 5000$ W/m °C, an interesting situation developed in that the band width decreased first as the shear stress at the specimen center dropped. It reached a plateau at $s_a/s_{max} = 0.85$, and then started to increase. The rate of decrease and subsequent increase of the band width with respect to s_a/s_{max} does depend upon the constitutive relation used. A plausible explanation for this computed decrease and increase of the band width is that as the shear stress at the specimen center drops and the plastic strain-rate increases sharply, the heat generated as a result of plastic working raises the temperature there more than at other points in the specimen. Initially, the rate of heat loss to outer parts of the specimen is less than the rate of heat generation at the specimen center, and the temperature there rises, making the material there softer and thus easier to deform. As the temperature gradient builds up, the rate of heat loss increases and eventually equals and exceeds the rate of heat generation at the specimen center. Thus the material surrounding the specimen center begins to deform severely, too, and the band width increases.

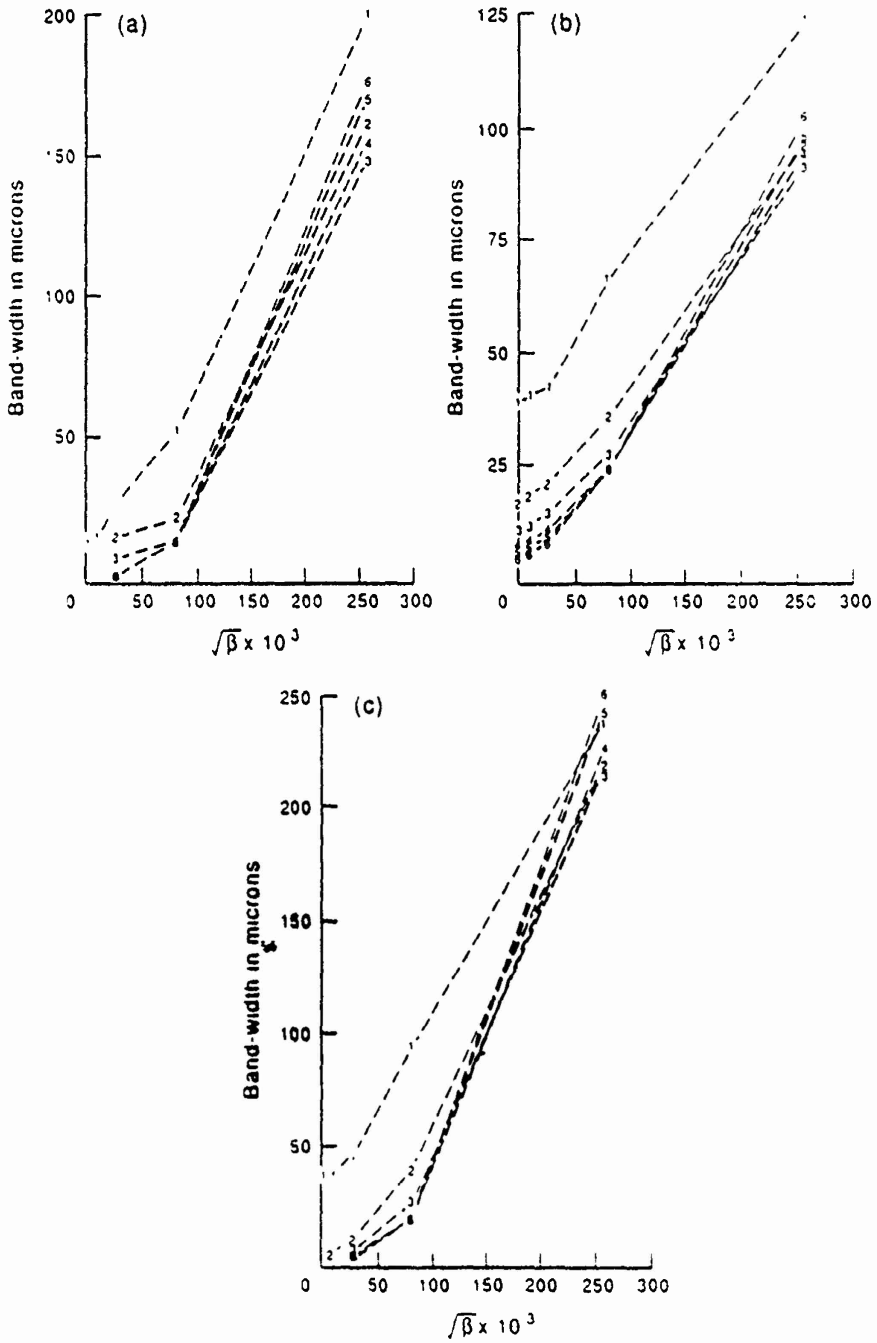

Fig. 6 Dependence of the band width upon the square-root of the non-dimensional thermal conductivity. (a) Litonski, (b) Bodner–Partom, (c) Johnson–Cook. Curve 1, $s_a/s_{max} = 0.95$; Curve 2, $s_a/s_{max} = 0.90$, Curve 3, $s_a/s_{max} = 0.85$; Curve 4, $s_a/s_{max} = 0.80$; Curve 5, $s_a/s_{max} = 0.75$; Curve 6, $s_a/s_{max} = 0.70$.

5. CONCLUSIONS

We have studied the problem of shear band development in a thermally softening viscoplastic block undergoing overall adiabatic deformations. The thickness of the block is assumed to vary smoothly with the thickness at the specimen center, being 5% smaller than that at the outer edges. Three constitutive relations, namely, the Litonski law, the Bodner–Partom law, and the Johnson–Cook law, have been used to represent the viscoplastic response of the material. The values of the material parameters used are such that each

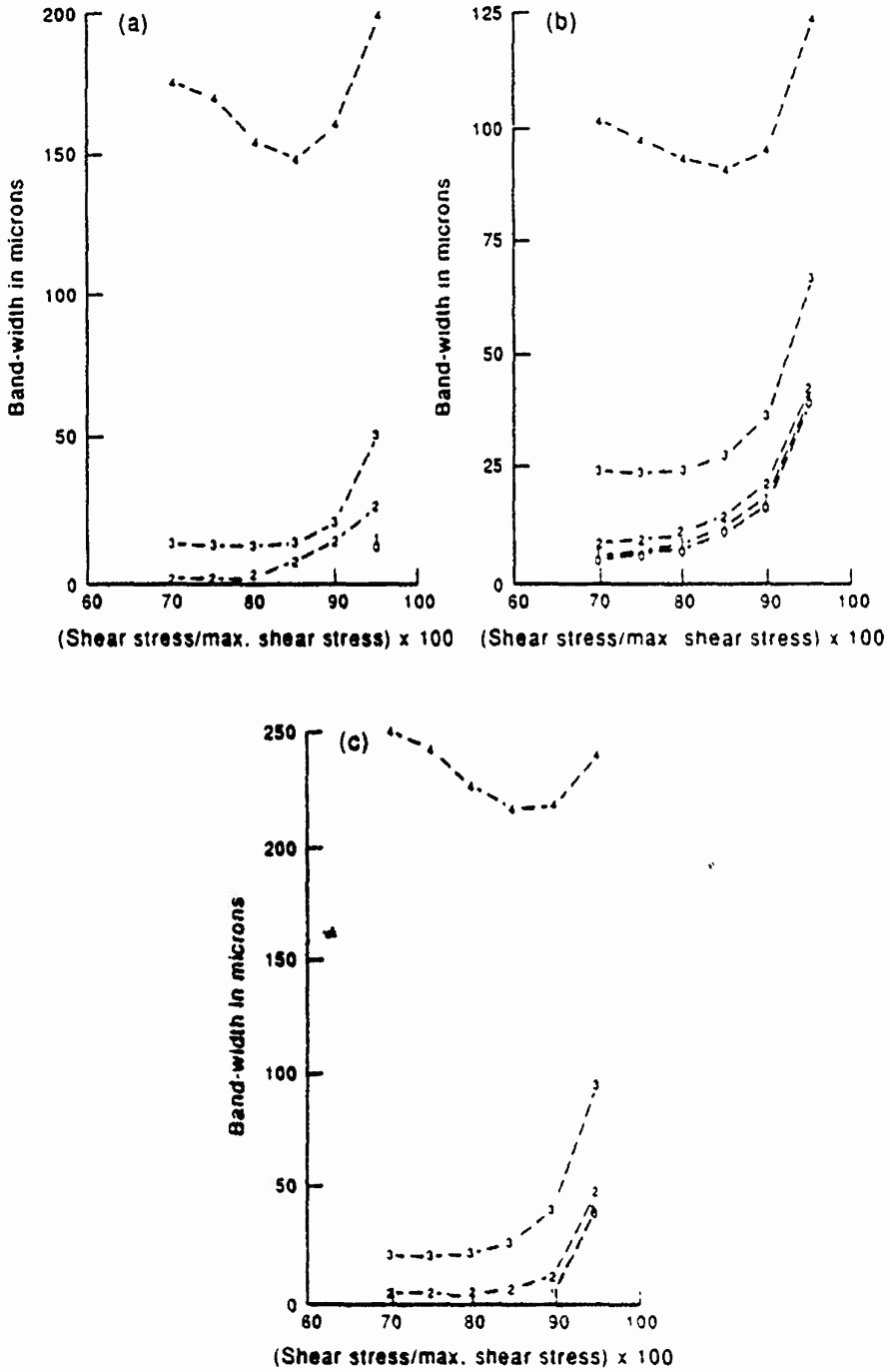

Fig. 7 Dependence of the band width upon s_a/s_{max}. Curve 0, $k = 0$; Curve 1, $k = 5$ W/m °C. Curve 2, $k = 50$ W/m °C. Curve 3, $k = 500$ W/m °C. Curve 4, $k = 5000$ W/m °C

constitutive relation gives essentially the same stress–strain curve as that observed by Marchand and Duffy [7] for a HY-100 steel deformed in torsion at a strain-rate of 3300 s^{-1}

Results have been computed for thermal conductivity k of 0, 5, 50, 500, and 5000 W/m °C. For the Bodner–Partom law, all of the results depend smoothly upon the thermal conductivity. Also, from a computational point of view, this constitutive relation was the most stable in the sense that satisfactory results could be computed for all values of k considered herein.

For each of the three constitutive relations studied, the rate of evolution of the temperature at the specimen center was steepest for $k = 0$ and decreased with an increase in the value of k. A similar behavior was noted for the development of the shear strain at the specimen center

When the time scale is changed to one which is proportional to s_a/s_{max}, the rate of temperature rise at the specimen center shows a transition for $k = 50$ W/m °C both for the Litonski law and the Johnson–Cook law. For the Litonski law and also for $k = 50$ W/m °C, the rate of localization ratio at the specimen center shows a transition at $s_a/s_{max} \simeq 0.85$. Otherwise, the results depend continuously upon s_a/s_{max} for the values of k considered herein.

The computed band width decreases nonlinearly with a decrease in the value of k. Both the Litonski law and the Johnson–Cook law predict that the band width will decrease to zero as k tends to zero. However, the Bodner–Partom law gives a finite value of the band width for $k = 0$. The band width was not found to be proportional to the square-root of the thermal conductivity as asserted by Dodd and Bai.

Acknowledgements—This work was supported by U.S. National Science Foundation grant MSM-871592, and U.S. Army Research Office Contract DAAL03-88-K-0184 to the University of Missouri–Rolla. Some of the computations were performed on the NSF sponsored supercomputer center at the Cornell University, Ithaca, NY.

REFERENCES

[1] A. M. MERZER, *J. Mech. Phys. Solids* **30**, 323 (1982).
[2] F. H. WU and L. B. FREUND, *J. Mech. Phys. Solids* **32**, 119 (1984).
[3] G. L. MOSS, In *Shock Waves and High Strain Rate Phenomenon in Metals* (Edited by M. A. MEYER and L. E. MURR), pp. 299–312. Plenum Press, New York, (1981).
[4] L. S. COSTIN, E. E. CRISMAN, R. H. HAWLEY and J. DUFFY, *Int. Phys. Conf. Ser.* **47**, 90 (1979).
[5] K. A. HARTLEY, J. DUFFY and R. H. HAWLEY, *J. Mech. Phys. Solids* **35**, 283 (1987).
[6] J. H. GIOVANOLA, *Mech. Mater.* **7**, 59 (1988).
[7] A. MARCHAND and J. DUFFY, *J. Mech. Phys. Solids* **36**, 251 (1988).
[8] M. R. STAKER, *Acta Metall.* **29**, 683 (1981).
[9] R. J. CLIFTON, NRC National Material Advisory Board (U.S.) Rep. 356 (1980).
[10] R. J. CLIFTON and A. MOLINARI, *J. Appl. Mech.* **54**, 806 (1987).
[11] T. J. BURNS, *Q. Appl. Math.* **43**, 65 (1985).
[12] L. ANAND, K. H. KIM and T. G. SHAWKI, Massachusetts Institute of Technology Report (1986).
[13] Y. L. BAI, *Shock Waves and High Strain Rate Phenomenon in Metals* (Edited by M. A. MEYERS and L. E. MURR), pp. 277–283 Plenum Press, New York (1981).
[14] B. D. COLEMAN and M. L. HODGDON, *Arch. Rational Mech. Anal.* **90**, 219 (1985).
[15] T. W. WRIGHT, *J. Mech. Phys. Solids* **38**, 515 (1990).
[16] R. J. CLIFTON, J. DUFFY, K. S. HARTLEY and T. G. SHAWKI, *Scripta Metall.* **18**, 443 (1984).
[17] T. W. WRIGHT and R. C. BATRA, *Int. J. Plasticity* **1**, 205 (1985).
[18] T. W. WRIGHT and R. C. BATRA, *Proc. IUTAM Symposium on Macro- and Micro-Mechanics of High Velocity Deformation and Fracture* (Edited by K. KAWATA and J. SHIOIRI), pp. 189–201. Springer-Verlag, Heidelberg (1987).
[19] T. W. WRIGHT and J. W. WALTER, *J. Mech. Phys. Solids* **35**, 701 (1987).
[20] R. C. BATRA, *Int. J. Plasticity* **3**, 75 (1987).
[21] R. C. BATRA, *Int. J. Solids Struct.* **23**, 1435 (1987).
[22] R. C. BATRA, *J. Appl. Mech.* **55**, 229 (1988).
[23] C. FRESSENGEAS, *Int. J. Impact Engr* **8**, 141 (1989).
[24] T. G. SHAWKI and R. J. CLIFTON, *Mech. Mater.* **8**, 13 (1989).
[25] J. LEMONDS and A. NEEDLEMAN, *Mech. Mater.* **5**, 339 (1986).
[26] J. LEMONDS and A. NEEDLEMAN, *Mech. Mater.* **5**, 363 (1986).
[27] A. NEEDLEMAN, *J. Appl. Mech.* **56**, 1 (1989).
[28] R. C. BATRA and D. S. LIU, *J. Appl. Mech.* **56**, 527 (1989).
[29] R. C. BATRA and D. S. LIU, *Int. J. Plasticity* **6**, 231 (1990).
[30] L. ANAND, A. M. LUSH and K. H. KIM, In *Thermal Aspects in Manufacturing* (Edited by M. H. ATTIA and L. KOPS), *ASME-PED* **30**, 89 (1988).
[31] Z. G. ZHU and R. C. BATRA, *Acta Mech.* **84**, 89 (1990).
[32] R. C. BATRA and X.-T. ZHANG, *Acta Mech.* **85**, 221 (1990).
[33] R. C. BATRA and Z. G. ZHU, *Int. J. Solids Struct.* **27**, 1829 (1991).
[34] Z. G. ZHU and R. C. BATRA, *Comput. Struct.* (in press).
[35] R. C. BATRA and Z. G. ZHU, *Acta Mech.* **86**, 31 (1991).
[36] T. G. SHAWKI, R. J. CLIFTON and G. MAJDA, Tech. Rep. ARO-DAAG29-81-K-0121/3, Brown University, Providence, RI (1983).
[37] A. V. SULIJOADIKUSUMO and O. W. DILLON, Jr, *J. Thermal Stresses* **2**, 97 (1979).
[38] W. S. FARREN and G. I. TAYLOR, *Proc. R. Soc. Lond.* **A107**, 422 (1925).
[39] S. R. BODNER and Y. PARTOM, *J. Appl. Mech.* **42**, 385 (1975).
[40] G. R. JOHNSON and W. H. COOK, *Proc. 7th Int. Symp. Ballistics*, The Hague, pp. 1–7 (1983).
[41] C. W. GEAR, *Numerical Initial Value Problems in Ordinary Differential Equations*. Prentice-Hall, Englewood Cliffs, NJ (1971).
[42] A. C. HINDMARSH, In: *Scientific Computing* (Edited by R. S. STEPLEMAN *et al.*), pp. 55–64. North-Holland, Amsterdam (1983).
[43] B. DODD and Y. BAI, *Mater. Sci. Technol.* **1**, 38 (1985).

(Received 27 September 1990; accepted 12 November 1990)